Improvements in Direct Torque Control of Induction Motors

Xavier del Toro García

PhD Thesis

A submission presented in partial fulfilment of the requirements of the University of Glamorgan/Prifysgol Morgannwg for the degree of Doctor of Philosophy

This research programme was carried out in collaboration with the Department of Electronic engiueering at the "Universitat Politècnica de Catalunya" (Spain)

Faculty of Advanced Technology

University of Glamorgan/Prifysgol Morgannwg

January 2008

Preface

The work presented in this thesis was carried out during the author's PhD studies at the former School of Electronics (nowadays part of the new Faculty of Advanced Technology) of the University of Glamorgan, under the supervision of Dr. Marcel G. Jayne (Director of Studies) and Prof. Phil A. Witting. The research project was realised in collaboration with the Department of Electronic Engineering at the "Universitat Politècnica de Catalunya" (UPC), in Spain, under the supervision of Dr. Antoni Arias Pujol. The collaboration between both institutions mainly involved the author's supervision and the use of the laboratory facilities and equipment of the collaborating group in Spain.

During the PhD studies the author received a Marie Curie Early Stage Training Fellowship at "Politecnico di Bari", in Italy, supported by the European Community's Sixth Framework Programme. The fellowship was in the training area of Electrical Energy Conversion and Conditioning Technology (ECCT) (EC Contract No: MEST-CT-2004-504243). The author spent one year working in the Converters, Electrical Machines and Drives (CEMD) Research Group at "Politecnico di Bari" under the supervision of Prof. Luigi Salvatore.

Abstract

Electrical motors have been increasingly employed for more than a century to convert electrical energy into mechanical energy. The wide variety of existing applications requires in many cases a very precise control of the electrical motor by means of a variable speed drive incorporating sophisticated control strategies. Besides the expectations that have to be met concerning the motion control, other aspects such as efficiency, reliability, generation of electromagnetic pollution, etc. have become very important and need to be addressed in the design of variable speed drives.

The work reported in this thesis is devoted to the investigation of speed and torque control methods for electrical motors with particular emphasis been given to a specific control strategy known as Direct Torque Control (DTC). DTC is one of the preferred control techniques for Induction Motor (IM) drives due to the high performance obtained and its structural simplicity. However, it has a number of inherent disadvantages such as: poor performance at low speed operation, unwanted torque and flux ripples, variable switching frequency and a higher harmonic distortion of the stator voltage and current waveforms compared with other methods, such as Field Oriented Control (FOC). It is the aim of this work to improve the control system in order to eliminate or considerably reduce the undesirable features that exist with the Classical DTC method.

The proposed solution investigated consists in the combination of the DTC principle with a multilevel power converter: the three-level Voltage Source Inverter (VSI). This type of VSI can deliver an increased number of voltage vectors when compared to the standard two-level VSI, and this feature enhances the possibilities of the controller when selecting the output voltage vector to be applied to the motor. A new controller has been developed to exploit this potential. The resulting control system is able to achieve a fast and precise control of the stator flux and torque, with a considerable reduction of the ripples. Moreover, the use of the three-level VSI provides reduced voltage derivatives, lower harmonic distortion in the stator voltages and currents, and a reduction of the Common-Mode (CM) voltage and leakage currents. The switching frequency and the voltage supported by the semiconductor devices are also reduced, and their stress and power losses are therefore lower.

Acknowledgements

I am most grateful to my supervisors Dr. Marcel Jayne, Prof. Phil A. Witting and Dr. Antoni Arias for their support, help and encouragement during all this time. I wish to express my gratitude to all the research students in the former School of Electronics at the University of Glamorgan for the enjoyable environment created and their help. In particular I would like to thank Andrew Chambers for his help while I was away in Italy and Spain. I am also thankful to the staff members of the former School of Electronics. I have to thank the student Ray De Grussa who taught me how personal effort and team work can break all barriers.

I would like to thank Josep Pou and Jose Luis Romeral for the possibility of using the laboratory facilities at the Department of Electronic Engineering in "Universitat Politècnica de Catalunya", Spain. A special mention should go to Vicenç Sala "Vite", German López and Héctor Lama for their work and help in setting up the equipment during the experimental work of this research.

I have to say "grazie mille" to Prof. Luigi Salvatore and the other colleagues from "Politecnico di Bari", in Italy, for the possibility to work with them and all the things I learnt during the year I spent there. I want to thank my good friends Branislav Zigmund and Rastislav Pavlanin from the University of Zilina, Slovakia, for their help, friendship and all the exciting discussions held while in Italy. I also have to thank Carlos Ortega for his collaboration and valuable comments.

I am also grateful to all the friends I made during my years in Wales and Italy, who made all this period of my life more enjoyable, especially to Ali Savvaris, Vicente Diaz and Erika Lino. I cannot forget thanking my friends back at home in Spain because in spite of the distance I always felt them very close. I really enjoyed every short return back home and their visits while being away. Among them I would like to mention Salvador Calls who spent a year in the University of Glamorgan while doing his final year project and who helped me to improve my cooking skills.

I wish to thank my family for their patience, care and continuous encouragement during all these years; without them it wouldn't have been possible.

Last but not least I have to say "gràcies" to Maria José for her love and support.

Xavier del Toro García, June 2007.

"On life's vast ocean diversely we sail,
Reason the card, but passion is the gale;"

"Essay on man", Alexander Pope (1688-1744)

Terminology

Symbols

a : 120° rotation operator $e^{j2\pi/3}$.

$\vec{B}$: Magnetic flux density.

c : Constant of the space vector, Clarke and Park transformations.

C_A, C_B, C_C : State of the VSI legs A, B and C.

D : Combined rotor and load viscous friction coefficient.

$d_{\Gamma e}$: Torque error label.

$d_{\psi s}$: Stator flux modulus error label.

$d_{\psi a}$: Phase a stator flux error label.

$d_{\psi b}$: Phase b stator flux error label.

$d_{\psi c}$: Phase c stator flux error label.

$e_{\Gamma e}$: Torque error.

$e_{\omega m}$: Rotor angular speed error.

$e_{\psi s}$: Stator flux modulus error.

$e_{\psi sa}$: Phase a stator flux modulus error.

$e_{\psi sb}$: Phase b stator flux modulus error.

$e_{\psi sc}$: Phase c stator flux modulus error.

$\vec{F}$: Force.

f_c : PWM carrier frequency.

f_o : VSI fundamental output frequency.

f_s : Sampling frequency.

f_{sw} : Mean switching frequency of the converter switches.

f_{sync} : Synchronous frequency.

h : Radius of exploration in the optimization algorithm.

$H_{\Gamma e}$: Torque hysteresis band.

$H_{\psi s}$: Stator flux hysteresis band.

I : Instantaneous electric current.

i_{NP} : NP current.

i_A, i_B, i_C : Instantaneous VSI output currents, legs A, B and C.

i_{ra}, i_{rb}, i_{rc} : Instantaneous rotor current, phases a, b and c.

i_{sa}, i_{sb}, i_{sc} : Instantaneous stator current, phases a, b, and c.

$\vec{i}_a$: Armature current of a DC motor.

$\vec{i}_m$: Magnetising current space vector.

$\vec{i}_r$: Rotor current space vector.

$\vec{i}_r'$: Rotor current space vector in the stator reference frame.

$\vec{i}_s$: Stator current space vector.

$\vec{i}_s'$: Stator current space vector in the rotor reference frame.

J : Combined rotor and load inertia coefficient.

k : Constant of a DC motor / number of levels of the line-to-line output voltage of a VSI.

K : Sector of the stator flux position.

$K_{\Gamma e}$: Proportional gain of the torque control loop.

$K_{\psi s}$: Proportional gain of the stator flux modulus control loop.

K_p : Proportional gain of the speed PI control.

K_i : Integral gain of the speed PI control.

$\vec{l}$: Length.

L_m : Total magnetising inductance.

L_r : Total rotor inductance.

L_s : Total stator inductance.

L_{rph} : Rotor phase inductance.

L_{sph} : Stator phase inductance.

M_r : Rotor mutual inductance between phases.

M_s : Stator mutual inductance between phases.

M_{sr} : Mutual inductance between the stator and rotor phases.

n : Rotor Speed / number of different voltage levels delivered by a power converter

N_r : Number of turns in the rotor windings.

N_s : Number of turns in the stator windings.

n_{sync} : Synchronous speed.

p : Number of levels of the phase voltage in a star-connected load fed by a VSI.

P : Number of pole pairs in an electrical motor.

P_{out} : Shaft output power.

P_T : Total instantaneous active power.

q : Electric charge.

R_r : Rotor phase resistance.

R_s : Stator phase resistance.

s : Derivative operator (Laplace domain).

S : Slip.

t : Time.

T_{DTC} : Time constant of the torque loop in DTC.

T_f : Time constant of the speed filter.

T_i : Integral time constant of the speed PI control.

T_{rotor} : Rotor electrical time constant.

T_s : Sampling period.

T_{sf} : Time constant of the speed reference smoothing filter.

T_{stator} : Stator electrical time constant.

T_Σ : Speed loop delay.

u : Voltage or electromotive force.

u_a, u_b, u_c : Generic instantaneous voltage of a three-phase system, phases a, b and c.

u_α, u_β, u_0 : Generic instantaneous voltage in α-β-0 coordinates.

u_i, u_j, u_0 : Generic instantaneous voltage in i-j-0 coordinates.

u_{ab} : Line voltage between phases a and b.

u_{ra}, u_{rb}, u_{rc} : Instantaneous rotor voltage, phases a, b and c.

u_{sa}, u_{sb}, u_{sc} : Instantaneous stator voltage, phases a, b and c.

u_{syBEMF} : Back Electromotive Force term of the stator voltage y component.

$u_{sy\Gamma e}$: Torque production term of the stator voltage y component.

u_{sx}^{*} : x component of the stator voltage reference vector.

u_{sy}^{*} : y component of the stator voltage reference vector.

$u_{s\alpha}^{*}$: α component of the stator voltage reference vector.

$u_{s\beta}^{*}$: β component of the stator voltage reference vector.

$\vec{u}$: Generic voltage space vector.

$\vec{u}_r$: Rotor voltage space vector.

$\vec{u}_s$: Stator voltage space vector.

$\vec{v}$: Speed / voltage space vector.

V_{AB} : Voltage between the A and B outputs of the VSI.

V_{AG}, V_{BG}, V_{CG} : A, B and C output voltages of the VSI referred to the ground of the power source.

V_{An}, V_{Bn}, V_{Cn} : A, B and C output voltages of the VSI referred to the neutral of a star-connected load.

$V_{ANP}, V_{BNP}, V_{CNP}$: A, B and C output voltages of the VSI referred to the middle point or NP of the DC-link.

V_{A-}, V_{B-}, V_{C-} : A, B and C output voltages of the VSI referred to the negative rail of the DC-link.

V_{C1} : Voltage of the capacitor connected between the positive rail and the NP of the DC-link.

V_{C2} : Voltage of the capacitor connected between the negative rail and the NP of the DC-link.

V_{CM} : CM voltage.

V_{DC} : DC-link Voltage.

V_{nNP} : Voltage between the neutral of a star-connected load and the NP.

V_{NP} : NP voltage (referred to the negative rail of the DC-link).

V_{FRMS} : RMS value of the fundamental harmonic of voltage.

α : Argument (angle) of a generic space vector.

Γ : Generic torque.

Γ_e : Electromagnetic torque.

$\hat{\Gamma}_e$: Estimated torque.

Γ_e^* : Torque reference.

Γ_F : Friction torque.

Γ_L : Load torque.

Γ_{lim} : Saturation value of the torque reference.

Γ_n : Nominal torque.

γ_r : Rotor flux angle.

γ_s : Stator flux angle.

$\hat{\gamma}_s$: Estimated stator flux angle.

θ_g : Angle between a generic coordinate system and the stator-fixed coordinate system.

θ_m : Angle between the rotor and the stator.

θ_s : Angle between the coordinate system fixed to the stator flux vector and the stator fixed coordinate system.

σ : Dispersion factor of the IM.

ω_g : Angular speed of a generic coordinate system.

ω_m : Rotor angular speed.

ω_{mf} : Rotor angular speed (filtered).

ω_m^* : Rotor angular speed reference.

ω_n : Nominal value of the rotor angular speed.

ω_r : Angular speed of the rotor flux vector.

ω_s : Angular speed of the stator flux vector.

$\hat{\omega}_s$: Estimated angular speed of the stator flux vector.

$\hat{\omega}_{sf}$: Estimated angular speed of the stator flux vector (filtered).

ψ : Magnetic flux.

$\psi_{ra}, \psi_{rb}, \psi_{rc}$: Instantaneous rotor flux linkage, phase a, b and c.

$\psi_{sa}, \psi_{sb}, \psi_{sc}$: Instantaneous stator flux linkage, phases a, b and c.

$\vec{\psi}_e$: Excitation flux of a DC motor.

$\vec{\psi}_r$: Rotor flux space vector.

$\vec{\psi}_r^{'}$: Rotor flux space vector in the stator reference frame.

$\vec{\psi}_s$: Stator flux space vector.

$\vec{\psi}_s^{'}$: Stator flux space vector in the rotor reference frame.

ψ_s^* : Stator flux modulus reference.

$\hat{\psi}_s$: Estimated stator flux modulus.

$\hat{\psi}_{sa}$: Estimated phase *a* stator flux modulus.

$\hat{\psi}_{sb}$: Estimated phase *b* stator flux modulus.

$\hat{\psi}_{sc}$: Estimated phase *c* stator flux modulus.

ψ_{sn} : Nominal stator flux modulus.

Subscripts

a / A : *a*/*A*-phase variable.

b / B : *b*/*B*-phase variable.

c / C : *c*/*C*-phase variable.

d : Direct component of the rotor-fixed coordinate system.

g : Generic coordinate system.

q : Quadrature component of the rotor-fixed coordinate system.

i : Direct component of a generic coordinate system.

j : Quadrature component of a generic coordinate system.

max: Maximum.

min: Minimum.

r : Rotor variable.

RMS: RMS value.

s : Stator variable.

x : Direct component of the stator flux vector coordinate system.

y : Quadrature component of the stator vector coordinate system

α : Direct component of the stator-fixed coordinate system.

β : Quadrature component of the stator-fixed coordinate system.

ψ_s : Stator flux vector reference frame.

0: Initial / homopolar component.

Mathematical operators

×: Cross vector product.

*: Complex conjugate.

Acronyms

AC: Alternating Current.

ADC: Analog-to-Digital Converter.

ANN: Artificial Neural Networks.

BEMF: Back Electromotive Force.

CM: Common-Mode.

DAC: Digital-to-Analog Converter.

DC: Direct Current.

DSC: Direct Self-Control.

DSP: Digital Signal Processor.

DTC: Direct Torque Control.

DTC2L: Classical DTC system with a two-level VSI.

EKF: Extended Kalman Filter.

EMI: Electromagnetic Interference.

EMC: Electromagnetic Compatibility.

FFT: Fast Fourier Transform.

FOC: Field Oriented Control.

GA: Genetic Algorithm.

GUI: Graphical User Interface.

HVAC: Heating, Ventilation and Air Conditioning.

IGBT: Insulated-Gate Bipolar Transistor.

IM: Induction Motor.

IPMSM: Interior Permanent Magnet Synchronous Motor

LPF: Low-Pass Filter.

NP: Neutral Point.

NPC: Neutral Point Clamped.

NTV: Nearest Three Vectors (modulation technique).

PDTC3L: Proposed control system with a three-level VSI.

PI: Proportional-Integral (controller).

PLD: Programmable Logic Device.

PM: Permanent Magnet.

PMSM: Permanent Magnet Synchronous Motor.

PPC: PowerPC.

PWM: Pulse Width Modulation.

RFOC: Rotor Field Oriented Control.

RISC: Reduced Instruction Set Computer.

RMS: Root-Mean-Square.

SFOC: Stator Field Oriented Control.

SO: Symmetrical Optimum.

SM: Synchronous Motor.

SMPMSM: Surface Mounted Permanent Magnet Synchronous Motor

SNR: Signal-to-Noise Ratio.

SVM: Space Vector Modulation.

THD: Total Harmonic Distortion.

UPS: Uninterruptible Power Supply.

VSI: Voltage Source Inverter.

VVVF: Variable Voltage Variable Frequency.

Table of Contents

List of Figures

List of Tables

Chapter 1: Introduction

Summary – *This chapter introduces the work contained in this thesis. First an historical review is presented in order to establish the context and justify the interest of the work reported. Next the aims and objectives of the research work are presented. Finally the structure of the document and the content of each chapter are described.*

1.1 Historical review

The asynchronous motor, also known as Induction Motor (IM), was invented in parallel by Nicola Tesla and Galileo Ferraris in the 1880s as a result of their studies on rotating magnetic fields. In 1889 Michail Dolivo-Dobrovolsky invented the three-phase IM with wound rotor and also the cage rotor type in a topology very similar to the IM used nowadays. Around 1900 the IM was ready for wide use in industry using the three-phase AC power grid [1]. Since that moment this type of motor has gained widespread application worldwide and a large percentage of the electrical energy generated is converted to its mechanical form by means of IMs.

Energy saving, improved energy efficiency and environmental protection have become some of the main concerns in Europe and worldwide. At present time, 40% of the overall energy consumption is electrical energy, but it is expected to grow to 60 % by 2040 [2]. In industry, 60% of the energy is used in electrical motors. Therefore IMs have a large impact on the total energy consumption, particularly in developed and industrialised countries.

Most IMs are still fed from three-phase or single-phase power grids and run at fixed speeds in a very inefficient way in most cases. By using variable speed drives incorporating power electronics a potential reduction in energy consumption of 30% is achievable [2]. Furthermore, variable speed in industrial processes leads to higher flexibility and controllability, better accuracy, higher productivity and easier maintenance. From the economical perspective the use of variable speed is also justified since for each euro spent to purchase a motor, 100 euros are spent for energy cost during its lifetime [2]. The increasing energy prices together with the declining prices of variable speed drives are shortening the payback period. Competitiveness is therefore gained by incorporating variable speed control.

Variable speed drives utilising IMs are used nowadays in a wide variety of application including transportation, pumps, compressors, ventilators, machine tools, robotics, hybrid or electric vehicles, washing machines, etc. It is expected that the share of electrical energy which will be controlled by power electronics in applications such as variable speed drives will increase from 40% in 2000 to 80% in 2015 [2]. The low and high power AC drives markets have experienced a strong growth which will continue in the next years according to the study presented in [3]. The high power AC drives market is expected to grow at a compounded annual growth rate of 9.1% over the next five year

(2007-2011). The market was over $4.7 billion in 2006 and is forecasted to be nearly $7.4 billion in 2011. Regarding the low power AC drives market, the compounded annual growth rate is expected to be 7.9% over the next five years. The market was nearly $6 billion in 2006 and is forecasted to be over $8.7 billion in 2011.

All these considerations and figures suggest that any improvements which can be made to the performance of variable speed drives can have a very considerable financial significance to the national economies and the environment. The use of variable speed drives, however, leads to the generation of current harmonics in the power grids and Electromagnetic Interference (EMI) in the environment. Power quality and EMI have become new constraints that the design of variable speed drives has to address.

The success of the IM is mainly attributed to its advantages over the rest of electrical motors. One of main advantages is that the cage rotor IM does not require an electrical connection between the stationary and the rotating parts of the motor. Moreover, the rotor construction and structure is very simple in the cage rotor type. The robustness and reliability are therefore increased, while the price and maintenance cost is reduced due to the absence of mechanical commutators (brushes). IMs are distinguished by their high efficiency and overload capability. They also have low weight and inertia which leads to higher operating speeds and faster acceleration. Furthermore, IMs can work in explosive environments, clean-room areas and low maintenance applications because no dust or sparks are generated. Taking into account all the advantages previously outlined, the IM can be considered one of the best options for converting electrical energy into mechanical energy.

Nowadays variable speed and torque control is a requirement for many applications where IM are employed. Moreover, many existing applications, where the IM is directly fed from the power grid and operated at fixed speed, can be improved regarding energy saving and performance by means of incorporating variable speed. From the control point of view, however, achieving variable speed and torque control with the IM is not a trivial matter. The complexity of the IM mathematical model requires more complex control schemes and more expensive power converters.

The only effective way of producing an infinitely variable speed drive is to supply the IM with three phase voltages of variable frequency and variable amplitude. Before the days of power electronics, a very limited speed control of the IM was achieved by switching the connection of the three stator windings from delta to star, allowing the voltage at the motor windings to be reduced. Some IMs are available with more than

three stator windings to allow a change of the number of pole pairs that in turn modifies the speed. However, a motor with several windings is more expensive and only certain discrete speeds are available according to the number of pole pairs. An alternative method of speed control can be realised by means of a wound rotor IM, where the rotor winding ends are brought out to slip rings and can be connected to resistances. However, this method obviously removes most of the advantages of the IM and it also introduces additional losses. Similarly, by connecting resistors or reactances in series with the stator windings of the IM poor performance is achieved.

In the past, only the methods previously described were available to control the speed of the IM. When infinitely variable speed drives with good performance were required, DC motors were the natural choice. DC motors not only permitted the operation in four quadrants but also covered a wide power range. Moreover, they provided high efficiency and good dynamic response with a suitable control. However, the main drawback of the DC motor is the utilisation of brushes in its mechanical structure, which in turn increases the inertia and friction, limits the maximum speed and voltage, and produces sparks. Furthermore their prices are higher and they require considerable maintenance.

With the enormous advances made in semiconductor devices, power electronics and digital electronics in the last decades, the required technologies to enable the development of variable speed drives for IMs were available. This development can be mainly attributed to the following factors:

- The decreasing cost and improved performance in power electronic switching devices, especially with the introduction of the Insulated Gate Bipolar Transistor (IGBT).
- The feasibility of implementing complex algorithms in the new microprocessors, and more recently in Digital Signal Processors (DSPs).

However, one precondition had to be satisfied, which was the development of suitable methods to control the motor speed. In contrast to the simplicity of the IM mechanical structure, the mathematical model that describes the mechanism of torque production (multivariable and non-linear with coupled variables) is considerably complex. It is to this field that an important research effort is devoted. In the past, several types of controller have been developed for variable speed IM drive systems, which can divided into scalar control and vector control methods.

Scalar control is based on relationships which are only valid when the IM is in steady-state conditions. The magnitude and frequency of voltages, currents and flux linkages

are controlled, to indirectly control the speed of the IM. Scalar control does not provide a fast and accurate speed control during transients since there is no control over the instantaneous state of the currents and fluxes that produce the electromagnetic torque.

Scalar control with constant voltage-frequency ratio (V/f) is the most widespread method and covers the majority of industrial applications. The structure is very simple and it is normally used without speed feedback. However, high accuracy in the speed response is not achieved, and the disturbance rejection capability is poor. This is mainly due to the fact that the motor flux and torque are not directly controlled. Control is instead provided by a frequency and voltage reference generator with constant volts per hertz output, which then drives a Pulse Width Modulation (PWM) block. Flux and torque levels are dictated by the response of the motor to the applied frequency and voltage, and they also depend on the motor load.

Vector control is based on relationships which are valid for transient and steady-state conditions. Not only the magnitude and frequency but also the instantaneous state of voltages, currents and flux linkages are controlled. All these motor variables can be expressed mathematically as space vectors. Vector control methods act on the position and amplitude of the space vectors during the transient and steady-state conditions, providing a better control performance. This type of control can be implemented in many different ways; the most popular solution is known as Field Oriented Control (FOC) and was proposed by Hasse [4] and Blaschke [5] in the early 1970s. In FOC, the motor equations are transformed to a coordinate system fixed to the rotor flux vector; the resulting control is known as Rotor Field Oriented Control (RFOC). In this new system of coordinates, under constant rotor flux amplitude, there is a linear relationship between torque and the control variables. Flux and torque are decoupled and can be controlled separately like in a DC motor. This method can reach high accuracy, but requires a considerable high computational capability and a good identification of the motor parameters. FOC is now highly developed and it can be considered as a mature and state of the art technique, being available on the market of variable speed drives from several manufacturers. Different versions of this control technique are obtained if the orientation of the coordinate system is changed. One of those possibilities is to fix the coordinate system to the stator flux vector. The resulting control is known as Stator Field Oriented Control (SFOC).

In the mid 1980s, when there was a trend toward standardization of the control system based on the FOC principle, a new technique called Direct Torque Control (DTC)

appeared. It was introduced by Isao Takahashi and Toshihiko Noguchi [6]. M. Depenbrock introduced a similar idea under the name Direct-Self Control (DSC) [7]. The basic motivation for their work was to obtain a faster torque response of the IM. This was achieved by directly controlling the stator flux vector by means of the stator voltage without employing current control loops and voltage modulators. This method has emerged over the last two decades to become one possible alternative to FOC. The main merits of DTC are the good performance achieved with its simpler control structure. The first commercial drive based on the DTC principle was developed by the AC drives division of the company Asea Brown Bovery (ABB), and it was commercially launched in 1995 [8-11]. Since then DTC has gained a large acknowledgement from industry and academia. Still nowadays, this particular control method is subject of study and research in order to improve and attenuate the existent drawbacks [12-14].

Besides the control algorithm, one of the core elements of the variable speed drive is the power converter. The standard solution adopted in most cases is the two-level Voltage Source Inverter (VSI). This type of VSI has a simple and robust structure, with a relatively small size and good regulation capabilities. It provides very high efficiency and open-circuit protection. Nevertheless, it has some technological limitations. One alternative to the standard two-level VSI is the multilevel power conversion technology, which is a very rapidly growing area of power electronics. A considerable effort is made in research and development in this field [15, 16]. The maximum voltage that the existing technologies for semiconductor devices can withstand is one the main limitations of the two-level VSI. For this reason, multilevel converters have emerged as the solution for working with higher voltage and power levels. Multilevel converters can synthesize waveforms by using more than two voltage levels. The quality of the voltage and current spectra is significantly improved when compared to the standard two-level VSI. Moreover lower voltage steps (dV/dt) and Common-Mode (CM) voltage and currents are produced. The main drawback of multilevel converters is the requirement of a higher number of switches, which reduces the reliability and increases the cost and the complexity of the control. Despite these drawbacks multilevel converters have turned out to be a very good alternative for high-power applications, since the cost of the control is a small portion of the whole cost of the system. Moreover, the requirement and size of additional passive components is reduced. As prices of power semiconductors and DSPs continue to decrease, the use of multilevel

topologies is expected to extend to low-power applications as well. Fast power devices, such as MOSFET transistors, which can operate at very high switching frequencies, can be used for low voltage applications. Furthermore, new power devices are expected to appear, and these may also extend the application of multilevel topologies.

The increased number of voltage vectors that can be delivered by a multilevel converter, when compared to the standard two-level VSI, is a very interesting feature from the control perspective. This feature can potentially lead to a considerable improvement of the performance in the resulting control system if it is employed in conjunction with the DTC principle. If the DTC algorithm can choose among a higher number of voltage vectors with different directions and amplitudes a better control performance is expected to be obtained. Despite the potential of the DTC method with multilevel converters the amount of research which has been dedicated to this area is still small.

1.2 Aims and objectives

The aims and objectives of the research work presented in this thesis can be summarized as follows:

- Study the DTC method for IMs and identify the existing drawbacks of this control method.
- Investigate ways to improve the performance of the DTC method.
- Study the power conversion technology for variable speed drives, in particular the existing types of multilevel converters.
- Study the three-level NPC VSI and compare it to the standard two-level VSI in order to identify the advantages and disadvantages.
- Investigate the combination of the DTC method with multilevel converter topologies, in particular with the three-level NPC VSI.
- Develop a new control system based on the combination of the DTC principle and the three-level NPC VSI.
- Implement the resulting control system and prove its validity. Establish the advantages and benefits achieved by the new control system.

1.3 Structure of the thesis

The thesis is structured in the following chapters:

Chapter 1, Introduction, presents the background, objectives and content of the thesis.

Chapter 2, The Induction Motor, is devoted to this type of electrical motor. A description of its structure and operational principle is given, followed by the mathematical model. A simulation model is obtained from the mathematical model and some simulation results are presented to show its validity.

Chapter 3, Voltage Source Inverters, presents the technology employed for power conversion in variable speed drives for IMs. The standard two-level VSI is described followed by a review of the technology for multilevel converters. A deeper description is given for the three-level VSI and the particularities of the NPC topology, which is employed in the work developed in this thesis. Finally, a comparison in simulation between the two-level VSI and the three-level VSI is presented.

Chapter 4, Direct Torque Control, is dedicated to this particular control method for IMs. A description of the Classical DTC method is given with its main features, advantages and disadvantages. Problems associated with DTC are presented and discussed. Finally, a variety of methods proposed in the past years to improve DTC are presented.

Chapter 5, New Control System, presents the novel control system developed, which is the main original contribution of this thesis. Sections 5.4 to 5.8 describe the structure and tuning methods of the new control system developed. Simulation results are shown to compare the proposed technique with the Classical DTC method and the benefits obtained are presented and discussed.

Chapter 6, Experimental Validation, describes the equipment used to test and evaluate the control algorithms developed. It gives a description of all the hardware components included in the laboratory setup and it also details the implementation of the control algorithms. The experimental results obtained are presented to prove the validity of the proposed control system.

Chapter 7, Conclusions and Suggestions for Further Research, summarizes the work presented in the thesis and states the contributions and conclusions extracted from it. Finally, some suggestions are given for further research.

The references and appendixes can be found at the end of the document. In particular, Appendix D contains the list of papers published by the author during the PhD studies, specifying those directly related to the research work presented in this thesis.

Chapter 2: The Induction Motor

Summary – *This chapter is dedicated to the IM. The structure, operational principle and mathematical model are described. For convenience, space vector notation is employed to formulate the model. A simulation model is obtained and some results are presented to prove its validity.*

2.1 Introduction

Electrical energy can be converted into mechanical energy and vice versa by means of electrical machines. When electrical energy is transformed into mechanical energy the electrical machine is said to be working as a motor, conversely, when the transformation is in the opposite direction it is said to be working as a generator. In electrical motors, mechanical forces and torque are produced due to the interaction between magnetic fields, which can be generated by electrical current flowing in conductors or permanent magnets. Electromagnetism is the field of physics which describes these interactions. A unified theory for electromagnetism was fully developed and presented by James C. Maxwell in 1873. The fundamental principle of electrical machines is based on the mechanical force experimented by electrical charges moving in a magnetic field. This principle is described by the Lorentz force law:

$$\vec{F} = q\vec{v} \times \vec{B} \tag{2.1}$$

For a straight wire carrying current in a uniform magnetic field the force will be:

$$\vec{F} = i\left(\vec{l} \times \vec{B}\right) \tag{2.2}$$

As can be deduced from the cross product of vectors in the previous equation, the force is maximum when the conductor is perpendicular to the magnetic field.

Another important effect is the electromagnetic induction discovered in the experiments carried out by Michael Faraday in 1831. The variation of a magnetic flux linking a conductor induces an electromotive force in the conductor. This principle explains how transformers, generators and IMs work.

$$u = -\frac{d\psi}{dt} \tag{2.3}$$

Most electrical motors are based on the electromagnetic principles described; however, some electrical motors are based on other electromechanical phenomena such as electrostatic forces and the piezoelectric effect.

Most electrical machines are rotary, but linear types also exist. A rotary electrical motor is divided in two main parts, the stationery part called stator and the rotating part called rotor, which is usually housed inside the stator. A motor contains electromagnets that

are wound on a frame usually made of a material with high magnetic permeability such as iron.

Regarding electrical motors various types have been developed with different structure, features and fields of application. A possible classification of the main types of electrical motors is as shown in Fig. 2-1.

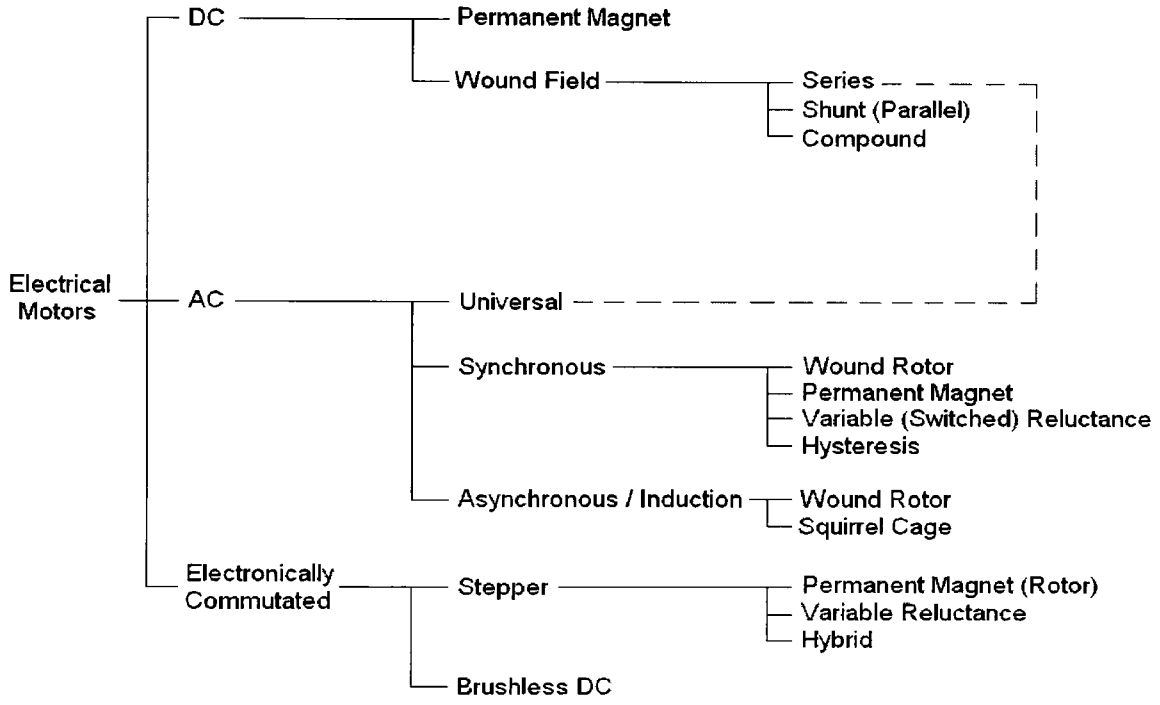

Fig. 2-1 Classification of the different types of electrical motors

Among the different types of motor presented in the previous figure the research presented in this thesis is focused on the control of the AC asynchronous motor also known as IM. A picture of an IM is shown in Fig. 2-2.

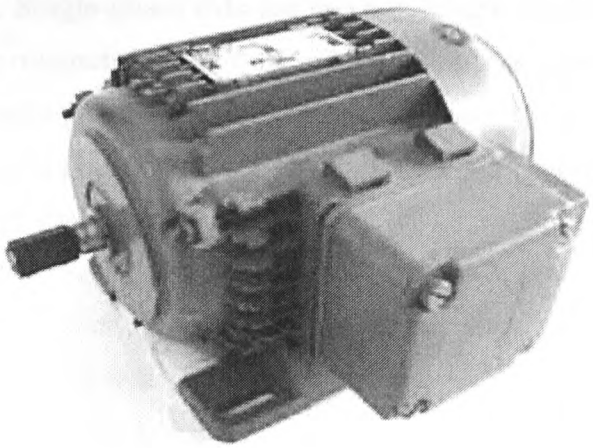

Fig. 2-2 Three-phase IM

The IM has found wide application in industry and appliances due to its advantageous characteristics. Some of the advantages of the IM that can be outlined are:

- Simple structure and low maintenance cost. No brushes are used in the squirrel cage rotor type.
- High robustness and reliability. High overload capability.
- Moderate cost, especially for the squirrel cage rotor type.
- Suitable in unfriendly and explosive environments with the appropriate enclosure.
- It can be directly fed from the three-phase and single-phase AC power grids. Only electromagnetic power switches and protection are required for a direct connection.
- Power range from tens of Watt to tens of Megawatt.
- Good power/weight ratio.

The disadvantages of the IM are basically related to the complexity of an accurate control in variable speed applications. This is mainly due to the fact that torque and flux are coupled and they are both generated by the stator voltages.

IMs are used in a broad variety of constant and variable speed applications, both in industry and appliances. Some examples of applications are: transportation, electric and hybrid vehicles, mills, pumps, compressors, ventilators, fans, conveyors, roller tables, machine tools, robotics and washing machines.

IMs can be single-phase or poly-phase, such as three-phase motors. Single-phase IMs are mainly used in low power applications, mainly home appliances. Their main advantages are the low cost, high reliability and the direct connection to the single-

phase AC power grid. Single-phase IMs are generally built with two stator windings to produce the travelling magnetic field in the air gap. The two windings are in general at 90 degrees shift. Single-phase motors are not self-starting and require a starting mechanism such as a split phase with resistance, reactance or capacitor start. A different option is the motor with shaded poles.

Three-phase IMs are the most common option due to its suitability for the three-phase AC power grid. The research work presented in this thesis will be focused on the control of the three-phase IM with squirrel cage rotor.

The structure of the IM mainly consists of two parts: the stator, which is the stationary part; and the rotor, which is the rotating part. Some other additional parts of the motor are: the rotor shaft, the stator frame with bearings, the cooling system and the terminal box.

The stator is normally wound with three-phase distributed winding, whereas the rotor can have a cage winding or a three-phase distributed winding similar to the stator one. The internal yoke of the stator and the rotor are generally constructed from laminations of ferromagnetic material with a very high permeability. The air gap between the stator and the rotor is symmetrical and normally designed to be minimal. Stator windings are housed in slots where they are enclosed in iron laminations as mentioned before.

The wound rotor IM has a three-phase symmetrical winding, which is housed in the rotor slots and insulated from the other parts of the rotor. The ends of the rotor windings can be connected in a star or delta configuration and these connections are brought out from the windings to slip rings. The slip rings and associated brushes provide a means for connecting the rotor windings to external resistors which may be used to increase the starting torque and decrease the starting current, or for speed control purposes. These motors are more expensive and the use of brushes makes them less advantageous.

The squirrel cage rotor IM, on the other hand, has a cage winding which is housed in the rotor. This winding consists of bars placed or cast in the rotor slots with their ends short-circuited by means of end rings. The bars and rings are made of copper or brass for high power motors, and aluminium in low and medium powers. This structure enables the casting of the rotor windings in the slots, which makes an inexpensive but reliable motor design. Because of the simple and low cost cage rotor construction techniques, cage rotor IMs have found wide application in industrial motor drive systems. Moreover, brushes are not necessary and therefore the result is a maintenance-free motor.

The stator windings of an IM are distributed around the stator to produce a roughly sinusoidal flux distribution. When three AC voltages shifted 120° between them are applied to the stator windings, a rotating magnetic field is produced. According to equation (2.3) an electromotive force is induced in the rotor bars or windings and current circulates. Then a force actuates on the conductors of the rotor according to (2.2) producing the rotor movement. The rotating magnetic field of the stator drags the rotor around. The rotor does not rotate at the same angular speed of the rotating magnetic field generated in the stator. It falls behind or slips as the field rotates. If the rotor and the magnetic field rotate at the same speed, no variation of magnetic fields occurs in the rotor windings and therefore no voltage is induced and no current circulates. The result is a null force applied on the rotor conductors and consequently the reduction of the rotor speed that produces the slip between the rotating field and the rotor. Due to this feature the IM is also known as asynchronous motor, because the rotating magnetic field and the rotor speeds are not equal or synchronized. The slip depends on the motor load and is defined by the following expression:

$$S = \frac{n_{sync} - n}{n_{sync}} \qquad n = n_{sync}(1 - S) \tag{2.4}$$

Where n is the rotor speed and n_{sync} is the speed of the rotating magnetic field (synchronous speed). The synchronous speed is obtained using the following expression:

$$n_{sync} = \frac{60 \cdot f_{sync}}{P} \tag{2.5}$$

Where f_s is the frequency of the stator voltages and currents and P is the number of pole pairs.

Three operating modes for the IM can be identified as follows according to the value of the slip:

- Motoring: $0 < S < 1$. Active power travels from the grid to the shaft.
- Generating: $S < 0$. Active power travels from the shaft to the grid.
- Braking: $S > 1$. Active power is drawn from the grid and the shaft and the summation of both is converted into motor losses, mainly in the rotor.

Another important characteristic of the three-phase IM is that at zero speed the torque produced is not null, therefore it is a self-starting motor. In general with the exception of

special motors, the standard speed-torque characteristic of the three-phase IM is as shown in Fig. 2-3.

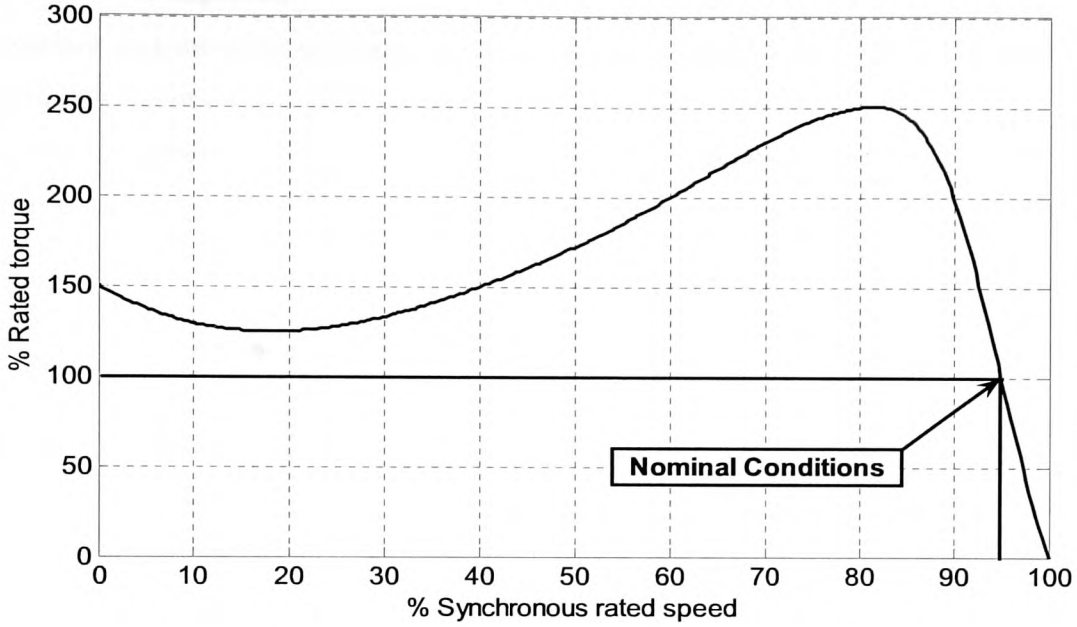

Fig. 2-3 Standard speed-torque curve of the three-phase IM

2.2 Mathematical model of the IM

The design of control strategies for variable speed drives requires the knowledge of the motor dynamic model. A precise model is particularly necessary for advanced control strategies such as vector control. However, the mathematical model of the motor is just an approximation of the real plant. In this section the equations that describe the dynamic behaviour of the IM are presented and a mathematical model is obtained. In this model some mathematical transformations are employed in order to simplify the analysis of the IM. These transformations are the following:

- The space vector theory [1] is used to reduce the set of twelve voltage and flux-current equations to four in the space vector form.
- The transformation of stator and rotor quantities, expressed with the space vector notation, to a common reference frame makes it possible to eliminate dependence of the mutual inductance on the relative position between the rotor and the stator. Different reference frames can be used to express the IM model.

For simplicity, the IM considered will have the following assumptions:

- Symmetrical two-pole three-phase windings.
- The slotting effects are neglected.

- The permeability of the iron parts is infinite.
- The flux density is radial in the air gap.
- Iron losses are neglected.
- The stator and the rotor windings are simplified as a single, multi-turn full pitch coil situated on the two sides of the air gap.
- The coil resistances and inductances are taken to be constant.

The cross section of this idealised IM with concentrated windings can be represented as in Fig. 2-4. It corresponds to a single pole pair motor, where the stator is represented by three concentrated coils shifted 120° one from the other. The rotor is represented by three concentrated coils in a similar way.

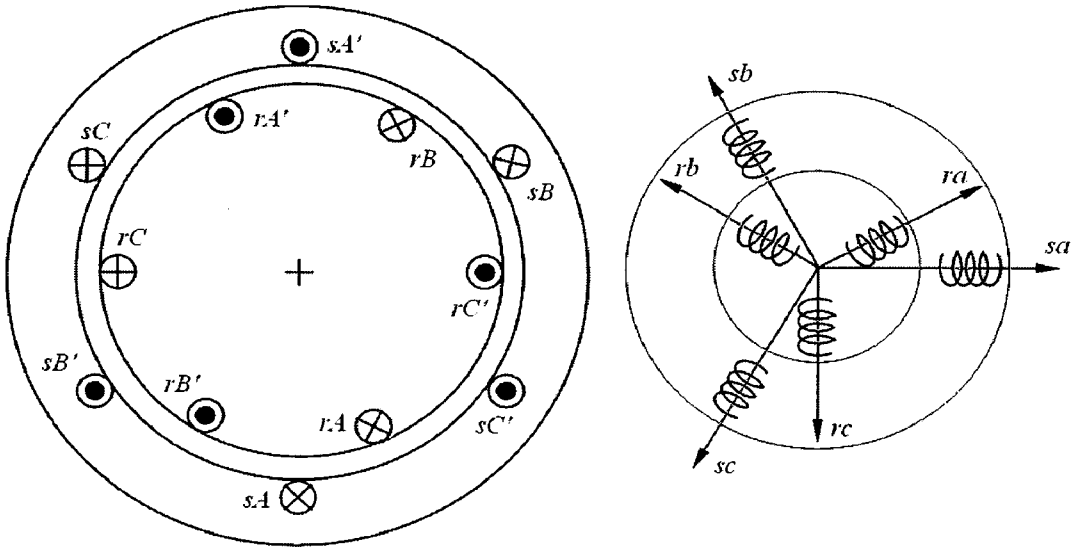

Fig. 2-4 Cross section of the three-phase IM and natural coordinates (*abc*) representation

2.2.1 Instantaneous equations of the IM model

The instantaneous stator phase voltages are given by the following expressions formulated from the stationary reference frame, which is fixed to the stator:

$$u_{sa} = R_s i_{sa} + \frac{d\psi_{sa}}{dt} \tag{2.6}$$

$$u_{sb} = R_s i_{sb} + \frac{d\psi_{sb}}{dt} \tag{2.7}$$

$$u_{sc} = R_s i_{sc} + \frac{d\psi_{sc}}{dt} \tag{2.8}$$

In a similar way the instantaneous rotor phase voltages in a reference frame fixed to the rotor can be expressed as:

$$u_{ra} = R_r i_{ra} + \frac{d\psi_{ra}}{dt} \tag{2.9}$$

$$u_{rb} = R_r i_{rb} + \frac{d\psi_{rb}}{dt} \tag{2.10}$$

$$u_{rc} = R_r i_{rc} + \frac{d\psi_{rc}}{dt} \tag{2.11}$$

The instantaneous stator flux linkages for each phase, in the stator reference frame, are expressed as:

$$\psi_{sa} = L_{sph} i_{sa} + M_s (i_{sb} + i_{sc}) + M_{sr} (\cos\theta_m i_{ra} + \cos(\theta_m + 2\pi/3) i_{rb} + \cos(\theta_m + 4\pi/3) i_{rc}) \tag{2.12}$$

$$\psi_{sb} = L_{sph} i_{sb} + M_s (i_{sa} + i_{sc}) + M_{sr} (\cos(\theta_m + 4\pi/3) i_{ra} + \cos\theta_m i_{rb} + \cos(\theta_m + 2\pi/3) i_{rc}) \tag{2.13}$$

$$\psi_{sc} = L_{sph} i_{sc} + M_s (i_{sa} + i_{sb}) + M_{sr} (\cos(\theta_m + 2\pi/3) i_{ra} + \cos(\theta_m + 4\pi/3) i_{rb} + \cos\theta_m i_{rc}) \tag{2.14}$$

It should be noted that in these equations it is considered that the motor only has one pair of poles. Otherwise the mechanical angle, θ_m, must appear multiplied by the number of pole pairs P.

In a similar way the instantaneous rotor flux linkages for each phase, in the rotor reference frame, are given by:

$$\psi_{ra} = M_{sr} (\cos(-\theta_m) i_{sa} + \cos(-\theta_m + 2\pi/3) i_{sb} + \cos(-\theta_m + 4\pi/3) i_{sc}) + L_{rph} i_{ra} + M_r (i_{rb} + i_{rc}) \tag{2.15}$$

$$\psi_{rb} = M_{sr} (\cos(-\theta_m + 4\pi/3) i_{sa} + \cos(-\theta_m) i_{sb} + \cos(-\theta_m + 2\pi/3) i_{sc}) + L_{rph} i_{rb} + M_r (i_{ra} + i_{rc}) \tag{2.16}$$

$$\psi_{rc} = M_{sr} (\cos(-\theta_m + 2\pi/3) i_{sa} + \cos(-\theta_m + 4\pi/3) i_{sb} + \cos(-\theta_m) i_{sc}) + L_{rph} i_{rc} + M_r (i_{ra} + i_{rb}) \tag{2.17}$$

From the previous equations a compact expression can be obtained using matrix notation as follows:

$$\begin{bmatrix} u_{sa} \\ u_{sb} \\ u_{sc} \\ u_{ra} \\ u_{rb} \\ u_{rc} \end{bmatrix} = \begin{bmatrix} R_s+sL_{sph} & sM_s & sM_s & sM_{sr}\cos\theta_m & sM_{sr}\cos\theta_{m1} & sM_{sr}\cos\theta_{m2} \\ sM_s & R_s+sL_{sph} & sM_s & sM_{sr}\cos\theta_{m2} & sM_{sr}\cos\theta_m & sM_{sr}\cos\theta_{m1} \\ sM_s & sM_s & R_s+sL_{sph} & sM_{sr}\cos\theta_{m1} & sM_{sr}\cos\theta_{m2} & sM_{sr}\cos\theta_m \\ sM_{sr}\cos\theta_m & sM_{sr}\cos\theta_{m1} & sM_{sr}\cos\theta_{m2} & R_r+sL_{rph} & sM_r & sM_r \\ sM_{sr}\cos\theta_{m2} & sM_{sr}\cos\theta_m & sM_{sr}\cos\theta_{m1} & sM_r & R_r+sL_{rph} & sM_r \\ sM_{sr}\cos\theta_{m1} & sM_{sr}\cos\theta_{m2} & sM_{sr}\cos\theta_m & sM_r & sM_r & R_r+sL_{rph} \end{bmatrix} \times \begin{bmatrix} i_{sa} \\ i_{sb} \\ i_{sc} \\ i_{ra} \\ i_{rb} \\ i_{rc} \end{bmatrix} \tag{2.18}$$

Where s is the derivative operator, $\theta_{m1}=\theta_m+2\pi/3$ and $\theta_{m2}=\theta_m+4\pi/3$. It should be noted that the mutual inductances depend on the rotor position and therefore the use of the model obtained in natural coordinates presents some difficulties. In order to simplify the model, space vector notation can be applied to reduce the number of equations and refer all quantities to a common reference frame.

2.2.2 Space vector notation

Space vector notation allows the transformation of the natural instantaneous values of a three-phase system into a vector located in a complex plane. In this plane, the space vector rotates with an angular frequency equal to the angular frequency of the three-phase supply system. The rotating magnetic field of the IM can be represented, for instance, by a space vector rotating with the same angular frequency in a complex plane located in the cross section of the motor.

In order to transform the IM model, in natural coordinates, into its equivalent space vector form, the following operator is introduced:

$$a = e^{j2\pi/3} \quad a^2 = e^{j4\pi/3} \tag{2.19}$$

A generic voltage space vector can be obtained by using the operator above and adding the instantaneous voltage values of the three-phase system.

$$\vec{u} = c\left[u_a(t) + a\,u_b(t) + a^2 u_c(t)\right] \tag{2.20}$$

The constant c can take the value of 2/3 to make the amplitude of the space vector equal to the amplitude of one of the phases. Alternatively it can take the value $(2/3)^{1/2}$ for a power invariant transformation.

Space vectors can be expressed in a rectangular coordinate system as shown in Fig. 2-5.

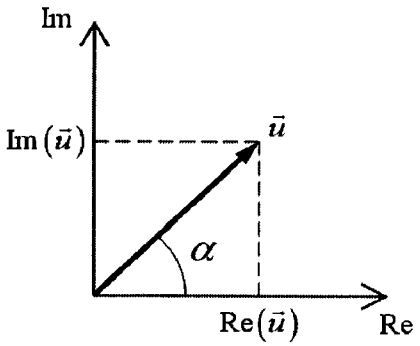

Fig. 2-5 Space vector in a rectangular coordinate system

In this way, the space vector can be expressed using complex notation:

$$\vec{u} = \mathrm{Re}(\vec{u}) + j\,\mathrm{Im}(\vec{u}) \tag{2.21}$$

Alternatively polar and Euler notation can also be used:

$$\vec{u} = |\vec{u}|\angle\alpha \qquad \vec{u} = |\vec{u}|e^{j\alpha} \tag{2.22}$$

The rectangular coordinate system can be stationary. The resulting coordinate system is commonly referred to as α-β coordinates and is defined as shown in Fig. 2-6. The instantaneous values of the three-phase system in natural coordinates can be converted to the equivalent α-β coordinates by means of the Clarke transformation.

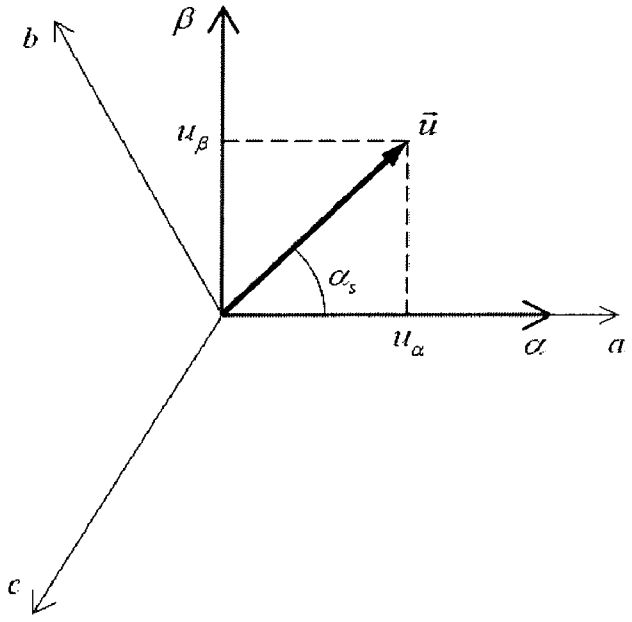

Fig. 2-6 Natural coordinates and α-β coordinates

The Clarke transformation is expressed as follows:

$$\begin{bmatrix} u_\alpha \\ u_\beta \\ u_0 \end{bmatrix} = c \begin{bmatrix} 1 & -1/2 & -1/2 \\ 0 & \sqrt{3}/2 & -\sqrt{3}/2 \\ 1/\sqrt{2} & 1/\sqrt{2} & 1/\sqrt{2} \end{bmatrix} \begin{bmatrix} u_a \\ u_b \\ u_c \end{bmatrix} \tag{2.23}$$

and the inverse Clarke transformation is defined as:

$$\begin{bmatrix} u_a \\ u_b \\ u_c \end{bmatrix} = c \begin{bmatrix} 1 & 0 & 1/\sqrt{2} \\ -1/2 & \sqrt{3}/2 & 1/\sqrt{2} \\ -1/2 & -\sqrt{3}/2 & 1/\sqrt{2} \end{bmatrix} \begin{bmatrix} u_\alpha \\ u_\beta \\ u_0 \end{bmatrix} \tag{2.24}$$

The value of c is taken according to Table 2-I.

Table 2-I Possible values of the Clarke transformation constant

Power invariant		$\lvert\vec{u}\rvert = u_{a\max}$	
a-b-c to *α-β-0*	*α-β-0* to *a-b-c*	*a-b-c* to *α-β-0*	*α-β-0* to *a-b-c*
$c = \sqrt{2/3}$	$c = \sqrt{2/3}$	$c = 2/3$	$c = 1$

The variable u_0 is the homopolar component, which is zero for a balanced three-phase system, where the sum of the phase quantities u_a, u_b and u_c is zero. This is the case of the IM as a three-phase balanced load, where the homopolar components of the phase voltages and currents are zero. The Clarke transformation can be simplified in this case to the two components α and β.

Instead of the stationary α-β coordinate system various rotating coordinate systems can be used according to the reference frame adopted. The coordinate system can be fixed to the rotor, the rotor flux vector or the stator flux vector for instance. Some coordinate systems and the nomenclature used are introduced in Fig. 2-7.

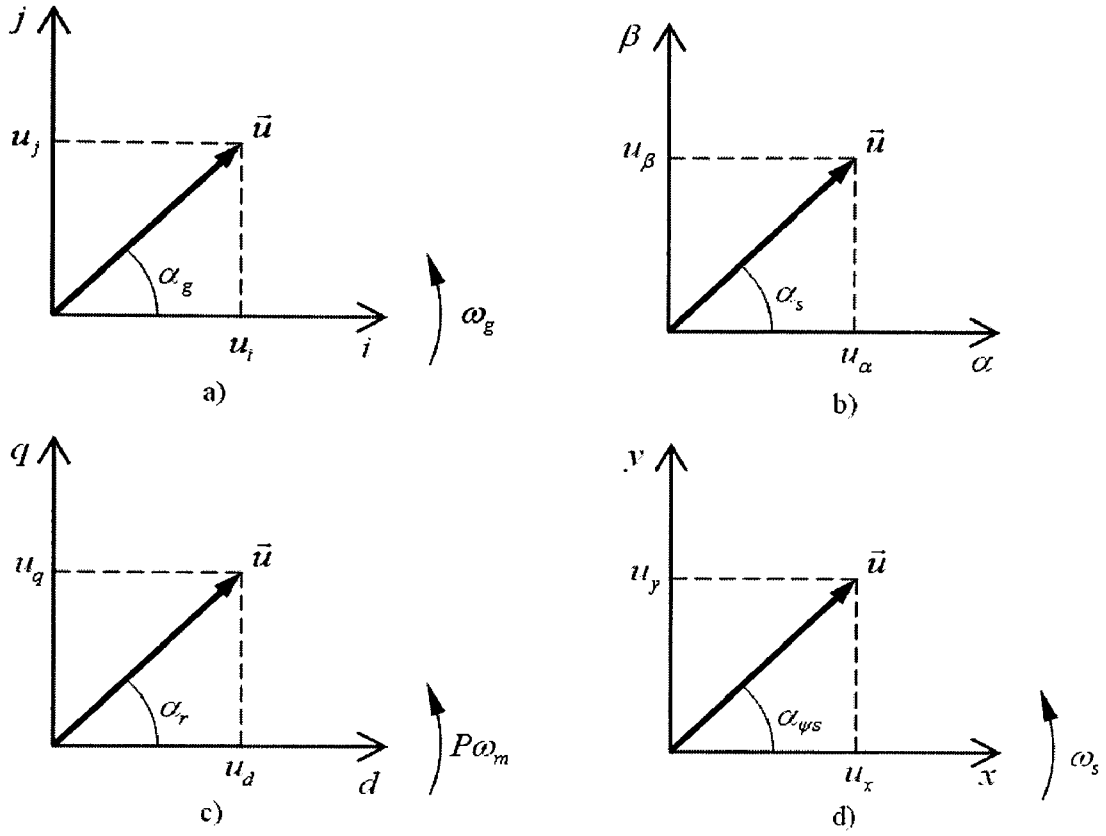

Fig. 2-7 Various coordinate systems: a) *i-j* generic rotating coordinate system, b) α-β coordinates fixed to the stator, c) *d-q* coordinates fixed to the rotor and d) *x-y* coordinates fixed to the stator flux vector.

A space vector expressed in a certain coordinate system can be transformed into a different coordinate system by means of a rotation. The angle of the rotation is equal to the angle between coordinate systems. The nomenclature for these rotations can be found in Fig. 2-8. It should be noted that the angle between the stator-fixed and the rotor-fixed is $P\theta_m$ to extend the model to motors with more than one pair of poles.

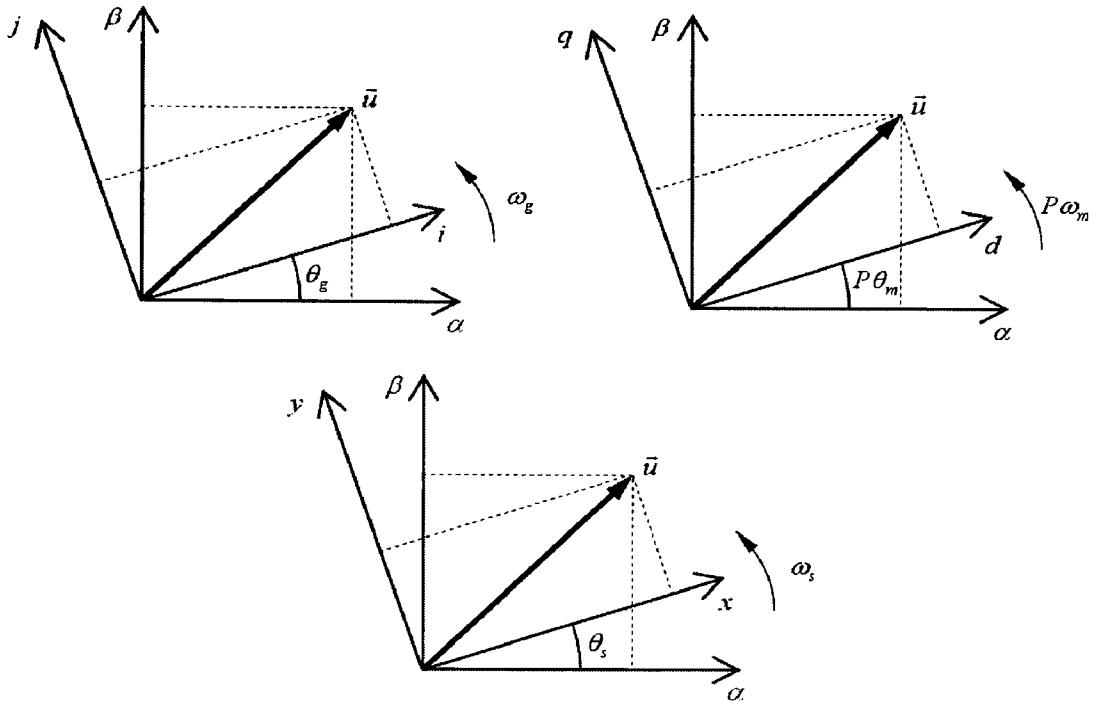

Fig. 2-8 Relationship between different coordinate systems and the coordinate system fixed to the stator

One particular case, which is commonly used, is the transformation of a space vector between the stator-fixed coordinates (α-β) and some other rotating coordinate system. For illustration, the transformation α-β to i-j is shown below:

$$\begin{bmatrix} u_i \\ u_j \\ u_0 \end{bmatrix} = \begin{bmatrix} \cos\theta_g & \sin\theta_g & 0 \\ -\sin\theta_g & \cos\theta_g & 0 \\ 0 & 0 & 1 \end{bmatrix} \begin{bmatrix} u_\alpha \\ u_\beta \\ u_0 \end{bmatrix} \tag{2.25}$$

and the inverse transformation i-j to α-β is as follows:

$$\begin{bmatrix} u_\alpha \\ u_\beta \\ u_0 \end{bmatrix} = \begin{bmatrix} \cos\theta_g & -\sin\theta_g & 0 \\ \sin\theta_g & \cos\theta_g & 0 \\ 0 & 0 & 1 \end{bmatrix} \begin{bmatrix} u_i \\ u_j \\ u_0 \end{bmatrix} \tag{2.26}$$

The Park transformation can be obtained by combining the Clarke transformation and the rotation of the stationary coordinate system to the rotating coordinate system. It can be defined as follows:

$$\begin{bmatrix} u_i \\ u_j \\ u_0 \end{bmatrix} = c \begin{bmatrix} \cos\theta_g & \cos(\theta_g - 2\pi/3) & \cos(\theta_g + 2\pi/3) \\ -\sin\theta_g & -\sin(\theta_g - 2\pi/3) & -\sin(\theta_g + 2\pi/3) \\ 1/\sqrt{2} & 1/\sqrt{2} & 1/\sqrt{2} \end{bmatrix} \begin{bmatrix} u_a \\ u_b \\ u_c \end{bmatrix} \tag{2.27}$$

The inverse Park transformation is then defined as follows:

$$\begin{bmatrix} u_a \\ u_b \\ u_c \end{bmatrix} = c \begin{bmatrix} \cos\theta_g & -\sin\theta_g & 1/\sqrt{2} \\ \cos(\theta_g - 2\pi/3) & -\sin(\theta_g - 2\pi/3) & 1/\sqrt{2} \\ \cos(\theta_g + 2\pi/3) & -\sin(\theta_g + 2\pi/3) & 1/\sqrt{2} \end{bmatrix} \begin{bmatrix} u_i \\ u_j \\ u_0 \end{bmatrix} \tag{2.28}$$

2.2.3 Voltage space vector

The stator voltage space vector can be expressed in the stator reference frame and α-β coordinates as follows:

$$\vec{u}_s = \tfrac{2}{3}\left[u_{sa} + a u_{sb} + a^2 u_{sc}\right] = |\vec{u}_s| e^{j\alpha_s} = u_{s\alpha} + j u_{s\beta} = \tfrac{2}{3}\left(u_{sa} - \tfrac{1}{2}u_{sb} - \tfrac{1}{2}u_{sc}\right) + j\tfrac{1}{\sqrt{3}}\left(u_{sb} - u_{sc}\right) \tag{2.29}$$

Similarly the rotor voltage space vector in the rotor reference frame and d-q coordinates is defined as:

$$\vec{u}_r = \tfrac{2}{3}\left[u_{ra} + a u_{rb} + a^2 u_{rc}\right] = |\vec{u}_r| e^{j\alpha_r} = u_{rd} + j u_{rq} = \tfrac{2}{3}\left(u_{ra} - \tfrac{1}{2}u_{rb} - \tfrac{1}{2}u_{rc}\right) + j\tfrac{1}{\sqrt{3}}\left(u_{rb} - u_{rc}\right) \tag{2.30}$$

The relationship between the space vectors and the instantaneous phase values can be obtained as follows:

$$u_{sa} = \mathrm{Re}(\vec{u}_s) \qquad u_{sb} = \mathrm{Re}(a^2\vec{u}_s) \qquad u_{sc} = \mathrm{Re}(a\vec{u}_s) \tag{2.31}$$

$$u_{ra} = \mathrm{Re}(\vec{u}_r) \qquad u_{rb} = \mathrm{Re}(a^2\vec{u}_r) \qquad u_{rc} = \mathrm{Re}(a\vec{u}_r) \tag{2.32}$$

The expressions above are equivalent to the inverse Clarke transformation.

In the particular case of a squirrel cage rotor IM the voltages applied to the rotor are zero because the rotor bars are short-circuited by the ending rings.

2.2.4 Current space vector

The current space vectors are obtained in the same way. The stator current space vector in the stator reference frame and α-β coordinates is as follows:

$$\vec{i}_s = \tfrac{2}{3}\left[i_{sa} + a i_{sb} + a^2 i_{sc}\right] = \left|\vec{i}_s\right| e^{j\alpha_s} = i_{s\alpha} + j i_{s\beta} = \tfrac{2}{3}\left(i_{sa} - \tfrac{1}{2} i_{sb} - \tfrac{1}{2} i_{sc}\right) + j\tfrac{1}{\sqrt{3}}\left(i_{sb} - i_{sc}\right) \quad (2.33)$$

and the relationship with the instantaneous phase values is given by:

$$i_{sa} = \mathrm{Re}\left(\vec{i}_s\right) \qquad i_{sb} = \mathrm{Re}\left(a^2 \vec{i}_s\right) \qquad i_{sc} = \mathrm{Re}\left(a \vec{i}_s\right) \quad (2.34)$$

The rotor current space vector in the rotor reference frame and *d-q* coordinates is as follows:

$$\vec{i}_r = \tfrac{2}{3}\left[i_{ra} + a i_{rb} + a^2 i_{rc}\right] = \left|\vec{i}_r\right| e^{j\alpha_r} = i_{rd} + j i_{rq} = \tfrac{2}{3}\left(i_{ra} - \tfrac{1}{2} i_{rb} - \tfrac{1}{2} i_{rc}\right) + j\tfrac{1}{\sqrt{3}}\left(i_{rb} - i_{rc}\right) \quad (2.35)$$

and the relationship with the instantaneous phase values is given by:

$$i_{ra} = \mathrm{Re}\left(\vec{i}_r\right) \qquad i_{rb} = \mathrm{Re}\left(a^2 \vec{i}_r\right) \qquad i_{rc} = \mathrm{Re}\left(a \vec{i}_r\right) \quad (2.36)$$

The rotor current space vector can also be expressed in the stator reference frame and α-β coordinates as follows:

$$\vec{i}_r' = \left|\vec{i}_r\right| e^{j\alpha_s} = \left|\vec{i}_r\right| e^{j(\alpha_r + P\theta_m)} = \vec{i}_r e^{jP\theta_m} = i_{r\alpha} + j i_{r\beta} \quad (2.37)$$

Similarly the stator current space vector in the rotor reference frame and *d-q* coordinates is expressed as follows:

$$\vec{i}_s' = \left|\vec{i}_s\right| e^{j\alpha_r} = \left|\vec{i}_s\right| e^{j(\alpha_s - P\theta_m)} = \vec{i}_s e^{-jP\theta_m} = i_{sd} + j i_{sq} \quad (2.38)$$

The magnetising current in the stator reference frame can be defined as:

$$\vec{i}_m = \vec{i}_s + \left(N_r/N_s\right)\vec{i}_r' \quad (2.39)$$

2.2.5 Stator flux linkage space vector

The stator flux linkage space vector in the stator reference frame and α-β coordinates can be expressed as:

$$\vec{\psi}_s = \tfrac{2}{3}\left[\psi_{sa} + a\psi_{sb} + a^2\psi_{sc}\right] = \left|\vec{\psi}_s\right| e^{j\alpha_s} = \psi_{s\alpha} + j\psi_{s\beta} \quad (2.40)$$

If equations (2.12), (2.13) and (2.14) are substituted in (2.40), the following expression is derived:

$$\vec{\psi}_s = \tfrac{2}{3}\begin{bmatrix} i_{sa}\left(L_{sph} + aM_s + a^2M_s\right) + i_{sb}\left(M_s + aL_{sph} + a^2M_s\right) + i_{sc}\left(M_s + aM_s + a^2L_{sph}\right) + \\ +i_{ra}\left(M_{sr}\cos\left(P\theta_m\right) + aM_{sr}\cos\left(P\theta_m + 4\pi/3\right) + a^2M_{sr}\cos\left(P\theta_m + 2\pi/3\right)\right) + \\ +i_{rb}\left(M_{sr}\cos\left(P\theta_m + 2\pi/3\right) + aM_{sr}\cos\left(P\theta_m\right) + a^2M_{sr}\cos\left(P\theta_m + 4\pi/3\right)\right) + \\ +i_{rc}\left(M_{sr}\cos\left(P\theta_m + 4\pi/3\right) + aM_{sr}\cos\left(P\theta_m + 2\pi/3\right) + a^2M_{sr}\cos\left(P\theta_m\right)\right) \end{bmatrix} \tag{2.41}$$

If the previous expression is developed it gives:

$$\vec{\psi}_s = \tfrac{2}{3}\begin{bmatrix} i_{sa}\left(L_{sph} + aM_s + a^2M_s\right) + a\cdot i_{sb}\left(a^2M_s + L_{sph} + aM_s\right) + a^2 i_{sc}\left(aM_s + a^2M_s + L_{sph}\right) + \\ +i_{ra}\left(M_{sr}\cos\left(P\theta_m\right) + aM_{sr}\cos\left(P\theta_m + 4\pi/3\right) + a^2M_{sr}\cos\left(P\theta_m + 2\pi/3\right)\right) + \\ +a\cdot i_{rb}\left(a^2M_{sr}\cos\left(P\theta_m + 2\pi/3\right) + M_{sr}\cos\left(P\theta_m\right) + aM_{sr}\cos\left(P\theta_m + 4\pi/3\right)\right) + \\ +a^2\cdot i_{rc}\left(aM_{sr}\cos\left(P\theta_m + 4\pi/3\right) + a^2M_{sr}\cos\left(P\theta_m + 2\pi/3\right) + M_{sr}\cos\left(P\theta_m\right)\right) \end{bmatrix} \tag{2.42}$$

and finally:

$$\begin{aligned} &\vec{\psi}_s = \left(L_{sph} + aM_s + a^2M_s\right)\vec{i}_s + \\ &+\left(M_{sr}\cos\left(P\theta_m\right) + aM_{sr}\cos\left(P\theta_m + 4\pi/3\right) + a^2M_{sr}\cos\left(P\theta_m + 2\pi/3\right)\right)\vec{i}_r = \\ &= \left(L_{sph} - M_s\right)\vec{i}_s + 1.5M_{sr}\vec{i}_r e^{jP\theta_m} = \left(L_{sph} - M_s\right)\vec{i}_s + 1.5M_{sr}\vec{i}_r' = L_s\vec{i}_s + L_m\vec{i}_r' \end{aligned} \tag{2.43}$$

where:

$$L_s = L_{sph} - M_s \tag{2.44}$$

and

$$L_m = 1.5M_{sr} \tag{2.45}$$

It should be noted how the dependence of the mutual inductance on the rotor position is eliminated due to the use of a common reference frame, which is fixed to the stator in this case. The α-β components of the stator flux vector are obtained as follows:

$$\psi_{s\alpha} = L_s i_{s\alpha} + L_m i_{r\alpha} \tag{2.46}$$

$$\psi_{s\beta} = L_s i_{s\beta} + L_m i_{r\beta} \tag{2.47}$$

and if the rotor reference frame is employed instead it gives:

$$\vec{\psi}_s' = \left|\vec{\psi}_s\right| e^{j\alpha_r} = \left|\vec{\psi}_s\right| e^{j(\alpha_s - P\theta_m)} = \vec{\psi}_s e^{-jP\theta_m} = L_s\vec{i}_s' + L_m\vec{i}_r \tag{2.48}$$

and the *d-q* components are given by:

$$\psi_{sd} = L_s i_{sd} + L_m i_{rd} \tag{2.49}$$

$$\psi_{sq} = L_s i_{sq} + L_m i_{rq} \tag{2.50}$$

2.2.6 Rotor flux linkage space vector

The rotor flux linkage space vector in the rotor reference frame and *d-q* coordinates can be expressed as:

$$\vec{\psi}_r = \tfrac{2}{3}\left[\psi_{ra} + a\psi_{rb} + a^2\psi_{rc}\right] = \left|\vec{\psi}_r\right| e^{j\alpha_r} = \psi_{rd} + j\psi_{rq} \tag{2.51}$$

If the equation above is combined with equations (2.15), (2.16) and (2.17) the following expression is obtained:

$$\vec{\psi}_r = L_r \vec{i}_r + L_m \vec{i}_s' \tag{2.52}$$

where:

$$L_r = L_{rph} - M_r \tag{2.53}$$

and the *d-q* components are given by:

$$\psi_{rd} = L_r i_{rd} + L_m i_{sd} \tag{2.54}$$

$$\psi_{rq} = L_r i_{rq} + L_m i_{sq} \tag{2.55}$$

The transformation to the stator reference frame gives:

$$\vec{\psi}_r' = \left|\vec{\psi}_r\right| e^{j\alpha_s} = \left|\vec{\psi}_r\right| e^{j(\alpha_r + P\theta_m)} = \vec{\psi}_r e^{jP\theta_m} = L_r \vec{i}_r' + L_m \vec{i}_s \tag{2.56}$$

and the α-β components are then given by:

$$\psi_{r\alpha} = L_r i_{r\alpha} + L_m i_{s\alpha} \tag{2.57}$$

$$\psi_{r\beta} = L_r i_{r\beta} + L_m i_{s\beta} \tag{2.58}$$

2.2.7 Space vector form of the motor equations

The motor equations need to be formulated in a common reference frame in order to avoid the dependence of the mutual inductance between the rotor and stator phases on the rotor mechanical angle θ_m.

The equations are initially expressed in a general rotating coordinate system, which rotates at a generic speed ω_g. The space vectors of currents, voltages and flux linkages are defined as follows:

$$\begin{aligned}\vec{i}_{sg} &= \vec{i}_s e^{-j\theta_g} = i_{si} + j i_{sj} \\ \vec{u}_{sg} &= \vec{u}_s e^{-j\theta_g} = u_{si} + j u_{sj} \\ \vec{\psi}_{sg} &= \vec{\psi}_s e^{-j\theta_g} = \psi_{si} + j\psi_{sj}\end{aligned} \tag{2.59}$$

$$\begin{aligned}\vec{i}_{rg} &= \vec{i}_r e^{-j(\theta_g - P\theta_m)} = i_{ri} + j i_{rj} \\ \vec{u}_{rg} &= \vec{u}_r e^{-j(\theta_g - P\theta_m)} = u_{ri} + j u_{rj} \\ \vec{\psi}_{rg} &= \vec{\psi}_r e^{-j(\theta_g - P\theta_m)} = \psi_{ri} + j\psi_{rj}\end{aligned} \tag{2.60}$$

The motor equations in this generic reference frame can be expressed as:

$$\begin{aligned}\vec{u}_{sg} e^{j\theta_g} &= R_s \vec{i}_{sg} e^{j\theta_g} + \frac{d\left(\vec{\psi}_{sg} e^{j\theta_g}\right)}{dt} \\ \vec{u}_{sg} e^{j\theta_g} &= R_s \vec{i}_{sg} e^{j\theta_g} + \frac{d\vec{\psi}_{sg}}{dt} e^{j\theta_g} + \vec{\psi}_{sg} e^{j\theta_g} j\omega_g \\ \vec{u}_{sg} &= R_s \vec{i}_{sg} + \frac{d\vec{\psi}_{sg}}{dt} + j\omega_g \vec{\psi}_{sg}\end{aligned} \tag{2.61}$$

$$\begin{aligned}\vec{u}_{rg} e^{j(\theta_g - P\theta_m)} &= R_r \vec{i}_{rg} e^{j(\theta_g - P\theta_m)} + \frac{d\left(\vec{\psi}_{rg} e^{j(\theta_g - P\theta_m)}\right)}{dt} \\ \vec{u}_{rg} e^{j(\theta_g - P\theta_m)} &= R_r \vec{i}_{rg} e^{j(\theta_g - P\theta_m)} + \frac{d\vec{\psi}_{rg}}{dt} e^{j(\theta_g - P\theta_m)} + \vec{\psi}_{rg} e^{j(\theta_g - P\theta_m)} j\left(\omega_g - P\omega_m\right) \\ \vec{u}_{rg} &= R_r \vec{i}_{rg} + \frac{d\vec{\psi}_{rg}}{dt} + j\left(\omega_g - P\omega_m\right)\vec{\psi}_{rg}\end{aligned} \tag{2.62}$$

where:

$$\vec{\psi}_{sg} = L_s \vec{i}_{sg} + L_m \vec{i}_{rg} \tag{2.63}$$

$$\vec{\psi}_{rg} = L_r \vec{i}_{rg} + L_m \vec{i}_{sg} \tag{2.64}$$

The model can be expressed using matrix form and *i-j* coordinates as follows:

$$\begin{bmatrix} u_{si} \\ u_{sj} \\ u_{ri} \\ u_{rj} \end{bmatrix} = \begin{bmatrix} R_s + sL_s & -\omega_g L_s & sL_m & -\omega_g L_m \\ \omega_g L_s & R_s + sL_s & \omega_g L_m & sL_m \\ sL_m & (P\omega_m - \omega_g)L_m & R_r + sL_r & (P\omega_m - \omega_g)L_r \\ (\omega_g - P\omega_m)L_m & sL_m & (\omega_g - P\omega_m)L_r & R_r + sL_r \end{bmatrix} \times \begin{bmatrix} i_{si} \\ i_{sj} \\ i_{ri} \\ i_{rj} \end{bmatrix} \tag{2.65}$$

If the generic coordinate system is fixed to the stator (ω_g=0), the motor model can be expressed in the stator reference frame and α-β coordinates as follows:

$$\begin{bmatrix} u_{s\alpha} \\ u_{s\beta} \\ u_{r\alpha} \\ u_{r\beta} \end{bmatrix} = \begin{bmatrix} R_s + sL_s & 0 & sL_m & 0 \\ 0 & R_s + sL_s & 0 & sL_m \\ sL_m & P\omega_m L_m & R_r + sL_r & P\omega_m L_r \\ -P\omega_m L_m & sL_m & -P\omega_m L_r & R_r + sL_r \end{bmatrix} \times \begin{bmatrix} i_{s\alpha} \\ i_{s\beta} \\ i_{r\alpha} \\ i_{r\beta} \end{bmatrix} \tag{2.66}$$

$$\vec{u}_s = R_s \vec{i}_s + \frac{d\vec{\psi}_s}{dt} \tag{2.67}$$

$$\vec{u}_r' = R_r \vec{i}_r' + \frac{d\vec{\psi}_r'}{dt} - jP\omega_m \vec{\psi}_r' \tag{2.68}$$

$$\vec{\psi}_s = L_s \vec{i}_s + L_m \vec{i}_r' \tag{2.69}$$

$$\vec{\psi}_r' = L_r \vec{i}_r' + L_m \vec{i}_s \tag{2.70}$$

If the generic coordinate system is fixed to the rotor (ω_g=$P\omega_m$), the motor model can be expressed in rotor reference frame and d-q coordinates as follows:

$$\begin{bmatrix} u_{sd} \\ u_{sq} \\ u_{rd} \\ u_{rq} \end{bmatrix} = \begin{bmatrix} R_s + sL_s & -P\omega_m L_s & sL_m & -P\omega_m L_m \\ P\omega_m L_s & R_s + sL_s & P\omega_m L_m & sL_m \\ sL_m & 0 & R_r + sL_r & 0 \\ 0 & sL_m & 0 & R_r + sL_r \end{bmatrix} \times \begin{bmatrix} i_{sd} \\ i_{sq} \\ i_{rd} \\ i_{rq} \end{bmatrix} \tag{2.71}$$

$$\vec{u}_s' = R_s \vec{i}_s' + \frac{d\vec{\psi}_s'}{dt} + jP\omega_m \vec{\psi}_s' \tag{2.72}$$

$$\vec{u}_r = R_r \vec{i}_r + \frac{d\vec{\psi}_r}{dt} \tag{2.73}$$

$$\vec{\psi}_s' = L_s \vec{i}_s' + L_m \vec{i}_r \tag{2.74}$$

$$\vec{\psi}_r = L_r \vec{i}_r + L_m \vec{i}_s' \tag{2.75}$$

If the generic coordinate system is fixed to the stator flux vector ($\omega_g=\omega_s$), the motor model can be expressed in the stator flux vector reference frame and x-y coordinates as follows:

$$\begin{bmatrix} u_{sx} \\ u_{sy} \\ u_{rx} \\ u_{ry} \end{bmatrix} = \begin{bmatrix} R_s + sL_s & -\omega_s L_s & sL_m & -\omega_s L_m \\ \omega_s L_s & R_s + sL_s & \omega_s L_m & sL_m \\ sL_m & (P\omega_m - \omega_s)L_m & R_r + sL_r & (P\omega_m - \omega_s)L_r \\ (\omega_s - P\omega_m)L_m & sL_m & (\omega_s - P\omega_m)L_r & R_r + sL_r \end{bmatrix} \times \begin{bmatrix} i_{sx} \\ i_{sy} \\ i_{rx} \\ i_{ry} \end{bmatrix} \tag{2.76}$$

$$\vec{u}_{s\psi_s} = R_s \vec{i}_{s\psi_s} + \frac{d\vec{\psi}_{s\psi_s}}{dt} + j\omega_s \vec{\psi}_{s\psi_s} \tag{2.77}$$

$$\vec{u}_{r\psi_s} = R_r \vec{i}_{r\psi_s} + \frac{d\vec{\psi}_{r\psi_s}}{dt} + j(\omega_s - P\omega_m)\vec{\psi}_{r\psi_s} \tag{2.78}$$

$$\vec{\psi}_{s\psi_s} = L_s \vec{i}_{s\psi_s} + L_m \vec{i}_{r\psi_s} \tag{2.79}$$

$$\vec{\psi}_{r\psi_s} = L_r \vec{i}_{r\psi_s} + L_m \vec{i}_{s\psi_s} \tag{2.80}$$

2.2.8 Electromagnetic torque expressions

The production of electromagnetic torque in a DC motor can be described by the following equation:

$$\Gamma_e = k\vec{\psi}_e \times \vec{i}_a \tag{2.81}$$

The instantaneous electromagnetic torque can be expressed as the cross vector product of the excitation flux linkage $\vec{\psi}_e$ and the armature current $\vec{i}_a$, where k is the motor constant. Since the excitation flux and the armature current are perpendicular, equation (2.81) can be written as the product of their moduli:

$$\Gamma_e = k|\vec{\psi}_e||\vec{i}_a| \tag{2.82}$$

If the flux is kept constant the electromagnetic torque can be controlled by varying the armature current.

In IMs the electromagnetic toque can be expressed in a vectorial expression similar to (2.81), that is to say:

$$\Gamma_e \propto \vec{\psi}_s \times \vec{i}_r' \tag{2.83}$$

By means of energy considerations the electromagnetic toque expression of an IM can be derived [2]. The overall instantaneous power of an IM can be expressed as follows:

$$P_T = \frac{3}{2}\mathrm{Re}\left(\vec{u}_s\vec{i}_s^{\,*}\right)+\frac{3}{2}\mathrm{Re}\left(\vec{u}_r'\vec{i}_r'^{\,*}\right) \tag{2.84}$$

If equations (2.67) and (2.68) are substituted in (2.84) this leads to the following expression in the stator reference frame.

$$P_T = \frac{3}{2}\left[\mathrm{Re}\left(R_s\vec{i}_s\vec{i}_s^{\,*}+\frac{d\vec{\psi}_s}{dt}\vec{i}_s^{\,*}\right)+\mathrm{Re}\left(R_r'\vec{i}_r'\vec{i}_r'^{\,*}+\frac{d\vec{\psi}_r'}{dt}\vec{i}_r'^{\,*}-jP\omega_m\vec{\psi}_r'\vec{i}_r'^{\,*}\right)\right] \tag{2.85}$$

$$P_T = \frac{3}{2}\left(R_s\left|\vec{i}_s\right|^2+R_r\left|\vec{i}_r'\right|^2\right)+\frac{3}{2}\mathrm{Re}\left(\frac{d\vec{\psi}_s}{dt}\vec{i}_s^{\,*}+\frac{d\vec{\psi}_r'}{dt}\vec{i}_r'^{\,*}\right)+\frac{3}{2}P\omega_m\,\mathrm{Re}\left(-j\vec{\psi}_r'\vec{i}_r'^{\,*}\right) \tag{2.86}$$

The first term of the above expression represents the copper losses in the stator and rotor windings; the second term represents the power in the magnetic field and the third term represents the shaft output power that is also defined by the following expression:

$$P_{out} = \Gamma_e\omega_m \tag{2.87}$$

From expressions (2.86) and (2.87) the following electromagnetic torque expression can be obtained.

$$\Gamma_e = -\frac{3}{2}P\,\mathrm{Re}\left(j\vec{\psi}_r'\vec{i}_r'^{\,*}\right) = -\frac{3}{2}P\,\mathrm{Im}\left(\vec{\psi}_r'^{\,*}\vec{i}_r'\right) = -\frac{3}{2}P\vec{\psi}_r'\times\vec{i}_r' \tag{2.88}$$

Several expressions for the electromagnetic torque can be derived if equation (2.88) is combined with the flux-current equations (2.69) and (2.70); that is to say:

$$\Gamma_e = -\frac{3}{2}PL_m\vec{i}_s\times\vec{i}_r' \tag{2.89}$$

$$\Gamma_e = \frac{3}{2}P\vec{\psi}_s\times\vec{i}_s \tag{2.90}$$

$$\Gamma_e = -\frac{3}{2}P\frac{L_m}{L_s}\vec{\psi}_s\times\vec{i}_r' \tag{2.91}$$

$$\Gamma_e = \frac{3}{2}P\frac{L_m}{L_r}\vec{\psi}_r'\times\vec{i}_s \tag{2.92}$$

$$\Gamma_e = -\frac{3}{2} P \frac{L_m}{L_s L_r - L_m^2} \vec{\psi}_s \times \vec{\psi}_r' \tag{2.93}$$

Once the torque expression is obtained, the motion equation can be derived from the following expression:

$$J \frac{d\omega_m}{dt} = \sum \Gamma \tag{2.94}$$

From this expression and considering the load torque and friction terms the motion equation can be written as:

$$J \frac{d\omega_m}{dt} = \Gamma_e - \Gamma_L - D\omega_m \tag{2.95}$$

2.3 Simulation model

From the expressions obtained in the previous sections a simulation model of the IM can be created. The stator reference frame (α-β coordinates) is chosen to implement the model and the software Matlab/Simulink from Mathworks is employed.

The equations of the IM model have been rearranged in order to use the integral operator $1/s$ instead of using the derivative operator s. The set of equations obtained is as follows:

$$u_{s\alpha} = \frac{2}{3}\left(u_{sa} - \frac{1}{2} u_{sb} - \frac{1}{2} u_{sc} \right) \tag{2.96}$$

$$u_{s\beta} = \frac{1}{\sqrt{3}} \left(u_{sb} - u_{sc} \right) \tag{2.97}$$

$$\psi_{s\alpha} = \frac{1}{s} \left(u_{s\alpha} - R_s i_{s\alpha} \right) \tag{2.98}$$

$$\psi_{s\beta} = \frac{1}{s} \left(u_{s\beta} - R_s i_{s\beta} \right) \tag{2.99}$$

$$\psi_{r\alpha} = \frac{1}{s} \left(u_{r\alpha} - R_r i_{r\alpha} - P\omega_m \psi_{r\beta} \right) = \frac{1}{s} \left(-R_r i_{r\alpha} - P\omega_m \psi_{r\beta} \right) \tag{2.100}$$

$$\psi_{r\beta} = \frac{1}{s} \left(u_{r\beta} - R_r i_{r\beta} + P\omega_m \psi_{r\alpha} \right) = \frac{1}{s} \left(-R_r i_{r\beta} + P\omega_m \psi_{r\alpha} \right) \tag{2.101}$$

$$i_{s\alpha} = \psi_{s\alpha} \frac{L_r}{L_x} - \psi_{r\alpha} \frac{L_m}{L_x} \tag{2.102}$$

$$i_{s\beta} = \psi_{s\beta}\frac{L_r}{L_x} - \psi_{r\beta}\frac{L_m}{L_x} \tag{2.103}$$

$$i_{r\alpha} = \psi_{r\alpha}\frac{L_s}{L_x} - \psi_{s\alpha}\frac{L_m}{L_x} \tag{2.104}$$

$$i_{r\beta} = \psi_{r\beta}\frac{L_s}{L_x} - \psi_{s\beta}\frac{L_m}{L_x} \tag{2.105}$$

where

$$L_x = L_s L_r - L_m^2 \tag{2.106}$$

The motion equation is expressed as follows:

$$\omega_m = \frac{\Gamma_e - \Gamma_L}{Js + D} \tag{2.107}$$

where according to equation (2.90):

$$\Gamma_e = \frac{3}{2}P\left(\psi_{s\alpha} i_{s\beta} - \psi_{s\beta} i_{s\alpha}\right) \tag{2.108}$$

The final motion equation is given by:

$$\omega_m = \frac{\frac{3}{2}P\left(\psi_{s\alpha} i_{s\beta} - \psi_{s\beta} i_{s\alpha}\right) - \Gamma_L}{Js + D} \tag{2.109}$$

The IM model is implemented in Simulink employing and the "Embedded MATLAB function" block as shown in Fig. 2-9. The notation 1-2-3 has been used instead of *a*-*b*-c for the motor phase values, because Greek letters are not supported. For the same reason the notation a-b-0 has been used in the model instead of α-β-0.

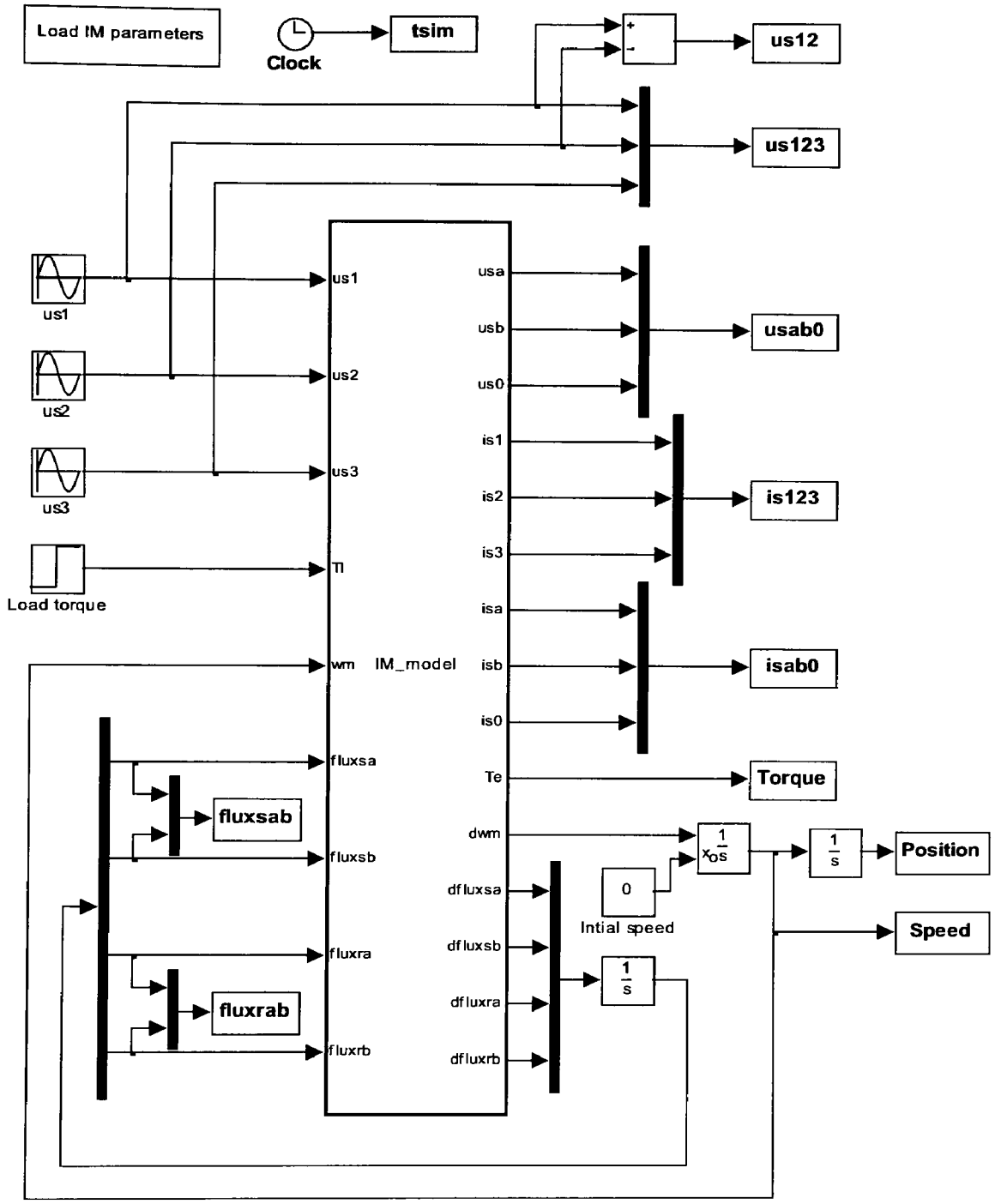

Fig. 2-9 Simulink model of the IM

The script of the embedded function block "IM model" is the following:

```
function [usa,usb,us0,is1,is2,is3,isa,isb,is0,Te,dwm,dfluxsa,dfluxsb,dfluxra,dfluxrb] =
IM_model(us1,us2,us3,Tl,wm,fluxsa,fluxsb,fluxra,fluxrb,Rs,Rr,Ls,Lr,Lm,Lx,P,J,D)
% IM model
% 1-2-3 (a-b-c) to alpha-beta-0 transformation
usa=(2/3)*(us1-(1/2)*us2-(1/2)*us3);
usb=(1/sqrt(3))*(us2-us3);
us0=(2/3)*(1/2*us1+1/2*us2+1/2*us3);
% Electrical equations
isa=fluxsa*Lr/Lx-fluxra*Lm/Lx;
isb=fluxsb*Lr/Lx-fluxrb*Lm/Lx;
ira=fluxra*Ls/Lx-fluxsa*Lm/Lx;
irb=fluxrb*Ls/Lx-fluxsb*Lm/Lx;
dfluxsa=usa-Rs*isa;
dfluxsb=usb-Rs*isb;
dfluxra=-Rr*ira-P*wm*fluxrb;
dfluxrb=-Rr*irb+P*wm*fluxra;
% Mechanical equations
Te=1.5*P*(fluxsa*isb-fluxsb*isa);
dwm=(1/J)*(Te-Tl-D*wm);
% alpha-beta to 1-2-3 (a-b-c) transformation
is1=(isa);
is2=(-1/2*isa+sqrt(3)/2*isb);
is3=(-1/2*isa-sqrt(3)/2*isb);
is0=(2/3)*(1/2*is1+1/2*is2+1/2*is3);
```

The motor parameters employed are taken from the IM used in the laboratory setup and can be found in Table 6-I in Chapter 6. The script employed to load these parameters is the following:

```
% Parameters Motor Siemens 1LA7090-4AA10-Z
% Electrical parameters
% Stator and Rotor resistances [Ohm]
Rs=9.21;
Rr=6.644;
% Inductances [H]
% Stator leakage inductance
Ls1=0.03207;
% Rotor leakage inductance
Lr1=0.00847;
% Magnetizing inductance
Lm=0.44415;
% Other inductances
Ls=Ls1+Lm;
Lr=Lr1+Lm;
Lx=(Ls*Lr)-(Lm^2);
% Number of pole pairs
P=2;
% Mechanical parameters
% Inertia [Kg*m^2]
J=0.00805;
% Damping [N*m*s]
D=0;
```

2.4 IM simulation

Some simulations have been executed with the Simulink model implemented. The following figures present the simulation results for the direct connection to a three-phase AC grid (380 V, 50 Hz) of the IM at t = 0 s. The nominal load torque is connected at t = 1 s.

Fig. 2-10, Fig. 2-11 and Fig. 2-12 show the stator line voltage, the stator phase voltages and the stator currents respectively. It can be observed how the stator currents start to increase when the load torque is connected at t = 1 s, and their delay with respect to the phase voltages decreases.

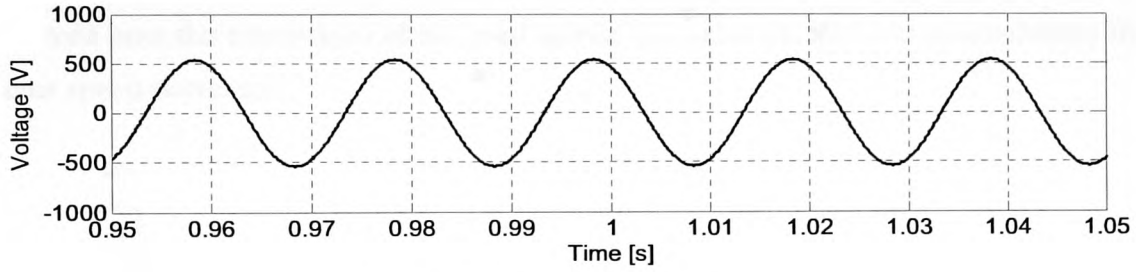

Fig. 2-10 Stator line voltage u_{ab}

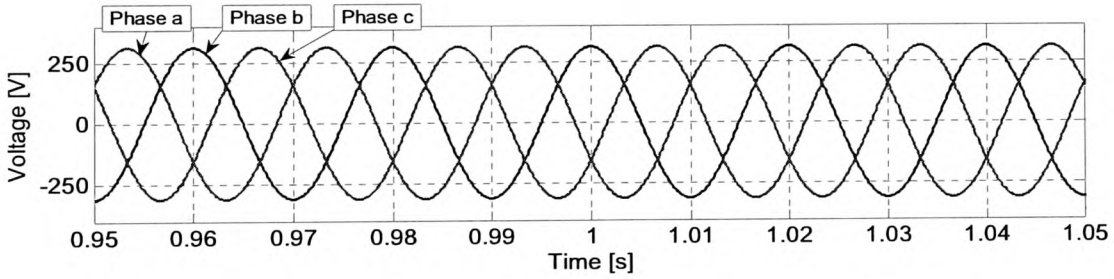

Fig. 2-11 Stator phase voltages

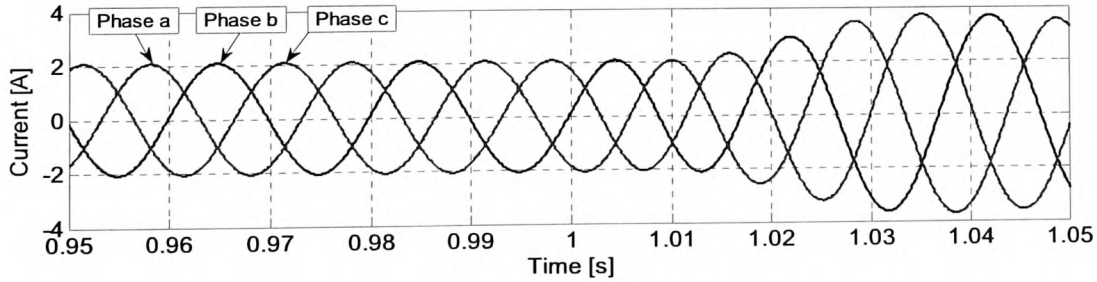

Fig. 2-12 Stator phase currents

Fig. 2-13 shows the power factor calculation. It can be observed how the active power and power factor increase when the load torque is connected.

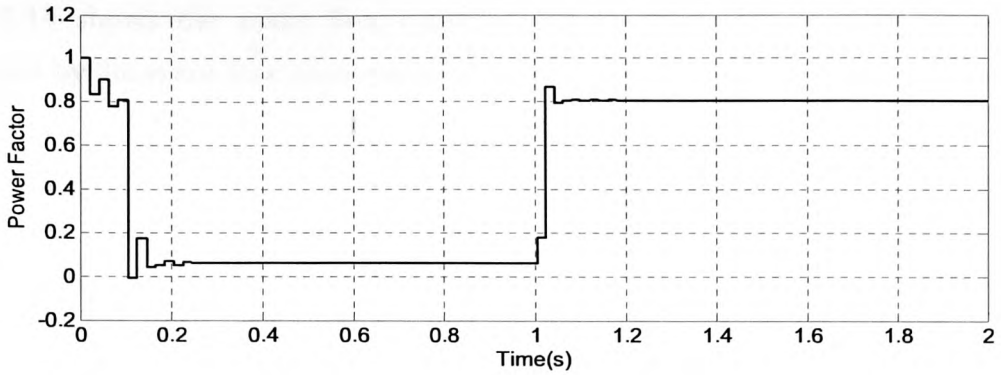

Fig. 2-13 Power Factor

Fig. 2-14 and Fig. 2-15 show the torque and speed responses respectively. It can be observed how the connection of the load torque increases the slip and consequently the motor speed decreases.

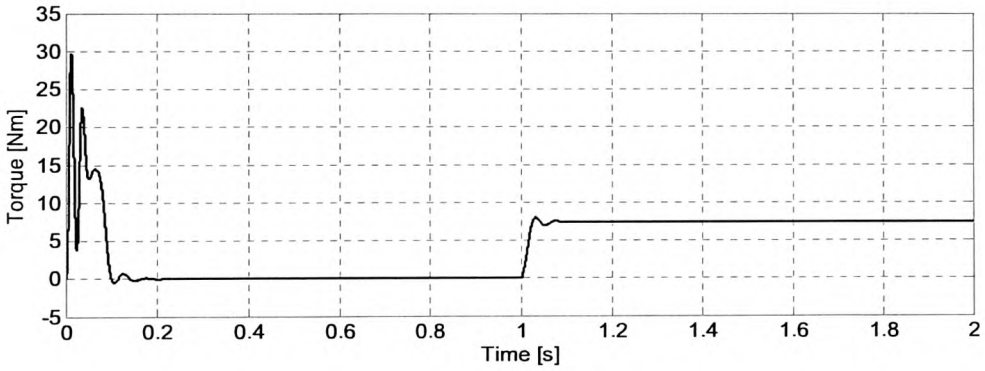

Fig. 2-14 Torque response

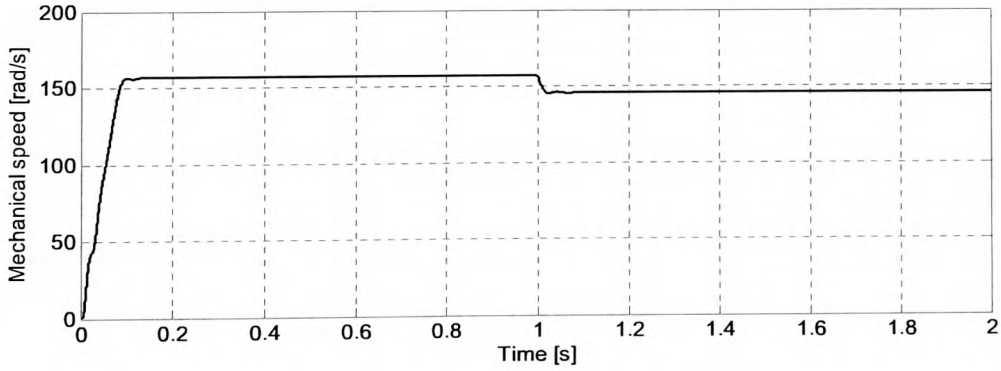

Fig. 2-15 Speed response

Fig. 2-16 shows the stator flux modulus response. In Fig. 2-17 the circular path followed by the stator flux space vector is shown

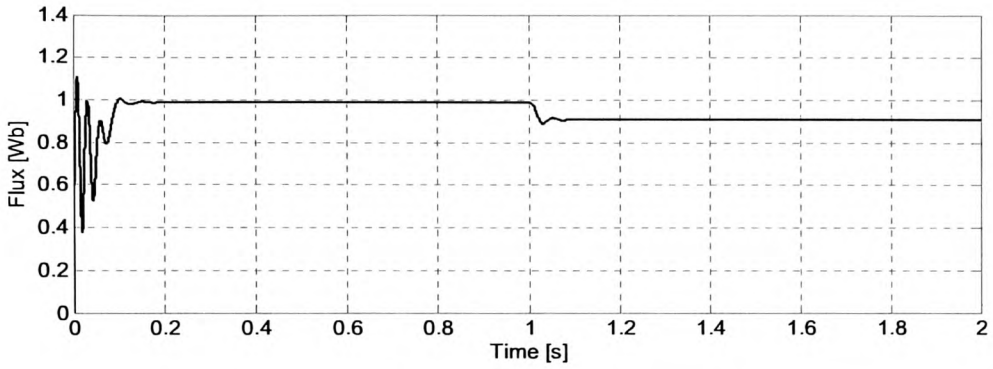

Fig. 2-16 Stator flux modulus response

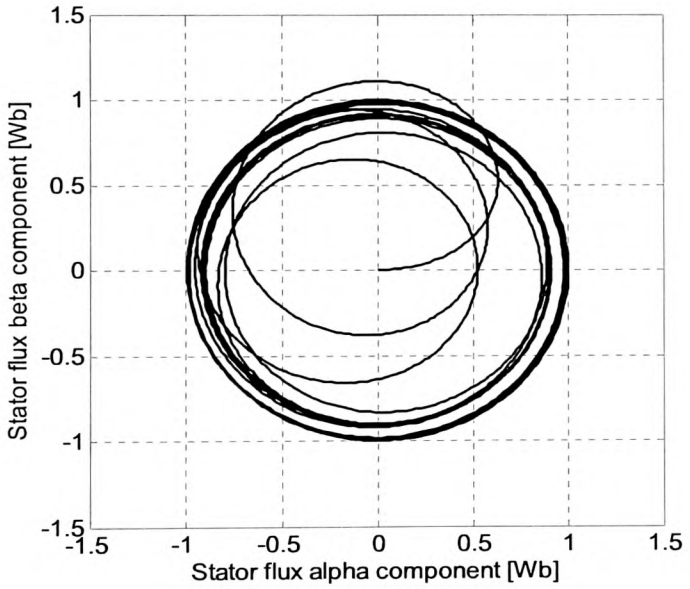

Fig. 2-17 Stator flux space vector path

Finally, Fig. 2-18 presents the speed-torque characteristic of the IM. Additionally a cubic curve fitting has been plotted in the same graph to show more clearly the similarity with the standard characteristic shown in Fig. 2-3. The cubic curve fitting performs a 3rd order polynomial interpolation. It can be observed how the speed-torque characteristic finishes in the nominal conditions reached at the end of the simulation presented.

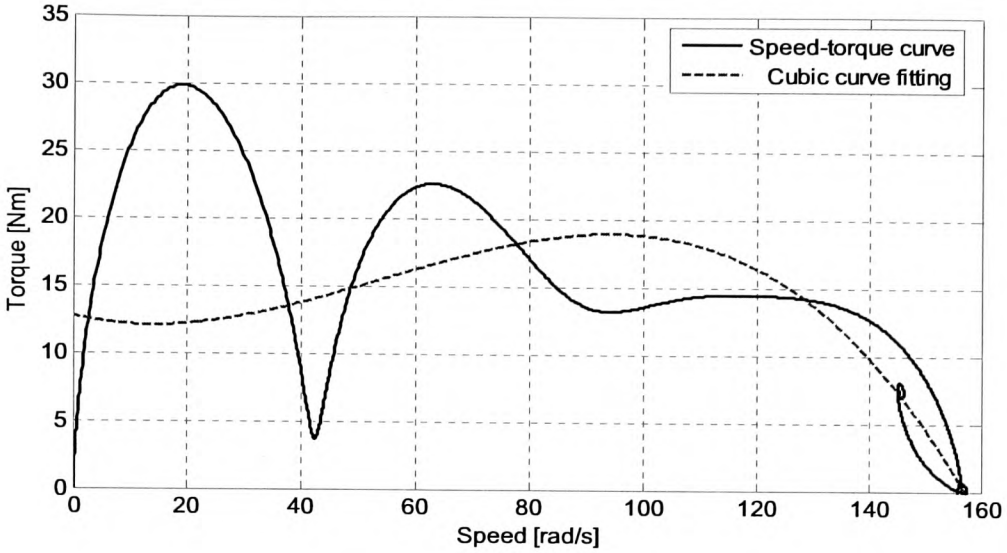

Fig. 2-18 Speed-torque curve during start-up

It can be observed how the simulation results match the nameplate values of the IM motor employed in the laboratory setup (see Table 6-I in Chapter 6).

2.5 Interim conclusions

The IM structure and principle of operation has been explained in this chapter. A mathematical model of the three-phase IM has been derived to study its dynamic behaviour. The employment of the space vector notation and a common reference frame provides a simplification of the model and eliminates the dependency of the mutual inductance on the rotor mechanical angle. The model has been expressed in different coordinate systems.

It can be conclude that a good understanding of the motor model is essential for the design of vector control strategies. A simulation model has been created using the software package Matlab/Simulink (by Mathworks) to develop the research work presented in this thesis. Some simulation results using the parameters of the IM used in the laboratory have been presented to prove the validity of the model.

Chapter 3: Voltage Source Inverters

Summary – *This chapter presents the technology employed for power conversion in variable speed drives for IMs. Most variable speed drives incorporate the two-level VSI, which has become the standard solution due to its low cost and simplicity. This type of converter is described and its technological limitations are discussed. One possible solution to overcome these technological limitations is the use of multilevel topologies, which are emerging to extend the range of application of power electronic systems to higher voltage and power levels. The main types of multilevel converters are described in this chapter and special attention is dedicated to the three-level diode-clamped converter, also known as Neutral Point Clamped (NPC) converter. This type of converter can be considered the most widely employed multilevel topology and some commercial drives incorporating the three-level technology are described. Finally, the three-level VSI is evaluated in comparison with the two-level VSI to illustrate the benefits it can offer.*

3.1 Introduction

Power electronic systems are employed to control the flow of electrical energy employed to supply loads in an optimal way regarding the voltages and currents delivered. The input of a power electronic system is in general coming form the AC power grid, with a line frequency of 50 or 60 Hz that can be single-phase or three-phase. The power electronic system is responsible for converting this input into an output with the desired characteristics regarding: voltage and current level, frequency and number of phases at the output. Moreover the power flow through the system might be reversible, thus interchanging the roles of the input and output.

Power electronics covers different fields of application such as:

- Switch-mode power supplies and Uninterruptible Power Supplies (UPS).
- Energy conservation and efficiency improvement.
- Process control and automation.
- Transportation.
- Power transmission.

Power electronic systems can be classified in terms of their input and output form. The AC power grid is in most cases the input to the power electronic system, while the load is connected to the output. Both input and output might be single-phase or multiple-phase, being the three-phase type the most common case. Depending on the application the output might have the following forms:

- DC with constant or adjustable magnitude.
- AC with constant or adjustable frequency and magnitude.

Power electronic systems usually consist of more than one power conversion stage. The various stages are decoupled by means of energy storage elements such as capacitors and inductors. Instantaneous power does not have to be equal at the input and output of the system. Converter is the name used to refer to each power conversion stage [19]. Therefore a converter is a basic module of a power electronic system. Based on the form of the electric power at both sides of the converter the following classification can be obtained:

- AC-DC converters.
- DC-AC converters.
- DC-DC converters.
- AC-AC converters.

More specifically, the word rectifier refers to the AC-DC converter where the average power flows from the AC to the DC side. In a similar way, inverter refers to the DC-AC converter where the average power flows from the DC side to the AC side. When the power is reversible in the converter the terms rectifier and inverter refer to the mode of operation.

An alternative to these multi-stage systems with energy storage elements that has attracted interest from researchers in the past years is the matrix converter. This type of converter contains a matrix of bidirectional semiconductor switches that allow the connection of any of the converter inputs to any of the outputs [20].

In general power electronic systems include power semiconductor devices controlled by electronic circuits, passive components for soft commutation (snubber circuits) and energy storage elements. Power semiconductor devices can be classified according to their level of controllability into three main groups:

- Diodes. The on and off states are controlled by the conditions of the power circuit.
- Thyristors (Silicon Controlled Rectifiers, SCR). They can be turned on by a control signal but must be turned off by the conditions of the power circuit.
- Controllable switches. They can be turned on and off by the control signals.

In the last group of controllable switches several types are included: Bipolar-Junction Transistors (BJT), Metal-Oxide-Semiconductor Field-Effect Transistors (MOSFET), Insulated-Gate Bipolar Transistors (IGBT), Integrated Gate-Commutated Thyristors (IGCT), MOS Controlled Thyristors (MCT), Static Induction Transistors (SIT), Static Induction Thyristors (SITH) and Gate Turn-Off Thyristors (GTO).

At the present time, much attention is devoted to new developments on power switching devices based on wide band gap semiconductors such as Silicon Carbide (SiC), Gallium Nitride (GaN) and diamond. These devices can offer several advantages over silicon devices. These advantages can be summarized as follows: operation at higher temperatures; good thermal conductivity and less cooling required; higher blocking voltages and current density; smaller size; lower losses, EMI and less sensitive to radiation [21].

The type of switch to be used is chosen depending on the application and the voltage and power rating. According to the way the power semiconductor devices are switched an alternative classification for converters can be done into the following types [19]:

- Line frequency converters (naturally commutated) converters. The input voltage facilitates the commutation of the devices, thus the devices switch on and off at the line frequency of 50 or 60Hz.
- Switching (forced-commutated) converters. Controllable switches are turned on and off at frequencies higher than the line frequency.
- Resonant and quasi-resonant converters. The controllable switches turn on and/or off at zero voltage and/or zero current minimising losses and stress on the semiconductor devices and reducing the generation of EMI.

Electrical motor drives are one of the main applications of power converters. Variable-frequency converters are used in IM drives to achieve variable speed. Except in high power applications where cycloconverters are employed (an AC to AC stage), variable speed drives usually utilise an AC to DC stage followed by a DC to AC stage. In general, the AC power grid input is rectified and converted into DC by means of a controlled or uncontrolled rectifier and then it is inverted to generate a number of AC outputs, generally three, with variable frequency and amplitude to feed the IM. A recent alternative to this structure is the matrix converter as it has been explained [20].

Regarding the standard structure and according to the type of rectifier and inverter the following classification can be made:

- Pulse-Width-Modulated Voltage Source Inverter (PWM-VSI) with a diode rectifier.
- Square-wave Voltage Source Inverter (square-wave VSI) with a thyristor rectifier.
- Current Source Inverter (CSI) with a thyristor rectifier.

In the VSI, the DC input appears as a DC voltage source to the inverter; while in the CSI the DC input appears as DC current source.

3.2 The two-level VSI

The standard three-phase two-level VSI is the topology used in most of the applications where three-phase supply is needed. It is possible to obtain three phases because it consists of three single-phase inverters. Fig. 3-1 shows a three-phase two-level VSI.

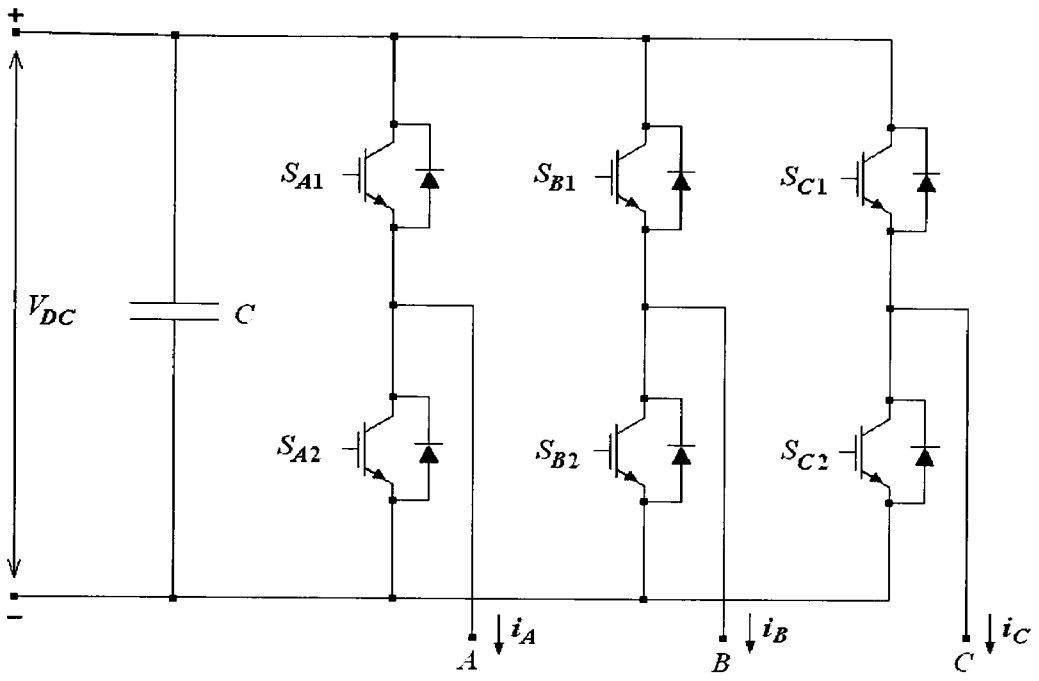

Fig. 3-1 The three-phase two-level VSI

The outputs of the VSI A, B and C can be connected through the semiconductor switches, either to the positive or negative rails of the DC-link. The pair of switches in each leg is controlled with complementary signals, when one of them is on the other one must be off. If both of them are on at the same time a short-circuit occurs. A dead time is used in transitions in order to avoid a possible temporary short-circuit and both switches are forced to the off state before one of them turns on again.

According to the schematic shown in Fig. 3-1, phase A will be connected to the positive of the DC-link when S_{A1} is on (1) and S_{A2} is off (0); and will be connected to the negative of the DC-link when S_{A1} is off (0) and S_{A2} is on (1). The following table illustrates the output voltage in each phase depending on the state of the switches.

Table 3-I Possible states of the two-level VSI

Leg *A*			
S_{A1}	S_{A2}	V_{A0}	C_A
0	0	-	-
0	1	0V	0
1	0	V_{DC}	1
1	1	Forbidden	-
Leg *B*			
S_{B1}	S_{B2}	V_{B0}	C_B
0	0	-	-
0	1	0V	0
1	0	V_{DC}	1
1	1	Forbidden	-
Leg *C*			
S_{C1}	S_{C2}	V_{C0}	C_C
0	0	-	-
0	1	0V	0
1	0	V_{DC}	1
1	1	Forbidden	-

As it can be seen the output voltage in each phase depends on the input voltage (V_{DC}) and the state of the switches. C_A, C_B and C_C are Boolean variables that describe the state of the converter leg during operation. The output voltage values referred to the neutral of a star-connected load are described by the following equations [23]:

$$V_{An} = \frac{V_{DC}}{3}(2C_A - C_B - C_C) \tag{3.1}$$

$$V_{Bn} = \frac{V_{DC}}{3}(2C_B - C_A - C_C) \tag{3.2}$$

$$V_{Cn} = \frac{V_{DC}}{3}(2C_C - C_A - C_B) \tag{3.3}$$

$$C_A, C_B, C_C \in \{0,1\}$$

Considering that each leg during operation can be on or off, and the variables C_A, C_B and C_C can take two possible values 0 and 1, the total number of possible combinations for the state of the switches is 2^3=8. One voltage space vector in the α-β plane is associated with each one of those combinations ($\vec{V}_0$ to $\vec{V}_7$) as shown in Fig. 3-2. The output voltage space vector can be written as:

$$\vec{v} = \frac{2}{3}\left(V_{An} + aV_{Bn} + a^2V_{Cn}\right) \tag{3.4}$$

where $a = e^{j\frac{2\pi}{3}}$, as explained in the previous chapter. If equations (3.1), (3.2) and (3.3) are substituted in (3.4) then:

$$\vec{v} = \frac{2}{3}\frac{V_{DC}}{3}\left(3C_A + 3aC_B + 3a^2C_C\right) \tag{3.5}$$

The amplitude of the voltage space vectors is $2/3V_{DC}$.

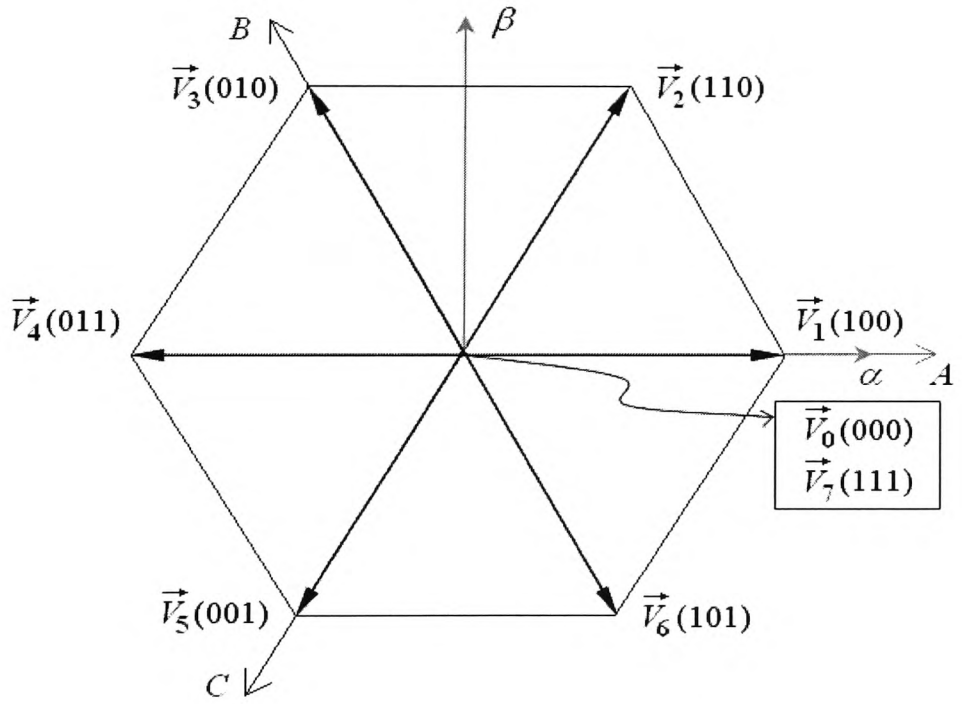

Fig. 3-2 Voltage space vectors delivered by three-phase two-level VSI

In the above figure the numbers in brackets show the state of the each leg for every voltage vector (C_A C_B C_C). For instance, $\vec{V}_1$ has the combination (100), which means: leg A connected to the positive of the DC-link (S_{A1} on and S_{A2} off; C_A=1); leg B connected to the negative of the DC-link (S_{B1} off and S_{B2} on, C_B=0); leg C connected to the negative of the DC-link (S_{C1} off and S_{C2} on; C_C=0).

There are six active vectors: $\vec{V}_1$, $\vec{V}_2$, $\vec{V}_3$, $\vec{V}_4$, $\vec{V}_5$ and $\vec{V}_6$, with and amplitude equal to $2/3 V_{DC}$; and two zero or null vectors: $\vec{V}_0$ and $\vec{V}_7$, with an amplitude equal to 0.

The success of the two-level VSI is due to several reasons such as its high efficiency, the open-circuit protection, the small relative size and the good regulation capabilities it offers. Although the standard two-level VSI is widely employed due to its advantages it has some technological limitations that can be summarized as follows [15, 22, 23]:

- The maximum voltages supported by different types of semiconductor devices limits the maximum DC-link voltage that can be employed. This limitation is particularly restrictive if fast switching technologies are employed. The solution to work with higher voltage levels based on series connection of switches presents some problems concerning the control and the voltage balance of the switches.
- The output line voltages of the VSI are composed of pulses with and amplitude equal to the DC-link voltage, which contain high harmonic distortion. PWM techniques have the property of moving the harmonics from low frequencies to the switching frequency zone and multiples of it, but with no significant reduction of the total voltage harmonic distortion.
- The strong voltage steps (*dV/dt*) in the output voltages produce high voltage peaks in the motor terminals due to the parasitic inductance and capacitance present in the motor cables. These voltage peaks contribute to the degradation of the windings insulation material. Moreover the high rate of voltage change also creates a non-uniform voltage distribution among the winding turns.
- A VSI is not an ideal balanced source and the CM voltage is therefore different from zero. In a two-level VSI none of the switching combinations produces a null CM voltage. The presence of high *dV/dt* due to the steps in the CM voltage waveform produces leakage currents (CM currents) to flow through the parasitic capacitances between cables, different parts of the motor and ground. The undesired effects of these currents are the generation of EMI and the degradation of the windings insulation and motor bearings.

3.3 Multilevel converters

The multilevel power conversion technology is a very rapidly growing area of power electronics. A considerable effort is made in research and development in this field [15, 16, 23]. The most attractive applications of this technology are in the medium to high-voltage range (2-13 kV), and include motor drives, power distribution, power quality and power conditioning applications. Nevertheless some developments are appearing for low-power applications as well [24, 25]. One of the main limitations of the two-level VSI is the maximum voltage that the existing power semiconductor devices can withstand. For these reasons, multilevel converters have emerged as the solution for working with higher voltage levels.

Multilevel converters can synthesize waveforms by using more than two voltage levels; consequently, the quality of the spectra is significantly improved when compared to the standard two-level VSI. The main drawback of multilevel converters is the requirement of a higher number of switches. Their control also becomes more complex due to the large number of devices. Several DC voltage sources are also required, which are usually provided by capacitors. In certain topologies the voltage balance of these capacitors during operation is a difficult challenge [23]. Moreover, the increase of complexity in the resulting structure decreases the reliability of the system.

Despite the drawbacks related to the mentioned increase of complexity and cost, multilevel converters have turned out to be a very good alternative for high-power applications, since the cost of the control is a small portion of the whole cost of the system. Furthermore, as prices of power semiconductors and DSPs continue to decrease, the use of multilevel topologies is expected to extend to low-power applications as well. Fast power semiconductor devices, such as MOSFETs, which can operate at very high switching frequencies, can be used for low voltages. Furthermore, new power devices are expected to appear in future, which may also extend the application of multilevel topologies.

Multilevel converters are built using an array of power semiconductors and capacitor voltage sources, the output of which generate voltages with stepped waveforms. The commutation of the switches permits the addition of the capacitor voltages. High voltage levels can be obtained at the output of the converter, while the power semiconductors must withstand only reduced voltages. The use of faster semiconductors with lower voltage capability is therefore possible.

Fig. 3-3 shows the schematic diagram of various single-phase VSIs with different number of levels. The action of the power semiconductors is represented by an ideal switch with several positions. A two-level VSI generates an output voltage with two values (levels) with respect to the negative terminal of the capacitor, while the three-level VSI generates three voltages and so on.

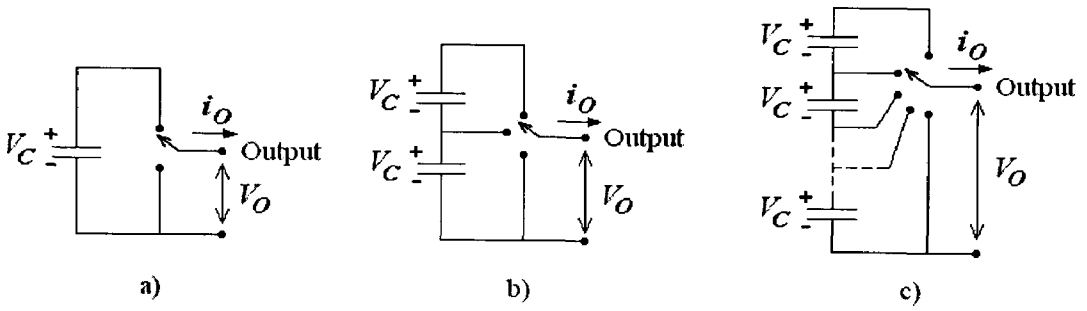

Fig. 3-3 VSI leg with a) two levels, b) three levels and c) n levels

By increasing the number of voltage levels in the VSI, the output voltages have more steps generating a staircase waveform, which has a reduced harmonic distortion.

Considering n as the number of levels of the output voltage referred to the negative rail of the DC-link, the number of levels k of the line-to-line voltage at the output of the VSI will be [23]:

$$k = 2n - 1 \tag{3.6}$$

And the number of levels p of the phase voltage in a star-connected three-phase load fed by the VSI will be [23]:

$$p = 4n - 3 \tag{3.7}$$

The output space vectors of a generic multilevel converter can be obtained with the same procedure followed for the two-level VSI. The output voltage values referred to the neutral of a star-connected load are described by the following equations:

$$V_{An} = \frac{V_{DC}}{3(n-1)}(2C_A - C_B - C_C) \tag{3.8}$$

$$V_{Bn} = \frac{V_{DC}}{3(n-1)}(2C_B - C_A - C_C) \tag{3.9}$$

$$V_{Cn} = \frac{V_{DC}}{3(n-1)}(2C_C - C_A - C_B) \tag{3.10}$$

$$C_A, C_B, C_C \in \{0,1,...,n-1\}$$

The output voltage space vector can be written as:

$$\vec{v} = \frac{2}{3}\left(V_{An} + aV_{Bn} + a^2 V_{Cn}\right) \tag{3.11}$$

$$\vec{v} = \frac{2}{3}\frac{V_{DC}}{3(n-1)}\left(3C_A + 3aC_B + 3a^2 C_C\right) \tag{3.12}$$

It can be deduced that some voltage space vectors will have several combinations of switches associated with them.

The most attractive features of multilevel converters can be summarized as follows [15, 16, 23, 26, 27]:

- Higher voltages and power levels can be achieved and faster semiconductor devices can be used. Series connection of semiconductors devices can be avoided.
- Distortion in the current and voltage waveforms is reduced.
- The average switching frequency in the semiconductor devices is reduced. Stress and losses in the semiconductor devices are therefore reduced.
- Lower voltage steps (*dV/dt*), CM voltage, CM current and EMI are generated. The stress caused in the stator windings insulation and motor bearings is therefore reduced.
- The requirement of extra passive components such as output filters or snubber circuits can be eliminated or reduced in size in some cases.
- The number of possible combinations of switching states and voltage vectors are both increased.
- There are redundant combinations of switching states that generate the same voltage vector at the output. This is useful to minimise switching frequency, CM voltage and for balancing the voltage in the capacitors of the DC-link in certain topologies. An *n*-level converter will have 1 vector with *n* redundant combinations of switches; 6 vectors with *n*-1 redundant combinations; 12 vectors with *n*-2 redundant combinations and so on.

Regarding the control of multilevel converters there is a wide variety of modulation techniques that can be grouped as shown in Fig. 3-4 [15, 23, 26, 27].

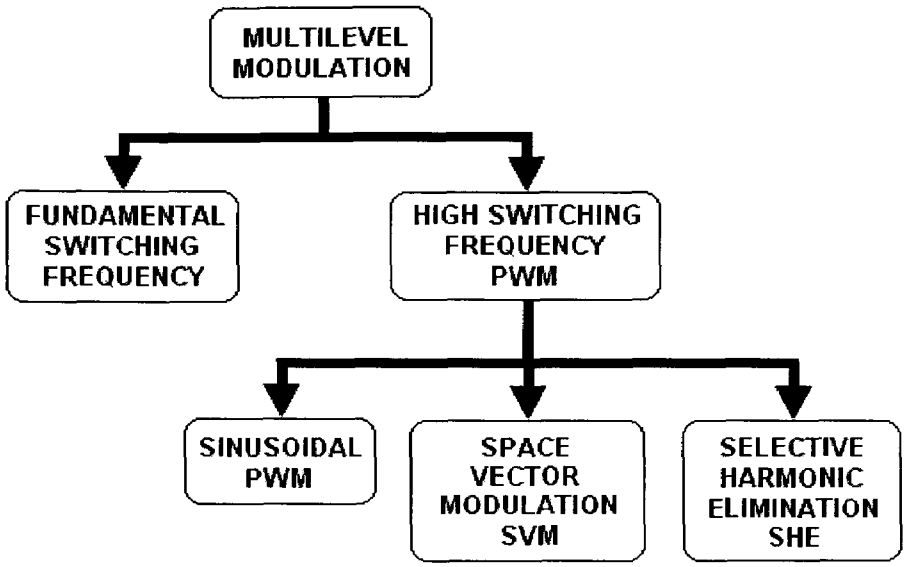

Fig. 3-4 Multilevel modulation techniques

So far, the most actively developed multilevel topologies are: the diode-clamped converter, the floating-capacitor converter and the cascaded multi-cell converter. These topologies are described in the following sections.

3.3.1 The diode-clamped converter

The diode-clamped converter (or NPC converter) was introduced in its three-level version by Nabae et al. in 1981 [28]. It is the most used topology nowadays for multilevel conversion [23]. This topology has been extended to higher numbers of levels. Fig. 3-5 shows the generic circuit diagram of a single-phase *n*-level diode-clamped converter.

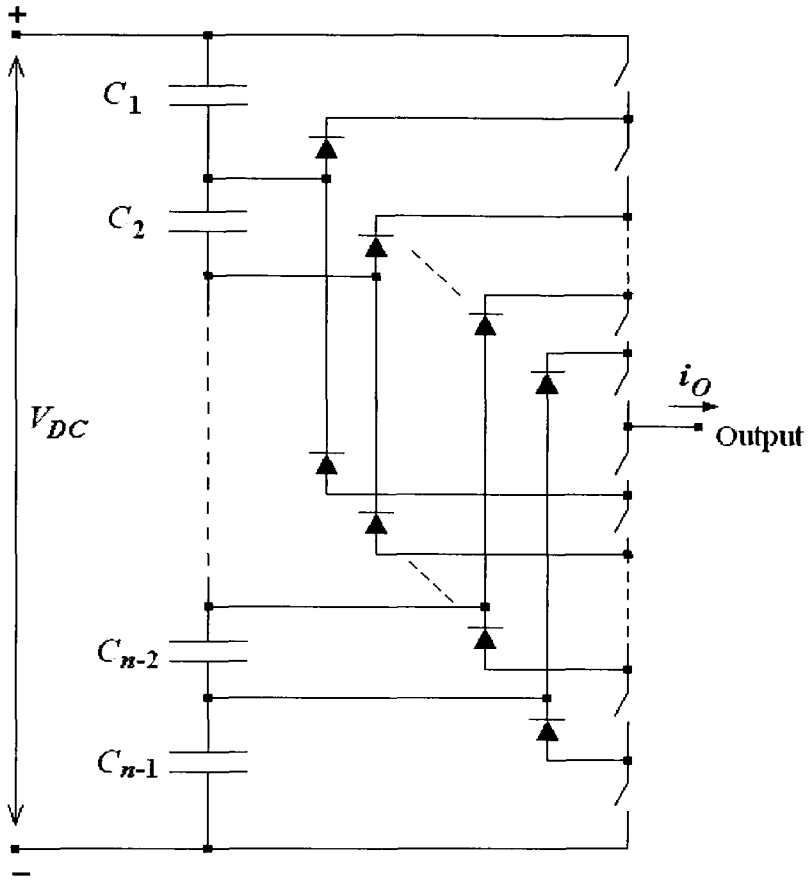

Fig. 3-5 Single-phase n-level diode-clamped converter

The required number of devices for each leg of this type of converter is shown in Table 3-II.

Table 3-II Number of devices used in each leg of a diode-clamped converter with n levels

Capacitors	n-1
Clamping diodes	2(n-2)
Fully controlled switches	2(n-1)

For the general case of an n-level topology, n-1 consecutive switches of each leg must be on. Consequently, a number of DC-link capacitors in series are connected to the output fixing a certain voltage level in it. The converter can be seen as a multiplexer that connects the output to a certain point or level of the DC-link as shown in Fig. 3-6.

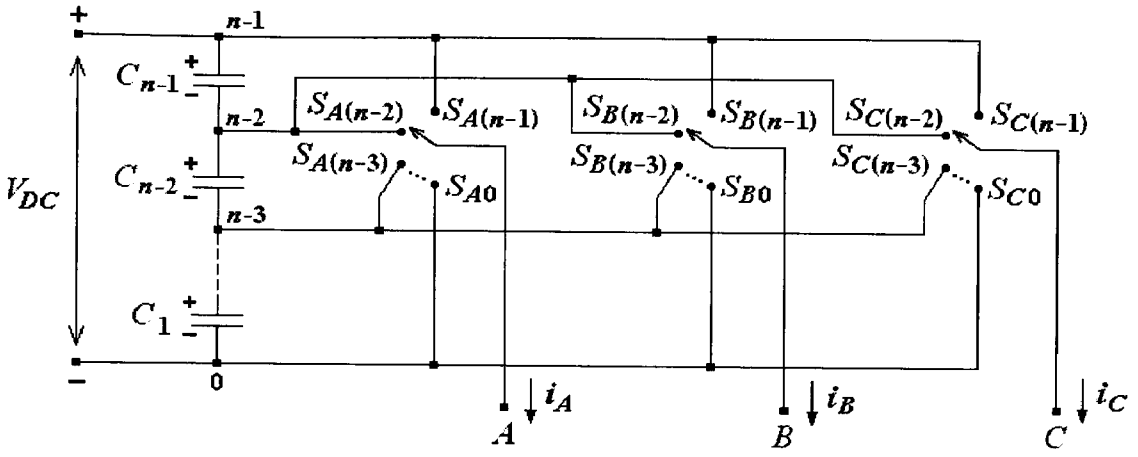

Fig. 3-6 Functional diagram of the n-level diode-clamped converter

In the previous functional diagram there are some variables (S_{ij}) that express the state of the multiplexers. These variables are equal to 1 when the output i is connected to the point j and otherwise they are 0. The output voltage referred to the negative rail of the DC-link (0) can be expressed as follows [23]:

$$v_{i0} = \sum_{j=0}^{n-1}\left(S_{ij} \sum_{p=1}^{j} V_{Cp} \right) \qquad with \quad i = \{A,B,C\} \tag{3.13}$$

And when the DC-link voltage is equally shared in the capacitors the following expression can be obtained:

$$v_{i0} = \frac{V_{DC}}{n-1} \sum_{j=0}^{n-1} jS_{ij} \qquad with \quad i = \{A,B,C\} \tag{3.14}$$

Under balanced conditions, the maximum voltage applied to the switches is the voltage of one capacitor $V_{DC}/(n\text{-}1)$.

The advantages of the diode-clamped converter compared with other multilevel topologies are [15, 22, 23, 26]:

- They use a lower number of capacitors. Although these topologies require some additional clamping diodes, the lower number of reactive components is usually preferred concerning the cost and compactness.
- They can be connected to a single DC-link voltage. The floating-capacitor topology also shares this advantage, but the cascade converter does not, since this converter requires multiple insulated DC power supplies.

Nevertheless, some practical experience with this topology reveals technical difficulties [23, 26]:

- For topologies with more than three levels, the clamping diodes are subject to high voltage stress equal to $V_{DC}(n\text{-}2)/(n\text{-}1)$. As a result, series connection of the diodes is required. This issue complicates the design and raises reliability and cost concerns. Even with the three-level topology high speed clamping diodes are required, able to carry full load and subject to severe reverse recovery stress.
- The objective of maintaining the charge balance of the capacitors in topologies with a high number of levels (more than three) has been demonstrated to be impossible for some operating conditions. These balancing problems appear when dealing with high modulation indices and active currents. Therefore, high AC output voltages cannot be achieved, which inhibits the most important attribute of multilevel converters.
- Although proper control of the three-level topology overcomes the voltage balance concern, a low-frequency ripple in the potential of the middle point of the DC-link appears when dealing with high modulation indices and low power factors. The maximum voltage applied to the devices is higher due to this oscillation, and additionally, it produces low-frequency distortion in the AC output voltages.
- Another issue to be considered is the fact that switching frequencies differ among the switches of a leg during operation. This may lead to different stress and lifetime of some semiconductors in relation to others.

3.3.2 The capacitor-clamped converter

This kind of topology is also known as flying-capacitor or floating-capacitor multilevel converter. It was introduced by Meynard et al. in 1992 [29], and it is considered to be the most serious alternative to the diode-clamped topology. The significant feature of this topology is that it eliminates the clamping diodes and replaces them by additional flying capacitors.

This converter is composed of several nested commutation cells. Each cell contains two fully-controlled switches with complementary states and dead times for switching transition, like in a two-level VSI. One flying capacitor is connected between two adjacent cells creating a flying DC voltage source. The generation of the output voltage level is based on the series connection of the necessary flying DC voltage sources. Fig. 3-7 shows an n-level leg of a flying-capacitor converter.

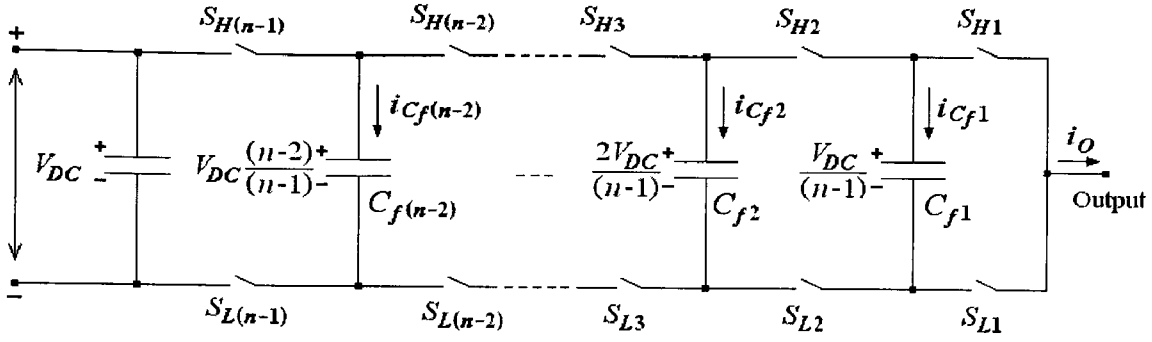

Fig. 3-7 Nested cells of a n-level flying-capacitor converter

One out of each pair of switches S_{Hi} and S_{Li} must be on in order to create a connection between the DC-link potential and the output through some of the capacitors. Additionally, both switches should not be on at the same time in order to avoid short-circuits between adjacent capacitors. Moreover, they should not be both off because inductive loads would produce overvoltages that would damage the switches.

The three-level version of the capacitor-clamped converter is shown in Fig. 3-8.

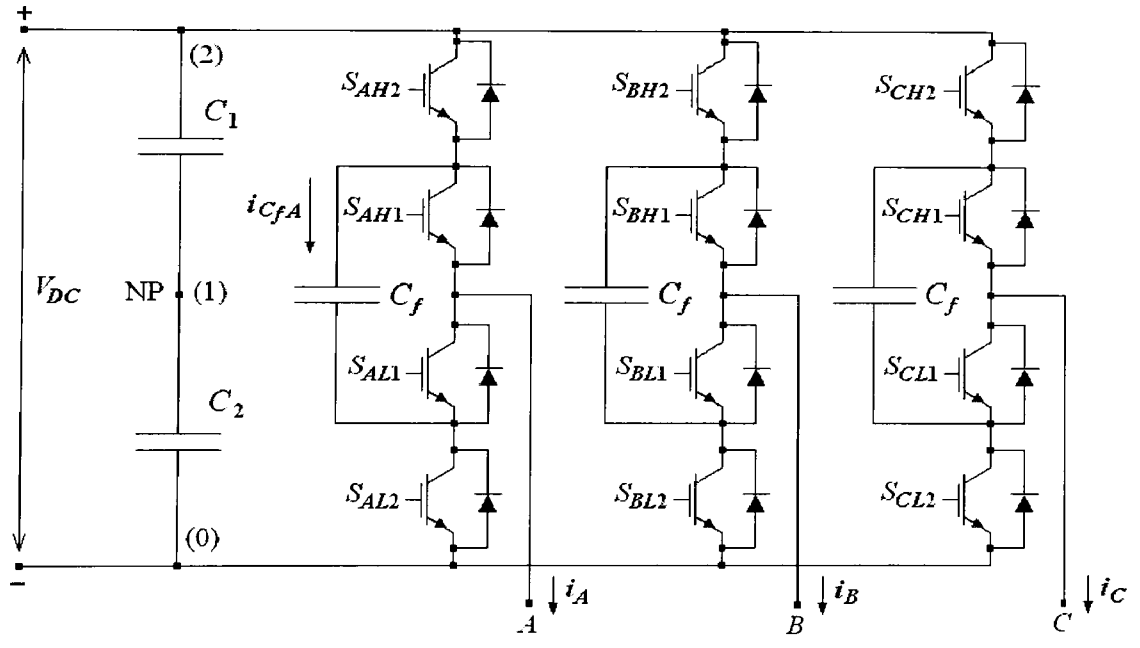

Fig. 3-8 Three-level capacitor-clamped converter

Table 3-III shows all the possible states of the switches in one leg of the converter. Only the state of the upper switches is given since the lower switches are complementary to them.

Table 3-III Possible state of the switches in a leg of a capacitor-clamped converter

S_{AH2}	S_{AH1}	V_{A0}	I_{CfA}
0	0	0	0
0	1	$V_{DC}/2$	$-i_A$
1	0	$V_{DC}/2$	i_A
1	1	V_{DC}	0

As it can be seen, the voltage balance in the flying capacitors can be controlled by choosing the appropriate combination of switches that gives $V_{DC}/2$ at the output.

Some additional features of the flying capacitor multilevel converter are:

- The voltage across each open switch is intrinsically limited to $V_{DC}/(n-1)$.
- The stress and life time of the switches can be equalised in the different switching cells by taking it into account in the control technique.
- Unlike the diode-clamped converter, the flying capacitor topology has enough switching states to control the charge balance in a single isolated leg in converters having any number of levels, even if the phase current is unidirectional. This makes this topology attractive even for DC to DC converters.
- Each leg can be analysed independently concerning the voltage balance of the capacitors.

The number of components required capacitor-clamped converters is shown in Table 3-IV.

Table 3-IV Number of devices used in each leg of an n-level capacitor-clamped converter

Capacitors	n-2
Additional diodes	0
Fully controlled switches	2(n-1)

At the present time it seems that this topology has some disadvantages [23, 26]:

- Higher number of capacitors required.

- The capacitor charge controller adds complexity to the control of the whole circuit.
- It might require more capacitance than the equivalent diode clamped topology.
- There is a potential for parasitic resonance between decoupling capacitors.

3.3.3 The cascade multi-cell converter

Cascade multi-cell converters are based on the series connection of multiple single-phase inverters with separate DC sources. Each individual converter is viewed as a power module and the output voltage is synthesized by adding each converter output voltage either indirectly, using an electromagnetic interface such as a multi-winding transformer, or directly using separate DC buses. Fig. 3-9 shows a basic schematic for a cascade multi-cell converter.

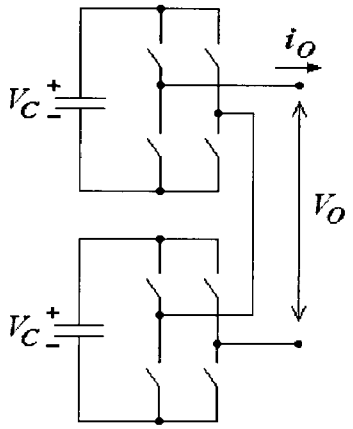

Fig. 3-9 Cascade multilevel converter concept

Other topologies have also been proposed based on the concept of cascade multi-cell, all of them providing modularity and low distortion in output voltages but a higher complexity at the same time concerning the structure of the system.

The basic three-phase structure for cascade converter is shown in Fig. 3-10.

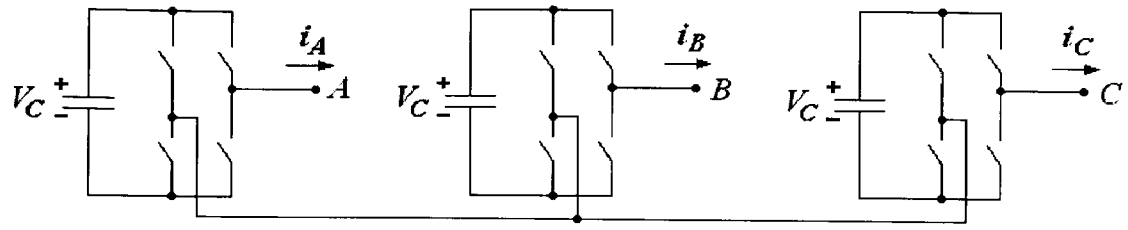

Fig. 3-10 Three-level cascade converter

A chain of H-bridge converters can create a converter with higher numbers of levels as shown in Fig. 3-11.

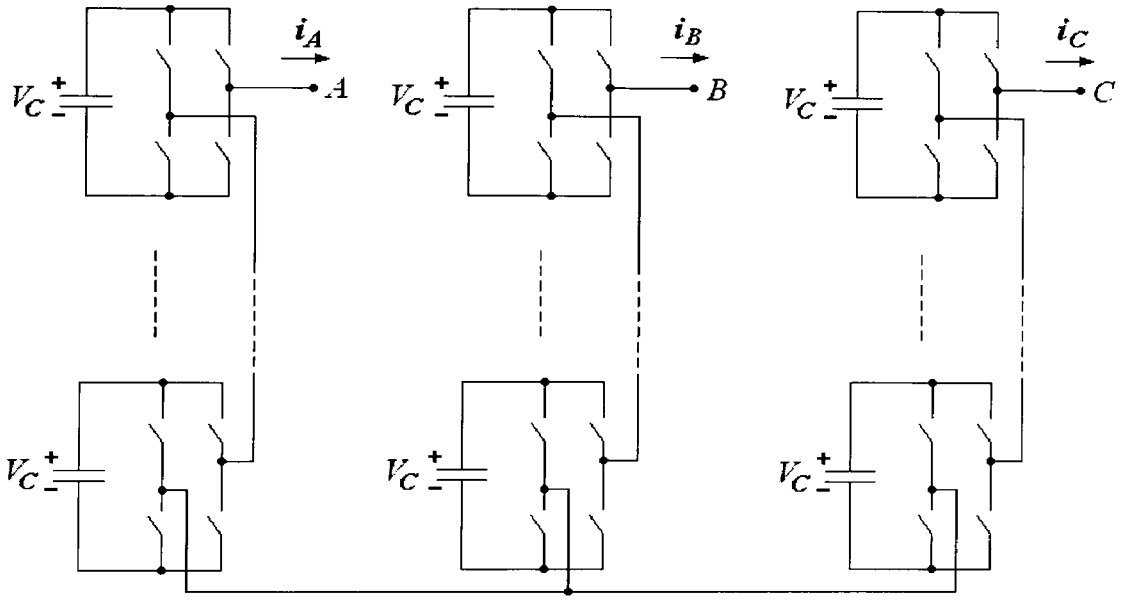

Fig. 3-11 n-level cascade converter

The modularity of this topology is an advantage. However, the fact that the DC-link voltages must be isolated is the major drawback of these structures. Several independent DC power supplies are required, which can be provided either by a transformer with multiple insulated secondaries or by several transformers. Another interesting feature is that for a given topology, a higher number of levels can be obtained by using different DC levels for the voltage sources [30]. Two H-bridges in cascade with equal DC voltages provide 5 levels at the output. If one of the H-bridges is fed with V_{DC} and the other with $2V_{DC}$, the obtained output contains 7 levels. Different types of semiconductor devices can be used according to the DC voltage for each H-bridge cell.

3.3.4 Summary of data for basic multilevel converters

A summary table containing all the main information related to the basic multilevel topologies presented in previous sections is given in Table 3-V [23].

Table 3-V Main characteristics of basic multilevel converter topologies

Concept	Topology					
	Diode-Clamped		Capacitor-Clamped		Cascade	
	3-level	*n*-level	3-level	*n*-level	3-level	*n*-level
A	12	$6(n\text{-}1)$	12	$6(n\text{-}1)$	12	$6(n\text{-}1)$
B	6	$6(n\text{-}2)$	0	0	0	0
C	6	$3(n\text{-}1)(n\text{-}2)$	0	0	0	0
D	2	$n\text{-}1$	4	$3n\text{-}5$	3	(n even) $(3n/2)\text{-}1.5$ (n Odd) $(3n/2)\text{-}2$
E	2	$n\text{-}1$	7	$(n-1)^2+3\sum_{i=1}^{n-2} i^2$	3	(n Even) $(3n/2)\text{-}1.5$ (n Odd) $(3n/2)\text{-}2$
F	$V_{DC}/2$	$V_{DC}/(n\text{-}1)$	$V_{DC}/2$	$V_{DC}/(n\text{-}1)$	$V_{DC}/2$	$V_{DC}/(n\text{-}1)$
G	5	$2n\text{-}1$	5	$2n\text{-}1$	5	$2n\text{-}1$
H	9	$4n\text{-}3$	9	$4n\text{-}3$	9	$4n\text{-}3$
I	27	n^3	64	$2^{3(n-1)}$	64	$2^{3(n-1)}$
J	19	$n^3\text{-}(n\text{-}1)^3$	19	$n^3\text{-}(n\text{-}1)^3$	19	$n^3\text{-}(n\text{-}1)^3$

A: number of switches (with free-wheeling diodes).

B: number of independent diodes (with different reverse voltages).

C: real number of independent diodes (series connection for same reverse voltage distribution).

D: number of capacitors (with different voltages).

E: real number of capacitors (series and parallel connections for the same voltage distribution and capacitance).

F: maximum voltage applied to the switches.

G: number of line-to-line output voltage levels.

H: number of phase voltage levels for a star-connected load.

I: number of switching combinations.

J: number of different space vectors delivered at the output.

3.4 The three-level NPC VSI

3.4.1 Description

The investigation carried out in this thesis has focused on the employment of three-level version of the diode-clamped VSI. The inclusion of this topology to the motor drive system is investigated due to the interesting characteristics it can offer. This converter (Fig. 3-12) is generally known as the three-level NPC VSI [28].

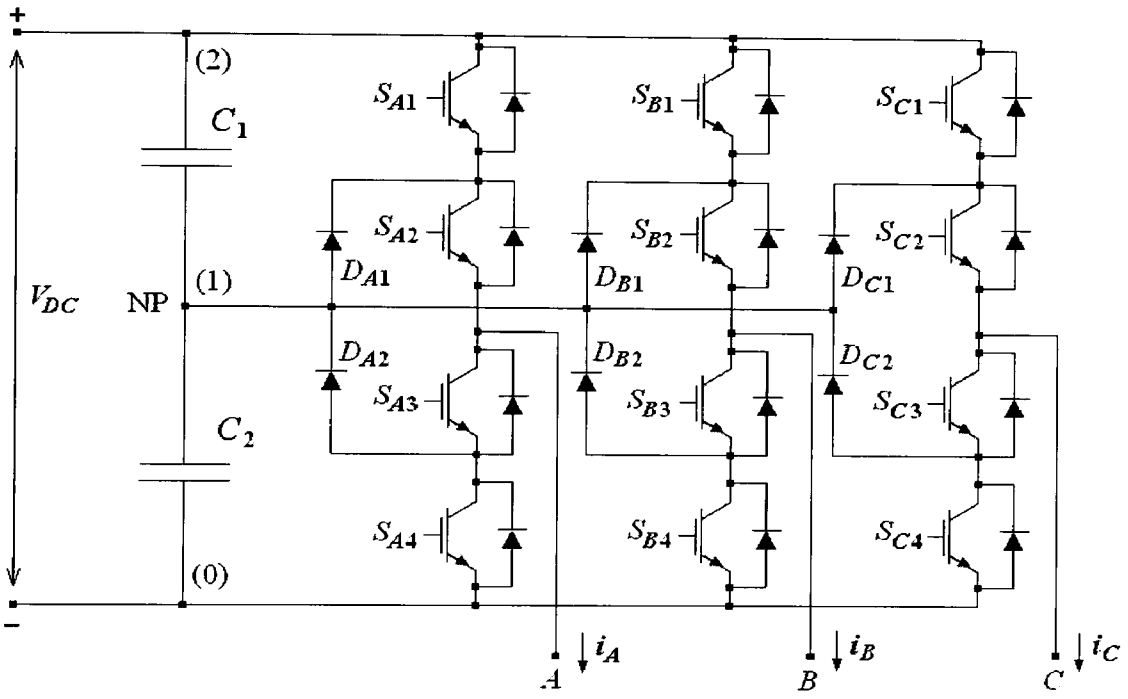

Fig. 3-12 The three-level NPC VSI

In this circuit the DC-link voltage is split into three levels by the two series-connected capacitors $C1$ and $C2$. The middle point of the two capacitors can be defined as the Neutral Point (NP). The output voltage has three different states between the outputs (A, B and C) and the NP: $V_{DC}/2$, 0, and $-V_{DC}/2$.

The voltage level at each output (A, B and C) is controlled by the state of the switches in each leg. For instance, leg A contains switches S_{A1}, S_{A2}, S_{A3} and S_{A4} that can be in on state (1) or off state (0). The state of the switches in leg A is expressed in brackets in the following form: (S_{A1}, S_{A2}, S_{A3}, S_{A4}); the state of the switches in legs B and C is expressed in the same way. The variables C_A, C_B and C_C are used to describe the state of each leg and the voltage delivered at the output. They can take three values 0, 1 and 2 according

to the three different voltage levels that can be delivered by this type of VSI. The following table describes the switching combinations and output voltages obtained:

Table 3-VI Possible states of a three-level NPC VSI

Leg *A*					
S_{A1}	S_{A2}	S_{A3}	S_{A4}	V_{ANP}	C_A
0	0	0	0	-	-
1	1	0	0	$V_{DC}/2$	2
0	1	1	0	0	1
0	0	1	1	$-V_{DC}/2$	0
Leg *B*					
S_{B1}	S_{B2}	S_{B3}	S_{B4}	V_{BNP}	C_B
0	0	0	0	-	-
1	1	0	0	$V_{DC}/2$	2
0	1	1	0	0	1
0	0	1	1	$-V_{DC}/2$	0
Leg *C*					
S_{C1}	S_{C2}	S_{C3}	S_{C4}	V_{CNP}	C_C
0	0	0	0	-	-
1	1	0	0	$V_{DC}/2$	2
0	1	1	0	0	1
0	0	1	1	$-V_{DC}/2$	0

As it can be seen, only 4 out of 16 possible combinations for each leg are used. Most of the unused combinations must be avoided because they would cause short-circuits of the DC-link, or the application of the total DC-link voltage in a single semiconductor switch. The last possibility must be avoided if the DC-link voltage employed is higher than the maximum voltage supported by the switches. Combinations (0,1,0,0) and (0,0,1,0) are not harmful for the converter and are used in transitions between valid states to avoid short-circuits.

Diodes D_{A1}-D_{A2}, D_{B1}-D_{B2} and D_{C1}-D_{C2} are the clamping diodes that connect the output to the NP when the combination in a leg is (0,1,1,0). High speed diodes are employed in order to withstand the recovery stress that the load currents can produce. For a three-level NPC VSI the blocking voltage for the clamping diodes is equal to $V_{DC}/2$.

The output voltage values referred to the neutral of a star-connected three-phase load are described by the following equations:

$$V_{An} = \frac{V_{DC}}{6}(2C_A - C_B - C_C) \tag{3.15}$$

$$V_{Bn} = \frac{V_{DC}}{6}(2C_B - C_A - C_C) \tag{3.16}$$

$$V_{Cn} = \frac{V_{DC}}{6}(2C_C - C_A - C_B) \tag{3.17}$$

$$C_A, C_B, C_C \in \{0,1,2\}$$

As it can be seen, the output voltage depends on the DC-link voltage and the state of the leg, which is defined by the variables C_A, C_B and C_C. The output voltage space vector can be written as:

$$\vec{v} = \frac{2}{3}\left(V_{An} + aV_{Bn} + a^2 V_{Cn}\right) \tag{3.18}$$

$$\vec{v} = \frac{2}{3}\frac{V_{DC}}{6}\left(3C_A + 3aC_B + 3a^2 C_C\right) \tag{3.19}$$

In Fig. 3-13 the different voltage vectors and the associated VSI states available in a three-level VSI are shown in the α-β plane. As it can be observed there are 4 different kinds of vectors:

- The zero vector: $\vec{V}_z$.
- Large vectors: $\vec{V}_{1l}$, $\vec{V}_{2l}$, $\vec{V}_{3l}$, $\vec{V}_{4l}$, $\vec{V}_{5l}$, $\vec{V}_{6l}$.
- Medium vectors: $\vec{V}_{1m}$, $\vec{V}_{2m}$, $\vec{V}_{3m}$, $\vec{V}_{4m}$, $\vec{V}_{5m}$, $\vec{V}_{6m}$.
- Small vectors: $\vec{V}_{1s}$, $\vec{V}_{2s}$, $\vec{V}_{3s}$, $\vec{V}_{4s}$, $\vec{V}_{5s}$, $\vec{V}_{6s}$.

Large and medium vectors have a unique combination of switches; small vectors have two possible configurations and the zero vector has 3 possible configurations. The redundancy of small vectors and the zero vector can be used to balance the voltage of the DC-link capacitors and reduce the switching frequency respectively. The state of the switches for each leg is shown in brackets (C_A C_B C_C).

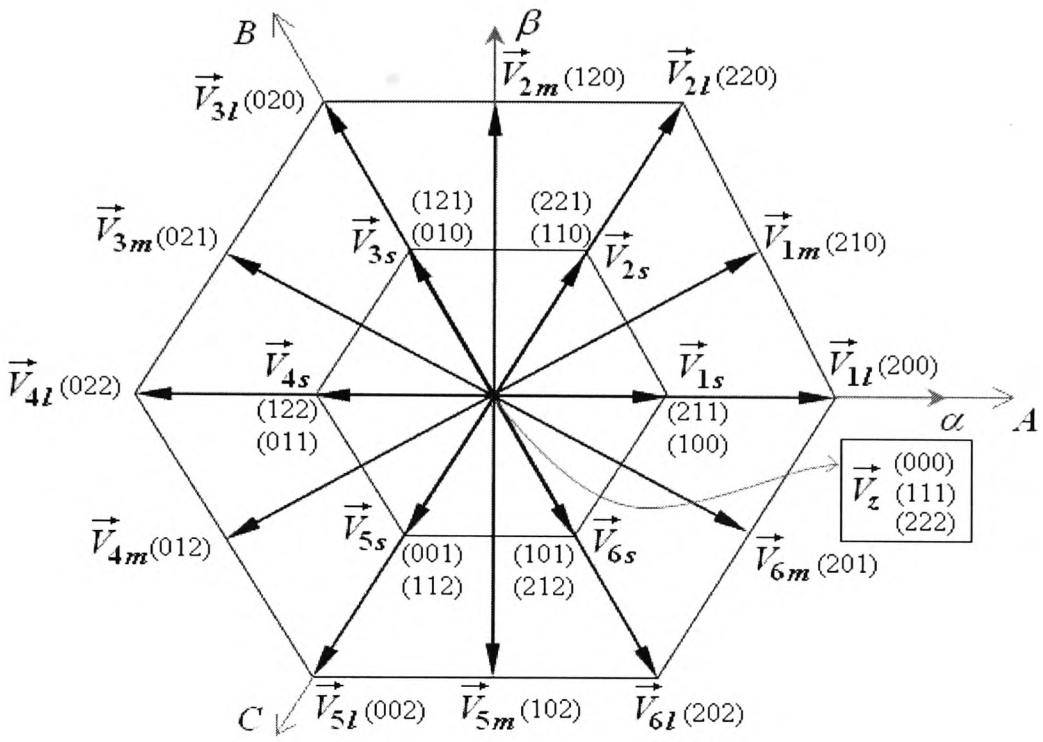

Fig. 3-13 Voltage vectors delivered by a three-level NPC VSI

The main characteristics of a three-level NPC VSI are shown in the previous section in Table 3-V. The column with the heading "Diode-Clamped/3-level" contains all the related information.

The advantages of the three-level VSI in comparison with the two-level VSI are the following [22, 23, 26, 28]:

- Higher number of VSI states available (27 vs. 8).
- Reduced harmonic distortion in the voltage and current waveforms.
- Lower voltage steps (*dV/dt*), CM voltage, CM currents and EMI are generated. The stress in the motor windings insulation and bearings is reduced.
- The switches only have to withstand half of the DC-link voltage. Fast semiconductors can be used for high-power applications.
- It can operate with lower switching frequency, reducing the power losses and stress in the semiconductor devices.

However, it presents the following disadvantages:

- The voltage of the DC-link capacitors has to be balanced.

- Higher cost since extra semiconductor devices are required (12 vs. 6). 6 additional clamping diodes are also required. Reliability is reduced due to the higher complexity and number of components.

3.4.2 Commercial drives

Some commercial drives for IMs already employ the three-level NPC technology. In 2001 Yaskawa introduced the Varispeed G7 which incorporates this technology for low voltage IM drives [25, 31, 32]. The main features of this drive are:

- Voltage input: three-phase 480 V.
- Power range: 0.55 kW to 300 kW.
- Maximum output frequency: 400 Hz.
- Control method: Sinusoidal PWM, V/f and flux vector control. Pulse generator feedback can be employed and sensorless versions are also available.
- Speed control accuracy: under flux vector control the accuracy is up to ±0.01% with pulse generator feedback and up to ±0.2% for sensorless versions.
- Speed response: 60 Hz.
- Torque control possible for flux vector control; the accuracy achieved is ±5%.
- Starting torque: 150% at 0.3 Hz for closed-loop flux vector control.
- Torque response: 300 Hz.

This manufacturer claims the following main benefits for the three-level technology:

- Lower voltage peaks are generated (30% less than conventional drives), which increases the life of the motor by reducing the stress on the insulation materials of the motor windings. Operation with longer cables is possible.
- Reduced CM voltage steps, which leads to a 50% reduction of the CM current.
- Leakage current through the motor bearings is reduced by 50%. Motor bearing lifetime is increased 4 times.
- Lower level of radio interference is generated. Conducted emission caused by the inverter is considerably reduced, which in turn reduces the cost of line filters.
- Quiet motor operation, 5 to 10 dB (20%) of noise reduction is achieved. The three-level technology reduces the noise due to magnetic transients in the motor.

The issue of the voltage balance in the DC-link capacitors is addressed in this drive by means of a modulation technique based on the Nearest Three Vectors (NTV) method, which is described in [33].

In 1998 ABB introduced the ACS 1000, which is a medium voltage AC drive for IMs [34-36]. The main features of this drive are:

- Type of converter: three-level VSI.
- Motor voltage: 2.3 kV, 3.3 kV and 4.0 kV (optional 6.0 and 6.6 kV).
- Power range: from 315 kW to 5 MW.
- Maximum output frequency: 66 Hz.
- 12/24-pulse uncontrolled diode bridge rectifier. Constant network power factor over the whole speed range (>0.95).
- It incorporates IGCT technology, which provides high switching speed and high voltage blocking with low losses. Snubber circuits are no required and it is self-protecting against destructive failures (fuseless).
- Control method: Direct Torque Control.
- A low pass LC filter is incorporated at the output to obtain sinusoidal voltages.
- Type of motor: induction motor.

The basic version of the ACS 1000 has evolved into the ACS 1000i, which incorporates the following components: integrated input transformer, input contactor, power supply and input surge protection.

For higher power ranges ABB developed and introduced in 1999 the ACS 6000 with similar characteristics to the ACS 1000:

- Type of converter: three-level VSI.
- Motor voltage: 3 kV, 3.3 kV.
- Power range: from 3 MW to 27 MW.
- Maximum output frequency: 75 Hz.
- 12/24-pulse uncontrolled diode bridge rectifier or IGCT active rectifier. Constant network power factor over the whole speed range.
- IGCT technology.
- Control method: Direct Torque Control.
- Special feature: multidrives with common DC bus.
- Type of motor: induction motor and synchronous motor.

3.4.3 Neutral Point balance

One of the main issues of the three-level NPC topology is the balance of the voltage level in the NP of the DC-link. Ideally both capacitors should equally share the DC-link

voltage level, which means that the voltage across each capacitor should be $V_{DC}/2$. However, during operation the voltage level in the two capacitors may differ when current is drawn or injected to the NP. In the worst case one of the two capacitors might be charged with the total voltage of the DC-link while the other is completely discharged. The consequences of the NP imbalance are the increase of the maximum voltage applied to the semiconductor devices and the generation of low-frequency distortion in the AC output voltages [23]. The NP potential fluctuation is particularly important when operating at maximum output voltage with low power factor [23, 33].

The imbalance of the NP voltage level occurs when current circulates from the NP to the outputs of the inverter or in the opposite direction. This situation takes place when medium and small vectors are applied. Large vectors and zero vectors have no effect on the NP voltage drift.

Table 3-VII shows the small and medium voltage vectors and their effect on the NP current. Voltage polarities and current directions are taken according to Fig. 3-14. Depending on the instantaneous value of the output currents (i_A, i_B and i_C) the NP voltage level will either increase ($i_{NP}<0$) or decrease ($i_{NP}>0$). Small vectors are grouped into positive and negative vectors according to how the positive directions of i_{NP}, i_A, i_B and i_C are defined (see Fig. 3-12 and Fig. 3-14).

Table 3-VII Effects of medium and small vectors on the NP current

Positive small vectors	i_{NP}	**Negative small vectors**	i_{NP}	**Medium vectors**	i_{NP}
100	i_A	211	$-i_A$	120	i_A
010	i_B	121	$-i_B$	210	i_B
001	i_C	112	$-i_C$	201	i_C
122	i_A	011	$-i_A$	102	i_A
212	i_B	101	$-i_B$	012	i_B
221	i_C	110	$-i_C$	021	i_C

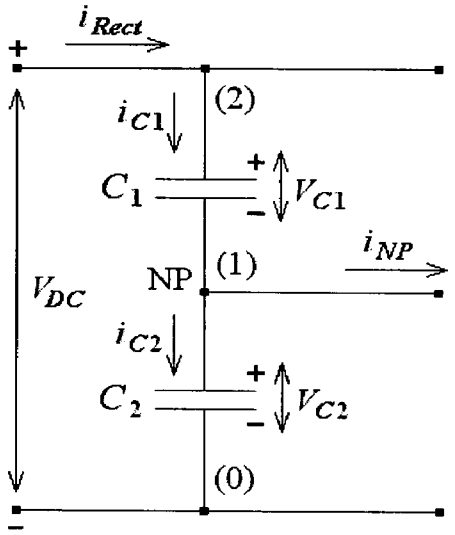

Fig. 3-14 NP current and capacitor voltages definition

Fig. 3-15 illustrates the effect of the different types of voltage vectors on the NP voltage level. Currents involved in the NP potential drift are also shown. Different vectors are applied every 0.05 s as shown in the figure and the variation of the voltage level in the capacitors is shown. A three-phase resistive load has been used in this simulation.

It can be observed how the voltage in the capacitors only changes when small and medium vectors are applied. When zero and large vectors are applied the voltage in the capacitors remains unchanged.

At t = 0.05 s the small voltage vector (211) is applied and C_1 is completely discharged while C_2 is charged until it reaches the total DC-link voltage. A similar situation with opposite effect occurs at t = 0.2 s, when the small vector (100) is applied.

Medium vectors tend to balance the voltage in the capacitors at the end of the voltage transient when they are applied continuously as in the simulation. This situation however, does not apply when the load is inductive and voltage vectors are applied for very short periods (much shorter than the capacitors charge and discharge time constant).

It can be observed how the NP current shown in Fig. 3-15b depends on the output currents as described in Table 3-VII. When the small vector (211) is applied at t = 0.05 s, i_{NP} is equal to $-i_A$. When the medium vector (120) is applied at t = 0.15 s, i_{NP} is equal to i_A. Finally, when the small vector (100) is applied at t = 0.2 s, i_{NP} is equal to i_A.

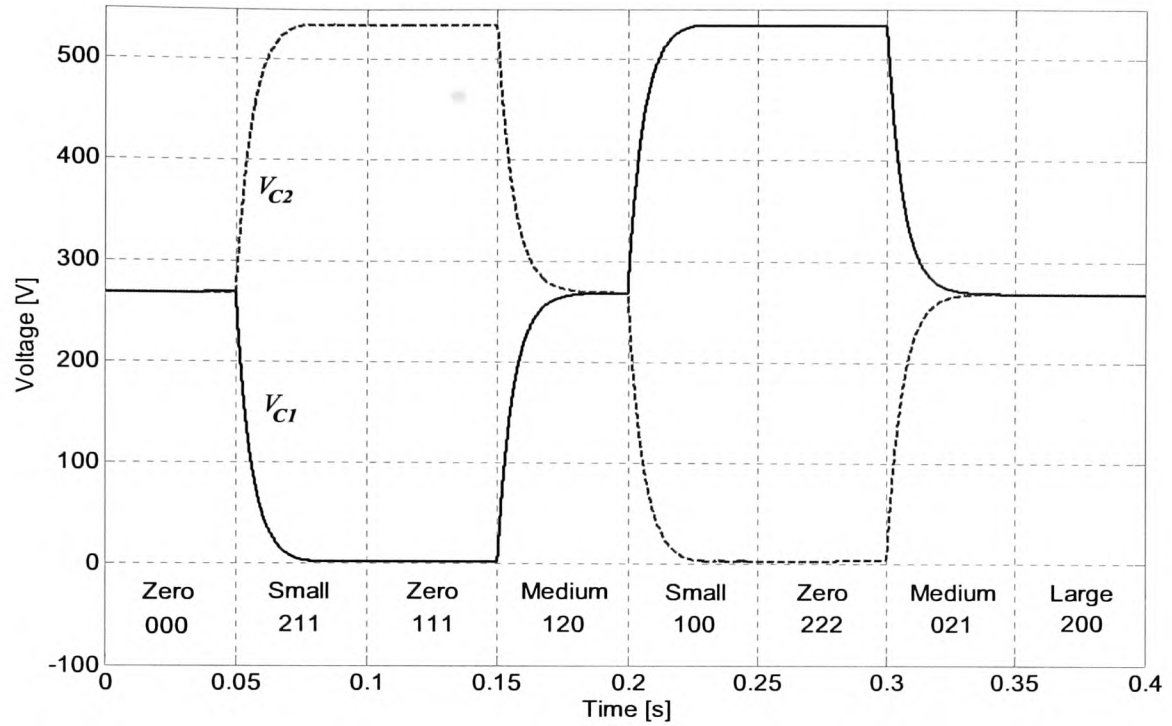

a) Voltage across the DC-link capacitors

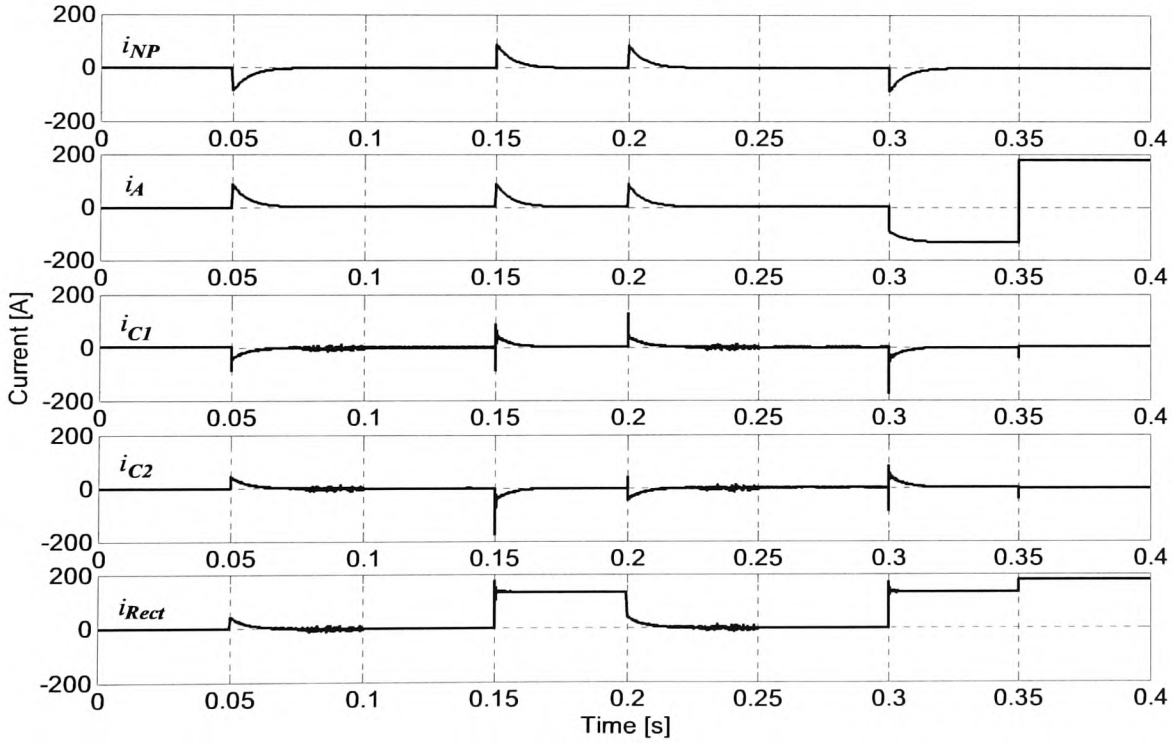

b) Currents related to the NP balance

Fig. 3-15 Effect of the different types of voltage vectors on the NP potential

Different solutions can be adopted to control the NP voltage level and minimise its drift. These solutions can be summarized as follows:

- The problem can be minimised by increasing the size of the capacitors and bleeding resistors that are usually placed in parallel with the capacitors. These solutions are not optimal from the cost and size reduction perspectives. Power losses are also increased due to the bleeding resistors [33].
- The voltage imbalance problem can also be solved by means of a back-to-back rectifier/inverter system and a proper voltage balancing control. Additional voltage balancing circuits, such as DC choppers, can be used [15, 23]. Despite the effectiveness of this kind of solution, the increase in cost and complexity is considerable.
- The most interesting solutions take advantage of the redundancy and opposite effects of small voltage vectors on the NP potential. These solutions generally incorporate the voltage control in the modulation algorithm [23, 26, 33, 37, 38].
- A simple solution which is applied to Direct Torque Control of IMs employs a hysteresis comparator to control the voltage drift in the NP [39-41]. In this solution, when a small vector is employed, the most convenient configuration among the redundant possibilities is selected to correct the voltage drift according to the hysteresis comparator.

3.5 Common-Mode voltage

The generation of CM voltage with high *dV/dt* is one of the undesirable effects when using a VSI [31, 42, 43]. The CM voltage can be defined as the voltage difference between the power source ground and the neutral of the star-connected load and can be expressed as follows:

$$V_{CM} = \frac{V_{AG} + V_{BG} + V_{CG}}{3} \tag{3.20}$$

It is apparent that with a balanced three-phase source the CM voltage is always zero. Nevertheless this is not the case for the VSI because it is not an ideal balanced source. The CM voltage when using a VSI can be redefined using the following expression:

$$V_{CM} \approx V_{nNP} = \frac{V_{ANP} + V_{BNP} + V_{CNP}}{3} \tag{3.21}$$

Although the NP or middle point of the DC-link does not have to be necessarily connected to the ground, from the high frequency point of view, they both can be considered to be the same point [31].

In a VSI, the output voltages referred to the NP can only take certain values according to the state of the switches. The sum of these voltages can be different from zero producing a non-zero CM voltage. In a two-level VSI, for instance, the CM voltage is always different from zero for all the possible switching combinations.

The CM voltage can generate currents (CM or leakage current) flowing from different parts the IM and the motor cables to ground. The existence of these currents is due to the parasitic inductances and capacitances between cables and ground, and the parasitic capacitance between different elements of the IM: stator windings and stator frame; stator windings and rotor frame; stator and rotor frames; and finally the shaft and the stator frame through the motor bearings. All these capacitances create the path for the CM current towards the stator frame which is connected to ground [31, 42, 43].

The generation of CM voltage and current can be attenuated by employing multilevel topologies such as the three-level NPC VSI. This reduction of the CM voltages can be achieved thanks to the reduction of the voltage step (*dV/dt*) between the different CM voltage levels that the VSI generates. Table 3-VIII shows the CM voltage produced by each switching configuration for a two-level and a three-level VSI.

Table 3-VIII CM voltage for each switching configuration

Two-level VSI	
V_{CM}	**Switching configuration**
$V_{DC}/2$	$\vec{V}_7(111)$
$V_{DC}/6$	$\vec{V}_2(110)$, $\vec{V}_4(011)$, $\vec{V}_6(101)$
$-V_{DC}/6$	$\vec{V}_1(100)$, $\vec{V}_3(010)$, $\vec{V}_5(001)$
$-V_{DC}/2$	$\vec{V}_0(000)$
Three-level VSI	
V_{CM}	**Switching configuration**
$V_{DC}/2$	$\vec{V}_z(222)$
$V_{DC}/3$	$\vec{V}_{2s}(221)$, $\vec{V}_{4s}(122)$, $\vec{V}_{6s}(212)$
$V_{DC}/6$	$\vec{V}_{2l}(220)$, $\vec{V}_{4l}(022)$, $\vec{V}_{6l}(202)$ $\vec{V}_{1s}(211)$, $\vec{V}_{3s}(121)$, $\vec{V}_{5s}(112)$
0	$\vec{V}_z$ (111) All medium vectors: $\vec{V}_{1m}(210)$, $\vec{V}_{2m}(120)$, $\vec{V}_{3m}(021)$, $\vec{V}_{4m}(012)$, $\vec{V}_{5m}(102)$, $\vec{V}_{6m}(201)$
$-V_{DC}/6$	$\vec{V}_{1l}(200)$, $\vec{V}_{3l}(020)$, $\vec{V}_{5l}(002)$ $\vec{V}_{2s}(110)$, $\vec{V}_{4s}(011)$, $\vec{V}_{6s}(101)$
$-V_{DC}/3$	$\vec{V}_{1s}(100)$, $\vec{V}_{3s}(010)$, $\vec{V}_{5s}(001)$
$-V_{DC}/2$	$\vec{V}_z(000)$

Due to the capacitive nature of the CM circuit, CM currents are generated by high frequency voltage components produced by large *dV/dt*, which appear during the step transitions of the CM voltage. Consequently CM currents are attenuated by keeping the CM voltage as constant as possible and by reducing the amplitude of the voltage transitions. In other words, CM currents can be attenuated by achieving a reduction of the high frequency content in the CM voltage spectrum. It can be observed how the voltage step between consecutive voltage levels is $1/3V_{DC}$ for the two-level VSI and $1/6V_{DC}$ for the three-level VSI. Moreover, the redundancy of some the switching configurations in the three-level VSI can be employed to reduce the number of step transitions in the CM voltage and the amplitude of these transitions.

Regarding the undesired effects produced by the CM current, they can be summarized as follows:

- Degradation of the motor bearings due to the current circulating through them, and the resulting reduction of their lifetime.
- Generation of EMI.
- Additional power losses.

The trend towards an increase of the switching frequency of the VSI to improve the control performance gives rise to these negative effects. From this point of view it is beneficial to keep the switching frequency as low as possible.

The reduction of the CM voltage and current achieved by means of multilevel converters can avoid in some cases alternative solutions such as:

- The utilisation of insulated bearings (ceramic bearings).
- The connection of the shaft to ground by means of a brush, which requires maintenance.
- The use of output filters.

These solutions increase the cost and installation issues resulting from the use of extra equipment.

3.6 Comparison: two-level VSI vs. three-level VSI

A simulation has been carried out to compare the standard two-level VSI and the three-level NPC VSI. The main parameters of the simulation are:

- Load: three-phase star-connected Resistive-Inductive load. R =1 Ω, L =200 mH.
- V_{DC} =537 V.
- Control: Sinusoidal PWM. Carrier frequency f_c =2000 Hz, output frequency f_o =50 Hz, modulation index m=0.8.

The results shown in the following figures are the output line voltage of the VSI (V_{AB}) (see Fig. 3-16 and Fig. 3-17); the phase voltage in the load (V_{An}) (see Fig. 3-18 and Fig. 3-19); and the line (or phase) current in the load (i_A) (see Fig. 3-20 and Fig. 3-21). The frequency spectrum of these variables is also calculated by means of the Fast Fourier Transform (FFT) and shown in those figures. Finally, the Total Harmonic Distortion (THD) calculation is made by means of the following expression:

$$THD = 100\frac{\sqrt{V_{RMS}^2 - V_{FRMS}^2}}{V_{FRMS}} = 100\sqrt{\frac{2V_{RMS}^2}{V_{F\max}^2} - 1} \tag{3.22}$$

The results obtained clearly show a reduction of the harmonic distortion in the output voltage and current waveforms when using a three-level VSI. It can also be observed the higher number of levels and reduced size of the steps in the voltage waveforms of the three-level VSI as stated in Table 3-V.

In Fig. 3-22 and Fig. 3-23 the CM voltage and its frequency spectrum is shown for the two-level VSI and the three-level VSI respectively. It can be seen how the voltage steps and high frequency content of the CM voltage is reduced when using a three-level VSI.

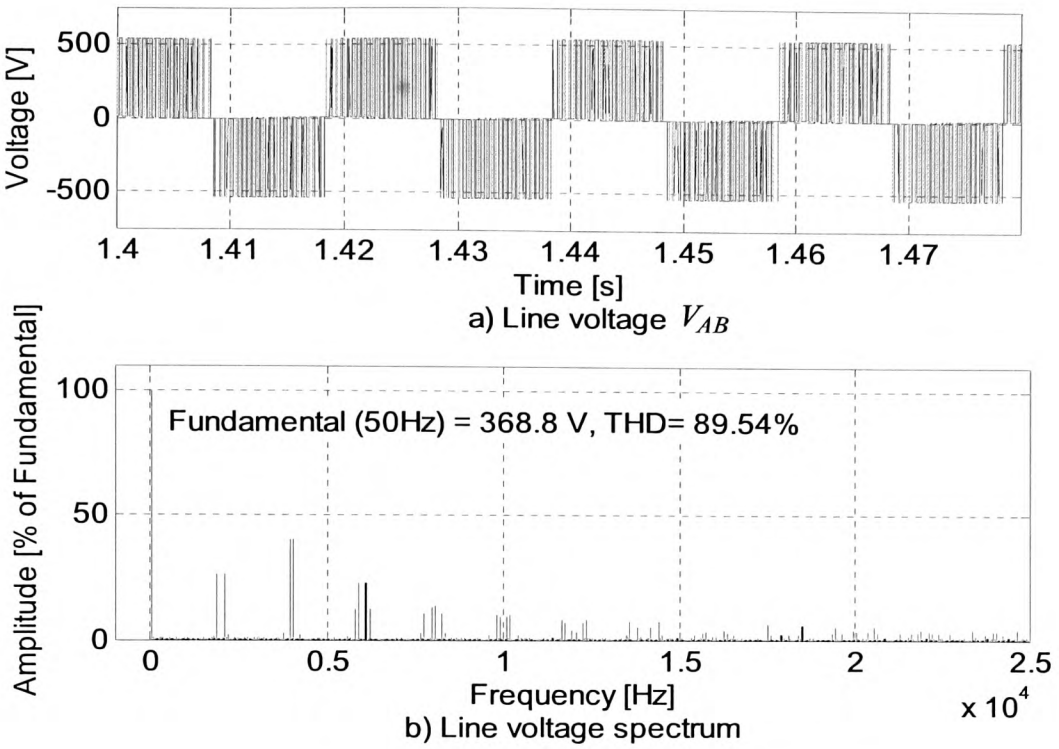

Fig. 3-16 Line voltage and frequency spectrum for the two-level VSI

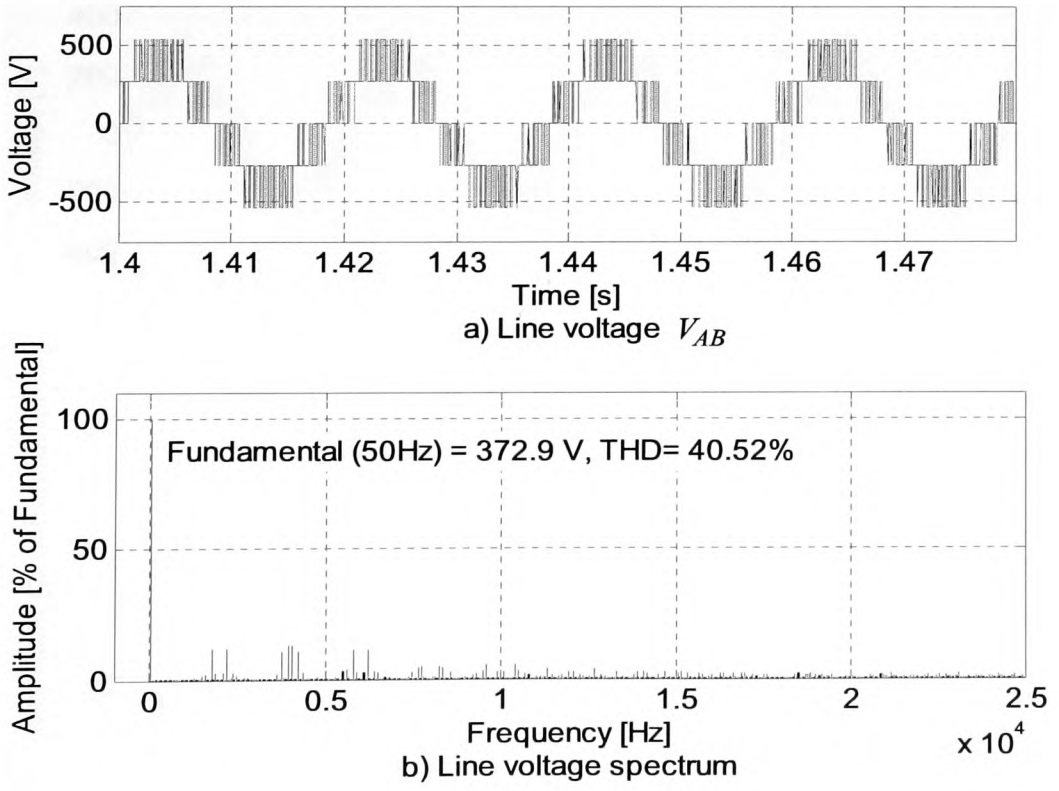

Fig. 3-17 Line voltage and frequency spectrum for the three-level VSI

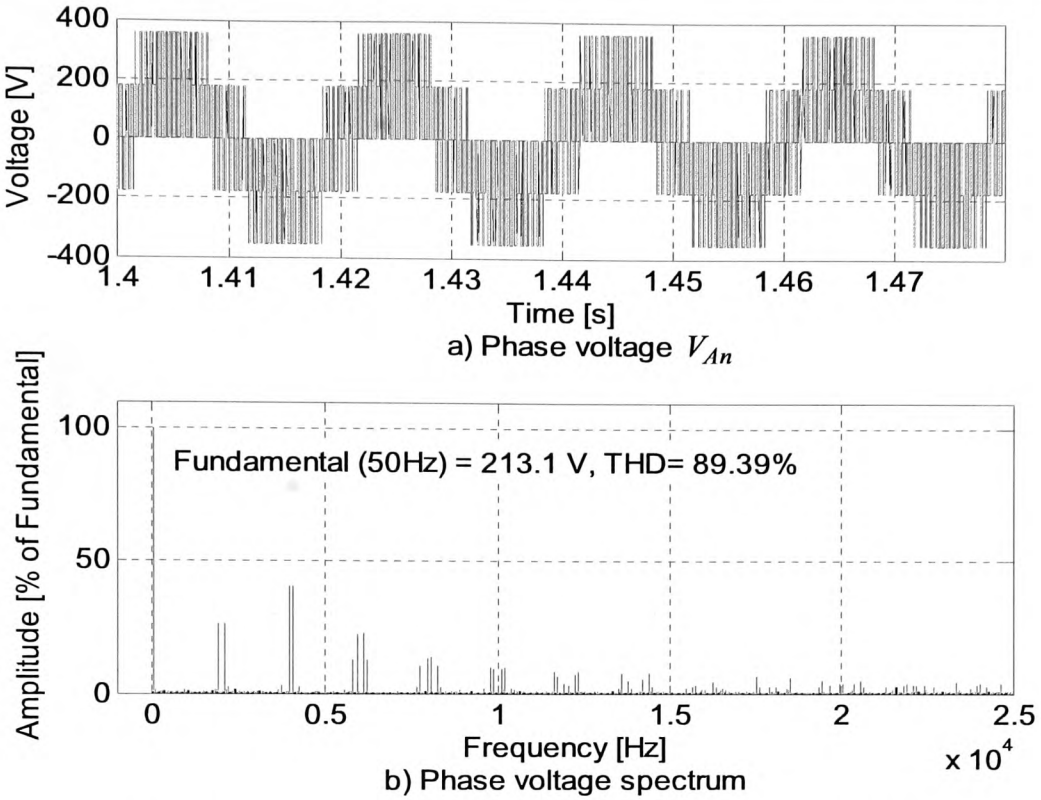

Fig. 3-18 Phase voltage and frequency spectrum for the two-level VSI

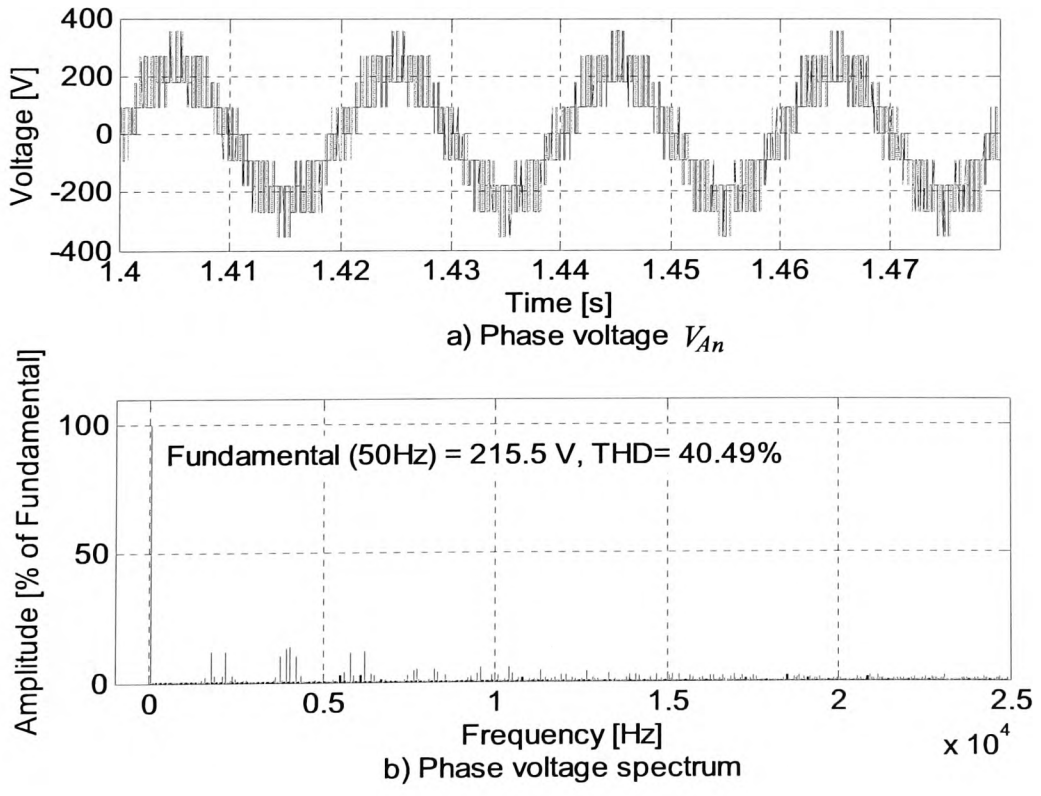

Fig. 3-19 Phase voltage and frequency spectrum for the three-level VSI

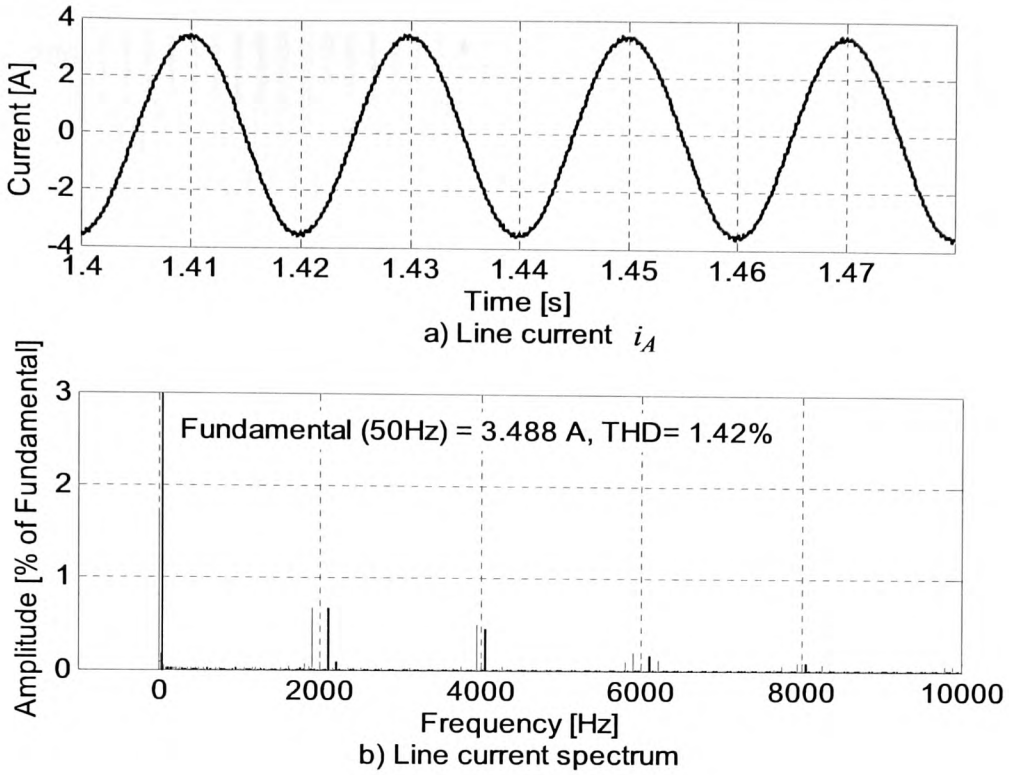

Fig. 3-20 Line current and frequency spectrum for the two-level VSI

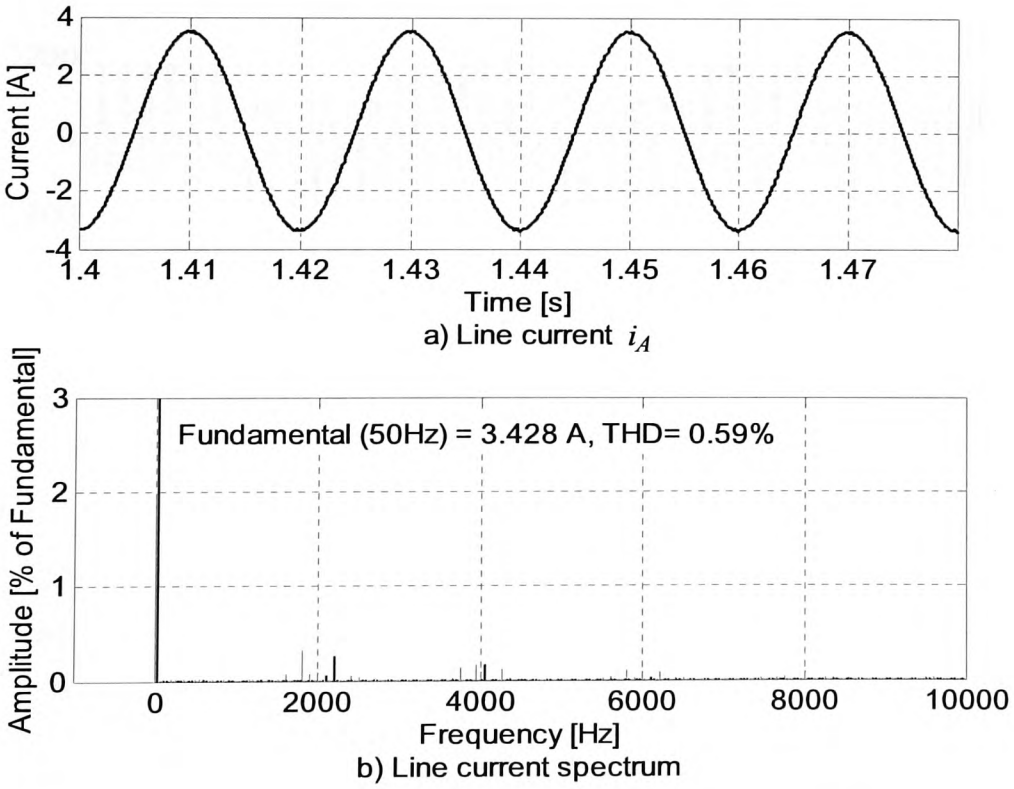

Fig. 3-21 Line current and frequency spectrum for the three-level VSI

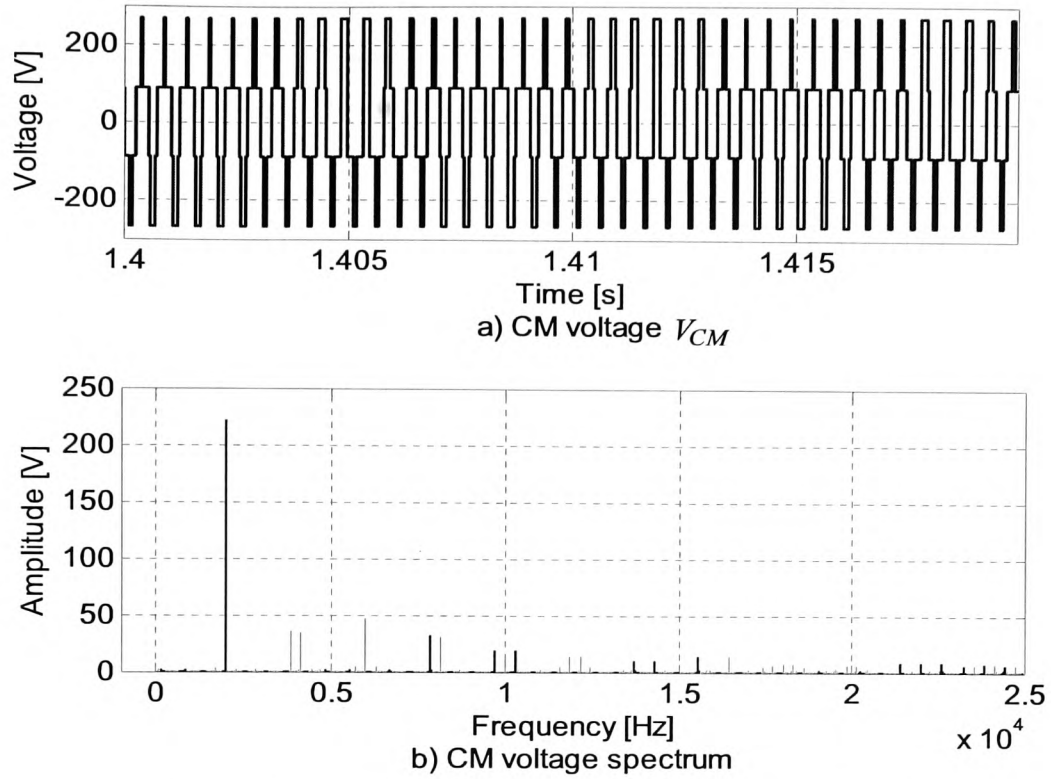

Fig. 3-22 CM voltage and frequency spectrum for the two-level VSI

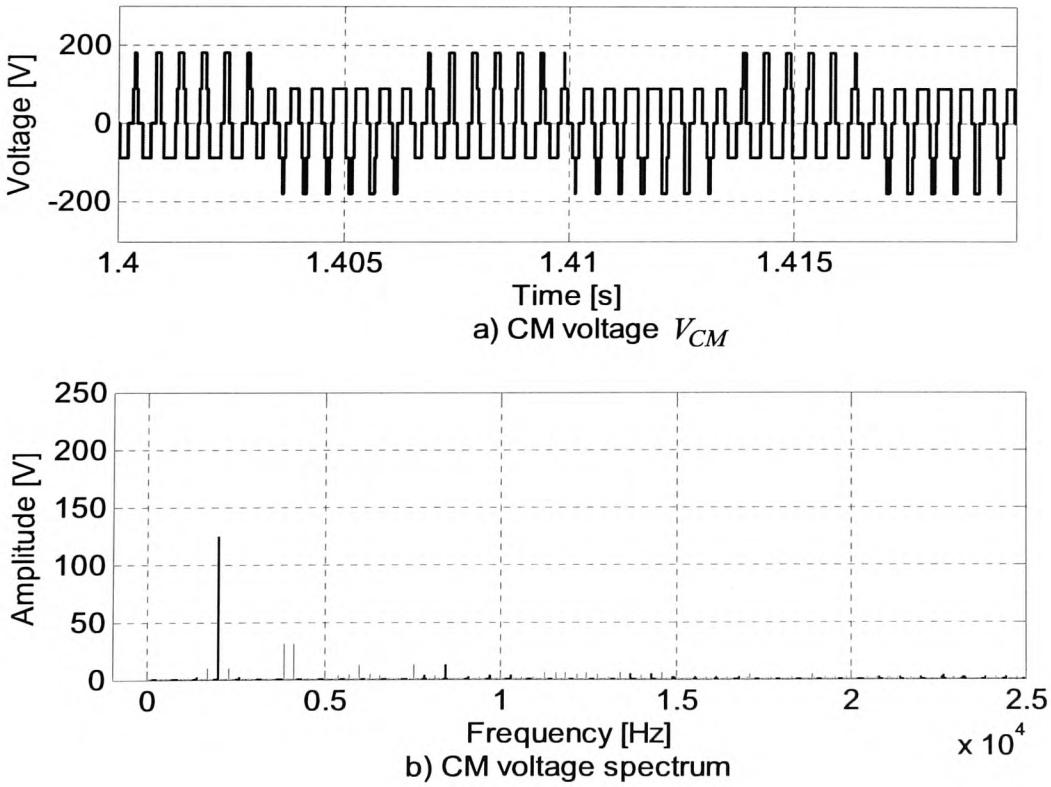

Fig. 3-23 CM voltage and frequency spectrum for the three-level VSI

The reduction in the THD of the voltage and current waveforms achieved by the three-level VSI in comparison with the two-level VSI is summarized in Table 3-IX. It can be observed how the THD values are approximately halved when the three-level VSI is employed.

Table 3-IX Comparison of THD values

	Two-level VSI	**Three-level VSI**
Line voltage	89.54 %	40.52 %
Phase voltage	89.39 %	40.49 %
Line current	1.42 %	0.59 %

The average switching frequency of semiconductor devices is equal to the carrier frequency (2000 Hz) for two-level VSI, while it is reduced to one half of the carrier frequency (1000 Hz) for the three-level VSI. This reduction leads to lower stress and power losses in the semiconductor devices.

3.7 Interim conclusions

The existing technology for power conversion in variable speed drives for IMs has been presented in this chapter. The two-level VSI is still the standard solution for DC to AC conversion due to its simple structure, compactness, low cost, good regulation capabilities, high efficiency and the open-circuit protection it offers.

Nevertheless the two-level VSI presents some technological limitations and undesired features that can be listed as follows:

- The maximum voltages supported by different types of semiconductor devices limits the maximum DC-link voltage that can be employed. This limitation is particularly restrictive if fast switching technologies are employed. The solution to work with higher voltage levels based on series connection of switches presents some problems concerning the control and the voltage balance of the switches.
- The output line voltages of the VSI are composed of pulses with and amplitude equal to the DC-link voltage, which contain high harmonic distortion. PWM techniques have the property of moving the harmonics from low frequencies to the switching frequency zone and multiples of it, but with no significant reduction of the total voltage harmonic distortion.

- The strong voltage steps (*dV/dt*) in the output voltages produce high voltage peaks in the motor terminals due to the parasitic inductance and capacitance present in the motor cables. These voltage peaks contribute to the degradation of the windings insulation material. Moreover the high rate of voltage change also creates a non-uniform voltage distribution among the winding turns.
- A VSI is not an ideal balanced source and the CM voltage is therefore different from zero. In a two-level VSI none of the switching combinations produces a null CM voltage. The presence of high *dV/dt* due to the steps in the CM voltage waveform produces leakage currents (CM currents) to flow through the parasitic capacitances between cables, different parts of the motor and ground. The undesired effects of these currents are the generation of EMI and the degradation of the windings insulation and motor bearings.

Multilevel converter topologies are the alternative to overcome and minimise these limitations and problems. Furthermore, they can extend the application of power electronic systems to higher power and voltage levels. The main advantages of multilevel converters can be summarized as follows:

- Higher voltages and power levels can be achieved and faster semiconductor devices can be used.
- Distortion in the current and voltage waveforms is reduced.
- Switching frequency is reduced. Stress and losses in the semiconductor devices are therefore reduced.
- Lower *dV/dt*, CM voltage, CM current and EMI are generated.
- The requirement of extra passive components such as output filters or snubber circuits can be eliminated or reduced in size in some cases.

The main disadvantage of multilevel converters is the higher number of components required which increases the cost and complexity, while the reliability is reduced. Regarding the control algorithm to be utilised it also becomes more complex.

The main types of multilevel converter described in this chapter are the diode-clamped converter, the floating-capacitor converter and the cascaded multi-cell converter.

Among multilevel converters, the three-level diode-clamped (or NPC) VSI can be considered the most widely studied and applied topology. Several commercial drives incorporate this technology for low voltage and medium voltage applications. One of the issues to be considered for this particular converter is the voltage balance of the DC-

link capacitors. The NP voltage balance is only affected by small and medium vectors due to the connection of one of the load phases to the NP. The existing redundancy of switching combinations for small vectors can be employed to balance the NP voltage. This can be done because the two redundant switching combinations that exist for each small vector produce opposite directions of the NP current.

The advantages of the three-level NPC VSI when compared to the standard two-level VSI have been demonstrated in the simulation results presented. These results illustrate the increased number of voltage levels provided by the three-level VSI, and the reduction in amplitude of the voltage steps. The frequency spectrum of the line and phase voltages shows a reduction of the harmonic distortion. This reduction is also present in the line currents. The CM voltage is reduced and presents smaller voltage steps, which result in a frequency spectrum with lower content at high frequencies. Finally, the average switching frequency of the semiconductor devices is halved in the three-level VSI (sinusoidal PWM is employed in the simulation). The lower frequency and voltage supported by the semiconductor devices reduces their stress and losses.

Chapter 4: Direct Torque Control

Summary – *The intention of this chapter is to introduce and describe the DTC method for control of IMs. The description of DTC includes its principle of operation, main features, advantages and disadvantages. Problems associated with DTC are then presented and discussed. Finally, a variety of methods proposed in the past years to improve the features of DTC are presented.*

4.1 Introduction

Variable speed and torque control is required by many applications employing electrical motors and leads to higher productivity and efficiency in the processes. In spite of the control complexity the advantages of the IM make it the most suitable choice to satisfy the requirements of most applications. In the past, appropriate control methods have been investigated to satisfy the requirement of variable speed and torque control and a family of control methods for IMs has been developed. These control methods can be divided into two main groups: scalar controllers and vector controllers. Scalar controllers are widely employed due to their simplicity and satisfactory performance in many applications. Nevertheless for more demanding applications vector controllers can provide torque control and the best response and precision.

Vector controllers are based on the motor model and the relationships which are valid for transients and steady-state operation. These methods aim to control the instantaneous voltage, current and flux linkage space vectors. In the early 1970s the concept of vector control was introduced with the FOC method proposed by Hasse [4] and Blaschke [5]. Like in a DC motor, FOC can achieve a decoupled control of the motor flux and torque. Nowadays it can be considered an established technique and it is available in many commercial drives from different manufacturers. Nevertheless, in the mid 1980s when the trend was to adopt FOC as the standard solution for high-performance drives, a possible alternative to FOC appeared introduced by Takahashi and Noguchi and known as DTC [6]. At the same time M. Depenbrock introduced a similar idea under the name Direct Self-Control (DSC) [7]. Theses two methods, which are based on the same principle, provide a decoupled control of torque and flux, with a very simple structure and a very fast toque response. The first commercial drive based on the DTC principle was developed by the company ABB and it was commercially launched in 1995 [8-11]. Patents related to the DTC method can be found in [44] and [45]. Nowadays DTC has gained a large acceptance from industry and academia, and is still the subject of study and further research [12, 13]. Since the introduction of the DTC method many authors have presented some modifications to improve the performance and solve some of the drawbacks of this strategy [12].

A possible classification of the variable speed control methods for IMs is presented in Fig. 4-1, and the DTC method is placed among them [12, 46]. In this figure the control

methods derived from the DTC principle are specified in more detail and will be described in the literature review presented in section 4.8.

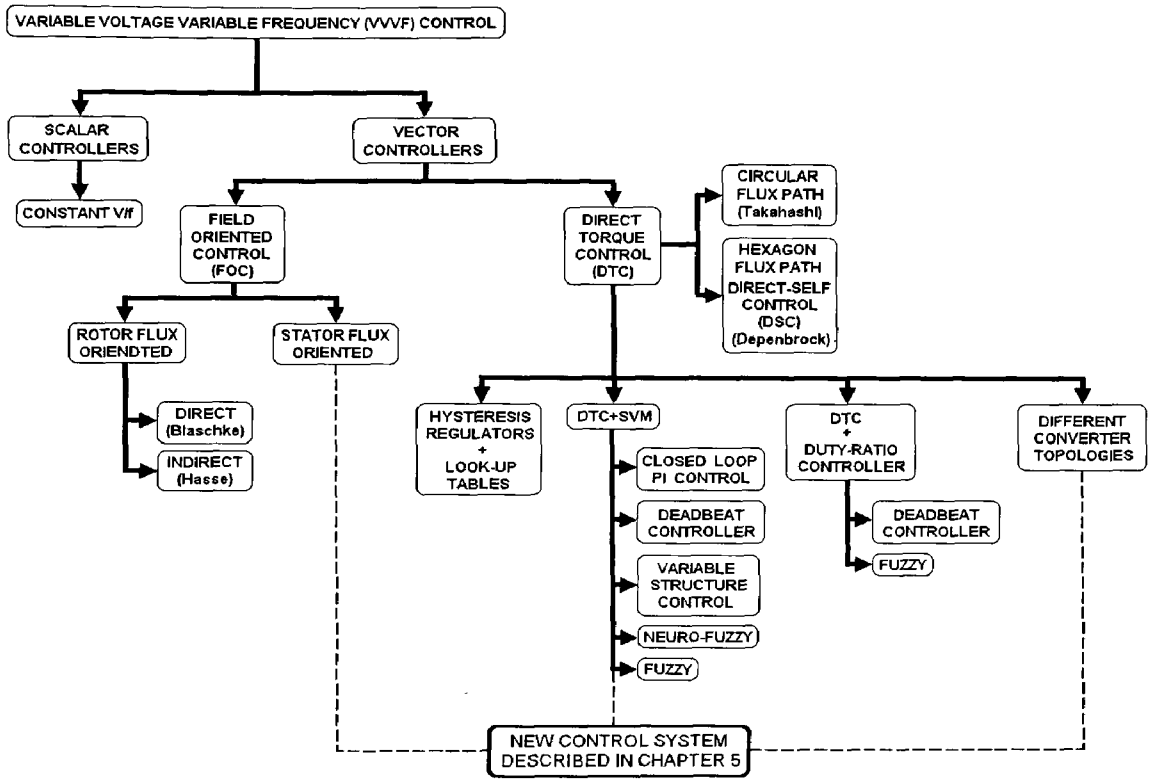

Fig. 4-1 Variable speed control methods for IMs

The new control method proposed in this thesis and described in Chapter 5 is also included in Fig. 4-1. It can be observed how the new method is connected with several solutions since it employs the stator flux orientation, a different converter from the standard two-level VSI and a reference voltage vector is generated similarly to the DTC with Space Vector Modulation (SVM) methods.

4.2 The Classical DTC method

In order to understand the DTC principle some of the equations of the IM need to be reviewed. The VSI is able to control the stator voltage vector applied to the IM. The relationship between the stator voltage vector and the stator flux vector is given by the following equation:

$$\vec{u}_s = R_s \vec{i}_s + \frac{d\vec{\psi}_s}{dt} \tag{4.1}$$

If the voltage drop in the stator resistance is neglected the following expression is obtained:

$$\vec{u}_s \approx \frac{d\vec{\psi}_s}{dt} \quad ; \quad \vec{u}_s \approx \frac{\Delta\vec{\psi}_s}{\Delta t} \quad ; \quad \Delta\vec{\psi} \approx \vec{u}_s \Delta t \tag{4.2}$$

From the above equation it is apparent that the variation of the stator flux vector has the direction of the stator voltage vector, and its amplitude is proportional to voltage amplitude and the time interval during which this voltage vector is applied.

In Chapter 2 various equations for the electromagnetic torque were presented. In one of those equations the electromagnetic torque is expressed as a function of the stator flux and the rotor flux vectors as follows:

$$\Gamma_e = -\frac{3}{2} P \frac{L_m}{L_s L_r - L_m^2} \vec{\psi}_s \times \vec{\psi}_r' \tag{4.3}$$

The above expression can be rewritten as follows:

$$\Gamma_e = \frac{3}{2} P \frac{L_m}{L_s L_r - L_m^2} |\vec{\psi}_s| |\vec{\psi}_r'| \sin(\gamma_s - \gamma_r) \tag{4.4}$$

By considering the moduli of the rotor flux and stator flux vectors to be constant, torque can be controlled by changing the relative angle between both flux vectors. It should be noted that the rotor time constant is larger than the stator one, and consequently the rotor flux changes more slowly than the stator flux. Thus torque can be controlled by quickly varying the stator flux vector angle, which in turn changes its relative angle with the rotor flux vector.

Taking into account the considerations above, the desired decoupled control of the stator flux modulus and torque is achieved by varying the radial (x) and tangential (y) components of the stator flux vector. According to equation (4.2) these two components will depend on the components of the stator voltage vector in the same direction. By considering the stator flux vector reference frame (x-y coordinates) with the x axis in the same direction of the stator flux vector, the y component of the stator voltage vector will affect the relative angle between the rotor flux and the stator flux vectors and in turn will control the torque variation according to equation (4.4). On the other hand, the x component of the stator voltage vector will affect the amplitude or modulus of the stator flux vector.

In a VSI-fed IM only a certain set of voltage vectors can be applied to the IM. Fig. 4-2 shows the stator flux vector in the α-β plane, and the effect of the different VSI states regarding torque and stator flux modulus variation. The α-β plane is divided into six different sectors as illustrated in Table 4-I.

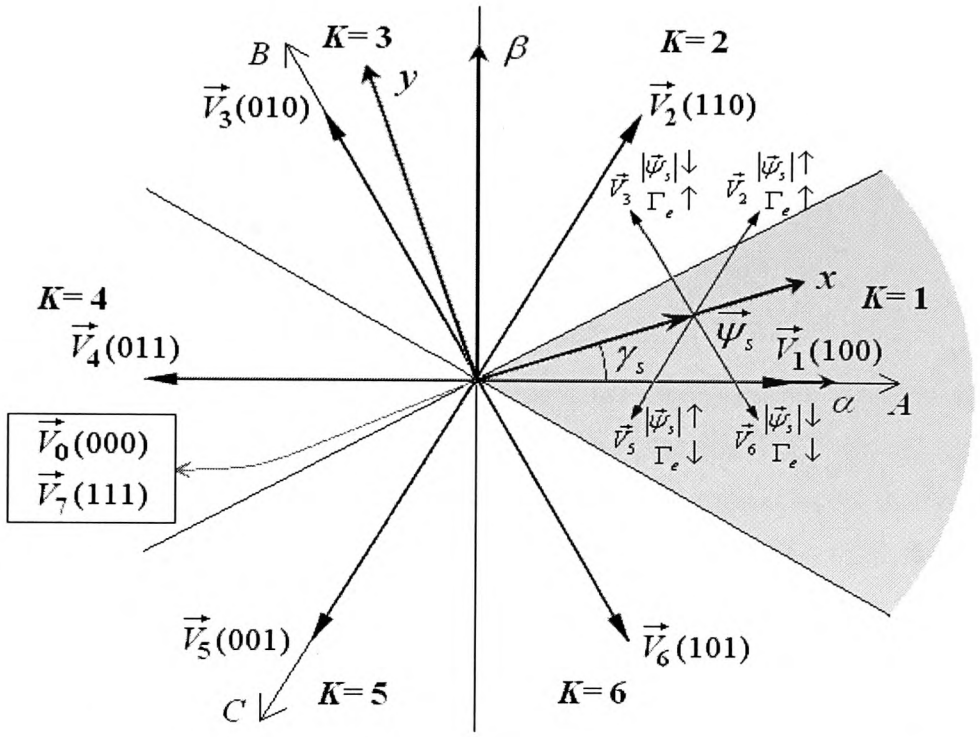

Fig. 4-2 Influence of the VSI voltage vectors on the variation of the stator flux modulus and torque

Table 4-I Sector division of the stator flux angle

K	γ_s
1	$-\frac{\pi}{6} \le \gamma_s < \frac{\pi}{6}$
2	$\frac{\pi}{6} \le \gamma_s < \frac{\pi}{2}$
3	$\frac{\pi}{2} \le \gamma_s < \frac{5\pi}{6}$
4	$\frac{5\pi}{6} \le \gamma_s < \frac{7\pi}{6}$
5	$\frac{7\pi}{6} \le \gamma_s < \frac{3\pi}{2}$
6	$\frac{3\pi}{2} \le \gamma_s < \frac{11\pi}{6}$

According to Fig. 4-2, Table 4-II can be written. It can be seen that for sector 1 the voltage vectors $\vec{V}_1$ and $\vec{V}_4$, can increase torque (first 30 degrees) or decrease it (next 30 degrees) depending on the stator flux position inside the sector and therefore they are not employed.

Table 4-II Effect of voltage vectors on the stator flux modulus and torque in sector K=1

Effect	Voltage Vectors
Stator flux modulus increase ($\psi_s\uparrow$)	$\vec{V}_1$, $\vec{V}_2$ and $\vec{V}_6$
Stator flux modulus decrease ($\psi_s\downarrow$)	$\vec{V}_3$, $\vec{V}_4$ and $\vec{V}_5$
Torque increase ($\Gamma_e\uparrow$)	$\vec{V}_2$ and $\vec{V}_3$
Torque decrease ($\Gamma_e\downarrow$)	$\vec{V}_5$ and $\vec{V}_6$

Based on the previous considerations the generic DTC scheme for a VSI-fed IM was developed [6]. This scheme will be referred to as the Classical DTC method (Fig. 4-3). As it can be seen, there are two different control loops corresponding to the magnitudes of the stator flux modulus and torque. The reference values for the stator flux modulus and torque are compared with the estimated values and the resulting error values are fed into a two-level and three-level hysteresis controller respectively (see Fig. 4-4). The outputs of the stator flux error and torque error hysteresis controllers, together with the position of the stator flux vector, are used as the inputs of a look-up table (Table 4-III). The position of the stator flux vector is divided into six different sectors according to Table 4-I. The output of the look-up table is the VSI switching state and the associated voltage vector that will be applied to the IM during a sampling period. The stator flux modulus and torque errors tend to be restricted within their respective hysteresis bands. The estimation of the stator flux and torque is required, which can be performed by means of two different phase currents, the state of the VSI and the voltage level in the DC-link. This estimator will be presented in section 4.4.1. An accurate estimation of the stator flux and torque is crucial in order to obtain a satisfactory performance when employing the DTC method. Several methods have been proposed to improve the accuracy of the estimator [46].

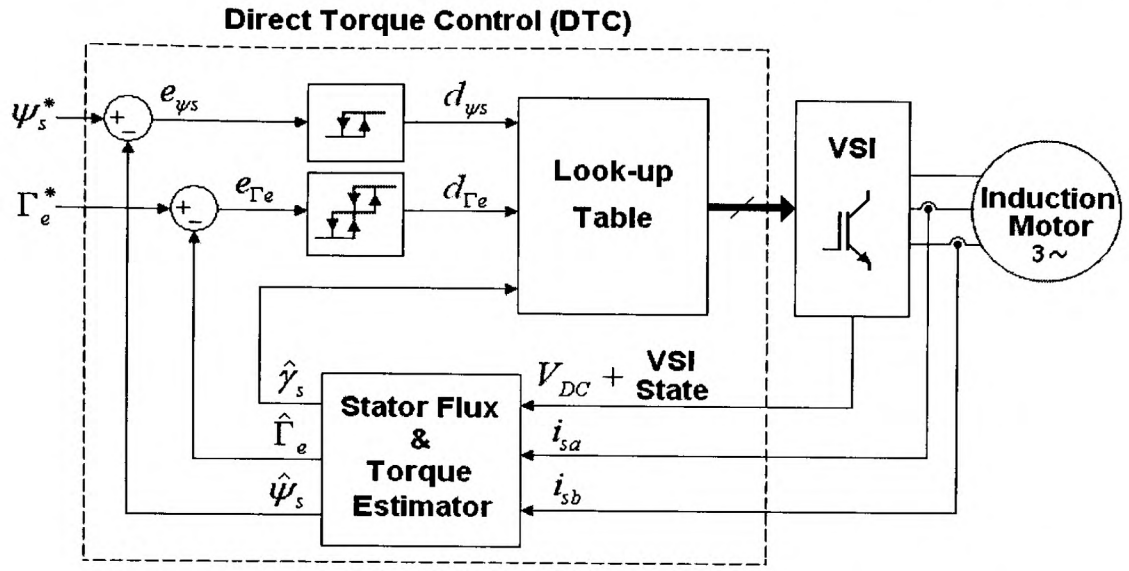

Fig. 4-3 The Classical Direct Torque Control scheme

The hysteresis controllers used in the previous control scheme are shown in Fig. 4-4.

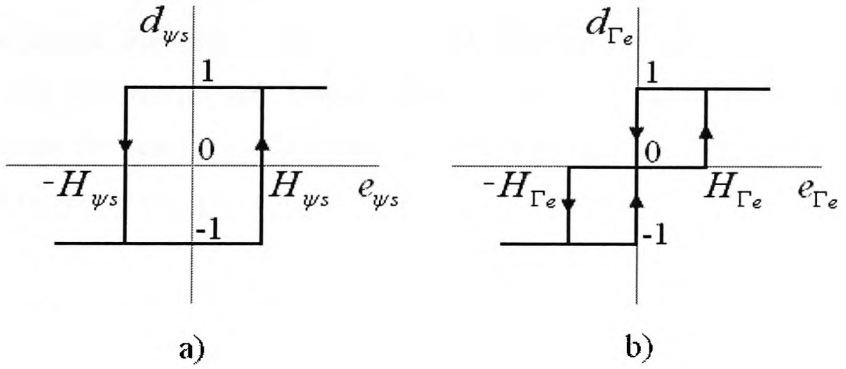

Fig. 4-4 Hysteresis controllers: a) two-level hysteresis controller for the stator flux modulus error; b) three-level hysteresis controller for the torque error

Finally, the Classical DTC look-up table is as follows:

Table 4-III The Classical DTC look-up table

$d_{\psi s}$ / $d_{\Gamma e}$ \ $K(\gamma_s)$		K=1	K=2	K=3	K=4	K=5	K=6
$d_{\psi s}=1$	$d_{\Gamma e}=1$	$\vec{V}_2(110)$	$\vec{V}_3(010)$	$\vec{V}_4(011)$	$\vec{V}_5(001)$	$\vec{V}_6(101)$	$\vec{V}_1(100)$
	$d_{\Gamma e}=0$	$\vec{V}_7(111)$	$\vec{V}_0(000)$	$\vec{V}_7(111)$	$\vec{V}_0(000)$	$\vec{V}_7(111)$	$\vec{V}_0(000)$
	$d_{\Gamma e}=-1$	$\vec{V}_6(101)$	$\vec{V}_1(100)$	$\vec{V}_2(110)$	$\vec{V}_3(010)$	$\vec{V}_4(011)$	$\vec{V}_5(001)$
$d_{\psi s}=-1$	$d_{\Gamma e}=1$	$\vec{V}_3(010)$	$\vec{V}_4(011)$	$\vec{V}_5(001)$	$\vec{V}_6(101)$	$\vec{V}_1(100)$	$\vec{V}_2(110)$
	$d_{\Gamma e}=0$	$\vec{V}_0(000)$	$\vec{V}_7(111)$	$\vec{V}_0(000)$	$\vec{V}_7(111)$	$\vec{V}_0(000)$	$\vec{V}_7(111)$
	$d_{\Gamma e}=-1$	$\vec{V}_5(001)$	$\vec{V}_6(101)$	$\vec{V}_1(100)$	$\vec{V}_2(110)$	$\vec{V}_3(010)$	$\vec{V}_4(011)$

According to Fig. 4-4 the stator flux modulus error after the hysteresis controller can take just two values (1, -1). The torque error after the hysteresis controller, however, can take three different values (1, 0, -1). The zero voltage vectors $\vec{V}_0$ and $\vec{V}_7$ are selected when the torque error is within the given hysteresis limits, and must remain unchanged. It should be noted that the system does not contain any motor parameters or PI controllers, and the decoupled control of both stator flux modulus and torque is achieved without the use of a coordinate transformation. The only adjustable variables are the bands of the hysteresis controllers.

A weakness of the Classical DTC method shown above is that the stator flux level cannot be controlled when the torque reference is zero, and the torque developed is zero, because the output of the look-up table in this situation is a zero vector ($\vec{V}_0$ or $\vec{V}_7$). This produces a slower torque response during the start-up of the IM. In order to overcome this problem the table should be expanded by adding a further state to the stator flux hysteresis comparator [18].

The results in Fig. 4-5 and Fig. 4-6 demonstrate the decoupled control of stator flux modulus and torque which can be achieved with the Classical DTC method.

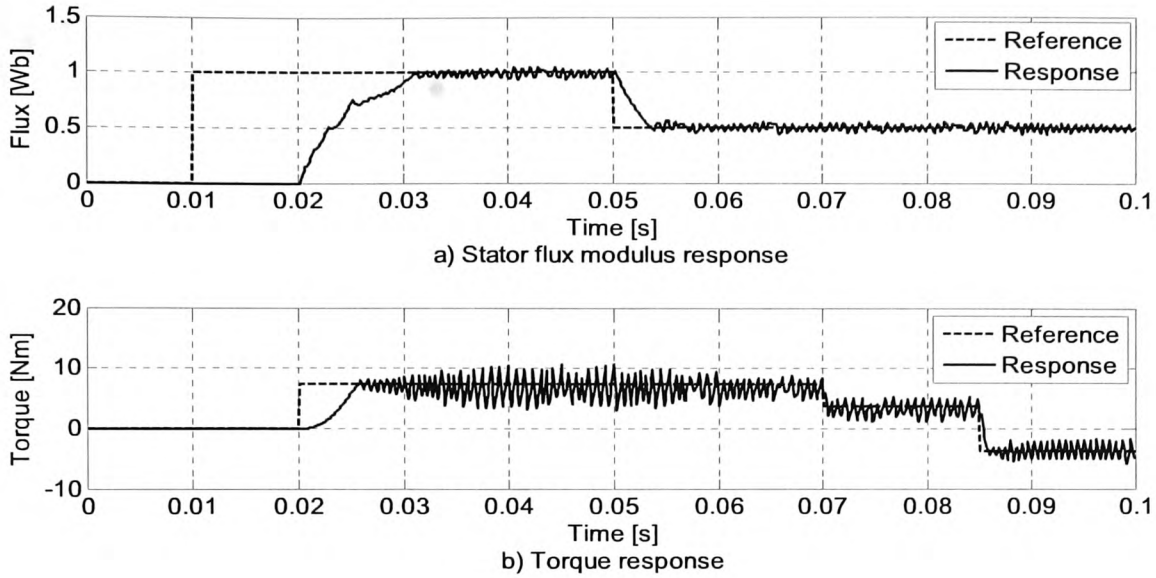

Fig. 4-5 Torque and stator flux modulus response for the Classical DTC method

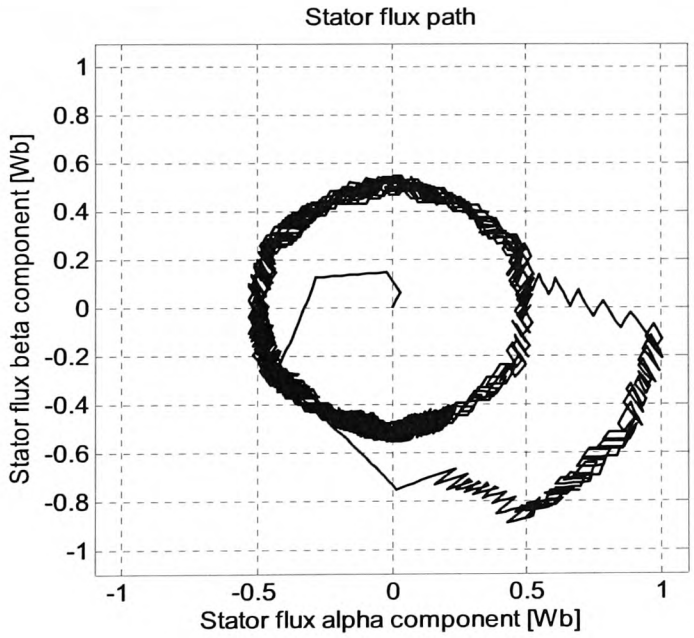

Fig. 4-6 Stator flux path in the α-β plane

It can be seen in Fig. 4-5 that stator flux is not produced until the torque reference is different from 0. The torque rise time is therefore increased during start-up due to the dependency of the torque on the stator flux modulus as can be deduced from equation (4.4). This dependency is also illustrated in Fig. 4-5 when the stator flux modulus is reduced after 0.05 s and the amplitude of the torque oscillation decreases. The stator

flux path is nearly circular in the DTC method proposed by Takahashi, as illustrated in Fig. 4-6 [6].

The main features of DTC are:

- Direct control of the stator flux and torque.
- Indirect control of the stator currents and voltages.
- Approximately sinusoidal stator fluxes and currents.
- Variable switching frequency depending on the hysteresis bands and the IM operating point.
- The estimation of the stator flux and torque is required. The most simple estimation method based on the integration of the stator voltage (see section 4.4.1) is only sensitive to stator resistance variation. Nevertheless, the estimation has to track the fast dynamics of the stator flux and therefore current measurements need to be very precise, with a low presence of noise and cannot employ filtering.
- The motor position or speed is not required to perform the torque control.

The main advantages of DTC are:

- Excellent torque dynamics and minimal torque response time.
- Absence of coordinate transformation (required in FOC).
- Absence of voltage modulator, as well as other controllers such as PID and current controllers (used in FOC).
- Robustness against rotor parameters variation. Only the stator resistance is needed when using the estimator based on the integration of the stator voltage (see section 4.4.1).

These merits are counterbalanced by some drawbacks that will be discussed in section 4.7.

4.3 Direct Self-Control (DSC)

Direct Self-Control (DSC) was mainly devised to reduce the switching frequency of the VSI switches for high power applications whilst keeping a good torque dynamic response [7]. The control scheme is presented in Fig. 4-7.

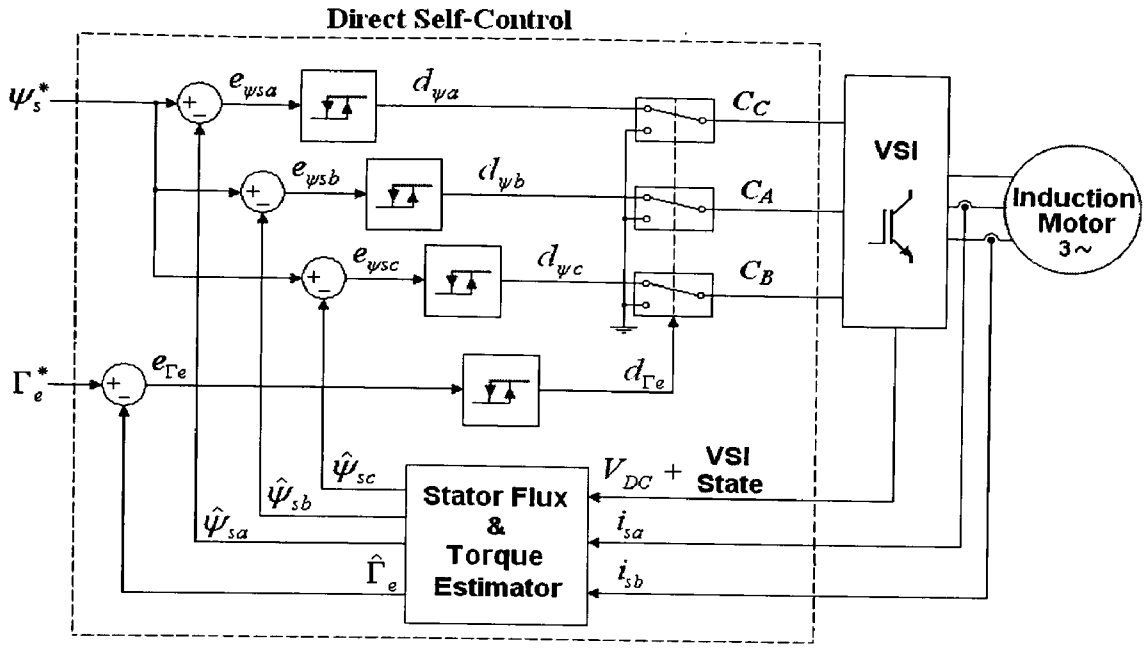

Fig. 4-7 Direct Self-Control scheme

In the DSC system the stator flux error in *a-b-c* components is digitized by means of three different two-level hysteresis controllers where the hysteresis bands are fixed to $\pm\psi_s^*$. The torque is also digitized by a two-level hysteresis controller. The control algorithm can be described as follows:

$$If\ d_{\Gamma e}=1 \quad then\ C_C=d_{\psi a}, C_A=d_{\psi b}, C_B=d_{\psi c}, (active\ vector\ selected)$$

$$If\ d_{\Gamma e}=0 \quad then\ C_A=0, C_B=0, C_C=0, (zero\ vector\ selected)$$

The main features of DSC are [7, 12, 46]:

- The stator flux vector moves along a hexagonal path.
- The stator flux and current waveforms are non-sinusoidal.
- Low switching frequency (dependent on the hysteresis torque band).
- Excellent torque dynamics.

Low switching frequency and fast torque control even in the field-weakening region are the main reasons why the DSC method is convenient for high power traction drives [12].

4.4 Stator flux and torque estimator

DTC can achieve a decoupled control of stator flux modulus and torque as shown in Fig. 4-5. As it can be seen in the control scheme in Fig. 4-3 the variables that need to be estimated to close the two existing control loops are the stator flux modulus and torque. Both variables are difficult and expensive to measure with transducers and this option is unfeasible in a commercial implementation. Thus they need to be estimated by other means. This estimation can be performed with the knowledge of the motor model and measuring other signals such as stator currents, stator voltages, rotor speed and position. Current and voltage transducers are inexpensive and can be easily incorporated into the drive system. Nevertheless, position and speed transducers are more expensive and difficult to integrate with the drive system. Thus an implementation which does not incorporate them is more desirable. This kind of implementation, without position and speed transducers, is generically known as sensorless.

The following sections will present two possibilities for implementing the stator flux and torque estimation.

4.4.1 Estimator using i_{sa}, i_{sb}, V_{DC} and the VSI state

Most of the estimators used for DTC are based on the voltage model of the IM, where only current and voltage are required to calculate the stator flux and torque. These methods are less sensitive to the variation of motor parameters and do not require the motor speed or position signals. The basic method of estimating the stator flux in DTC is based on the integration of the motor stator voltage as follows:

$$\vec{\psi}_s = \int_0^t \left(\vec{u}_s - R_s \vec{i}_s\right) dt + \vec{\psi}_{s0} \tag{4.5}$$

The implementation of this method starts by measuring the following variables: i_{sa}, i_{sb}, V_{DC} and the VSI state (represented by C_A, C_B and C_C) as shown in Fig. 4-3.

The α-β components of the stator current vector are first calculated as follows:

$$i_{s\alpha} = i_{sa} \tag{4.6}$$

$$i_{s\beta} = \frac{1}{\sqrt{3}}\left(2i_{sb} + i_{sa}\right) \tag{4.7}$$

Then the α-β components of the stator voltage vector are calculated using the following expressions:

$$u_{sa} = \frac{V_{DC}}{3(n-1)}(2C_A - C_B - C_C) \tag{4.8}$$

$$u_{sb} = \frac{V_{DC}}{3(n-1)}(2C_B - C_A - C_C) \tag{4.9}$$

$$u_{sc} = \frac{V_{DC}}{3(n-1)}(2C_C - C_A - C_B) \tag{4.10}$$

$$u_{s\alpha} = \frac{2}{3}\left(u_{sa} - \frac{1}{2}u_{sb} - \frac{1}{2}u_{sc}\right) \tag{4.11}$$

$$u_{s\beta} = \frac{1}{\sqrt{3}}(u_{sb} - u_{sc}) \tag{4.12}$$

The number of voltage levels of the VSI topology employed is represented by n. The variables C_A, C_B and C_C define the state of each VSI leg, which can take the values {0, 1} in a two-level VSI (n=2); and {0, 1, 2} in a three-level VSI (n=3).

The stator flux α-β components are then calculated using the stator voltage equation as follows:

$$\vec{\psi}_{s\alpha} = \int_0^t \left(\vec{u}_{s\alpha} - R_s\vec{i}_{s\alpha}\right)dt \tag{4.13}$$

$$\vec{\psi}_{s\beta} = \int_0^t \left(\vec{u}_{s\beta} - R_s\vec{i}_{s\beta}\right)dt \tag{4.14}$$

Finally the modulus and angle of the stator flux vector are calculated. It should be noted that for the calculation of the stator flux angle the $\tan^{-1}$ function is used and gives a solution in the range $[-\pi/2, \pi/2]$. The solution can be extended to $[-\pi, \pi]$ by considering the sign of the stator flux α-β components.

$$\left|\vec{\psi}_s\right| = \sqrt{\psi_{s\alpha}^2 + \psi_{s\beta}^2} \tag{4.15}$$

$$\gamma_s = \begin{cases} 0 & (\psi_{s\alpha} = 0 \;\; \& \;\; \psi_{s\beta} = 0) \\ \pi & (\psi_{s\alpha} = 0 \;\; \& \;\; \psi_{s\beta} > 0) \\ -\pi & (\psi_{s\alpha} = 0 \;\; \& \;\; \psi_{s\beta} < 0) \\ \tan^{-1}\left(\dfrac{\psi_{s\beta}}{\psi_{s\alpha}}\right) & (\psi_{s\alpha} > 0) \\ \tan^{-1}\left(\dfrac{\psi_{s\beta}}{\psi_{s\alpha}}\right) + \pi & (\psi_{s\beta} > 0 \;\; \& \;\; \psi_{s\alpha} < 0) \\ \tan^{-1}\left(\dfrac{\psi_{s\beta}}{\psi_{s\alpha}}\right) - \pi & (\psi_{s\beta} < 0 \;\; \& \;\; \psi_{s\alpha} < 0) \end{cases} \tag{4.16}$$

The torque value is then obtained using the following expression:

$$\Gamma_e = \frac{3}{2} P\left(\psi_{s\alpha} i_{s\beta} - \psi_{s\beta} i_{s\alpha}\right) \tag{4.17}$$

The only motor parameter involved in the calculations is the stator resistance, which can be easily measured. The main drawback of this method is the application of an open-loop pure integrator because of its DC drift and initial condition problem [46]. Some solutions have been proposed to improve the method described which entail using a closed-loop integrator with a low-pass filter instead of the pure integrator to correct the DC offset caused by the wrong initial conditions [13, 46]. Another alternative to correct the estimation is the use of current feedback [10].

In order to improve the estimator performance and robustness several solutions have been proposed to estimate the variation of the stator resistance. Some solutions are based on the thermal model of the motor as the variation of the resistance is due to thermal changes [10]. Other alternatives employ PI or fuzzy logic techniques to correct the stator resistance value depending on the stator current variation [47].

4.4.2 Estimator using i_{sa}, i_{sb} and ω_m

An alternative to the method described above is an estimator using i_{sa}, i_{sb} and ω_m. This estimator has the disadvantage of requiring the motor speed information. Since the speed sensor is available in the laboratory setup described in Chapter 6, this method has been considered because it has proved to be effective and good estimation is achieved [18, 48].

First the α-β components of the stator current vector are calculated as in equation (4.6) and equation (4.7). The rotor voltage and rotor flux equations in α-β components are expressed as follows:

$$0 = R_r i_{r\alpha} + \frac{d\psi_{r\alpha}}{dt} + P\omega_m \psi_{r\beta} \tag{4.18}$$

$$0 = R_r i_{r\beta} + \frac{d\psi_{r\beta}}{dt} - P\omega_m \psi_{r\alpha} \tag{4.19}$$

$$\psi_{r\alpha} = L_r i_{r\alpha} + L_m i_{s\alpha} \tag{4.20}$$

$$\psi_{r\beta} = L_r i_{r\beta} + L_m i_{s\beta} \tag{4.21}$$

If the previous equations are combined, the rotor flux can be calculated using the following equations:

$$R_r \psi_{r\alpha} + L_r \frac{d\psi_{r\alpha}}{dt} = L_m R_r i_{s\alpha} - L_r P\omega_m \psi_{r\beta} \tag{4.22}$$

$$R_r \psi_{r\beta} + L_r \frac{d\psi_{r\beta}}{dt} = L_m R_r i_{s\beta} - L_r P\omega_m \psi_{r\alpha} \tag{4.23}$$

The stator flux α-β components can be defined using the following expression:

$$\psi_{s\alpha} = L_s i_{s\alpha} + L_m i_{r\alpha} \tag{4.24}$$

$$\psi_{s\beta} = L_s i_{s\beta} + L_m i_{r\beta} \tag{4.25}$$

Combining (4.22), (4.23), (4.24) and (4.25) the following equations are obtained to calculate the stator flux:

$$\psi_{s\alpha} = \frac{L_x}{L_r} i_{s\alpha} + \frac{L_m}{L_r} \psi_{r\alpha} \tag{4.26}$$

$$\psi_{s\beta} = \frac{L_x}{L_r} i_{s\beta} + \frac{L_m}{L_r} \psi_{r\beta} \tag{4.27}$$

The stator flux modulus and angle are obtained using the expressions (4.15) and (4.16). The torque value is obtained by means of (4.17).

4.5 Motor speed estimation

The motor speed can be measured using different types of sensors, mainly incremental and absolute encoders or resolvers. Alternatively, it can be estimated to reduce the cost and installation issues of speed and position sensors. Intense research is devoted to improve the speed estimation and nowadays several sensorless methods have been developed. The biggest challenge nowadays is still the measurement in the low speed range at near zero speed.

One of the possibilities to calculate the speed of the motor is presented in the following expression [10, 46]:

$$\omega_m = \frac{\omega_s - \omega_r}{P} \tag{4.28}$$

The synchronous speed ω_s can be obtained from the stator flux estimation. The angular frequency of the rotor flux can be obtained from the following expressions:

$$\omega_r = \frac{\Gamma_e R_r}{|\vec{\psi}_r|^2} \tag{4.29}$$

$$|\vec{\psi}_r| = \sqrt{\psi_{r\alpha}^2 + \psi_{r\beta}^2} \tag{4.30}$$

$$\psi_{r\alpha} = \frac{L_r}{L_m}\psi_{s\alpha} + \frac{L_x}{L_m} i_{s\alpha} \tag{4.31}$$

$$\psi_{r\beta} = \frac{L_r}{L_m}\psi_{s\beta} + \frac{L_x}{L_m} i_{s\beta} \tag{4.32}$$

This method requires the knowledge of almost all the parameters of the IM.

4.6 Industrial applications of DTC

The first motor drive incorporating DTC was developed by ABB and launched in 1995. The ABB ACS 600 has become a benchmark product in the AC drives industry since then [8-11]. The ACS 600 product family has found wide application in industry. Examples of fields of application are:

- Heating, Ventilation and Air conditioning (HVAC): fans, pumps, compressors.
- Cement industry: fans, kilns, conveyors.
- Chemical industry: pumps, fans, mixers, processing lines.

- Cranes and harbours.
- Food and beverage: mixers, conveyors, centrifuges, ovens, bottling tables.
- Marine applications.
- Material handling: conveyors, hoists, positioning.
- Metal industry: roller tables, processing lines, cranes.
- Mining and mineral processing: conveyors, dredgers, crushers.
- Oil and gas industry: fans, pumps, centrifuges, compressors.
- Plastic and rubber industry: mixers, extruders, conveyors, processing lines.
- Power plants: pumps, fans, conveyors.
- Printing: printing machinery, winders.
- Pulp and paper industry: sectional drives, pumps, fans, kilns, debarking, screws, washers.
- Textile industry: mixers, extruders, textile machines.
- Water treatment: pumps, compressors, conveyors.
- Wood handling: sawmills, debarking lines, lathes, plywood lines.

In the ACS600, thanks to its 40 MHz Toshiba DSP and ASIC hardware, the entire control loop is closed every 25 μs, calculating the modulus of the stator flux, its position, the electromagnetic torque and the rotor speed. It allows an accurate control of motor speed (error between ±0.1% and ±0.5% for sensorless speed control; and ±0.01% for speed control with pulse encoder). Torque rise time is very short, typically below 3 ms [8, 11].

Some additional features and functionalities can be summarized as follows:

- Some motor parameters can be automatically identified during initialization and commissioning (stator resistance, stator inductance, magnetising inductance, inertia and some others).
- The switching frequency can be controlled by varying the hysteresis parameters depending on the electrical frequency.
- A compensation of the stator resistance is made by means of the temperature estimation obtained from the thermal model of the motor.
- Some other special functions are included such as flying start (the motor can be started as fast as possible for DTC in all electromagnetic states), flux braking, flux optimization, supply voltage loss (the DC level is kept constant in power failures

within appropriate limits and the motor remains magnetized, this allows the motor to be loaded immediately as soon as the network recovers).

In 2002 the ACS 600 product family was replaced by a new series of low voltage industrial drives, the ACS 800 (230 to 690 V; 0.55 to 5600 kW), which also incorporates DTC.

As explained in section 3.4.2, DTC is also incorporated in the following series of medium voltage drives: ACS 1000, ACS 6000 and ACS 5000.

4.7 Main drawbacks of DTC

The merits of the Classical DTC method have been highlighted in the previous sections of this chapter. These merits, as for any technical progress, are counterbalanced by several problems and drawbacks that are described in this section. The main drawbacks associated with the Classical DTC method are presented and discussed in the following sections.

4.7.1 Low speed operation

Low speed operation can be problematic when employing the Classical DTC method. As described in section 4.4.1, the basic stator flux estimation method depends on the stator resistance. The variation of the stator resistance caused by temperature changes makes the system behaviour worse due to inaccuracies in the estimation of the stator flux. This effect is particularly important at low speed where the voltage drop in the stator resistance is more significant and cannot be neglected.

Demagnetization effects can also appear at low speed operation due to the more frequent utilisation of zero vectors, which produce a reduction of the stator flux modulus [46, 49].

Furthermore the voltage level required at low speed operation is considerably smaller and far from the voltage delivered to the IM by an active vector applied during the whole sampling period. The consequence is the increase of the torque slopes and ripples at low speed operation.

4.7.2 Problems during start-up

In section 4.2, it was shown that the stator flux modulus cannot be controlled when the torque reference is null. During start-up, the stator flux modulus and torque have to be increased simultaneously. Since both variables are not completely decoupled (torque

depends on the stator flux modulus as shown in equation (4.4)) the result is a slow torque response during start-up [13, 46, 50]. This situation is illustrated in the torque start-up shown in Fig. 4-5. It can be observed how the torque response in the start-up (after 0.02 s) is significantly slower than in the other torque transients shown at 0.07 s and 0.085 s.

4.7.3 Requirement of torque and flux estimators

This implies the necessary parameters identification (the same as for other vector control methods). The estimation is only dependant on the stator resistance for the estimator presented in section 4.4.1. Consequently it is not as sensitive to the variation of the IM parameters as in RFOC, where the rotor parameters are required as well [13]. The stator flux estimation is particularly difficult at low speed operation. Moreover current measurement system has to be very precise (with very low noise and delay) and filtering cannot be employed.

4.7.4 Variable switching frequency

Variable switching frequency is caused by the use of hysteresis controllers and the application of a single switching state during the whole sampling time. Unlike in the PWM methods with fixed PWM frequency, variable switching frequency produces a spread spectrum in the stator voltages and currents [8, 18]. The spread spectrum of the stator phase voltage can be observed in Fig. 4-8.

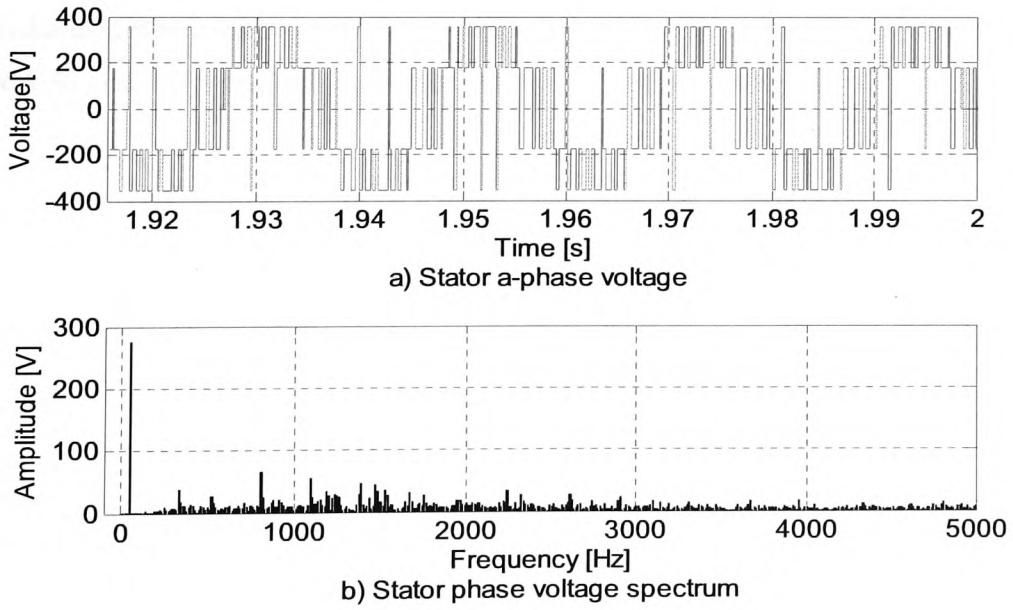

Fig. 4-8 Spread spectrum of the stator phase voltage due to the variable switching frequency

4.7.5 Torque and stator flux ripple

The torque and flux ripple can be high when using the Classical DTC method. This is due to the nature of the control, which incorporates hysteresis controllers and because only a certain set of voltage vectors associated with the VSI can be applied. If the sampling period of the control system is increased these ripples become larger. The reduction of the sampling period can reduce the ripples. This solution, however, has some limitations which are related to the feasibility to implement the control due to the processing capabilities required. Moreover, it implies an increase of the switching frequencies in the semiconductor devices and the resulting increase of the power losses and stress on them. The presence of high torque and flux ripple is one of the main drawbacks of the Classical DTC method [13].

4.7.6 Torque steady-state mean error

The discrete-time digital implementation of the DTC algorithm and the system delays make the control response diverge from the expected behaviour [12]. The result is that the stator flux modulus and torque can exceed the hysteresis bands. A steady-state mean error appears in the torque response as the motor speed increases. This effect is illustrated in Fig. 4-9 and is caused by the torque slopes. At high speed operation negative slopes are more accentuated than the positive ones causing the torque to exceed the upper band of the torque hysteresis controller.

This effect can be attenuated by reducing the sampling time of the control system. Nevertheless, the sampling frequency is limited by the maximum switching frequency of the VSI and the processing speed of the digital control system.

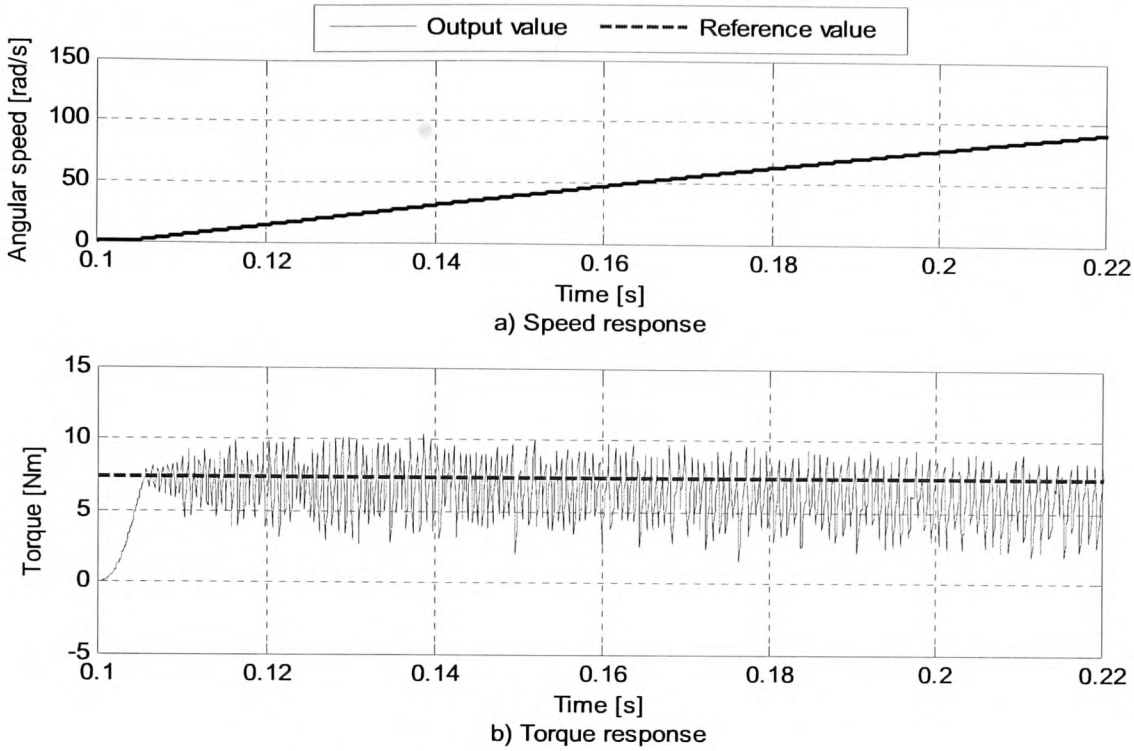

Fig. 4-9 Increase of the torque steady-state mean error

4.7.7 Stator flux modulus distortion in the sector boundaries

The vector selection behaviour is not optimal when the stator flux is in the sector boundaries defined in Table 4-I. The reason is that the effect of a selected voltage vector is considerably different depending on the position of the stator flux vector inside the sector. This effect is illustrated in Fig. 4-10. In order to understand it, the situation when the stator flux vector crosses the border between sector 1 and 2 can be considered. When the stator flux vector enters sector 2, vectors $\vec{V}_3$ and $\vec{V}_4$ are selected to increase the torque according to Table 4-III. In this position of the stator flux vector, the radial component of $\vec{V}_3$ is zero while for $\vec{V}_4$ it has a large negative value. Consequently when torque has to be increased the vectors selected produce a drop of the stator flux modulus (particularly when $\vec{V}_4$ is selected). This drop in turn produces distortions in the stator currents and torque. This effect is more visible when the angular speed of the stator flux vector is high and the amount of voltage vectors employed to drive the stator flux across the sector is smaller.

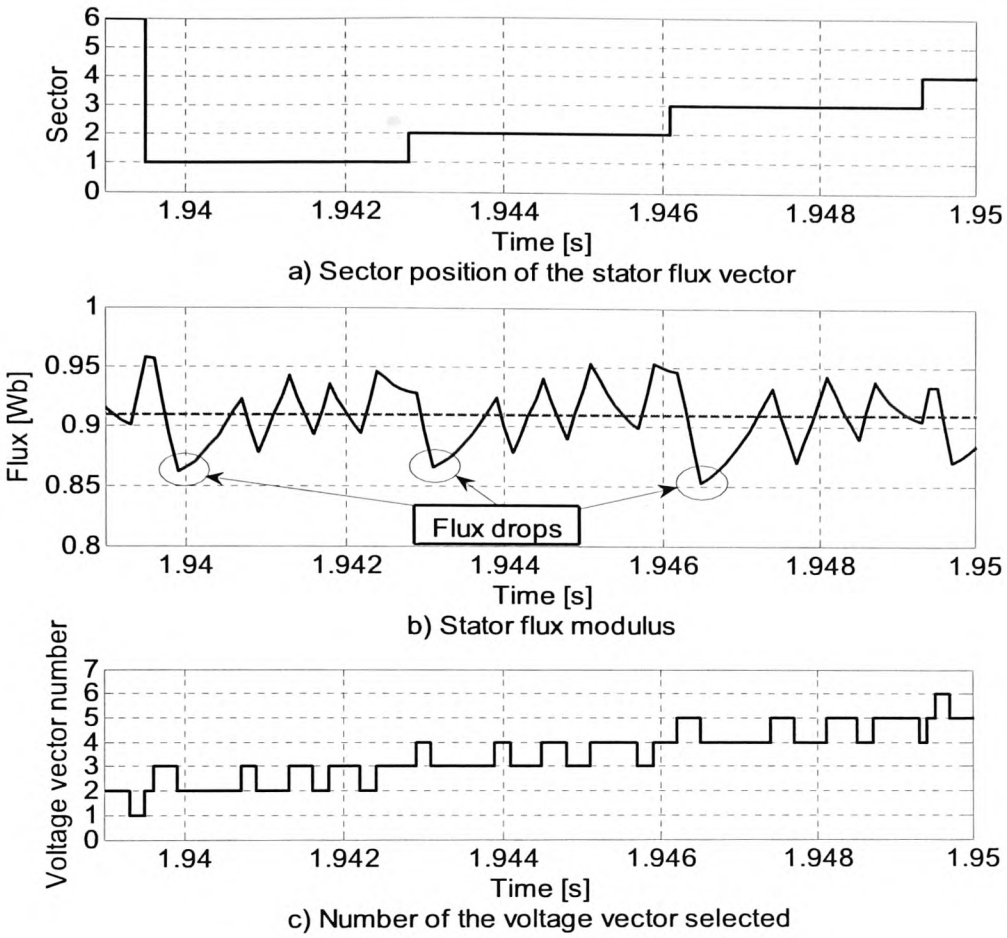

Fig. 4-10 Distortion of the stator flux modulus in the sector boundaries

4.7.8 High harmonic distortion in the stator voltage and current waveforms

The harmonic distortion in the voltage and current waveforms is higher for a similar switching frequency, when compared to other methods which use modulation techniques such as FOC [51, 52]. Furthermore, the distortion caused by the effect of the sector boundaries previously described produces low harmonic components. This situations is illustrated in more detail in the simulation results presented in Fig. 5-30 of Chapter 5.

4.7.9 Large voltage transitions

High voltage transitions can occur due to the vector selection strategy in the Classical DTC method, where no rules regarding allowed transitions are considered. This produces higher *dV/dt* and the associated voltage peaks in the motor terminals and CM

currents described in section 3.5 [12, 37]. Fig. 4-11 shows a strong voltage step in u_{sa} due to a transition between $\vec{V}_1$ and $\vec{V}_4$.

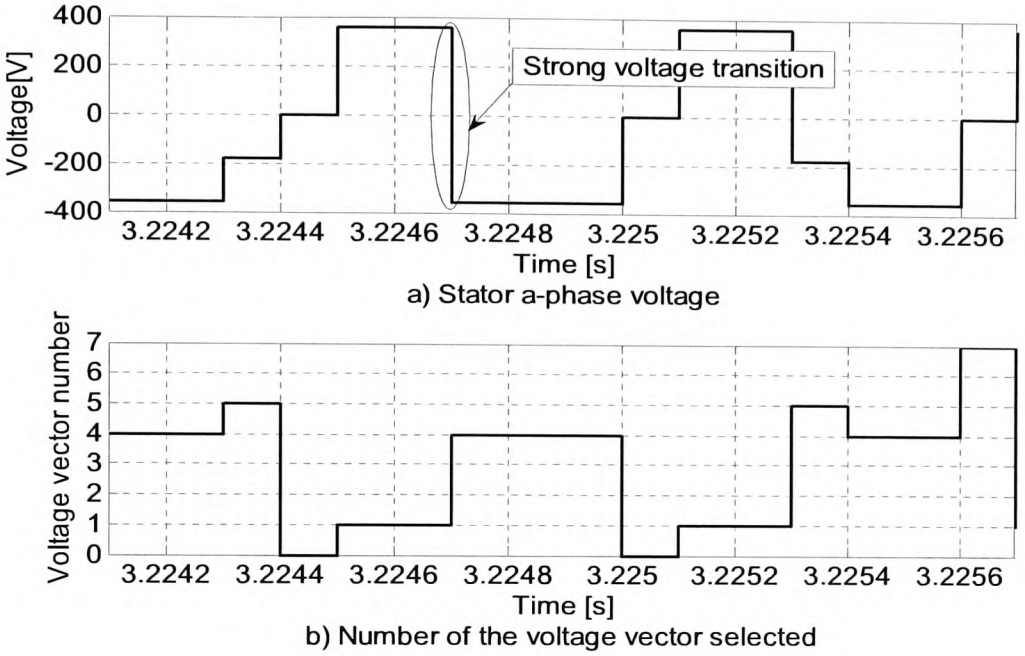

Fig. 4-11 Strong voltage transition in the stator phase voltage

4.7.10 Audible noise

A high level of noise can be produced, particularly at low speed operation, due to the variable switching frequency and the presence of harmonic components at low frequencies inside the audible noise band [51, 53].

4.8 Improvements in Direct Torque Control

A considerable number of methods have been proposed to improve the features of the Classical DTC method and solve some of the drawbacks described above. A possible classification for these methods can be done as follows:

- Modified look-up tables and hysteresis controllers.
- Constant switching frequency DTC with modulation techniques.
- DTC with duty-ratio control.
- DTC using different converter topologies from the standard two-level VSI.

Besides the classification presented above some other remarks can be made concerning the improvement of the Classical DTC method:

- Artificial intelligence techniques have also been employed to improve DTC features and section 4.8.5 is dedicated to them.
- Flux optimization can be employed, as for other IM control techniques, to improve the performance of the control system.
- It should be noted that an accurate estimation of torque and stator flux is of paramount importance in the performance of the DTC method. An intense research effort is made to improve the estimation methods as mentioned in section 4.4.

4.8.1 Modified look-up tables and hysteresis controllers

These methods are basically intended to improve the Classical DTC method by using more sophisticated strategies for the voltage vector selection. In these selection strategies the operating point of the motor is also taken into account [54]. For instance, in high speed operation zero vectors produce a strong torque decrease, while at low speeds they keep it almost equal. Therefore, different optimum tables can be obtained for different operating points. In [55] a composition of different switching tables for different operating regions is proposed. A precise consideration of the flux and torque changes produced by the voltage vectors at different operating points is used to obtain several tables. However these methods are still based on the Classical DTC scheme (use of a look-up table, division of the stator flux position in 6 sectors and hysteresis controllers) and although torque ripple can be reduced they keep some of the undesired features such as the distortion problem in the sector boundaries.

Another interesting approach is proposed in [51, 56, 57]. In this method the sampling time is divided into three intervals and new virtual voltage vectors can be synthesized. A new switching selection table can be devised by increasing the number of levels in the torque hysteresis comparator. A considerable reduction of the torque ripple and current distortion is achieved.

The design of the hysteresis controller can also bring some improvement. The three-level torque hysteresis controller used in the Classical DTC method presents one problem. During steady-state operation the torque error operates in only one of the hysteresis region, and as a result there is a steady-state mean error that increases with the speed. A different kind of three-level hsyteresis controller is proposed in [58] to solve this problem.

4.8.2 Constant switching frequency DTC with modulation techniques

At the beginning of the 1990s a new DTC-based scheme incorporating SVM was introduced instead of the optimum switching table [59]. It can be considered a predictive method which employs a deadbeat controller. This method calculates the reference voltage vector which can cancel the torque and flux errors in one sampling period. This reference voltage vector is then synthesized in the SVM block and constant switching frequency is achieved. This method involves the calculation of the voltage reference vector and its decomposition by means of the SVM algorithm. Specific hardware for PWM is also required. Higher computational capabilities are required for this algorithm when compared to the simplicity of the look-up table and the hysteresis controllers employed in the Classical DTC method. Moreover an accurate IM model and a precise identification of the IM parameters that appear in the calculation of the voltage reference vector are necessary. The advantages of this method are:

- Very good steady-state and transient performance.
- The highest reduction in torque ripple is achieved.
- Low harmonic distortion in currents.
- Constant switching frequency.

However the disadvantages are the complexity of the algorithm compared with the Classical DTC, the increase of the switching frequency and the sensitivity to IM parameters variation.

Other methods have been presented which generate a reference voltage vector to be synthesized by means of SVM [12, 60, 61]. These strategies employ closed-loop torque and flux schemes with PI controllers that provide the components of the reference voltage vector. These methods are very similar to FOC and particularly to Stator Field Oriented Control (SFOC), current control loops are not used though. Their features are very similar to the DTC with SVM based on a deadbeat controller. The main differences are that the IM parameters are not involved in the calculation of the reference voltage vector which is done by means of PI controllers. The torque and flux responses are not as quick due to the integral action of the PI controllers.

Finally, variable structure control has also been used in conjunction with SVM following the DTC principle with very interesting results [53]. The features are also very similar to the previous methods described in this section and the steady-state behaviour is significantly improved. The advantage of this method is that no motor

parameters are involved in the reference voltage vector calculation whilst a fast torque and flux response is kept.

4.8.3 Duty-ratio control

A different alternative to the Classical DTC method is the DTC scheme with duty-ratio control. The Classical DTC method produces high torque and flux ripple because none of the voltage vectors available in a two-level VSI is able to produce the desired changes in both torque and stator flux modulus during the sampling period. The reduction of this ripple is possible in DTC with SVM because modulation is introduced and the switching frequency is considerably increased. DTC with duty-ratio control can achieve a significant reduction of torque ripple without increasing the switching frequency as occurs in DTC with SVM. This method applies the VSI state selected by the look-up table during some portion of the sampling period and then a zero vector is applied during the remaining part of the sampling period. The portion of the sampling period that the VSI state from the look-up table is applied is given by a duty ratio (δ). This duty ratio has to be determined for each sampling period in order to minimise torque ripple. By means of varying the duty-ratio between its extreme values [0, 1] it is possible to apply the voltage vectors that can be delivered by the VSI with the desired amplitude. Different methods for obtaining the value of δ have been developed [13, 62-64]. The main advantages of the DTC with the duty-ratio control method are:

- Torque ripple is considerably reduced.
- The average switching frequency in steady-state conditions is almost constant and approximately equal to one third of the sampling frequency [62].

However, the complexity of the resulting system is higher than the Classical DTC method, and the harmonic distortion for currents is considerably high [52]. Moreover the method presented in [62] requires all the IM parameters, the instantaneous speed and a coordinate transformation.

4.8.4 DTC with different converter topologies

As explained in Chapter 3, the standard two-level VSI is a simple and low-cost converter employed in most of the variable speed IM drives. Regarding DTC, most of the literature is focused on drive systems employing the standard two-level VSI, and the research carried out on DTC with different topologies is still scarce.

Following the approach which combines DTC with different converter topologies, one of the earliest studies was presented by Takahashi, the inventor of DTC, and Ohmori in 1989 [65]. In their work DTC is employed to control a particular converter topology which consists of two sets of three-phase VSIs with GTO switches and a reactor to suppress the zero phase sequence current feeding an open delta-connected IM. The resulting converter is a multilevel topology able to deliver the same set of 19 different voltage vectors of a three-level VSI. Some of these 19 vectors have redundant VSI configurations since 64 different VSI configurations are possible. This redundancy is employed to reduce the zero phase sequence current and the switching frequency in this order of priority. The modifications of the Classical DTC scheme introduced for this particular converter topology are the following:

- The torque hysteresis controller with two hysteresis loops (three-level) is replaced by a four-loop hysteresis controller.
- The stator flux vector position is divided into 12 sectors.
- A look-up table is defined and extended according to the previous modifications.
- An additional input, the zero-phase sequence current, is added. An extra look-up table is employed to minimise this current by choosing among the redundant switching configurations that exist for each voltage vector.
- A switching frequency equalizing circuit is added.

The resulting system can achieve a very fast torque response and the mean switching frequency of the semiconductor devices is 60% lower when compared to the Classical DTC with a two-level VSI. This switching frequency is below 600 Hz for all operating conditions and allows the use of GTO devices. The disadvantages of this system are the increase in complexity and cost, and the requirement of a reactor.

This initial work by Takahashi and Ohmori stated the suitability and potentialities of DTC with multilevel topologies. In the last years, several authors have investigated in this direction and different solutions have been proposed, most of them employing the three-level VSI. Chapter 5 includes a more detailed literature review of these solutions in section 5.2.

Following the approach of using different converter topologies with DTC some authors have investigated DTC with matrix converters [66, 67]. The proposed control systems employ new look-up tables designed to control the matrix converter and exploit the potentiality of the resulting system. The power factor at the input of the converter is

incorporated in the control system to achieve unity power factor. Moreover in [67] the torque hysteresis controller and the look-up table are modified in order to use the small voltage vectors and achieve a reduction of the torque ripple.

In [68] DTC is developed for a quasi-resonant converter and also for a converter with a reduced number of components consisting of a four-switches H bridge.

4.8.5 Artificial intelligence techniques in DTC

The progress experienced by artificial intelligence techniques in the last decades has also reached electrical motor drives as a field of application [50, 69]. Artificial intelligence provides powerful tools to assist in the resolution of complex problems. Several solutions incorporating Fuzzy Logic, Artificial Neural Networks (ANN) and Genetic Algorithms (GA), or a combination of them like Neuro-Fuzzy, have been proposed to improve DTC.

4.8.5.1 Fuzzy logic

Several papers have proved that Fuzzy Logic techniques can help in overcoming some of the disadvantages present in the Classical DTC method. The authors of [70] made the assumption that the Classical DTC method could be improved by distinguishing between very large and relatively small torque errors. In the Classical DTC method the VSI states selected for large errors, mainly during start-up or during a torque reference step change, are the same as for fine control in steady-state conditions. The authors have proposed a Fuzzy Logic controller that replaces the hysteresis controllers and the look-up table. The new controller has three inputs: the torque error, the stator flux error and the stator flux position, as in the Classical DTC method. The selection of the optimum VSI state is done according to the state of these inputs. The new system has a similar behaviour when compared to the Classical DTC regarding torque ripples, but a faster response for torque and stator flux modulus step changes is achieved. The control structure is more complicated due to the high number of membership functions, resulting in a very high number of rules to be computed.

A Fuzzy Logic controller can be used to generate a reference voltage vector employing as inputs: the stator flux modulus and torque errors, and the stator flux position. This voltage vector is then synthesized by means of SVM, similarly to the methods described in section 4.8.2 [71].

Fuzzy Logic has also been used to determine the value of δ in the duty-ratio control strategy explained in the previous section [63, 64]. The resulting system is more complex than the Classical DTC method, but a high reduction of torque ripple is achieved.

4.8.5.2 Artificial Neural Networks

Despite the number of publication on the application of ANNs in IM drives, it seems like they find difficulties in practical applications [69]. This situation is probably caused by the high price of neural network ASIC devices. Regarding the DTC method there are just a few publication involving ANN.

In [72] an ANN is used as a voltage vector selector. Nevertheless this paper is mainly devoted to the demonstration of the potential application of ANNs to control AC drives, and the ANN is just emulating the Classical DTC method. Thus no advantage is achieved. In [73] an ANN is also used as the VSI state selector but no significant improvement is achieved.

4.8.5.3 Neuro-Fuzzy

The use of a Neuro-Fuzzy controller for DTC has been proposed to provide the systems with a learning mechanism [46, 74]. The controller obtained has the following features: constant switching frequency, low flux and torque ripple and auto-tuning. In this scheme the Neuro-Fuzzy controller has the same inputs as the Classical DTC method and calculates a voltage reference vector, which is then synthesized by means of SVM.

4.8.5.4 Genetic Algorithms

GA's are very powerful optimization tools that can be used to solve complex problems with a large number of parameters to be adjusted and a poor knowledge of the system behaviour.

GA's have been used in [75] to assist in the training of an ANN used as a voltage vector selector. The GA is used to tune the weights of the ANN.

4.8.6 Flux optimization

Optimizing the level of magnetization according to the load conditions improves the total efficiency of the motor drive system and achieves a reduction of the reactive power taken from the grid. This is particularly true for low motor loads, where losses can be reduced by more than 60%. In applications where the load is normally below the

nominal value, such as in ventilation systems, flux optimization also reduces the noise level in the motor [8]. Moreover, a reduction in the torque and stator flux modulus ripples is obtained [64]. Nevertheless, torque dynamics becomes slower due to the dependency on the stator flux modulus (see equation (4.4)).

Flux optimization is achieved by setting the stator flux reference to the appropriate value, which should be just large enough to produce the desired torque. It should be noted that flux optimization is not only valid for the DTC system but can also be applied to other vector control methods [13, 64].

4.9 Interim conclusions

In this chapter the Classical DTC method for IMs has been described. This method can be considered to be part of the family of vector control strategies and an alternative to FOC. The principle of operation of DTC is based on the relationship between the stator voltage vector and the variation of the stator flux vector, which in turn affects the torque produced in the IM.

The main merit of DTC is the high performance achieved with a very simple control structure. It has been demonstrated that the decoupled control of the stator flux modulus and torque is possible. The main advantages of DTC are:

- The stator flux and torque are directly controlled.
- Stator fluxes and currents are approximately sinusoidal.
- Excellent torque dynamics is achieved with minimal torque response time.
- The motor position or speed is not required to perform the torque control.
- Absence of coordinate transformation (required in FOC).
- Absence of voltage modulator, as well as other controllers such as PID and current controllers (used in FOC).

Nevertheless, some problems and drawbacks are associated to the DTC method. These problems can be summarized as follows:

- Poor performance at low speed operation.
- Slow start-up.
- Stator flux and torque estimators are required.
- The switching frequency is variable and produces a spread frequency spectrum in the stator voltages and currents.
- Higher torque and stator flux ripple is generated.

- The torque steady-state mean error is not null due to the discrete-time implementation and delays of the control system. This error increases with the speed.
- The stator flux is distorted due to the effect of the sector boundaries.
- The stator voltage and current waveforms contain higher harmonic distortion when compared to other methods, such as FOC, with a similar switching frequency.
- Large voltage transitions can appear in the stator voltages.
- Audible noise is produced.

A considerable number of methods have been proposed to improve the features of DTC and solve some of the drawbacks described above. A possible classification of these methods can be done as follows:

- Modified look-up tables and hysteresis controllers.
- Constant switching frequency DTC with modulation techniques.
- DTC with duty-ratio control.
- DTC using different converter topologies from the standard two-level VSI.

All the improvements presented in those methods are generally counterbalanced by an increase in the complexity of the resulting control method. Finally, it should be noted that an accurate estimation of torque and stator flux is of paramount importance in the performance of the DTC method.

Chapter 5: New Control System

Summary – *This chapter presents the new control system developed and reported in this thesis. The new controller is based on the DTC principle and it has been designed to be applied in the control of the IM fed with the three-level NPC VSI. The characteristics of the new controller are described, and the advantages and disadvantages of the proposed solution are discussed. Simulation results are presented to compare the new control system with the Classical DTC method employing the two-level VSI.*

5.1 Introduction

The objective when designing a new control system for a high performance electrical motor drive is to meet a certain set of features. Some of these required features are listed in Table 5-I, where they have been classified into different groups according to different perspectives [46].

Table 5-I Required features of an electrical motor drive system from different perspectives

Requirements from the control point of view:
• Very fast and precise flux, torque and speed response.
• Low flux, torque and speed oscillations (low ripples).
• Good disturbance rejection.
• Maximum output torque available in the full operating region.
• A simple tuning method or even auto-tuning.
• Robustness and low sensitivity to motor parameters variation.
Requirements from the power conversion point of view:
• Four-quadrant operation.
• Low and constant switching frequency.
• Low power losses and high efficiency.
• Low voltage and current harmonic distortion.
• Low reactive power with a power factor ideally equal to one.
Requirements from the environment point of view:
• Low EMI.
• Low audible noise.
Requirements from the mechanical point of view:
• Simple and robust structure, without moving parts if possible.
• Small dimensions and compactness.
Requirements from the end user point of view:
• Simple commissioning and operation.
• Reliability.
• Low cost.
• Low maintenance.

As in every engineering problem, some of the required features are connected and some benefits are gained at the expense of loosing some others in a certain degree. A trade-off has to be therefore established to obtain a satisfactory solution.

The achievement, however, of some of the features listed above is outside the scope of the research carried out. The research reported in this thesis is mainly focused on the achievement of the required features from the control and power conversion perspective. In order to improve the control of the IM the research undertaken has been devoted to the following areas:

- The use of DTC which has proved to be an alternative to FOC.
- The use of a different VSI topology from the standard two-level VSI. In this case the topology selected is the three-level NPC VSI.

The initial hypothesis is that a better control of the IM can be achieved by means of using DTC in conjunction with a VSI topology which provides an increased number of voltage vectors at the output. This is the case of the three-level VSI, as described in Chapter 3, where more vectors with different directions and modulus can be obtained at the output of the VSI. As it has been explained in Chapter 4, the Classical DTC method presents some drawbacks that need to be addressed to improve the control of the IM. In the design of the new controller, priority has been given to reduce the torque and flux ripples, eliminate stator flux distortion produced in the boundaries of the sectors and reduce harmonic distortion in voltages and currents. It is expected that the use of a multilevel topology will bring improvement in these features in the resulting control system.

5.2 Review of DTC with the three-level VSI

As it has been explained Chapter 4, a possible approach to improve DTC is to employ different converter topologies from the standard two-level VSI. Some authors have presented different implementations of DTC for the three-level VSI.

In references [40, 49, 76, 77] it is proposed to use new optimised look-up tables to select the most appropriate voltage vector among all the possibilities following the Classical DTC method approach [65]. These solutions increase the complexity and size of the look-up table in order to exploit the enhanced possibilities for the voltage vector selection. The stator flux modulus and torque errors are quantified by means of modified hysteresis controllers which incorporate more levels. Several tables are, in some cases, defined for different speed regions. Moreover, in some cases, the direction

of rotation needs to be taken into account due to the asymmetry of the look-up tables. The resulting systems are therefore more complex, difficult to tune and cannot be applied to different types of converter.

In references [41] and [78] some of the authors belong to the motor drives division of the ABB company. These publications contain a description of a drive system incorporating DTC with a three-level NPC VSI, which probably corresponds to the ACS 1000 described in section 3.4.2. The control scheme is based on hysteresis controllers and a look-up table that is not specified.

A different approach based on the concept of "virtual vectors" is presented in [37]. A new look-up table is defined using these virtual vectors that can be synthesized by means of a defined modulation pattern, which consists in a fixed sequence of the available voltage vectors in the three-level VSI. The modulation patterns are defined to maintain the voltage balance in the DC-link capacitors. This system, however, doesn't seem to exploit the potentialities of the topology employed because only 12 virtual vectors plus the zero vector are defined in comparison with the 19 non-redundant vectors available in the three-level VSI.

Predictive control methods have also been proposed where a deadbeat controller can be used to find the optimum voltage vector to be applied [22]. In this case results are shown for a four-level VSI but the proposed technique can also be employed in a three-level VSI. A different possibility is to assess the effect of the available voltage vectors and choose the optimum one [79]. All these methods are based on the IM model, which consequently increases the complexity and processing requirements of the resulting control algorithm. The increase of sensitivity to parameter variation is another drawback of these methods.

A different approach based on the concept of Output Regulation Subspaces (ORS) is presented in [80]. This method consists in the definition of sets of input points (voltage vectors) that have a certain effect on the output (torque and stator flux modulus variation). In a VSI-fed IM, four different quadrants result from the application of this concept and every quadrant contains several VSI voltage vectors. All the voltage vectors inside a quadrant produce a variation of the stator flux modulus and torque with equal signs. The selection of the optimum voltage vector is performed by means of a cost function that minimises the quadratic error of torque and stator flux modulus. A prediction of these errors is therefore necessary for all the possible vectors in the selected quadrant.

The DTC method with duty-ratio control has also been developed in [81], where torque ripple reduction is the main goal. The algorithm employed is based on the approach presented in [62] for a DTC system with a two-level VSI. A similar approach is presented in [39, 82]. The same authors present in [83] a back-to-back connection of two three-level NPC VSIs, one of them used as a rectifier and the other one as an inverter controlling an IM with their proposed DTC method. The main advantage of the proposed control system is that a more precise control of the DC-link voltage and the voltage balance the DC-link capacitors can be achieved with appropriate control of the three-level rectifier. Moreover nearly sinusoidal currents can be obtained in the network side with unity power factor.

Some other methods, not devised in particular for the three-level VSI or other multilevel topologies, can also be applied such as the constant switching frequency DTC methods with SVM [12, 53, 59]. The only modification required is to adopt an appropriate modulation technique for the multilevel topology employed. It should be noted that the complexity of modulation techniques for multilevel topologies is higher. The performance of these methods is very good particularly in steady-state operation when compared to the hysteresis controller with a look-up table alternative. Moreover the potential of the three-level VSI can be better exploited. On the other hand, the complexity of the control system is considerably increased.

A comparative analysis between different control techniques (FOC, Classical DTC, DTC with duty-ratio control and DTC with SVM) for an electric vehicle application employing an IM and a three-level NPC VSI is presented in [52]. The results of the comparison, according to the authors, show that the control technique that offers better performance is DTC with SVM. This method is superior due to the fast torque response, low steady-state torque ripple and low current distortion achieved. The solution selected from the comparison is then fully described in [84].

From the study of the literature review presented about the implementation of DTC with the three-level VSI and other multilevel topologies the following conclusions are extracted:

- The approach based on hysteresis controllers and a look-up table, as in the Classical DTC method, presents some limitations and does not exploit the full potential of three-level VSI. It is difficult to establish the optimum structure and tuning of the hysteresis controllers and devise the look-up table.

- An appropriate control system to balance the voltage of the DC-link capacitors is necessary and this issue is not reported in some of the studied control systems.
- The use of modulation techniques for multilevel topologies is more complex, not only considering the modulation algorithm, but also regarding the hardware requirements.

5.3 Review of the DTC principle

A brief review of the IM model described in Chapter 2 will be helpful to understand the structure of the new controller presented in this chapter.

DTC is based on the direct control of the motor stator flux vector by means of the applied stator voltage as explained in Chapter 4. The principle of operation can also be understood from the analysis of the IM stator voltage equation in the stator flux reference frame, which is written as follows:

$$\vec{u}_{s\psi_s} = R_s \vec{i}_{s\psi_s} + \frac{d\vec{\psi}_{s\psi_s}}{dt} + j\omega_s \vec{\psi}_{s\psi_s} \tag{5.1}$$

If equation (5.1) is expressed in a coordinate system fixed to the stator flux vector (x-y coordinates, with the x axis in the same direction of the stator flux vector) the stator voltage vector can be separated into the direct component (x) and the quadrature component (y) and the following expressions are obtained:

$$u_{sx} = R_s i_{sx} + \frac{d\psi_{sx}}{dt} \tag{5.2}$$

$$u_{sy} = R_s i_{sy} + \omega_s \psi_{sx} \tag{5.3}$$

The particularity of the stator flux reference frame (x-y coordinates) is that the y component of the stator flux vector is zero.

Equation (5.2) can be rewritten to obtain the following expression:

$$\frac{d\psi_{sx}}{dt} = u_{sx} - R_s i_{sx} \tag{5.4}$$

From the above expression it is apparent that the variation of the stator flux modulus can be controlled by means of the u_{sx} voltage.

In the same reference frame, fixed to the stator flux vector, the electromagnetic torque can be expressed as follows:

$$\Gamma_e = \frac{3}{2} P \vec{\psi}_{s\psi_s} \times \vec{i}_{s\psi_s} \tag{5.5}$$

If the equation above is expressed in x-y coordinates, taking into account that ψ_{sy}=0, the electromagnetic torque can be written as follows:

$$\Gamma_e = \frac{3}{2} P\left(\psi_{sx} i_{sy} - \psi_{sy} i_{sx}\right) = \frac{3}{2} P \psi_{sx} i_{sy} \tag{5.6}$$

Combining equations (5.3) and (5.6) the following torque expression is obtained:

$$\Gamma_e = \frac{3P}{2R_s} \psi_{sx}\left(u_{sy} - \omega_s \psi_{sx}\right) \tag{5.7}$$

From the expression above it is apparent that torque can be controlled by means of the u_{sy} voltage. Some additional conclusions can be extracted from equation (5.7) as follows:

- Torque also depends on the stator flux modulus. A decoupled control of both magnitudes can be achieved if the stator flux modulus is maintained at a constant value. This value is generally the nominal value and can be reduced if operation beyond the rated speed of the IM (field weakening region) is required. This value can also vary if flux optimization or flux braking are employed.
- For a given value of u_{sy}, torque production depends on the stator flux angular speed, which in turn depends on the operating point of the machine.

In order to control torque by means of u_{sy} it is interesting to study the relationship between both variables. For this purpose equation (5.7) can be rewritten as follows:

$$u_{sy} = \frac{2R_s \Gamma_e}{3P\psi_{sx}} + \omega_s \psi_{sx} \tag{5.8}$$

Considering ψ_{sx} is constant and equal to the nominal stator flux modulus, u_{sy} can be plotted in a graph as a function of Γ_e and ω_s as shown in Fig. 5-1, making this relationship valid in steady-state conditions. The parameters used are taken from the IM used in the laboratory setup and can be found in Table 6-I in Chapter 6.

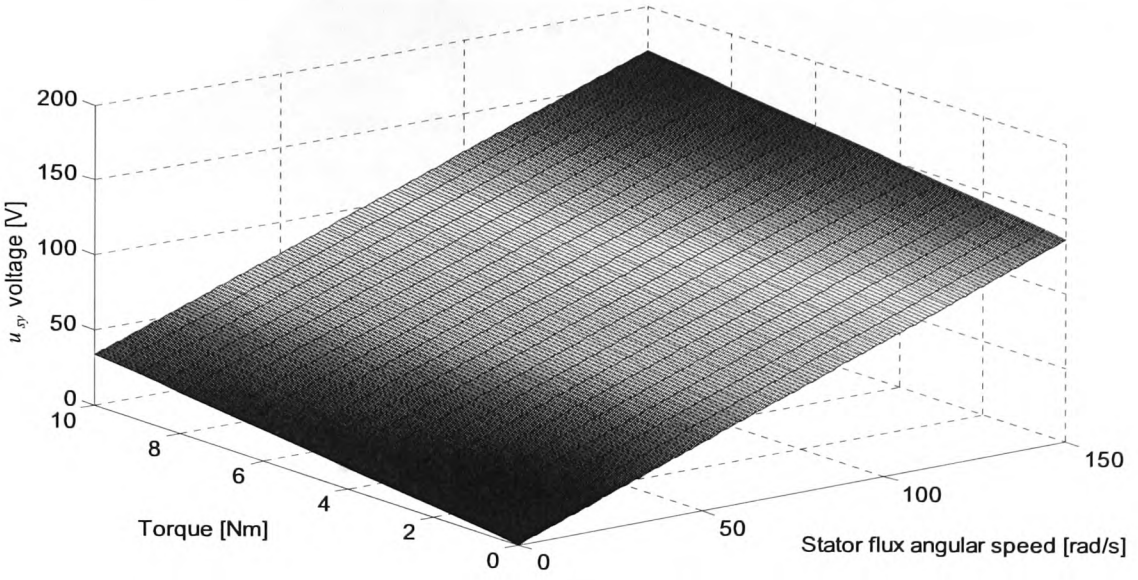

Fig. 5-1 u_{sy} dependency on torque and stator flux angular speed

The previous figure illustrates the required u_{sy} voltage at different operating points of the IM in steady-state conditions. Equation (5.8) can be divided into two different terms. One of the terms depends on Γ_e. The other one depends on ω_s and is known as the Back Electromotive Force (BEMF). The resulting expressions for the two terms are written as follows:

$$u_{sy\Gamma e} = \frac{2R_s\Gamma_e}{3P\psi_{sx}} \tag{5.9}$$

$$u_{syBEMF} = \omega_s\psi_{sx} \tag{5.10}$$

It can be seen in Fig. 5-1 how the BEMF term takes a bigger share of the u_{sy} voltage in most of the operating region. This conclusion can be further illustrated by plotting the percentage of the u_{sy} voltage that corresponds to each term for different operating conditions, as shown in Fig. 5-2.

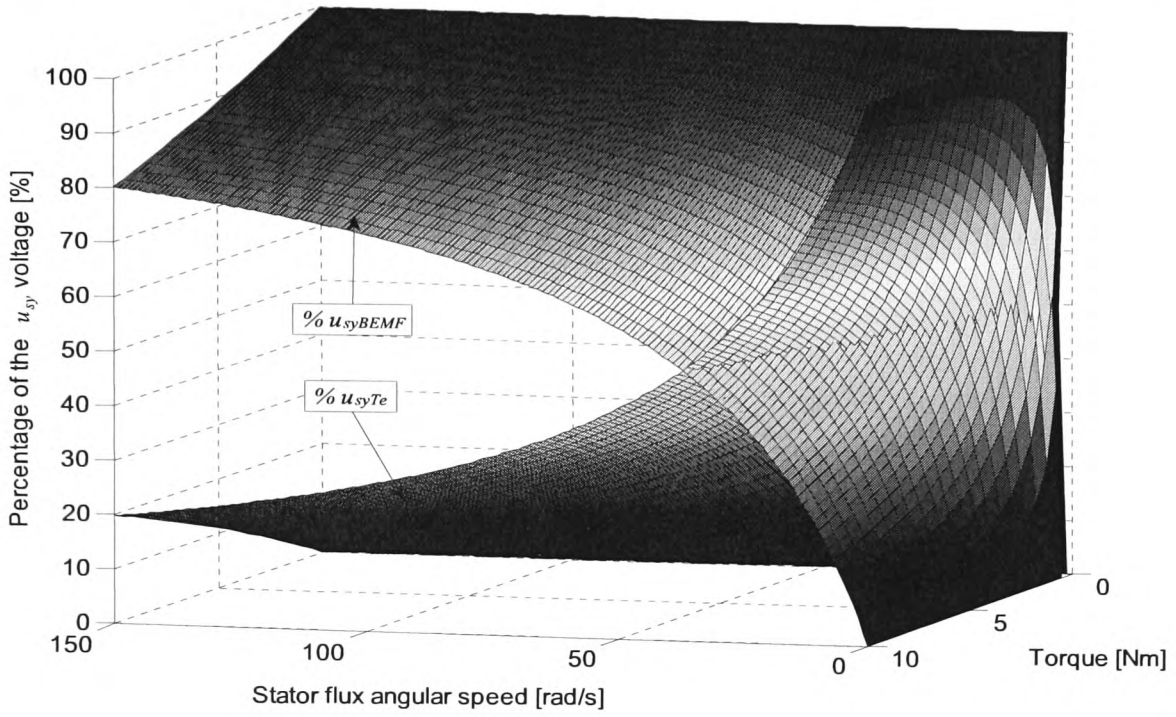

Fig. 5-2 Percentage of u_{sy} corresponding to the torque and BEMF terms

This can also be illustrated by plotting the percentage of the u_{syBEMF} term in the ω_s-Γ_e plane by means of lines with equal percentage of this term as shown in Fig. 5-3. This graph clearly illustrates how in most of the operating region the term u_{syBEMF} is more than 50% of u_{sy}.

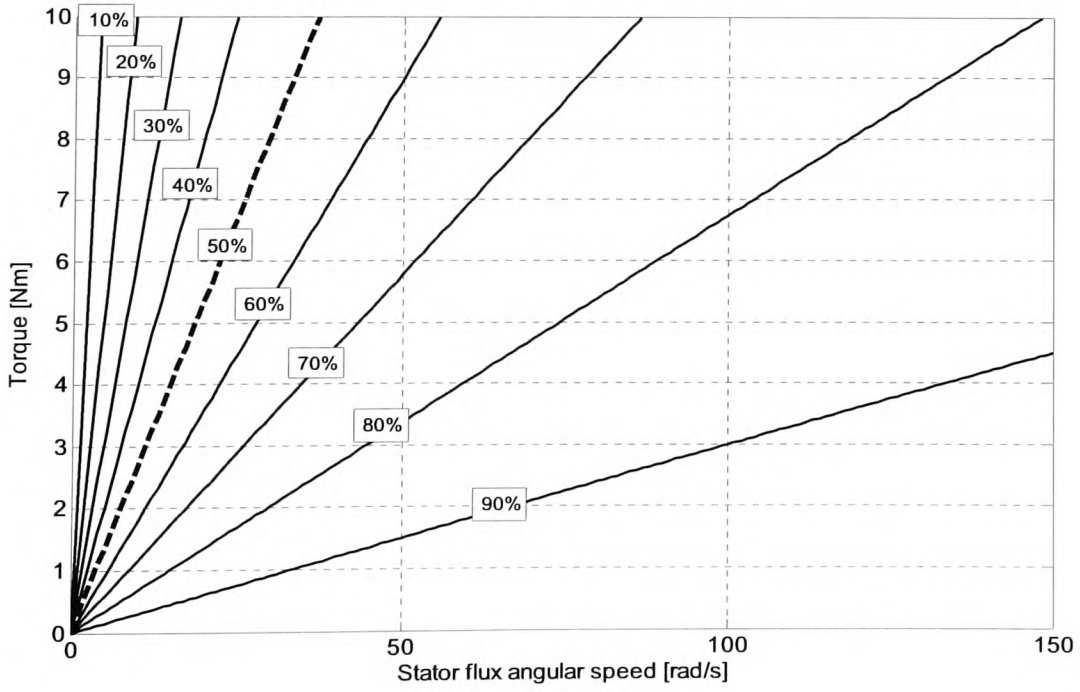

Fig. 5-3 Percentage of the u_{syBEMF} term in the ω_s-Γ_e plane

Fig. 5-1 also shows that for low speed and load conditions the level of the u_{sy} voltage required is very low and far from the voltage level provided by the DC-link.

From the analysis presented the following conclusions can be extracted:

- The stator flux modulus can be controlled by means of u_{sx}.
- Torque can be controlled by means of u_{sy}.
- The BEMF term, which depends on ω_s, strongly influences the effect of u_{sy} on the produced torque.

These conclusions have to be taken into account when designing an improved control strategy. If torque has to be directly controlled by means of the stator voltage applied to the motor, as in the Classical DTC method, the performance of the control can be improved if the u_{sy} voltage is more precisely controlled and the BEMF term is compensated. These two conditions explain some of the limitations present in the Classical DTC method. Due to its simplicity, the BEMF term is not considered and the precision of the u_{sy} voltage control is limited by:

- The reduced choice of voltage vector delivered by a two-level VSI.
- The absence of modulation techniques.
- The division of the stator flux position in a discrete number of sectors. The u_{sy} component of a voltage vector can vary a lot depending on the position of the stator flux vector inside the sector.

The Classical DTC method can overcome these limitations by reducing the sampling time, but this solution is in turn limited by the processing capabilities of the controller and the switching capabilities of the semiconductor devices. A possible alternative to improve the precision of the u_{sy} control is to use a converter topology with an increased number of voltage levels. The alternative considered in this case is the three-level VSI, which has been described in Chapter 3.

In Chapter 3, Fig. 3-2 and 3-13 show the voltage vectors delivered by a two-level VSI and a three-level VSI respectively in the α-β plane. In those figures a nomenclature is defined to identify the voltage vectors. Following this nomenclature, Fig. 5-4 shows the u_{sx} and u_{sy} components of the different voltage vectors that can be delivered by a three-level VSI in a range going from $-\pi/6$ rad to $\pi/6$ rad, which corresponds to sector 1. Zero vectors are not plotted because their voltage components are obviously zero. The first column of graphs corresponds to the large vectors of a three-level VSI, which are equivalent to the vectors $\vec{V}_1$ to $\vec{V}_6$ of a two-level VSI if the same DC-link voltage is

employed (V_{DC}=537 V). It is apparent that the possibilities of selection are considerably enhanced with a three-level VSI as described in Chapter 3.

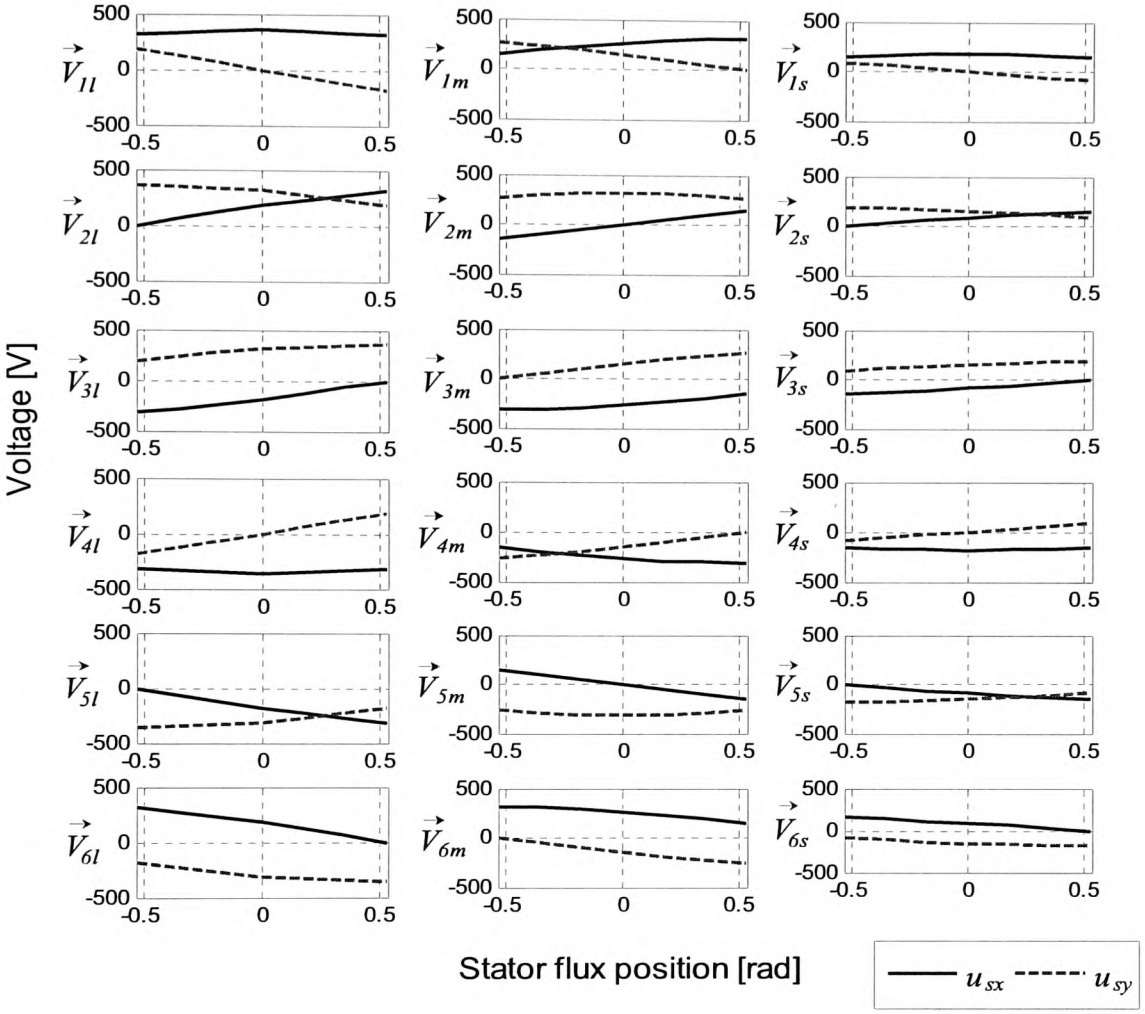

Fig. 5-4 u_{sx} and u_{sy} components of the three-level VSI voltage vectors in the $-\pi/6$ rad to $\pi/6$ rad range

In order to further illustrate how the choice of vectors is considerably increased in a three-level VSI, Fig. 5-5 and Fig. 5-6 show the u_{sx} and u_{sy} components respectively of all the voltage vectors and both VSI topologies in the same graph. It is clear that the precision of the u_{sx} and u_{sy} control can be improved by using a three-level VSI.

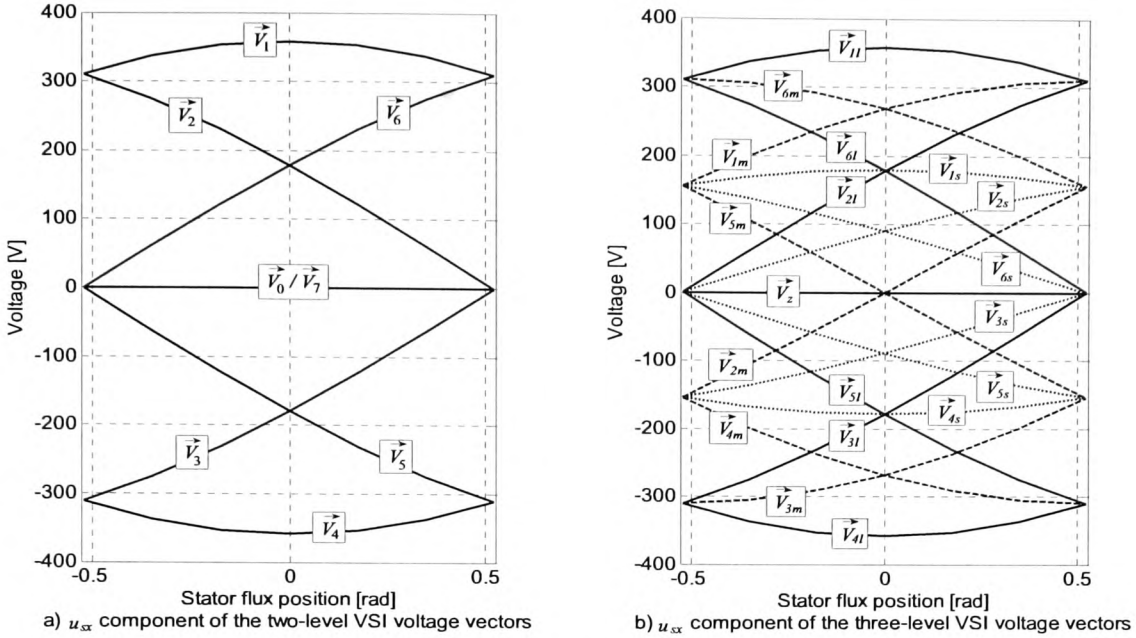

a) u_{sx} component of the two-level VSI voltage vectors

b) u_{sx} component of the three-level VSI voltage vectors

Fig. 5-5 u_{sx} components of the voltage vectors in the $-\pi/6$ rad to $\pi/6$ rad range: a) two-level VSI, and b) three-level VSI

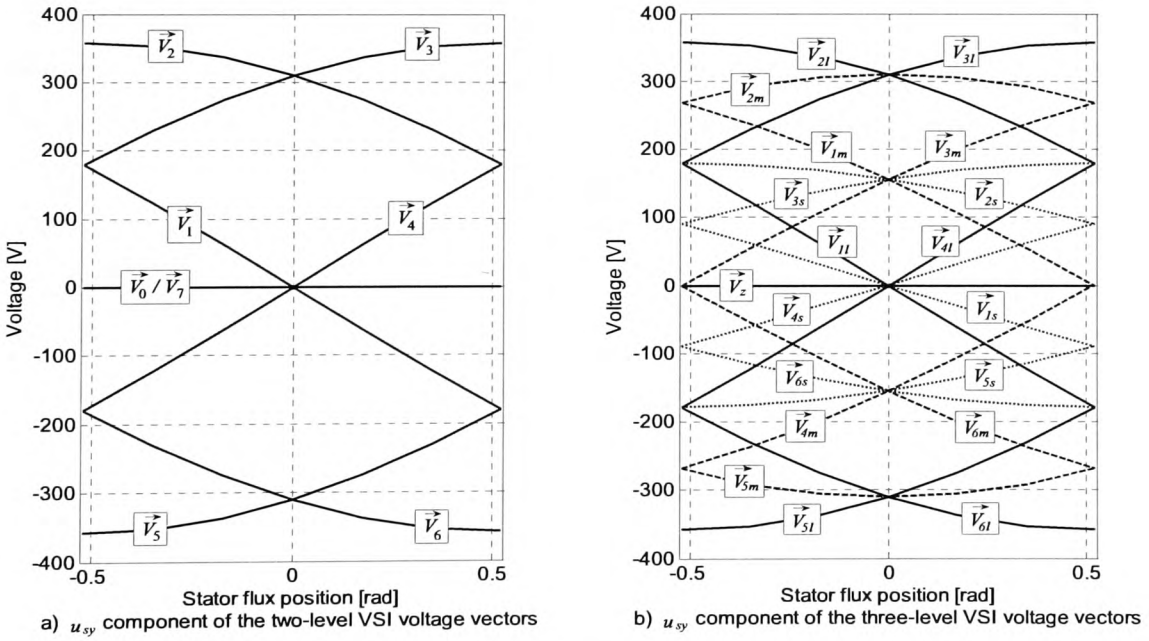

a) u_{sy} component of the two-level VSI voltage vectors

b) u_{sy} component of the three-level VSI voltage vectors

Fig. 5-6 u_{sy} components of the voltage vectors in the $-\pi/6$ rad to $\pi/6$ rad range: a) two-level VSI, and b) three-level VSI

5.4 Description of the new controller

The design of the new controller tries to meet the following objectives and premises:

- Employ the DTC principle and directly control stator flux and torque by means of the stator voltage applied. No current control loops are therefore employed.
- Employ the three-level VSI topology and fully exploit the potential provided by the higher number of voltage vectors available.
- Obtain a flexible solution with a simple tuning, which can be easily adapted to different converter topologies.
- Maintain the characteristic fast torque dynamics of DTC.
- Take into account the operating point of the machine incorporating ω_s in the controller. It has been shown in the previous section how this variable affects the torque produced.
- Reduce the switching frequency.
- Reduce the voltage and current distortion.
- Eliminate the stator flux distortion caused by the effect of the sector boundaries.

In order to incorporate all the features described above, the structure of the Classical DTC method (hysteresis controllers, look-up table and the division of the stator flux position in sectors) has not been considered due to the limitations stated in section 5.2. The alternative approach adopted entails the calculation of a reference voltage vector, which is then synthesized by the VSI. This structure provides more flexibility and makes it easier to incorporate the operating point to the control system calculations. The resulting improvement is achieved at the expense of increasing the complexity of the controller. The aim of the design is to keep the complexity of the control system as close as possible to that of the Classical DTC method.

The new controller calculates a reference voltage vector in x-y coordinates. The control laws of the controller have been derived from the stator voltage equations expressed in the stator flux reference frame (x-y coordinates) in equations (5.2) and (5.3).

From (5.2) it is deduced that the stator flux modulus can be controlled by means of u_{sx}. This equation can be rewritten as follows:

$$u_{sx} = R_s i_{sx} + \frac{d\psi_{sx}}{dt} = R_s i_{sx} + \frac{\Delta\psi_{sx}}{\Delta t} \tag{5.11}$$

Considering that between two sampling instants the variation of time is equal to T_s and the desired variation of stator flux modulus is equal to the stator flux modulus error, the resulting control is defined as follows:

$$u_{sx}^{*} = R_s i_{sx} + \frac{\psi_s^{*} - \hat{\psi}_s}{T_s} \tag{5.12}$$

The resulting control structure obtained in equation (5.12) corresponds to a deadbeat controller as in [59], which imposes the u_{sx} voltage necessary to eliminate the error in one sampling period.

From equation (5.7) it is deduced that torque can be controlled by means of u_{sy}. The torque control law is derived from this equation and it is based on two different terms. The first term is a feed-forward action based on equation (5.8), which is valid for steady-state conditions and calculates the required voltage to produce the torque reference. The second term is a feed-back loop which incorporates the torque error and employs a proportional controller. This term is mainly responsible for the transient response of the controller. The resulting control law can be written as follows:

$$u_{sy}^{*} = \frac{2R_s\Gamma_e^{*}}{3P\hat{\psi}_s} + \hat{\omega}_{sf}\hat{\psi}_s + K_{\Gamma e}\left(\Gamma_e^{*} - \hat{\Gamma}_e\right) \tag{5.13}$$

Both components of the reference voltage vector (equations (5.12) and (5.13)) are saturated due to the limitation of the DC-link voltage available. The saturation values are equal to the maximum amplitude of the VSI voltage vectors, $\pm 2/3 V_{DC}$, that corresponds to the amplitude of the large vectors in a three-level VSI.

The resulting controller only has one parameter to be tuned, the proportional gain of the torque feed-back loop $K_{\Gamma e}$. Moreover the only parameter of the IM involved is the stator resistance R_s, which is already required in the stator flux estimation. No integral action is used in the control algorithm. The stator flux angular speed is calculated from the discrete derivation of the stator flux vector position (γ_s), and it is then filtered by means of a Low-Pass Filter (LPF) to obtain the steady-state average value of ω_s for the current operating point.

Once the reference voltage vector is calculated in x-y coordinates, it has to be synthesized by the VSI, which feeds the IM. In order to obtain the VSI state and the corresponding firing signals to command the VSI, the reference voltage vector is first

converted to α-β coordinates. This operation requires the stator flux vector position which is obtained from the stator flux estimation.

$$u_{s\alpha}^{*} = u_{sx}^{*}\cos(\hat{\gamma}_s) - u_{sy}^{*}\sin(\hat{\gamma}_s) \tag{5.14}$$

$$u_{s\beta}^{*} = u_{sx}^{*}\sin(\hat{\gamma}_s) + u_{sy}^{*}\cos(\hat{\gamma}_s) \tag{5.15}$$

The reference voltage vector in α-β coordinates can be synthesized by the VSI employing modulation techniques. An alternative, to reduce the complexity of the control, is to avoid the use of modulation and find the nearest voltage vector, from those provided by the VSI, to the reference voltage vector [22]. The nearest vector is calculated by finding the voltage vector among those delivered by the VSI that has the minimum distance to the reference voltage vector. The expression employed for this calculation is the distance between two generic vectors:

$$Dist = \left|\vec{a} - \vec{b}\right| = \sqrt{(a_\alpha - b_\alpha)^2 + (a_\beta - b_\beta)^2} \tag{5.16}$$

The approach adopted for the new controller has similarities with some of the proposed schemes for DTC with SVM. These methods employ deadbeat controllers [59] or closed-loop flux and torque PI controllers in a similar way to that of Stator Field Oriented Control [12, 60]. The new control scheme is shown in Fig. 5-7.

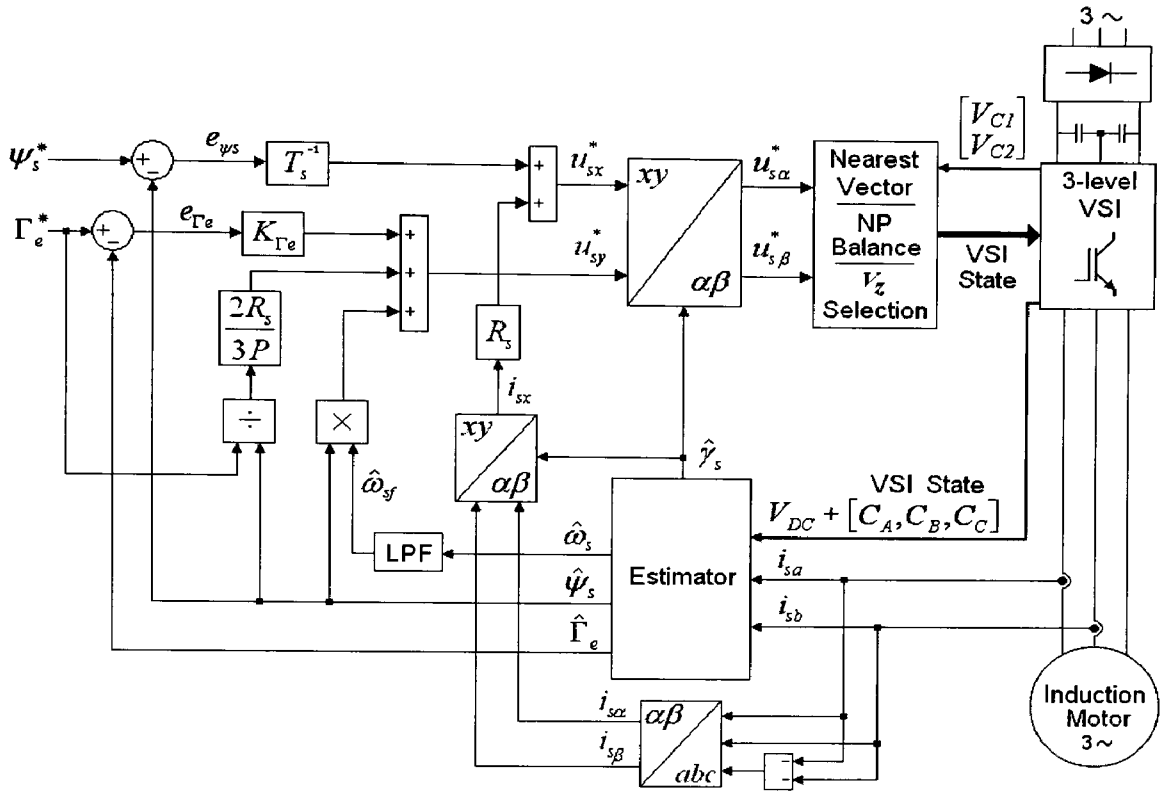

Fig. 5-7 New control scheme

5.5 Tuning of the torque controller

The only parameter which requires to be tuned in the new controller presented is the proportional gain of the torque feed-back loop $K_{\Gamma e}$. Due to the complexity and non-linearity of the IM model, the power converter and the proposed control scheme, the problem of tuning the value of $K_{\Gamma e}$ is addressed by means of optimization techniques.

The first step in applying an optimization method is to define a fitness function (or cost function) to grade results obtained with different values of $K_{\Gamma e}$. The cost function has to be minimised or maximised during the optimization process. In this case the main objective is to minimise the torque error and the selected fitness function has been the RMS value of the torque error, which is defined as follows:

$$e_{\Gamma eRMS} = \sqrt{\frac{1}{T}\int_t^{t+T} e_{\Gamma e}(t)^2} \tag{5.17}$$

and the discrete-time form of (5.17) is given by the following expression:

$$e_{\Gamma eRMS} = \sqrt{\frac{\sum_{i=1}^{N} e_{\Gamma ei}^2}{N}} \tag{5.18}$$

where N is the total number of samples and i is the number of each torque error sample. The next step is to define a test to evaluate the fitness function. The test is devised to incorporate different operating points and transitions between them in order to obtain a satisfactory solution in all operating conditions. Fig. 5-8 shows the fitness evaluation test which consists of a speed and load torque profile.

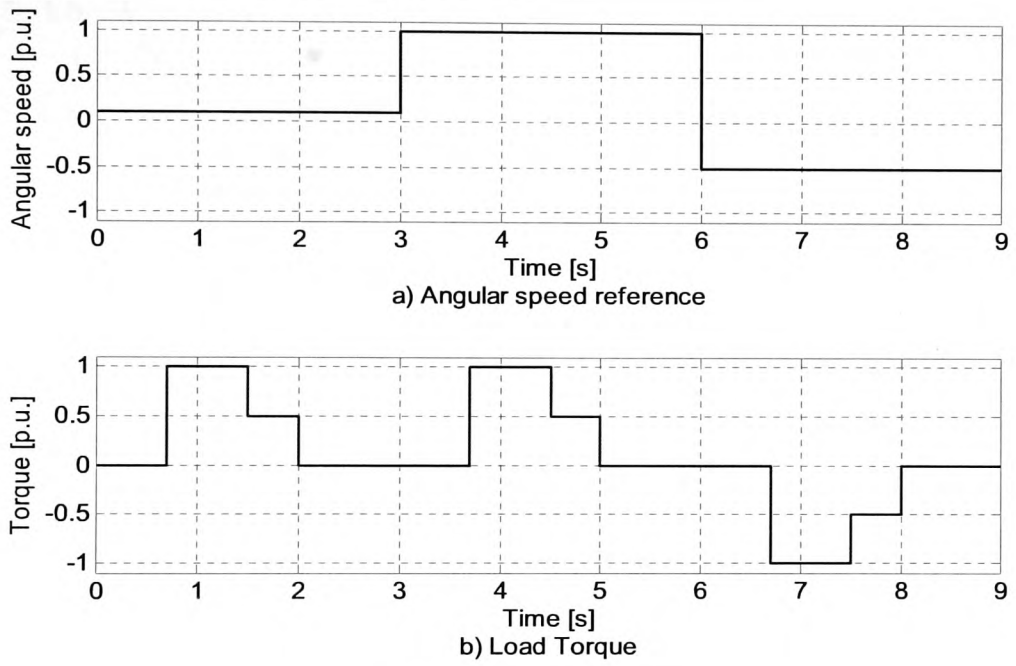

Fig. 5-8 Fitness evaluation test

The optimization problem to be solved is considerably simplified because of its one-dimensional nature; just one parameter, $K_{\Gamma e}$, has to be tuned. It is therefore feasible to execute a set of tests in order to gain some knowledge regarding the shape of the "fitness landscape" and be able to choose the appropriate optimization technique. The concept "fitness landscape" refers to graphical representation of the fitness function, $e_{\Gamma eRMS}$, as a function of the parameters that have to be optimised, in this case $K_{\Gamma e}$.

The set of tests entails executing the simulation of the fitness evaluation test for different values of $K_{\Gamma e}$ in the range of 0 to 250 with increments of 5 units. The fitness landscape obtained is shown in Fig. 5-9.

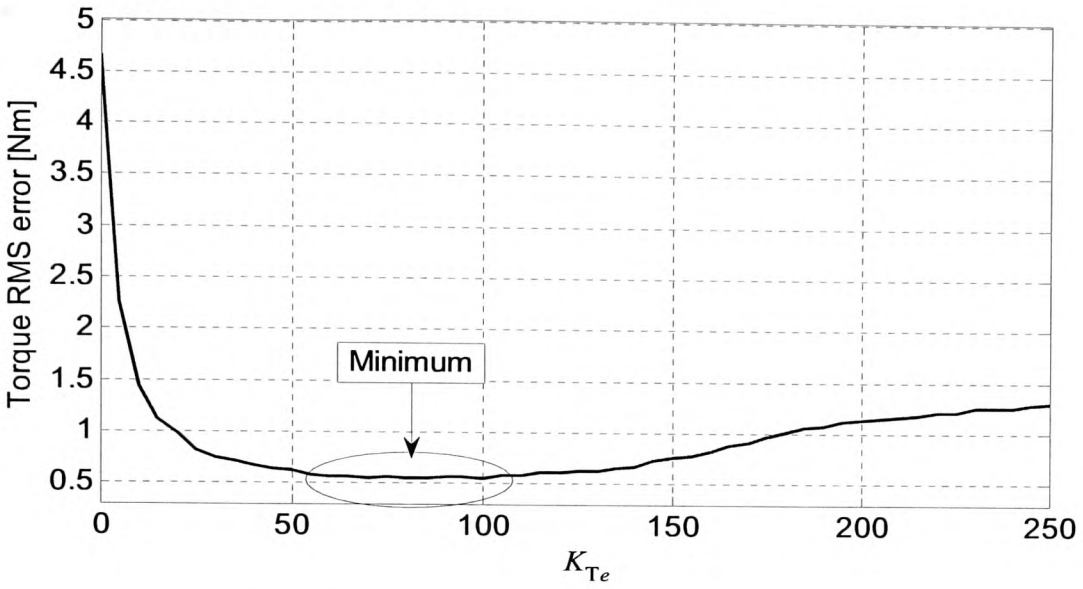

Fig. 5-9 Fitness landscape

From the fitness landscape it is apparent that there is only one basin of attraction, which is the area between 50 and 100 where the minimum is located. It can be observed how for low values of $K_{\Gamma e}$ the goodness of the solutions is considerably worse. This is due to the improvement obtained during transients, which is introduced by the closed-loop proportional control. It can also be seen how the value of the fitness tends to stabilize to a certain value when the value of $K_{\Gamma e}$ increases. This is explained by the fact that for high values of $K_{\Gamma e}$ the behaviour of the system is almost the same due to the saturation of the u_{sy} component of the reference voltage vector. This saturation is caused by the limitation of the DC-link voltage available. For high values of $K_{\Gamma e}$ the system tends to operate in a very similar way to that of the Classical DTC method with a two-level VSI due to the saturation of u_{sy}.

The existence of only one basin of attraction makes it feasible to employ local searchers to find the optimum solution. Local searchers are used to find the nearest local minimum starting from an initial solution. One efficient method of this kind that can be employed is the Hooke-Jeeves algorithm [85]. This method is based on the steepest descent pivot rule and can be employed to find the closest local minimum. In this case and according to the fitness landscape there is only one minimum, which is therefore the global minimum. The optimization algorithm consists of the following steps:

Step 1: Initialization.

The initial solution ($K_{\Gamma e0}$) and the initial radius of exploration ($h=h_0$) are chosen. The fitness of $K_{\Gamma e0}$ is evaluated and $K_{\Gamma e0}$ becomes the current best solution $K_{\Gamma ec}$. The ending conditions, which consist of the minimum radius of exploration (h_{min}) and the maximum number of fitness evaluations (*budget*), are initialized.

Step 2: Exploratory move.

The solutions $K_{\Gamma ec}\pm h$ are evaluated and the solution with the best fitness value is found.

Step 3: Pattern move.

If $K_{\Gamma ec}$ is the best solution, $K_{\Gamma ec}$ remains as the best point and h is halved.

If $K_{\Gamma ec}+h$ is the best solution, the solution $K_{\Gamma ec}+2h$ is evaluated; the best solution among both, $K_{\Gamma ec}+h$ and $K_{\Gamma ec}+2h$, becomes the current best point ($K_{\Gamma ec}$) and h remains the same.

If $K_{\Gamma ec}-h$ is the best, the solution $K_{\Gamma ec}-2h$ is evaluated; the best solution among both, $K_{\Gamma ec}-h$ and $K_{\Gamma ec}-2h$, becomes the current best point ($K_{\Gamma ec}$) and h remains the same.

Step 4: Ending condition.

Repeat process from Step 2 until $h=h_{min}$ or the *budget* is exceeded.

The script of the optimization algorithm employed to tune $K_{\Gamma e}$ is shown in Appendix A. The algorithm has been executed for two different initial solutions in order to test the reliability of the method. In both cases the algorithm has converged to the same solution. The initialization of the algorithm for both executions is shown in Table 5-II.

Table 5-II Initialization parameters of the optimization algorithm

Parameters	Test 1	Test 2
$K_{\Gamma e0}$	0	200
h_0	16	16
h_{min}	1	1
budget	100	100

Table 5-III and Table 5-IV show the progress of Test 1 and Test 2 respectively. Both tests converge to the same solution $K_{\Gamma e} = 81$. In Test 1 the initial solution is closer to the optimum solution and only 21 fitness evaluations are required, while Test 2 takes 27 fitness evaluations to find the optimum solution. The ending condition for both tests is reached when the exploratory radius is less than 1.

Table 5-III Progress of the optimization algorithm for Test 1

$K_{\Gamma e}$	$e_{\Gamma eRMS}$ (fitness)	h	Number of Evaluations
0	4,657	16	1
32	0,775	16	4
64	0,573	16	7
80	0,549	16	10
80	0,549	8	12
80	0,549	4	14
80	0,549	2	16
80	0,549	1	18
81	0,539	1	21
81	0,539	0,5	23

Table 5-IV Progress of the optimization algorithm for Test 2

$K_{\Gamma e}$	$e_{\Gamma eRMS}$ (fitness)	h	Number of Evaluations
200	1,138	16	1
168	0,899	16	4
136	0,666	16	7
104	0,575	16	10
72	0,560	16	13
72	0,560	8	15
80	0,549	8	18
80	0,549	4	20
80	0,549	2	22
80	0,549	1	24
81	0,539	1	27
81	0,539	0,5	29

Fig. 5-10 shows the number of evaluations versus the fitness value to illustrate the progress of the algorithm towards the optimum solution for Test 1 and Test 2. It can be seen how both tests converge after a considerably low number of fitness evaluations. Fig. 5-11 shows the torque response for the initial solution of both tests and the optimum solution found. The improvement achieved when using the optimum value of K_{Te} is apparent.

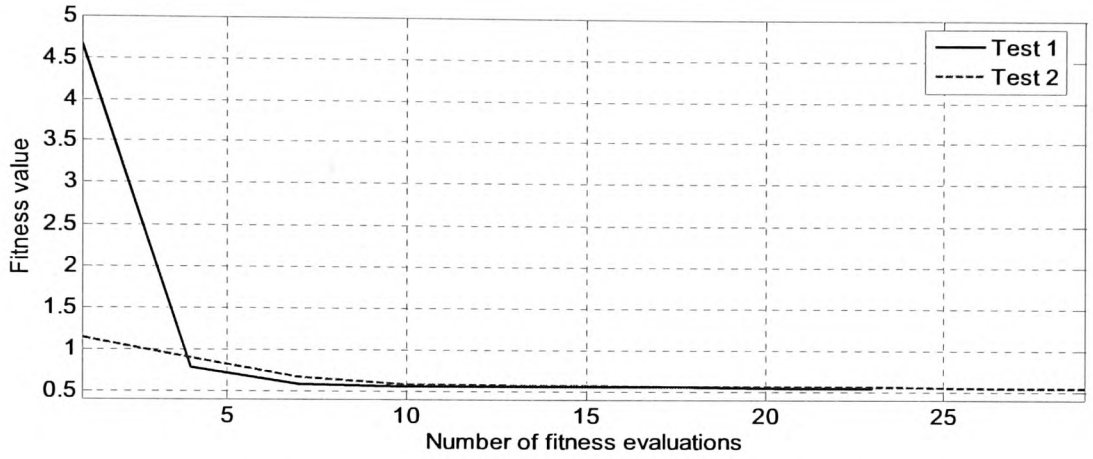

Fig. 5-10 Progress of Test 1 and Test 2 towards the optimum solution

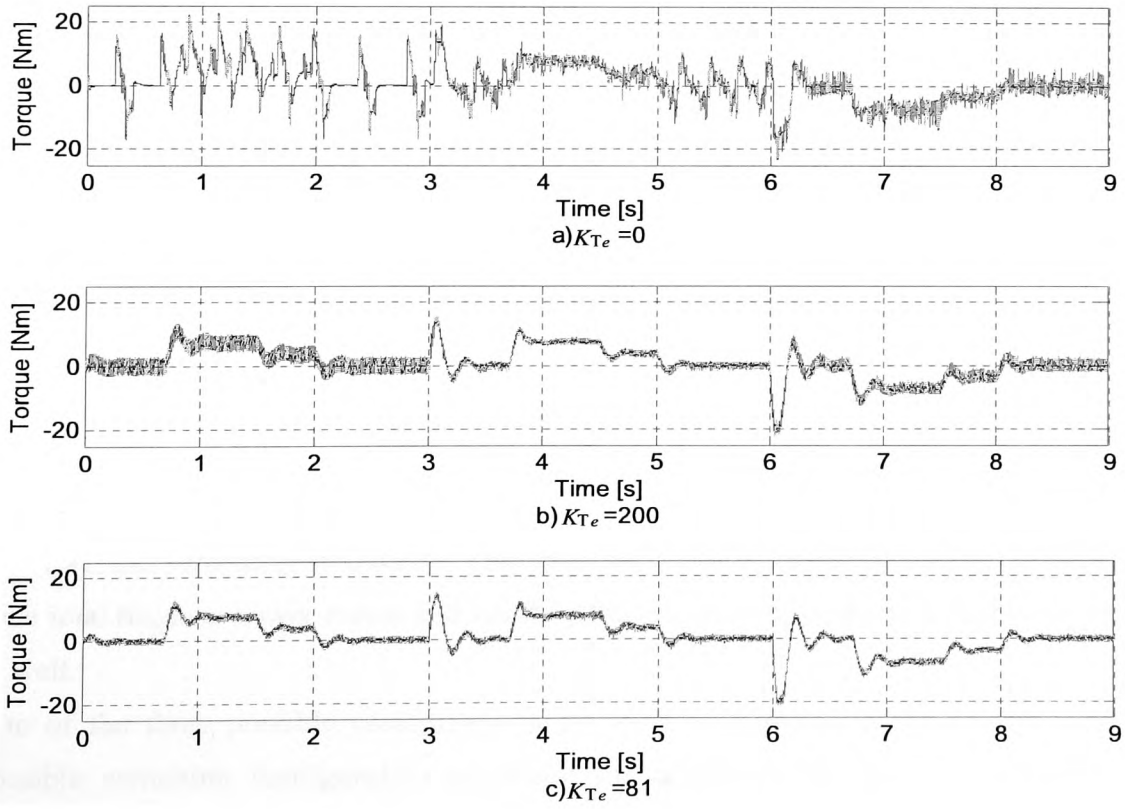

Fig. 5-11 Torque response of the initial solution of both tests and the optimum solution

It can be concluded that the optimization method employed to tune $K_{\Gamma e}$ has proved to be simple, efficient, reliable and considerably quick. These characteristics suggest that this optimization algorithm presents a good potential to be integrated in the motor drive system providing auto-tuning capabilities in a self-commissioning solution.

The results obtained in Test 1 and Test 2 suggest that it is better to start the algorithm with the initial solution taking a high value as in Test 2. It can be observed in Fig. 5-9 how the controller tends to have similar performance for high values of $K_{\Gamma e}$ due to the saturation of the control action. In this situation the system behaves similarly to the Classical DTC method with a two-level VSI. This is because large vectors are selected most of the time. Such solutions despite not being optimum provide a stable torque response and it is therefore recommendable to start with a high value of $K_{\Gamma e}$ as initial solution of the optimization algorithm.

Furthermore, if the algorithm is executed in a particular application, the fitness evaluation test can be adapted to the requirements and constraints of such application. In this way the potential of the optimization process can be fully exploited and the performance of the control can be improved.

Additionally, the algorithm presented could be used to perform a fine adjustment of $K_{\Gamma e}$ during operation. In steady-state conditions (when the torque reference is approximately constant) the optimization algorithm can be executed with a small radius of exploration and the torque RMS error can be evaluated for neighbour solutions in order to find the optimum value for the current operating conditions. This optimum may be slightly different from the optimum value of $K_{\Gamma e}$ found with the training test presented.

5.6 Zero vector selection

As explained in section 3.4.1, three different switching configurations correspond to the zero vector in a three-level VSI. This redundancy provides an additional degree of freedom that can be employed in order to reduce the number of commutations and therefore the switching frequency. This reduction of the switching frequency will be beneficial because power losses and stress in the semiconductor devices will be reduced as well.

One of the three possible configurations for zero vectors can be associated to each possible switching configuration to obtain the minimum number of commutations during transitions.

Table 5-V gives the zero vector configuration associated to each switching configuration in order to minimise the number of commutations during transitions.

Table 5-V Zero vector configuration associated to each switching configuration to minimise commutations

Large Vectors	Zero Vector	Medium Vectors	Zero Vector	Small Vectors	Zero Vector	Small Vectors	Zero Vector
200	000	210	111	211	111	100	000
220	222	120	111	221	222	110	111
020	000	021	111	121	111	010	000
022	222	012	111	122	222	011	111
002	000	102	111	112	111	001	000
202	222	201	111	212	222	101	111

It can be observed that the zero vector configuration 111 has the minimum number of commutations for transitions with medium vectors. This is because a transition in a VSI leg between the possible states 0, 1 and 2 has different number of commutations as illustrated in Fig. 5-12. A transition between the configurations 210 and 000 or 210 and 222 will produce 6 commutations, while a transition between 210 and 111 will only produce 4 commutations. The configuration 111 should be therefore employed after a medium vector in order to minimise the number of commutations.

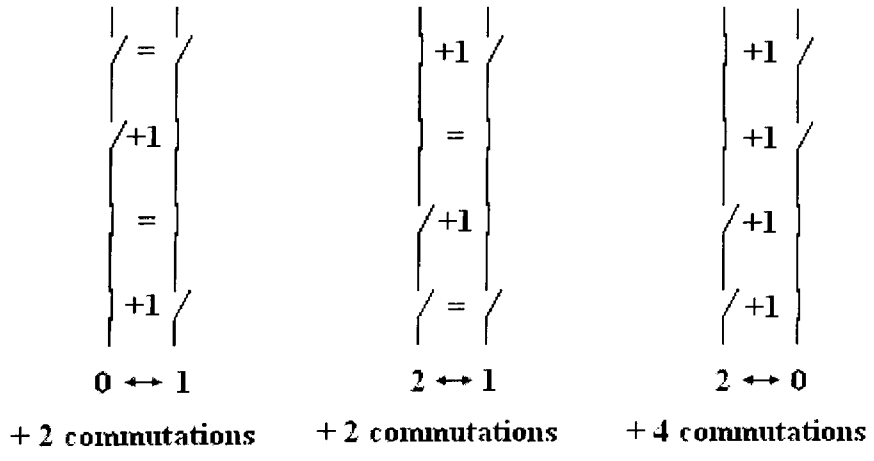

Fig. 5-12 Number of commutations for different transitions of a three-level NPC VSI leg

The redundancy of zero vectors can also be used for a different purpose like the reduction of CM voltages and currents. In this case, for each switching configuration there is a zero vector configuration with a minimum variation of V_{CM} according to Table

3-VIII in section 3.5. The objective of reducing the CM voltage and currents might be in conflict with the minimisation of commutations, which has been prioritised in the proposed system. This is the case of large vectors, where the smallest variation of V_{CM} is achieved if the zero vector configuration 111 is employed. However, according to Table 5-V, the configurations 000 and 222 are employed in order to minimise the number of commutations. For medium and small vectors Table 5-V satisfies both objectives: the minimisation of commutations and the minimisation of the variations in V_{CM}.

5.7 Balance of the Neutral Point voltage

The balance of the NP voltage is an important issue in the control of the three-level NPC VSI. As explained in section 3.4.3, only small and medium vectors affect the voltage balance in the DC-link capacitors. The redundancy of small vectors makes it possible to select the configuration that will correct the voltage drift. The appropriate selection of the small vector configuration is given for all the possible conditions in Table 5-VI. The conditions in the circuit are given by the voltage in the capacitors and the NP current, which is related to the VSI output currents. Voltage polarities and current sense is taken according to Fig. 3-14.

Table 5-VI Small vector selection to balance the NP voltage

Small vector	Configuration	Condition				
		$V_{C1} \geq V_{C2}$	$V_{C1} < V_{C2}$	$i_A - i_{sa}$	$i_B - i_{sb}$	$i_C - i_{sc}$
$\vec{V}_{1s}$	100	√		<0		
			√	≥0		
	211	√		≥0		
			√	<0		
$\vec{V}_{2s}$	110	√				≥0
			√			<0
	221	√				<0
			√			≥0
$\vec{V}_{3s}$	010	√			<0	
			√		≥0	
	121	√			≥0	
			√		<0	
$\vec{V}_{4s}$	011	√		≥0		
			√	<0		
	122	√		<0		
			√	≥0		
$\vec{V}_{5s}$	001	√				<0
			√			≥0
	112	√				≥0
			√			<0
$\vec{V}_{6s}$	101	√			≥0	
			√		<0	
	212	√			<0	
			√		≥0	

Medium vectors only have one possible configuration and their effect on the voltage drift depends on the output current of the leg connected to the NP. This lack of control when medium vectors are selected can be limited by selecting the second nearest vector when the effect of the medium vector tends to increase the voltage drift beyond a certain limit. As a side effect of this solution, the control performance in terms of torque and stator flux response will be worse since the nearest voltage vector to the reference voltage vector cannot be selected.

Fig. 5-13 shows the results of a test performed to asses the efficiency of the NP voltage balance. The test consists of a speed and load torque profile. It can be observed how the voltage level of the NP remains stable during the whole test and has a considerably small ripple. This ripple is a bit accentuated when the motor is rotating at nominal speed because medium vectors are selected more frequently and current values are higher. As explained before, this type of vector complicates the balance of the NP voltage,

consequently if medium vectors are employed more frequently the ripple of the NP voltage increases. Fig. 5-14 illustrates in a small window of the test performed the behaviour of the NP voltage depending on the type of voltage vector selected and the NP current. It can be observed how the NP current is zero when small and large vectors are selected. It can also be seen how small vectors tend to balance the voltage of the DC-link capacitors, while the biggest voltage drift occurs when medium vectors are more frequently selected at the end of the window.

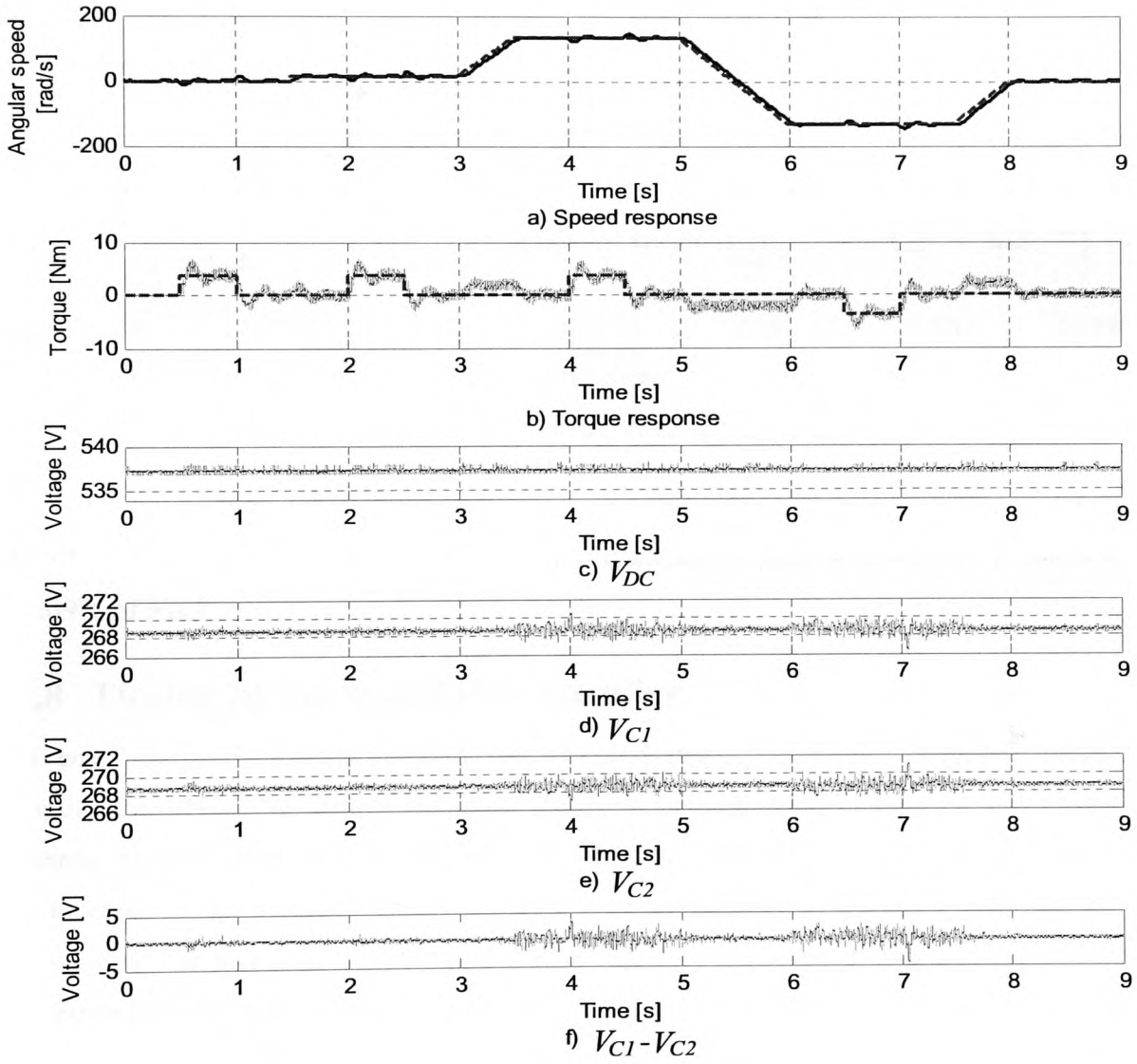

Fig. 5-13 Voltage balance of the DC-link capacitors

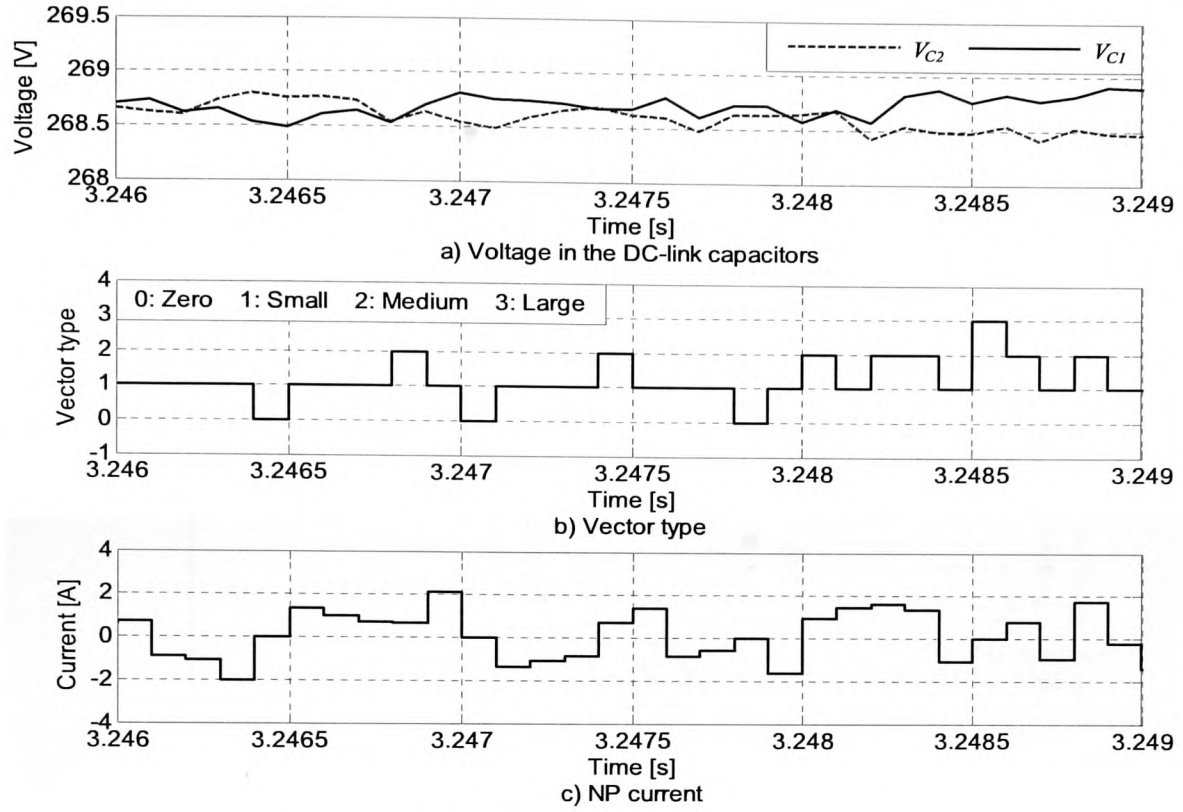

Fig. 5-14 Detail of the voltage drift in the DC-link capacitors

The maximum difference registered during the test between V_{C1} and V_{C2} is 4.5 V (0.84% of V_{DC}), and the RMS value of the difference between V_{C1} and V_{C2} is 0.533 V (0.09% of V_{DC}).

5.8 Tuning of the speed PI controller

PI controllers are widely used in industry and more specifically in speed control applications due to its simple structure and good performance. In the new DTC-based control system described in the previous sections the torque control loop can be connected to an external speed control loop employing a PI controller. In this application the speed PI controller is tuned employing the Symmetrical Optimum (SO) criterion [86-89], which is a very suitable methodology for electrical drive systems due to the presence of small time delays in the control loop and larger time constants in the plant under control. This tuning method, as a main advantage, offers a good disturbance rejection, which is a very desirable feature in speed control applications. The complete control scheme incorporating the speed control loop is shown in Fig. 5-15.

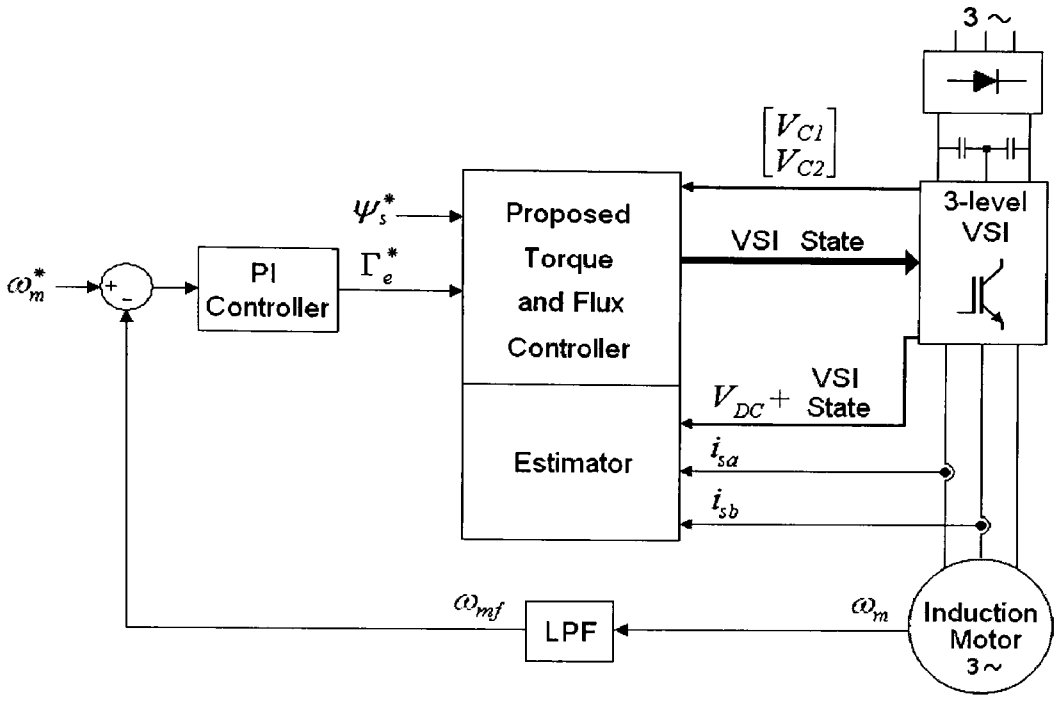

Fig. 5-15 Complete control scheme including the speed controller

The speed control loop can be approximated by the block diagram shown in Fig. 5-16 in order to obtain a transfer function in the *S* domain.

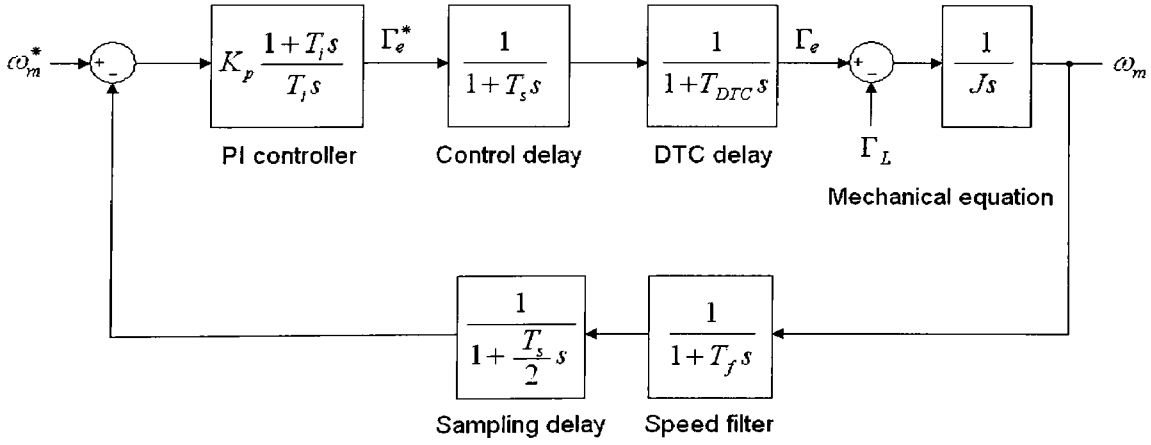

Fig. 5-16 Speed control loop block diagram

The different delays of the control loop are approximated by 1st order transfer functions. This approximation is acceptable since these delays are very small when compared to the motor mechanical time constant. A further simplification can be done by replacing

all the small delays by a single delay, T_Σ, as the sum of all of them. The resulting open-loop transfer function that approximates the speed control loop is the following [90]:

$$G_\omega(s) = K_p \frac{1+T_i s}{T_i s} \frac{1}{1+T_\Sigma s} \frac{1}{Js} \tag{5.19}$$

Where the sum of the small delays in the speed loop, T_Σ, has the following expression:

$$T_\Sigma = \frac{T_s}{2} + T_s + T_f + T_{DTC} \tag{5.20}$$

The delay of the DTC torque control loop is considered to be the equivalent armature time constant of an IM which is given by the following expression:

$$T_{DTC} = \sigma \frac{T_{stator} T_{rotor}}{T_{stator} + T_{rotor}} \tag{5.21}$$

The dispersion factor and the stator and rotor time constants are calculated as follows:

$$\sigma = 1 - \frac{L_m^2}{L_s L_r}; \qquad T_{stator} = \frac{L_s}{R_s}; \qquad T_{rotor} = \frac{L_r}{R_r} \tag{5.22}$$

The transfer function obtained in (5.19) has the same form of the SO criterion transfer function [90], which is expressed as follows:

$$G(s) = \frac{1+4T_\Sigma s}{8T_\Sigma^2 s^2 (1+T_\Sigma s)} \tag{5.23}$$

If expression (5.19) is made equal to (5.23), the resulting PI parameters have the following values:

$$T_i = 4T_\Sigma; \qquad K_p = \frac{J}{2T_\Sigma}; \qquad K_i = \frac{K_p}{T_i} = \frac{J}{8T_\Sigma^2} \tag{5.24}$$

From the application of this method the resulting values of the PI parameters for the IM used in the laboratory setup (see Table 6-I in Chapter 6), with the values T_s=0.0001 s and T_f=0.0032 s, are:

$$K_p = 0.6909; \qquad T_i = 0.0233 \qquad K_i = 29.6488$$

The characteristic response of the SO has a 43.4% overshoot. In order to attenuate this overshoot while keeping the disturbance rejection capability a smoothing filter can be

applied to the speed reference [88, 89, 91]. The transfer function of the smoothing filter is the following:

$$G_{sf} = \frac{1}{1 + T_{sf} s} \tag{5.25}$$

The time constant of the smoothing filter is chosen according to the bandwidth of the speed control loop. In this case and observing the response in simulation for several values it has been decided to set its value to $T_{sf} = 4T_{\Sigma}$, which provides the desired attenuation of the overshoot.

Due to the limitations in real systems some additional blocks must be added to the basic PI scheme. In real systems there are always operational limits for the actuator. The limitation of the PI controller output will have as a result oscillations, overshoots and delays caused by the integral action when the output limit is reached. One solution to this problem is called the integral anti-windup method and it is employed to stop integration when the limit of the output is reached. Several ant-windup methods are proposed in literature and the solution adopted in this case [46] is shown in Fig. 5-17.

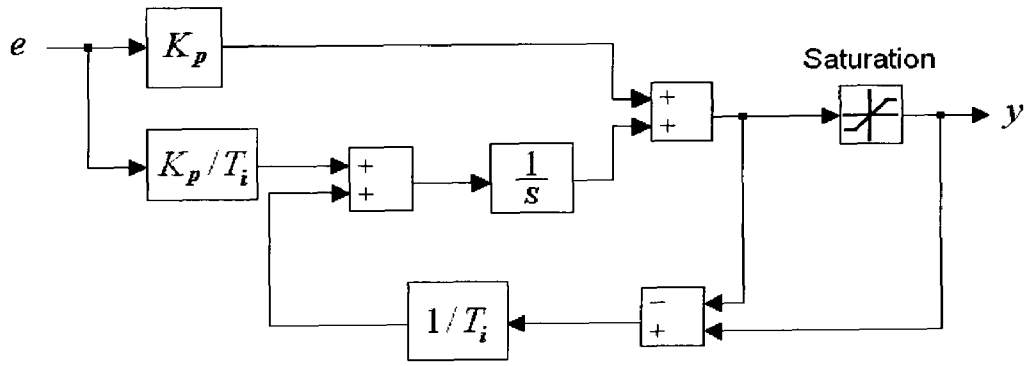

Fig. 5-17 PI controller with anti-windup

Due to the simplifications and approximations done in the process of calculation of the PI parameters, the speed response obtained is slightly different from the theoretical one. The divergences observed are the increase of the rise and settling times and a smaller overshoot in comparison with the SO characteristic response. These divergences are considerably small and the validity of method is proved. Fig. 5-18 shows the speed response of the new control system employing the PI parameters obtained with the tuning method presented. The reference value for the speed is set to 50% of the nominal

speed at 0 s, while the load torque is set to 50% of the nominal torque at 0.25 s in order to observe the disturbance rejection. The response is shown with and without smoothing filter. It can be observed how the smoothing filter decreases the overshoot while the disturbance rejection is kept equal. It can also be seen the reference obtained at the output of the smoothing filter which has the characteristic response of a 1st order system as expected.

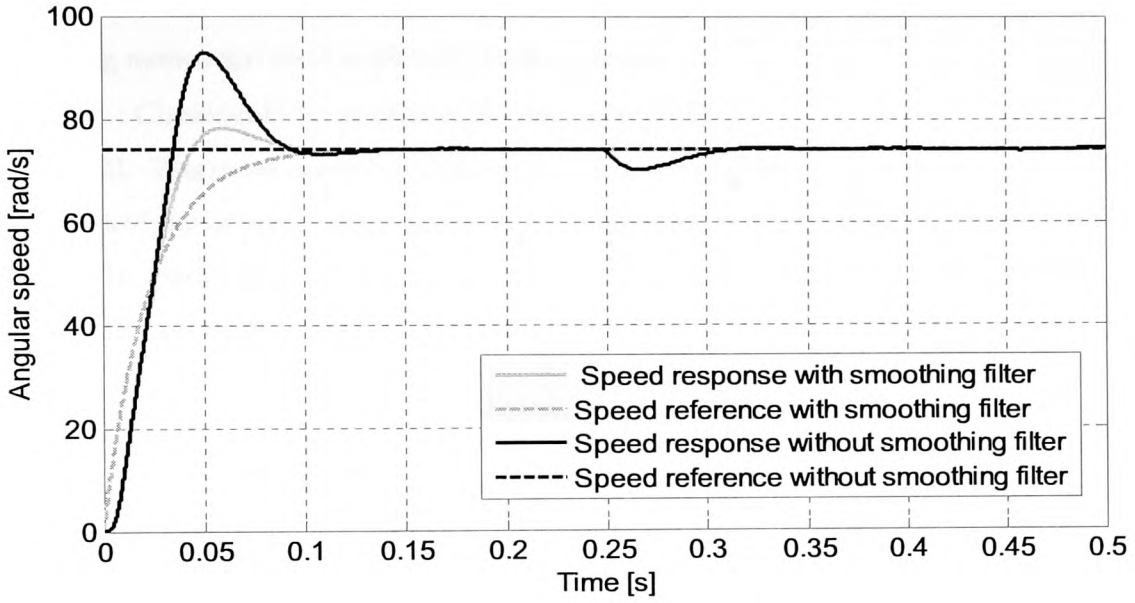

Fig. 5-18 Speed response obtained with the SO tuning method

5.9 Simulation results

The performance of the proposed controller when employing a three-level VSI has been analysed by means of simulation tests. In order to assess the improvements achieved a comparative analysis with the Classical DTC method with a two-level VSI is presented. The characteristics and implementation of the Classical DTC method are well known and it can be considered a good reference to benchmark the proposed system. The simulation tests are divided into two groups, steady-state tests and transient tests. The following names are used to identify both systems:

- DTC2L: Classical DTC system with a two-level VSI.
- PDTC3L: Proposed control system with a three-level VSI.

The control parameters employed in all the tests for both systems are shown in Table 5-VII. The parameters of the speed control loop are common for both systems. The torque and flux hysteresis bands in DTC2L are defined according to Fig. 4-4.

Table 5-VII Control parameters employed in simulation

DTC2L	
Parameter	**Value**
Flux hysteresis bands ($H_{\psi s}$,-$H_{\psi s}$)	(0.001,-0.001) Wb
Torque hysteresis bands ($H_{\Gamma e}$,-$H_{\Gamma e}$)	(0.1,-0.1) Nm
Sampling period (T_s)	0.0001 s
PDTC3L	
Parameter	**Value**
Torque control proportional gain ($K_{\Gamma e}$)	81
Sampling period (T_s)	0.0001 s
Speed control loop	
Parameter	**Value**
PI proportional gain (K_p)	0.6909
PI integral time (T_i)	0.0233
PI output saturation (Γ_{lim})	±17 Nm
Speed filter time constant (T_f)	0.0032 s
Smoothing filter time constant (T_{sf})	0.0233 s

5.9.1 Steady-state performance

The steady-state performance of the both systems, DTC2L and PDTC3L, has been tested in five different operating points defined by the speed reference and load torque values. The operating points chosen are shown in Table 5-VIII, where values are given as percentages of the speed and torque nominal values.

Table 5-VIII Operating points tested in simulation for steady-state conditions

ω_m^*	Γ_L
$10\%\omega_n$	$10\%\Gamma_n$
$10\%\omega_n$	$100\%\Gamma_n$
$100\%\omega_n$	$100\%\Gamma_n$
$50\%\omega_n$	$50\%\Gamma_n$
$100\%\omega_n$	$10\%\Gamma_n$

The variables plotted for each test are:

- Stator flux modulus response.
- Stator flux vector path.
- Torque response.
- Speed response.
- i_{sa} current and frequency spectrum.

Moreover several performance indexes are calculated:

- Mean and RMS stator flux modulus error ($e_{\psi s}$).
- Mean and RMS torque error ($e_{\Gamma e}$).
- RMS speed error ($e_{\omega m}$).
- Stator current THD.
- Mean switching frequency of the semiconductor devices (f_{sw}). (Considering the ON-OFF sequence in a switch as one period).
- Percentage of utilisation for each type of voltage vector. (Large vector also refers to active vector in the system which employs the two-level VSI).

The steady-state results obtained for the different operating points defined in Table 5-VIII are shown in the following figures (Fig. 5-19 to Fig. 5-28). In these figures, the results obtained are presented in two columns; the first column shows the results of the DTC2L system, while the second column presents the results for the PDTC3L system.

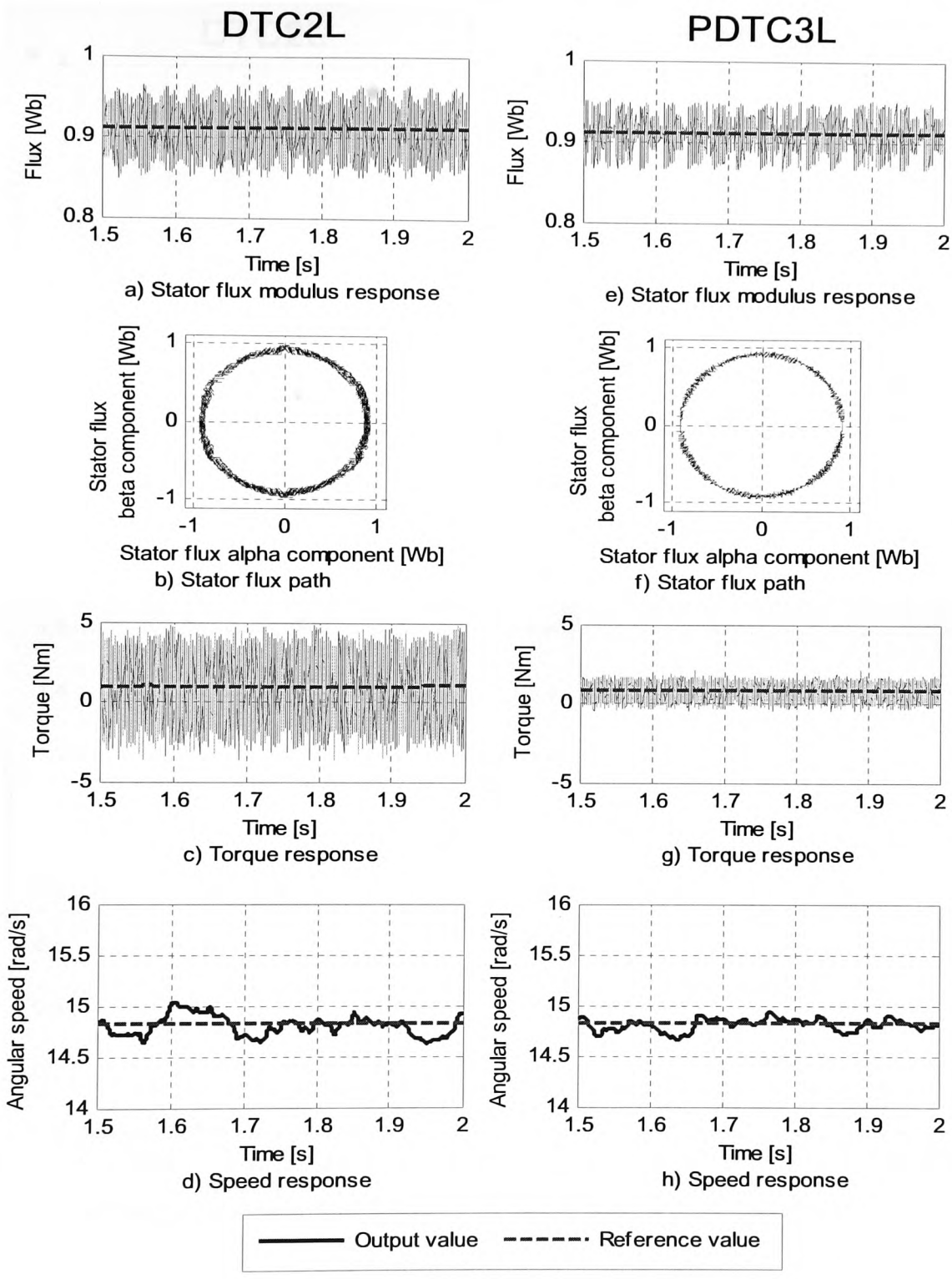

Fig. 5-19 Steady-state results at $10\%\omega_n$ and $10\%\Gamma_n$ part I

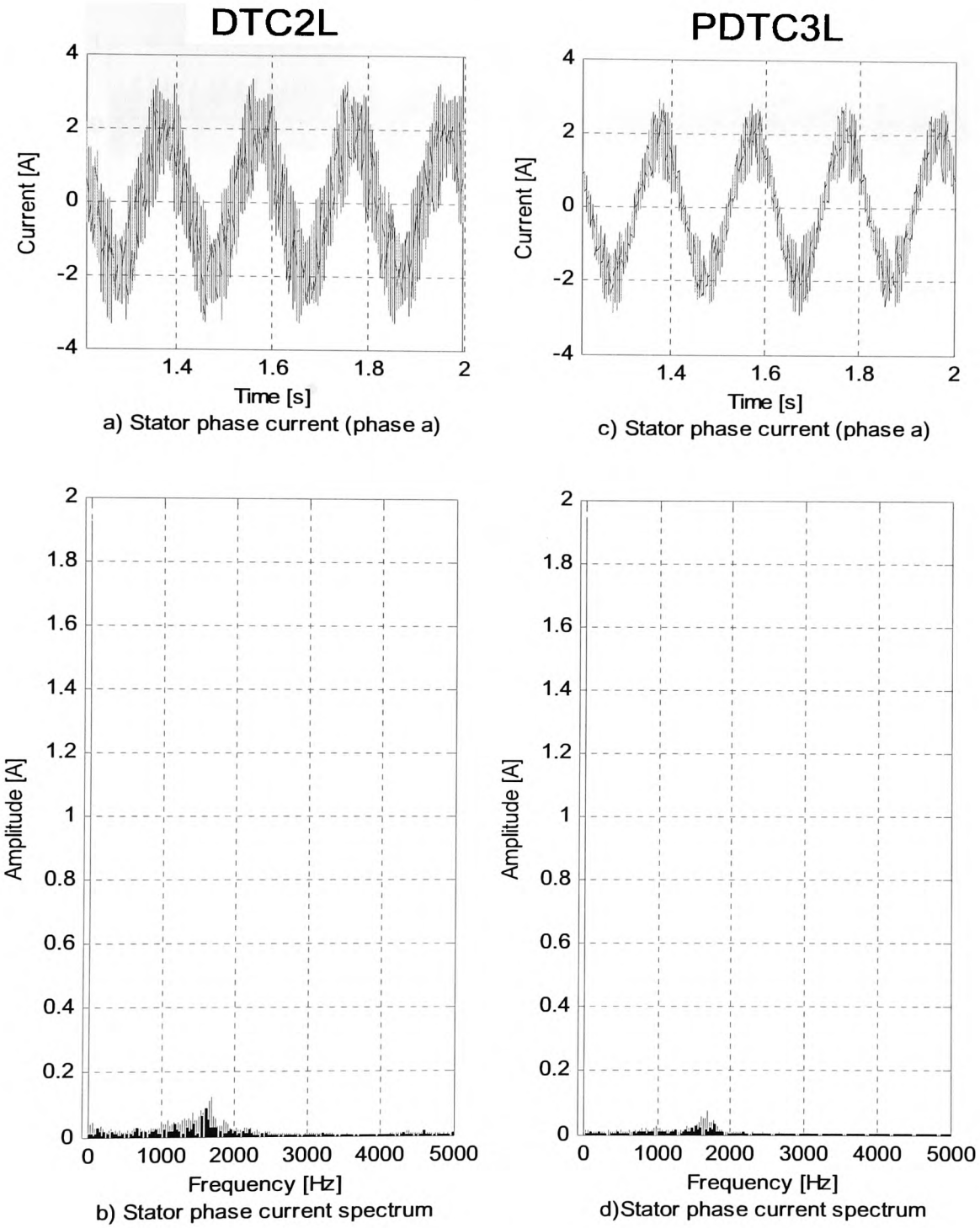

Fig. 5-20 Steady-state results at 10%ω_n and 10%Γ_n part II

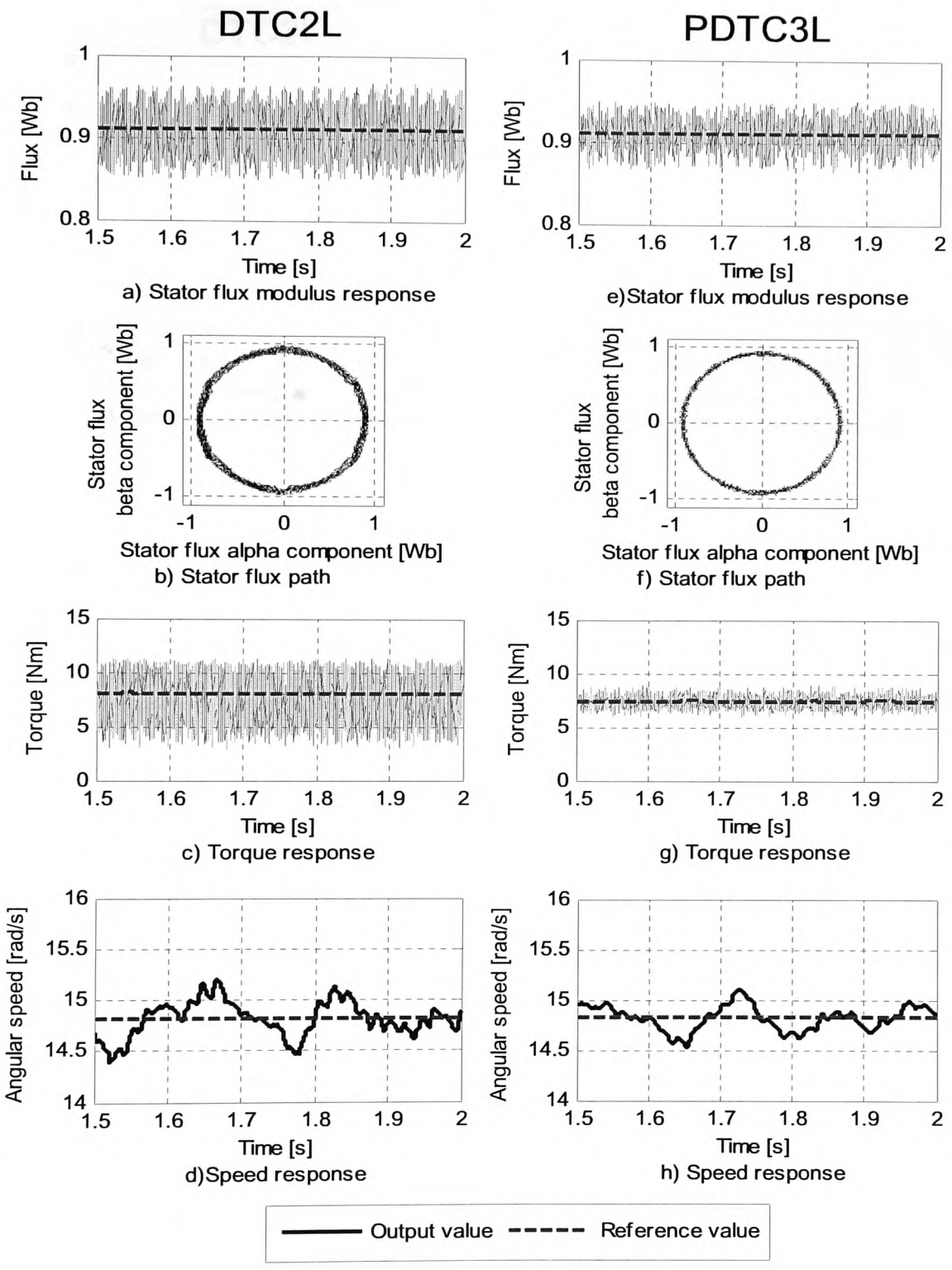

Fig. 5-21 Steady-state results at $10\%\omega_n$ and $100\%\Gamma_n$ part I

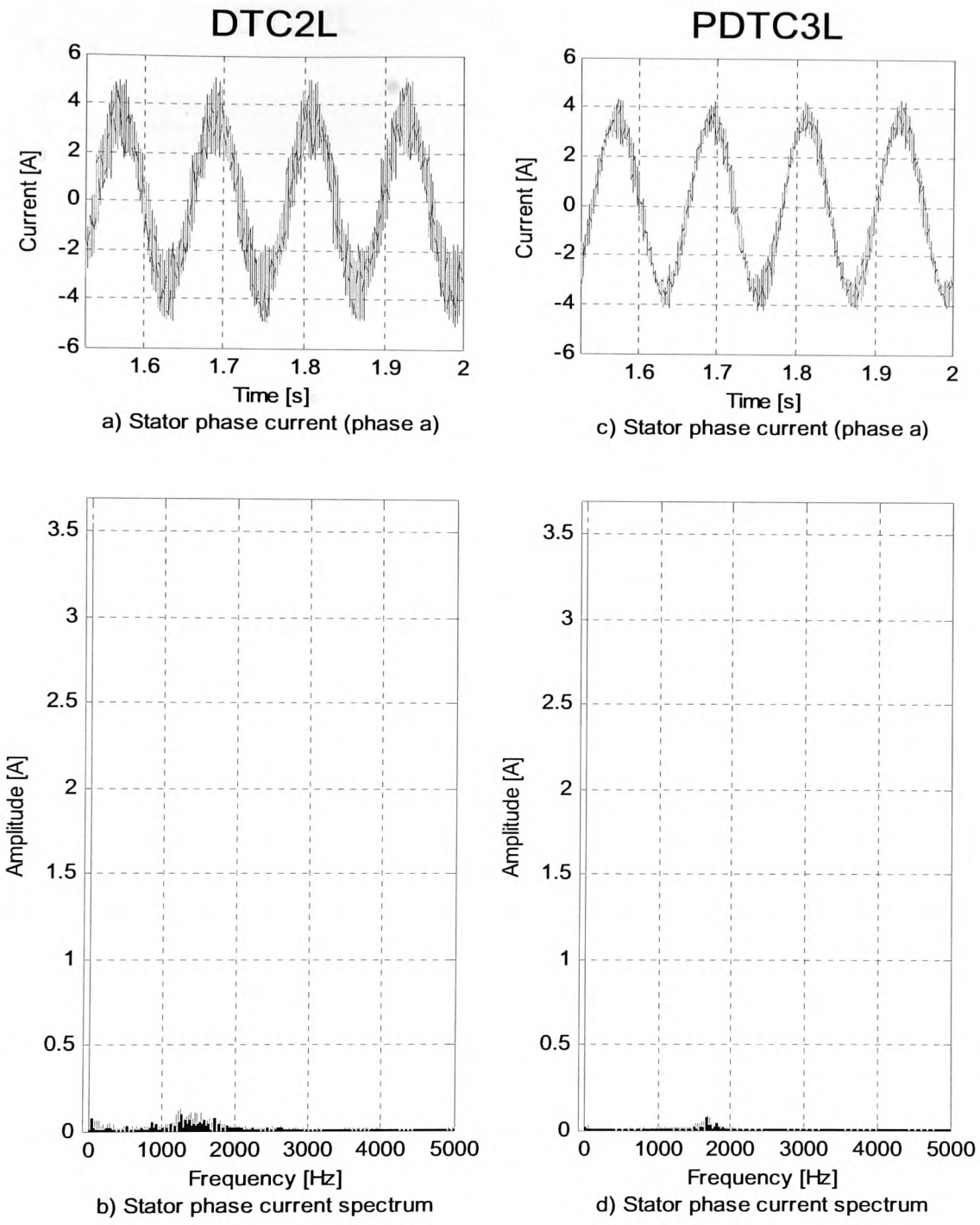

Fig. 5-22 Steady-state results at $10\%\omega_n$ and $100\%\Gamma_n$ part II

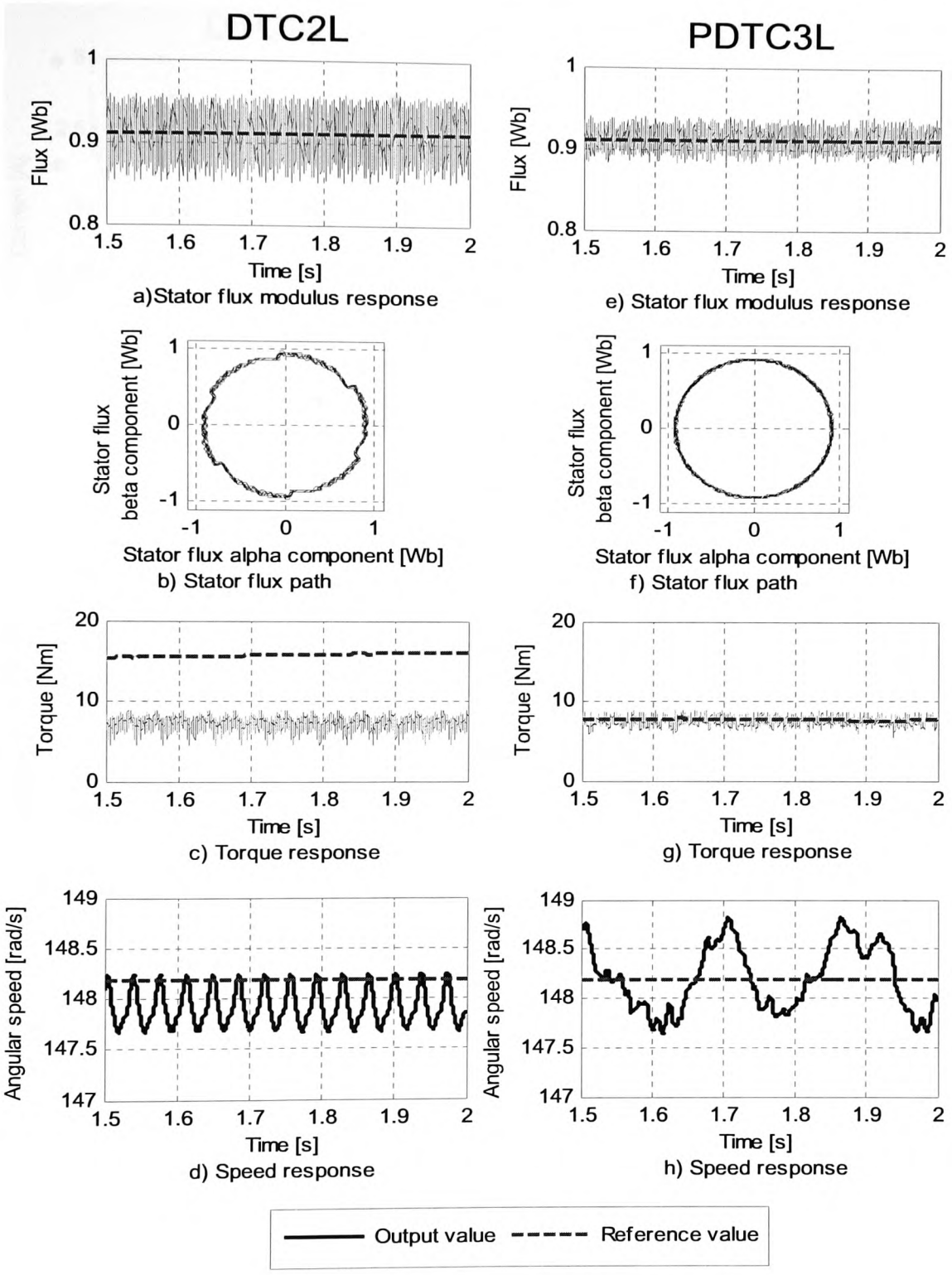

Fig. 5-23 Steady-state results at 100%ω_n and 100%Γ_n part I

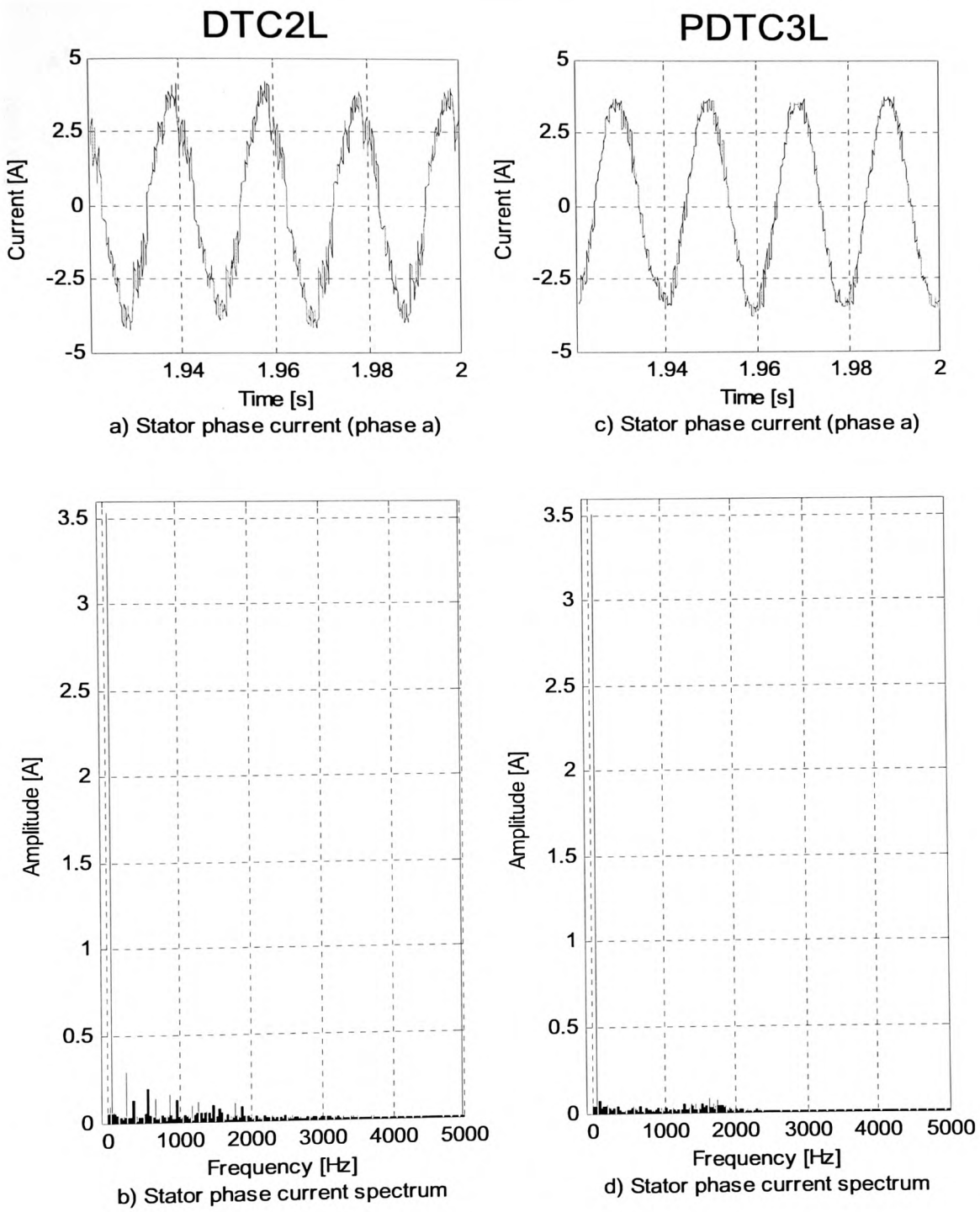

Fig. 5-24 Steady-state results at $100\%\omega_n$ and $100\%\Gamma_n$ part II

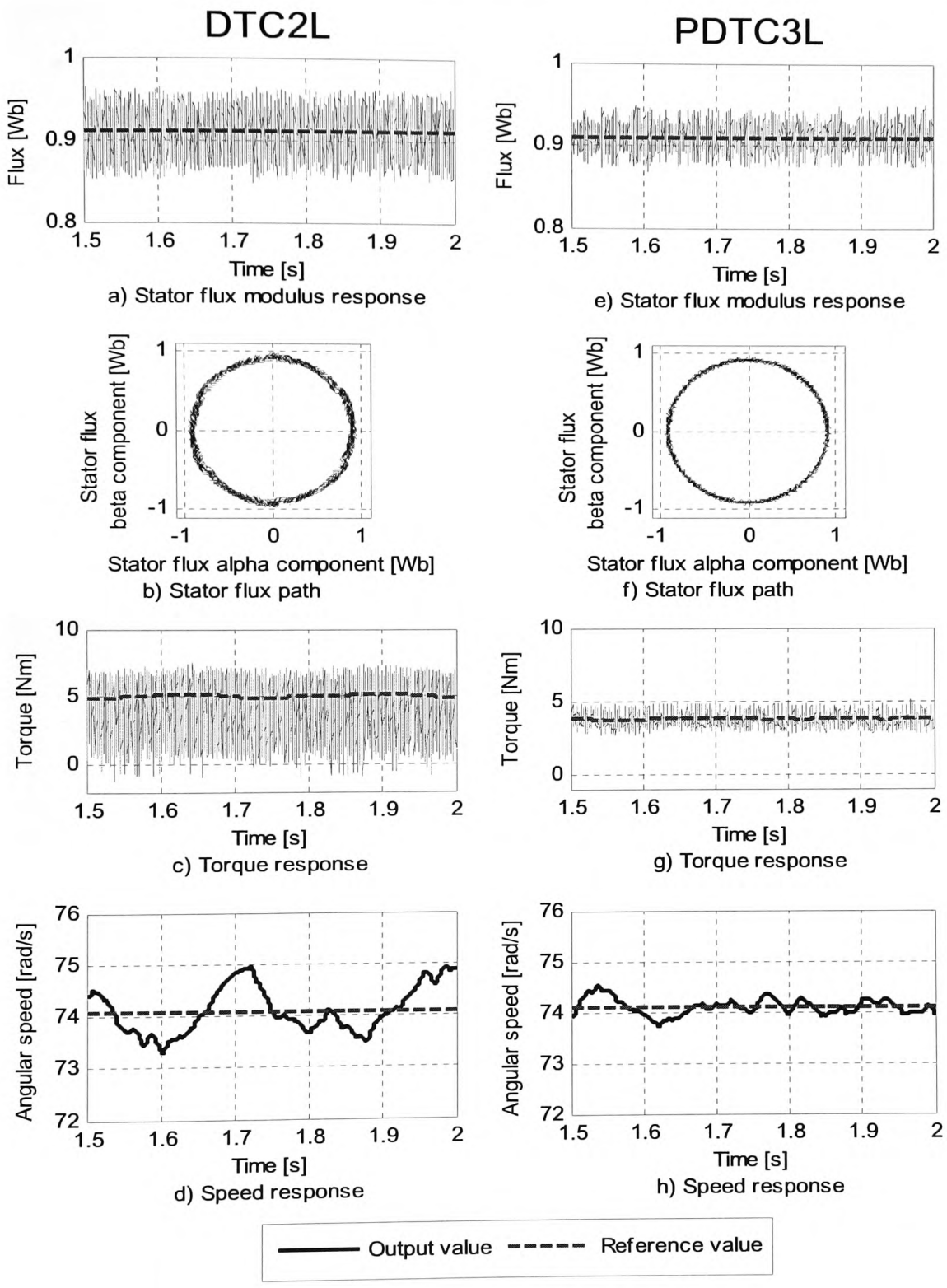

Fig. 5-25 Steady-state results at 50%ω_n and 50%Γ_n part I

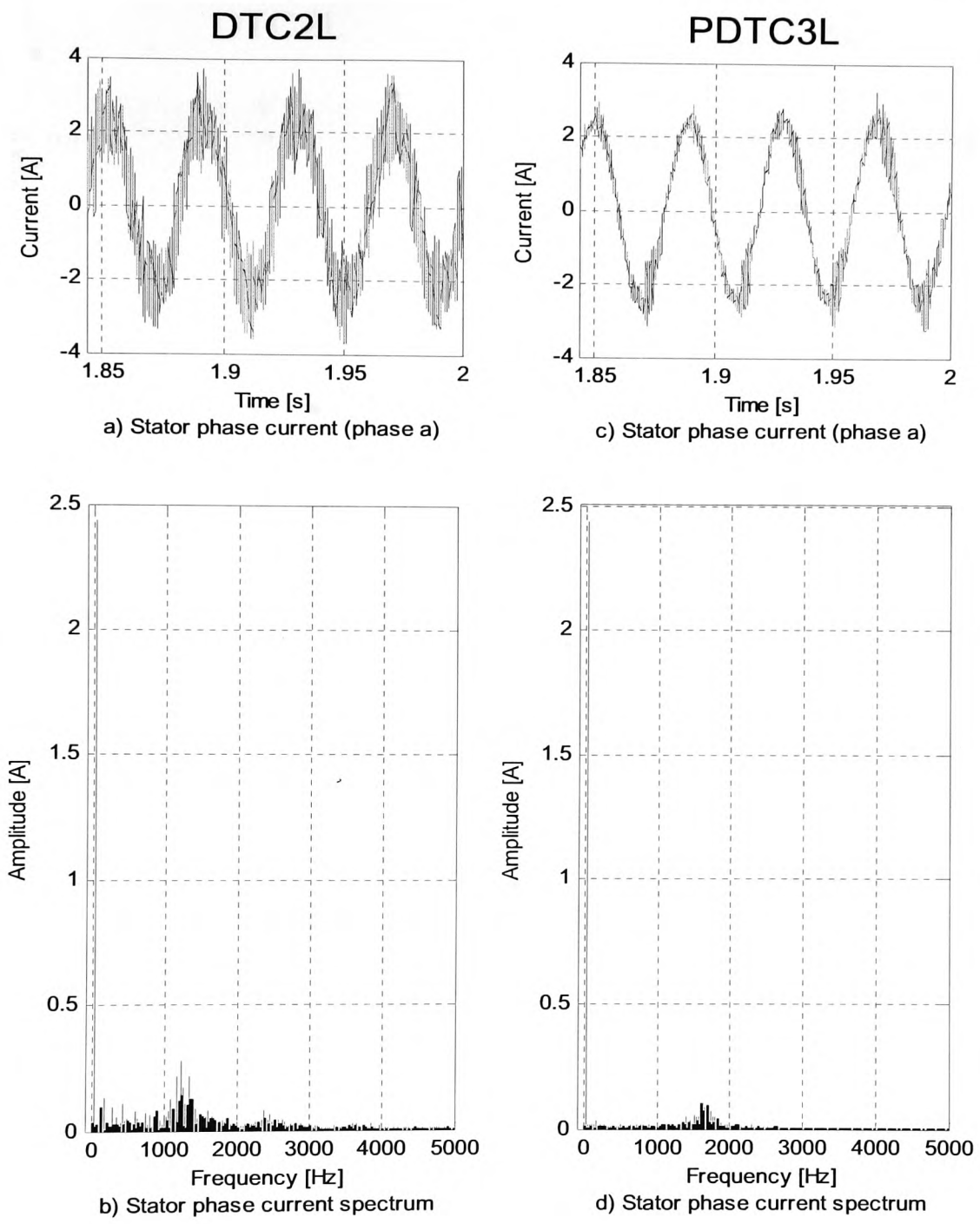

Fig. 5-26 Steady-state results at 50%ω_n and 50%Γ_n part II

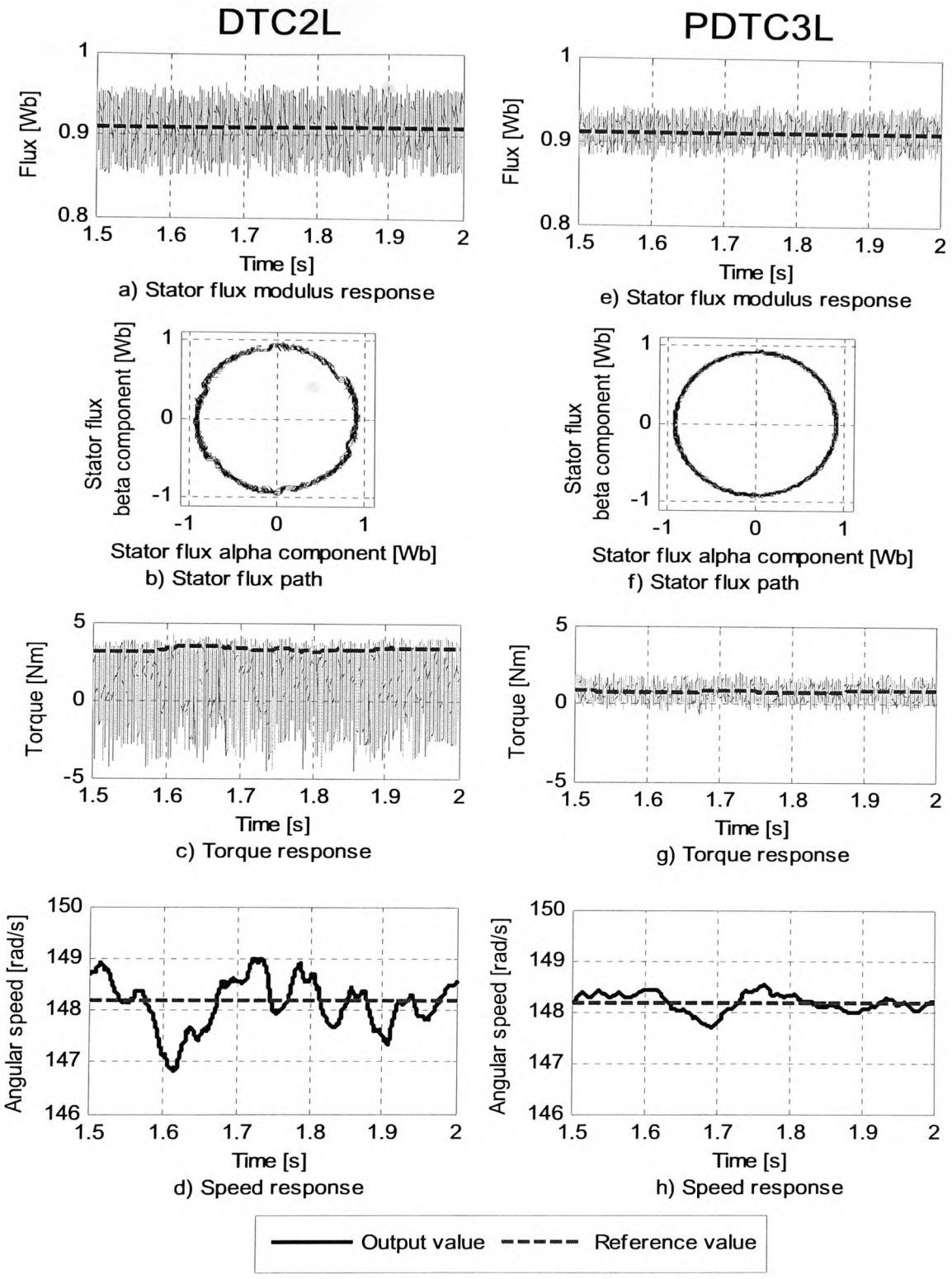

Fig. 5-27 Steady-state results at $100\%\omega_n$ and $10\%\Gamma_n$ part I

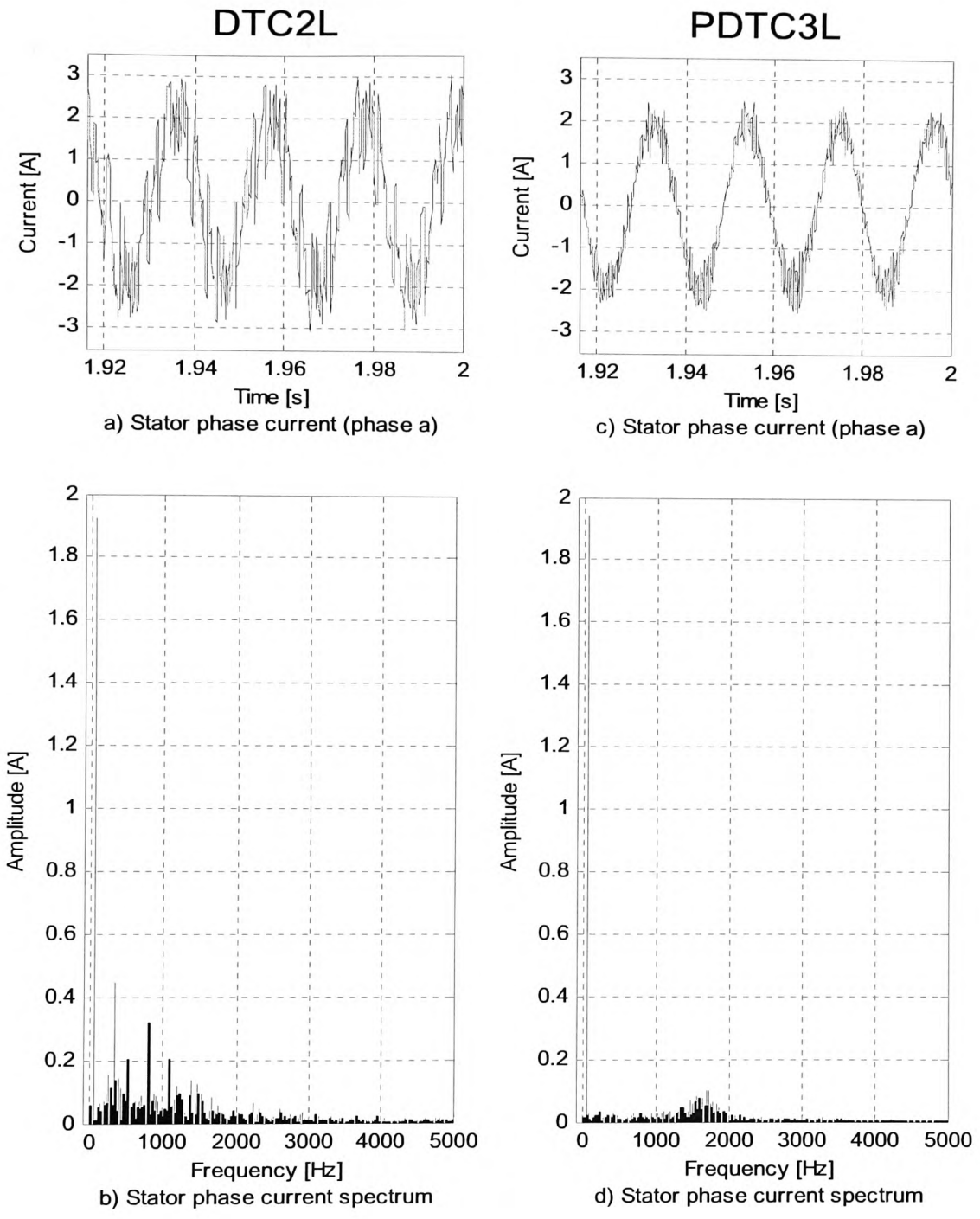

Fig. 5-28 Steady-state results at 100%ω_n and 10%Γ_n part II

The results presented for steady-state conditions show a reduction in the stator flux and torque ripples achieved with the PDTC3L system. The speed oscillation is also lower (except for the operating point $100\%\omega_n$-$100\%\Gamma_n$). The stator phase currents waveforms and spectrum also show lower distortion with the PDCT3L system.

The DTC2L system presents some distortion in the stator flux path due to the effect of the sector boundaries for the operating points $100\%\omega_n$-$100\%\Gamma_n$ and $100\%\omega_n$-$10\%\Gamma_n$. The effect can be observed with more attenuation at $50\%\omega_n$-$50\%\Gamma_n$. It can be conclude from these results that this effect is more noticeable when the stator flux vector rotates at high angular speeds. The distortion consists in a flux drop when the stator flux vector is crossing the sector border and can also be observed in the torque and stator phase current waveforms illustrated in Fig. 5-29. The spectrum of the currents also reflects this distortion with the presence of low frequency harmonics (harmonics 5^{th}, 7^{th}, 11^{th}, 13^{th}, 17^{th}, 19^{th},...) as can be seen in the current spectrum shown in Fig. 5-30. The stator flux amplitude drop produces in turn a torque drop which affects the speed control for the operating point $100\%\omega_n$-$100\%\Gamma_n$ as can be seen in Fig. 5-23. In this situation with the IM in nominal conditions, the produced torque cannot reach the reference value due to the flux drops and it can be observed how the integral action of the speed PI keeps increasing the control action due to existing error.

The PDTC3L system does not employ the sector division and the results show that the distortions observed with the DTC2L system disappear as it can be clearly seen in the stator flux paths.

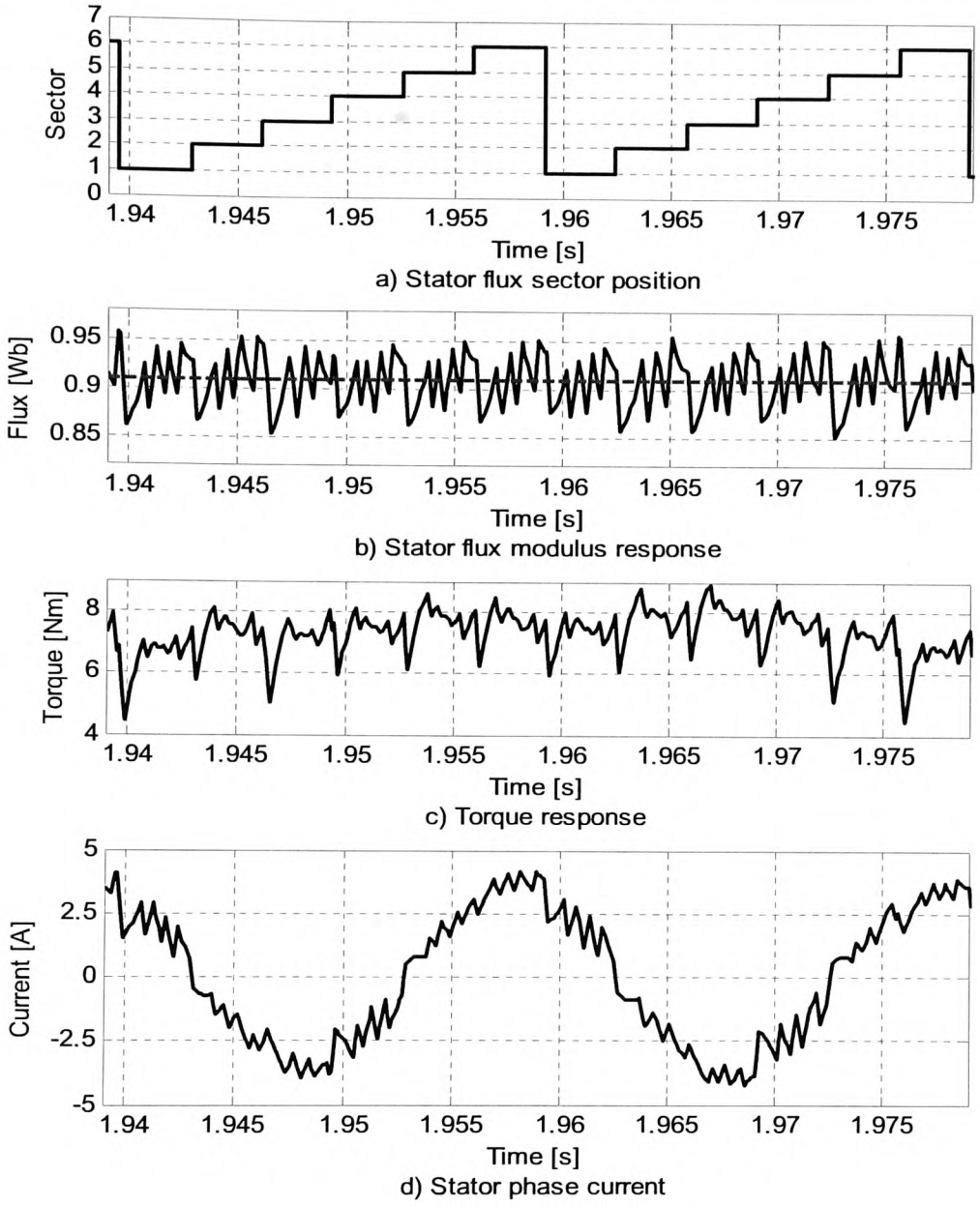

Fig. 5-29 Stator flux, torque and current distortion due to the sector boundaries in the DTC2L system

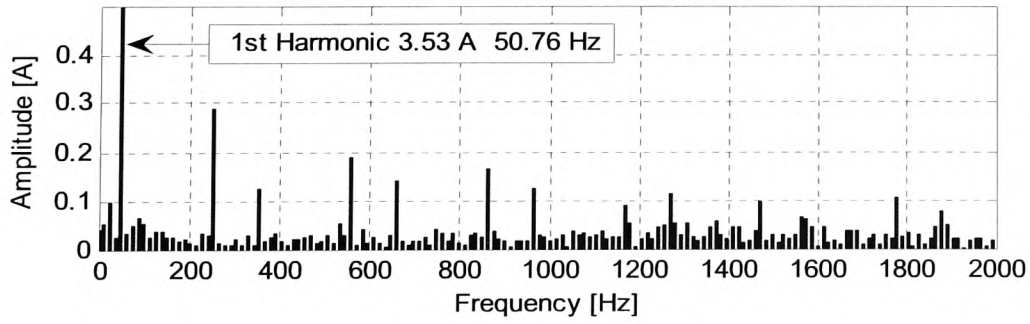

Fig. 5-30 Spectrum of the distorted stator phase current due to the sector boundaries effect

Table 5-IX presents the performance indexes obtained in the steady-state tests for the DTC2L and the PDTC3L systems.

Table 5-IX Performance indexes of the simulated steady-state tests

Index	System	Operating points (%ω_n-%Γ_n)					Mean Reduction %
		10%-10%	10%-100%	100%-100%	50%-50%	100%-10%	
Mean $e_{\psi s}$ [Wb]	DTC2L	0.0023	0.0034	0.0015	0.0020	0.0018	**54.32**
	PDTC3L	-0.0001	-0.0001	-0.0016	-0.0004	-0.0017	
RMS $e_{\psi s}$ [Wb]	DTC2L	0.0242	0.0253	0.0241	0.0254	0.0258	**40.17**
	PDTC3L	0.0169	0.0176	0.0108	0.0153	0.0141	
Mean $e_{\Gamma e}$ [Nm]	DTC2L	0.254	0.595	8.629	1.267	2.524	**90.8**
	PDTC3L	0.087	-0.006	0.214	0.080	0.049	
RMS $e_{\Gamma e}$ [Nm]	DTC2L	1.767	1.894	8.655	2.164	3.124	**81.53**
	PDTC3L	0.501	0.477	0.512	0.402	0.446	
RMS $e_{\omega m}$ [rad/s]	DTC2L	0.102	0.160	0.316	0.388	0.578	**34.28**
	PDTC3L	0.053	0.115	0.361	0.247	0.155	
THD i_{sa} [%]	DTC2L	47.77	27.07	17.69	38.35	52.23	**53.51**
	PDTC3L	24.65	12.76	9.30	16.62	19.72	
Mean f_{sw} [Hz]	DTC2L	1640	1503	458	1303	693	**30.16**
	PDTC3L	804	899	380	851	638	
Mean ω_s [rad/s]	DTC2L	31.752	52.959	318.95	160.77	298.76	
	PDTC3L	31.89	52.874	319.19	159.48	298.58	
% zero vectors	DTC2L	2.17	2.14	0.08	1.30	1.50	
	PDTC3L	33.91	21.53	0.005	0.47	0.005	
% large vectors	DTC2L	97.83	97.86	99.92	98.70	98.50	
	PDTC3L	4.70	5.72	53.12	4.12	32.37	
% medium vectors	DTC2L						
	PDTC3L	14.72	11.72	44.69	20.49	53.35	
% small vectors	DTC2L						
	PDTC3L	46.64	61.01	2.17	74.91	14.26	

The last column of the table shows the mean reduction of the performance indexes obtained for all the operating points. It can be observed how the PDTC3L system considerably reduces all the indexes and proves its superiority in comparison with the DTC2L system. Results show that the PDTC3L system offers a more precise control of stator flux modulus, torque and speed with less distorted currents and a lower switching frequency in the semiconductor devices. The reduction of the torque RMS error is particularly remarkable and it is achieved thanks to the feed-forward term of the torque control law (see equation (5.13)).

The resulting mean switching frequency for both systems and each operating point is shown in Fig. 5-31. It can be observed how the switching frequency is considerably reduced particularly for low angular speeds of the stator flux vector (ω_s). This is caused by the frequent utilisation of small and medium vectors for low and medium ω_s. For high values of ω_s the resulting switching frequency is similar for both systems because the PDTC3L system employs large vectors most of the times. Just a small reduction is achieved thanks to the medium vectors that are also selected quite frequently.

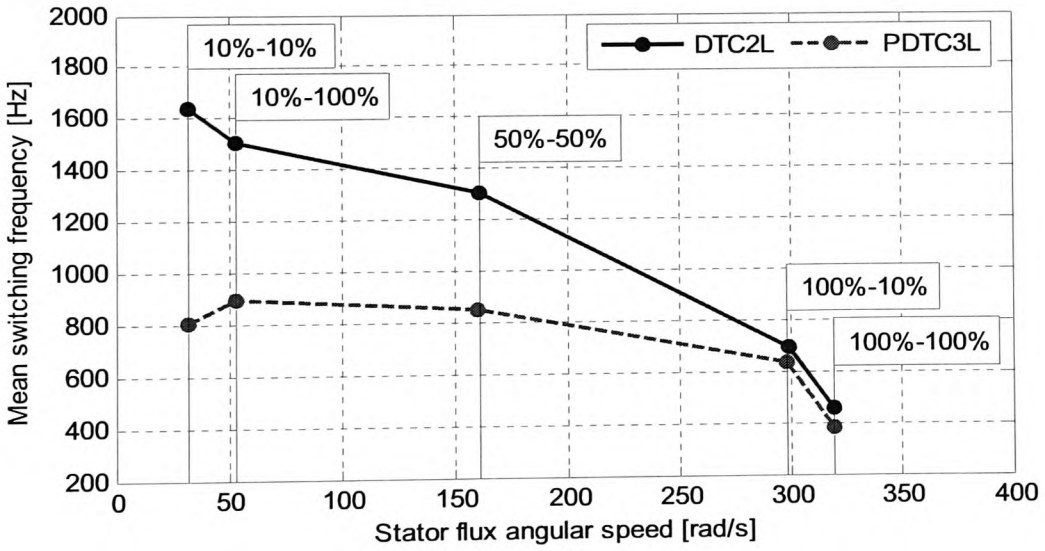

Fig. 5-31 Mean switching frequency depending on the operating point

The last 4 rows of Table 5-IX present the percentage of utilisation of the different types of voltage vector in order to analyse how they contribute to the improvement of the control system response.

The DTC2L system employs active or large vector most of the time and zero vectors are employed less than 3% of the time for all operating points.

The PDTC3L system employs all the different types of vectors with a significant variation of the percentages depending on the operating point as shown in Fig. 5-32. Zero vectors have a big contribution for low ω_s but their percentage of utilisation for high ω_s is very small. Small vectors have the biggest contribution for small and medium values of ω_s. Medium and large vectors have the biggest contribution for high values of ω_s. Moreover it should be noted that medium vectors also have an important contribution for medium and even small values of ω_s. This analysis clearly confirms the goodness of the solution based on the combination of DTC and the three-level VSI.

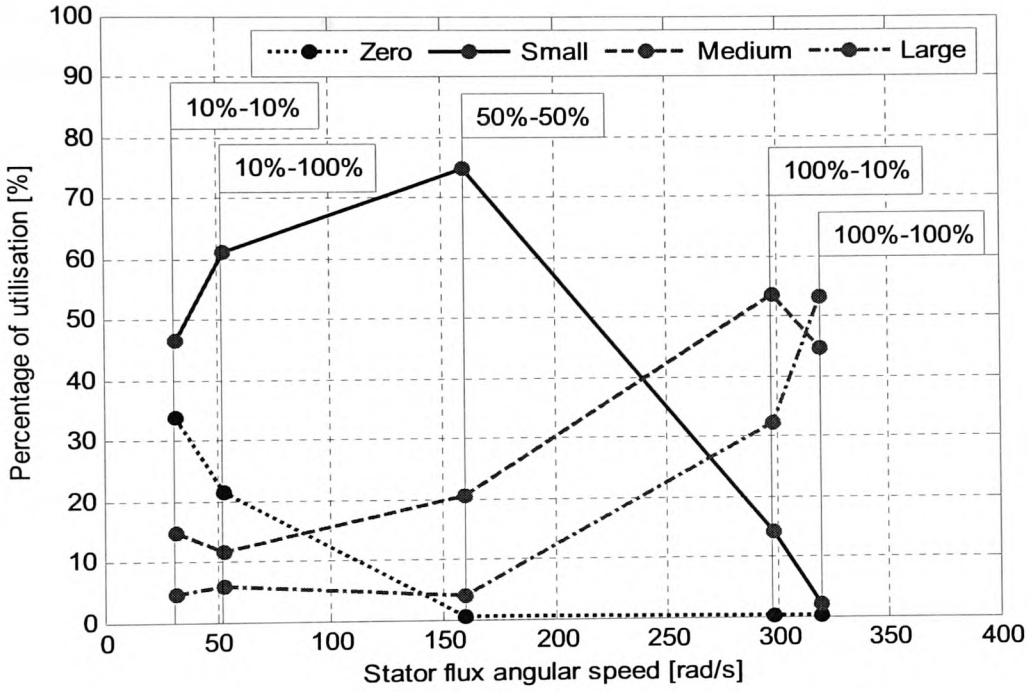

Fig. 5-32 Percentage of utilisation of the different types of vector depending on the operating point

An additional benefit that multilevel topologies can offer as explained in Chapter 3 is the reduction of CM voltage and currents. The RMS value of the CM voltage has been calculated for the DTC2L and PDTC3L systems and all the operating points. It can be observed in Table 5-X how the reduction achieved is around 30% for all the operating points.

Table 5-X V_{CMRMS} for different operating points

Operating point	V_{CMRMS} [V]	
	DTC2L	PDTC3L
$10\%\omega_n$ and $10\%\Gamma_n$	97.332	66.416
$10\%\omega_n$ and $100\%\Gamma_n$	97.516	76.698
$100\%\omega_n$ and $100\%\Gamma_n$	89.567	64.606
$50\%\omega_n$ and $50\%\Gamma_n$	94.255	79.838
$100\%\omega_n$ and $100\%\Gamma_n$	91.253	61.697

Regarding CM currents, it is important to reduce CM voltage transitions and the size of the voltage step in these transitions as much as possible due to the capacitive nature of the CM circuit. Fig. 5-33 shows the spectrum of the CM voltage for both systems and all operating points. It should be noted that the CM voltage has a spread spectrum due to the variable frequency of both systems. A qualitative analysis of the spectrums obtained shows a reduced presence of harmonics at high frequencies for the PDTC3L system. In order to have an accurate study of CM voltage and the effects it can produce, the CM circuit should be modelled to obtain the CM currents [42].

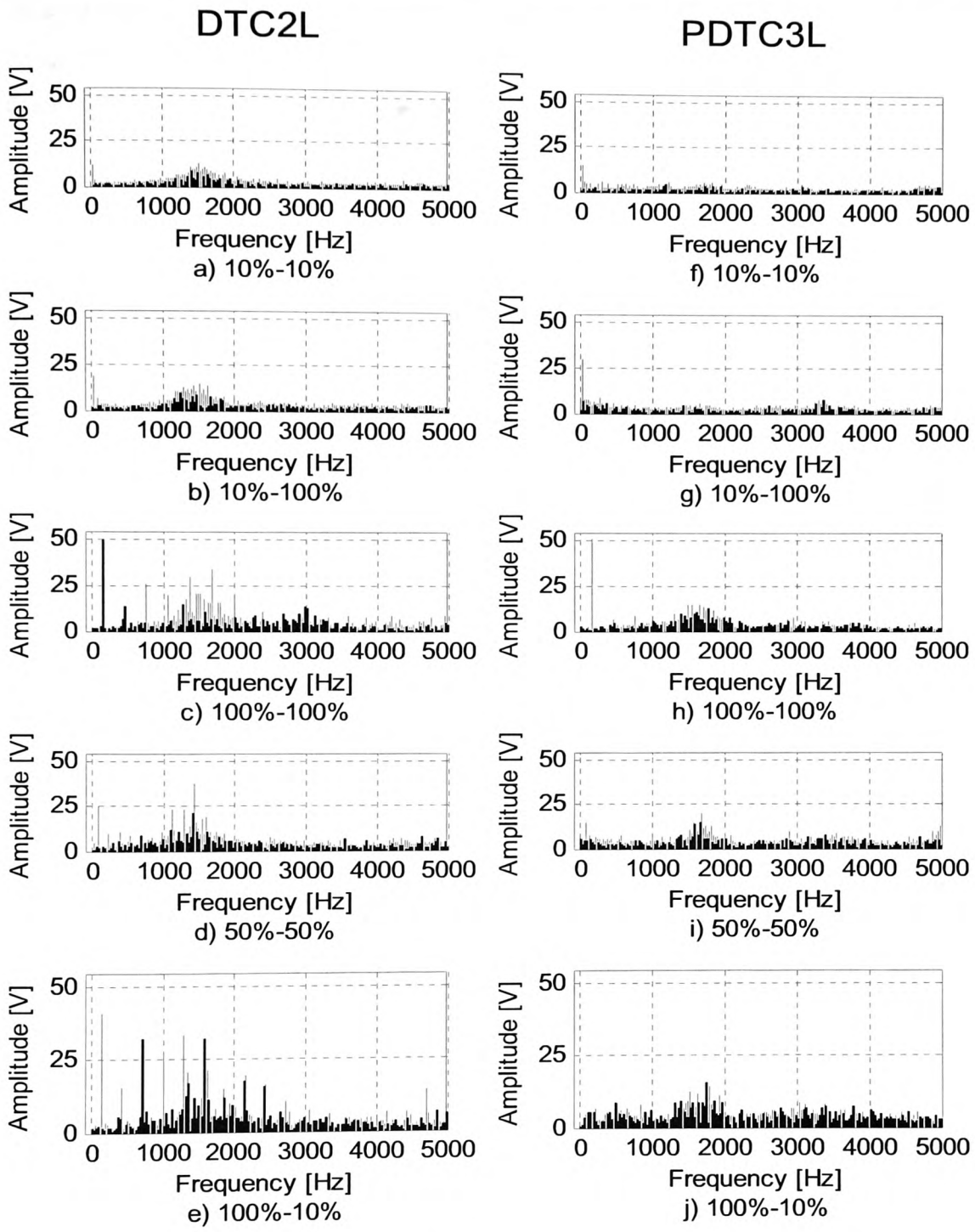

Fig. 5-33 CM voltage spectrum for the different operating points

5.9.2 Transient performance

The transient performance of the proposed control system has been analysed by means of two different dynamic tests. The first dynamic test (Speed Test) consists of a speed and load torque profile as shown in Fig. 5-34.

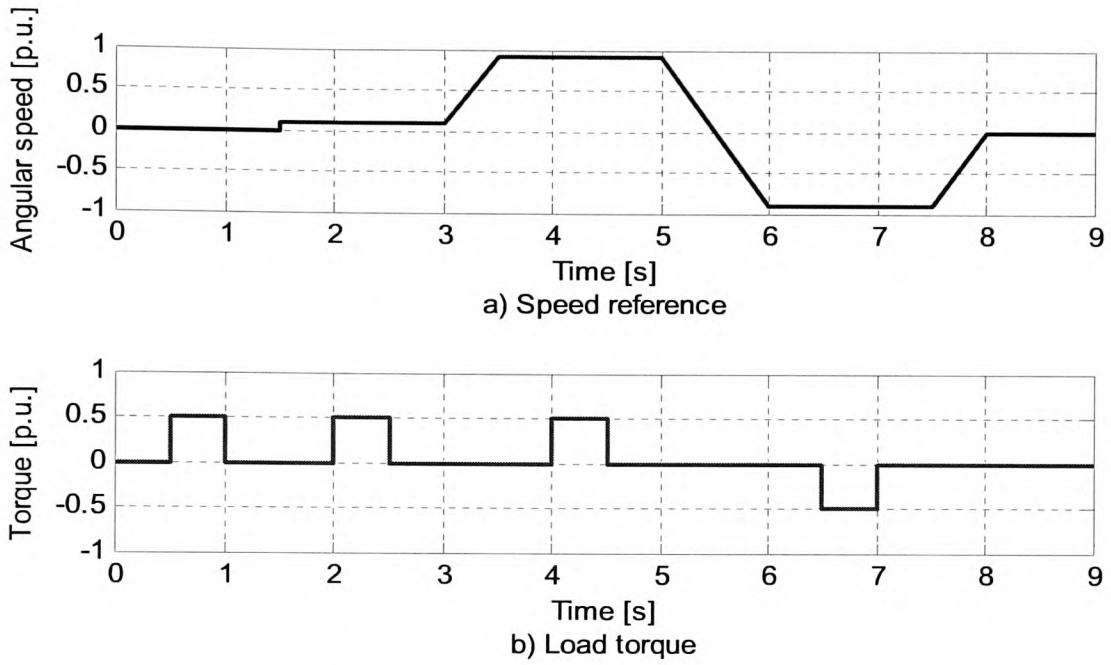

Fig. 5-34 Speed and torque profile of the Speed Test

The second dynamic test (Torque Test) consists in a torque reference profile. At 0.1 s the torque reference is set to the nominal torque value (Γ_n) and this reference is kept until the motor speed reaches its nominal value (ω_n), then the torque reference changes to $-\Gamma_n$ until the motor speed reaches $-\omega_n$ and the torque reference is changed back to Γ_n.

The variables plotted for each test are:

- Torque response.
- Speed response.
- Stator flux modulus response.
- Stator phase currents.
- NP voltage (only for PDTC3L).

Moreover several performance indexes are calculated:

- RMS speed error ($e_{\omega m}$) (only for the Speed Test).
- RMS torque error ($e_{\Gamma e}$).
- RMS stator flux modulus error ($e_{\psi s}$).

- RMS value of the difference between the voltages of the DC-link capacitors (only for PDTC3L).
- Mean difference between the voltages of the DC-link capacitors (only for PDTC3L).
- Mean NP current (i_{NP}) (only for PDTC3L).

The Speed Test results obtained for the DTC2L system and the PDTC3L system are shown in Fig. 5-35 and Fig. 5-36 respectively. It can be observed how both systems provide a satisfactory speed control with similar dynamic performance. Flux and torque ripple is reduced with the PDTC3L system, and the stator current is less distorted. Moreover, the control of the NP voltage proves to be efficient during the Speed Test.

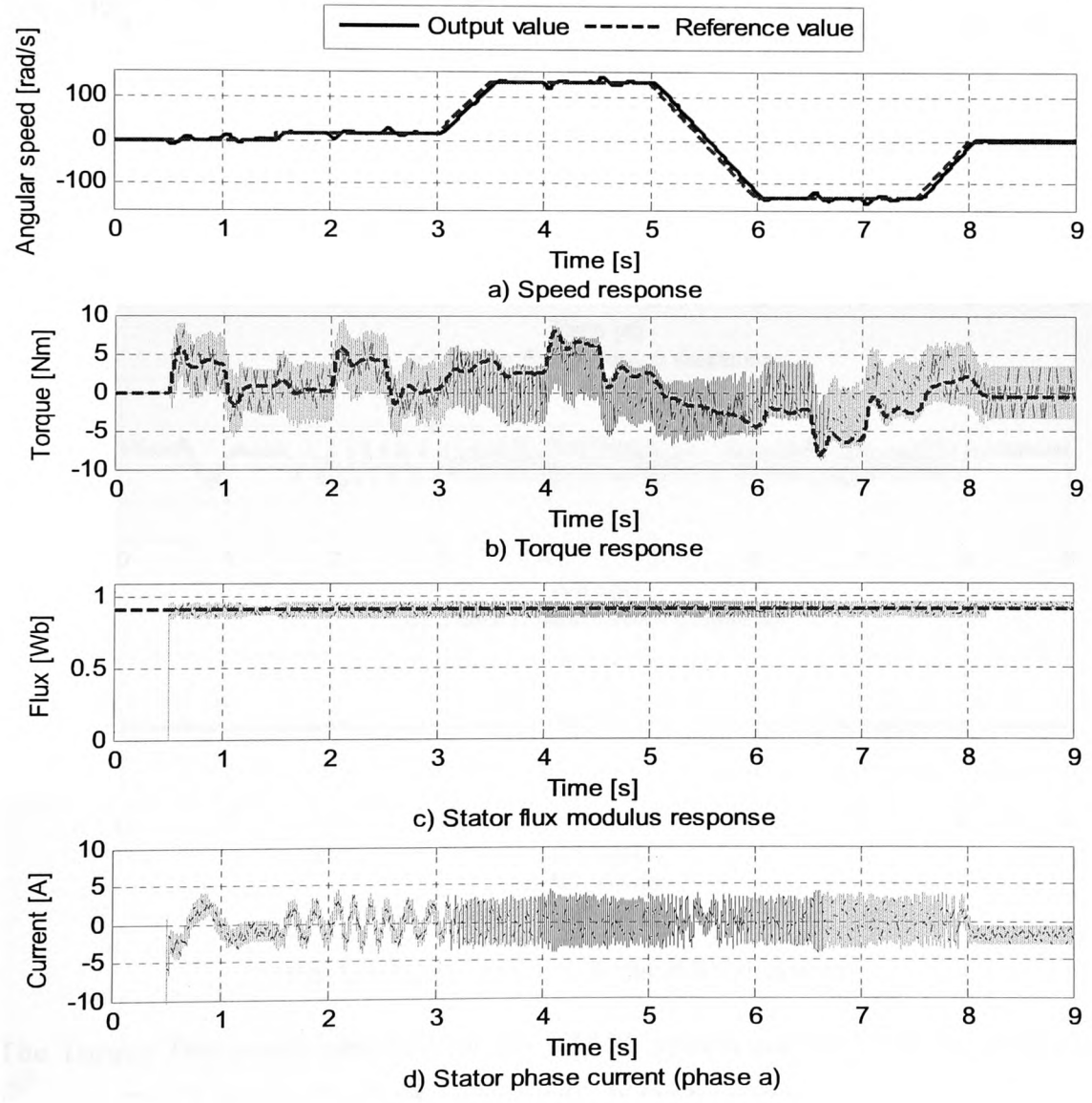

Fig. 5-35 Speed Test results for the DTC2L system

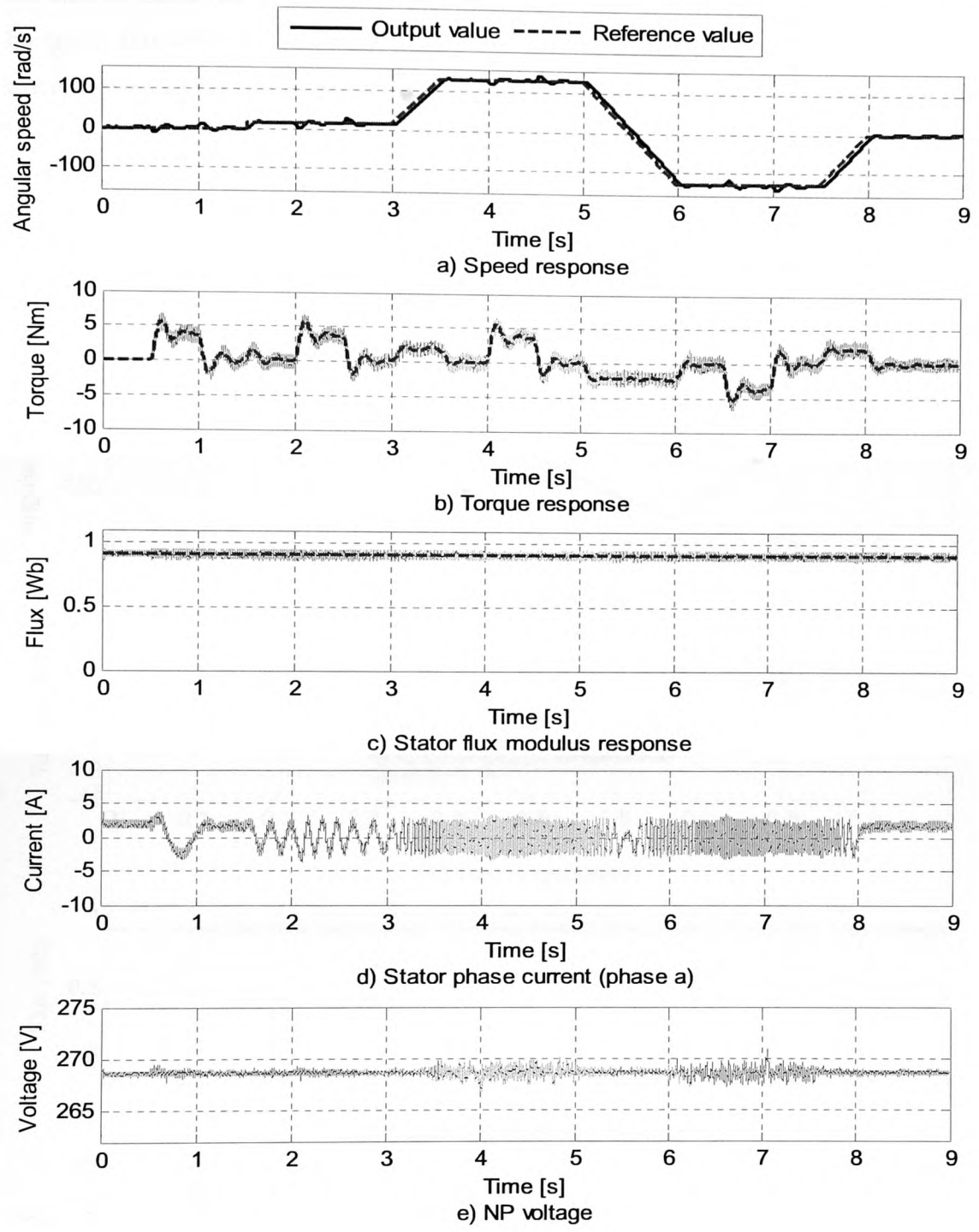

Fig. 5-36 Speed Test results for the PDTC3L system

The Torque Test results obtained for the DTC2L system and the PDTC3L system are shown in Fig. 5-37 and Fig. 5-38 respectively. It can be observed how torque control is considerably superior with the PDTC3L system, not only regarding the torque ripple reduction but also due to the elimination of the mean error in the whole speed range. It

can also be observed in the stator flux modulus response of the PDTC3L system how the stator flux can be controlled even when the reference value for torque is zero. A faster start-up is therefore possible. The stator phase currents have less distortion in the PDCT3L system results, and the current amplitude remains almost equal during the whole test, even in the torque inversion instants. The control of the NP voltage proves to be again efficient during the Torque Test.

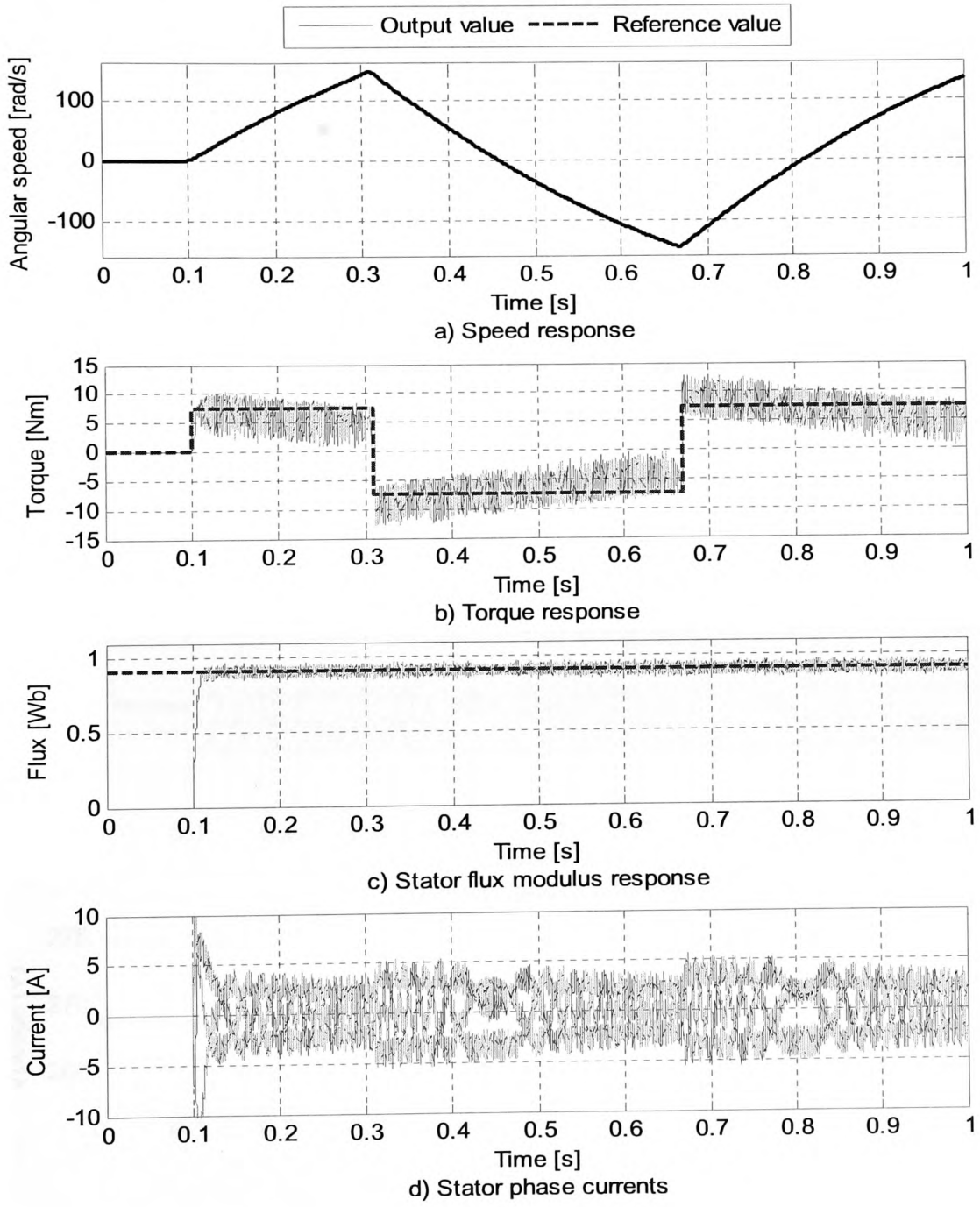

Fig. 5-37 Torque Test results for the DTC2L system

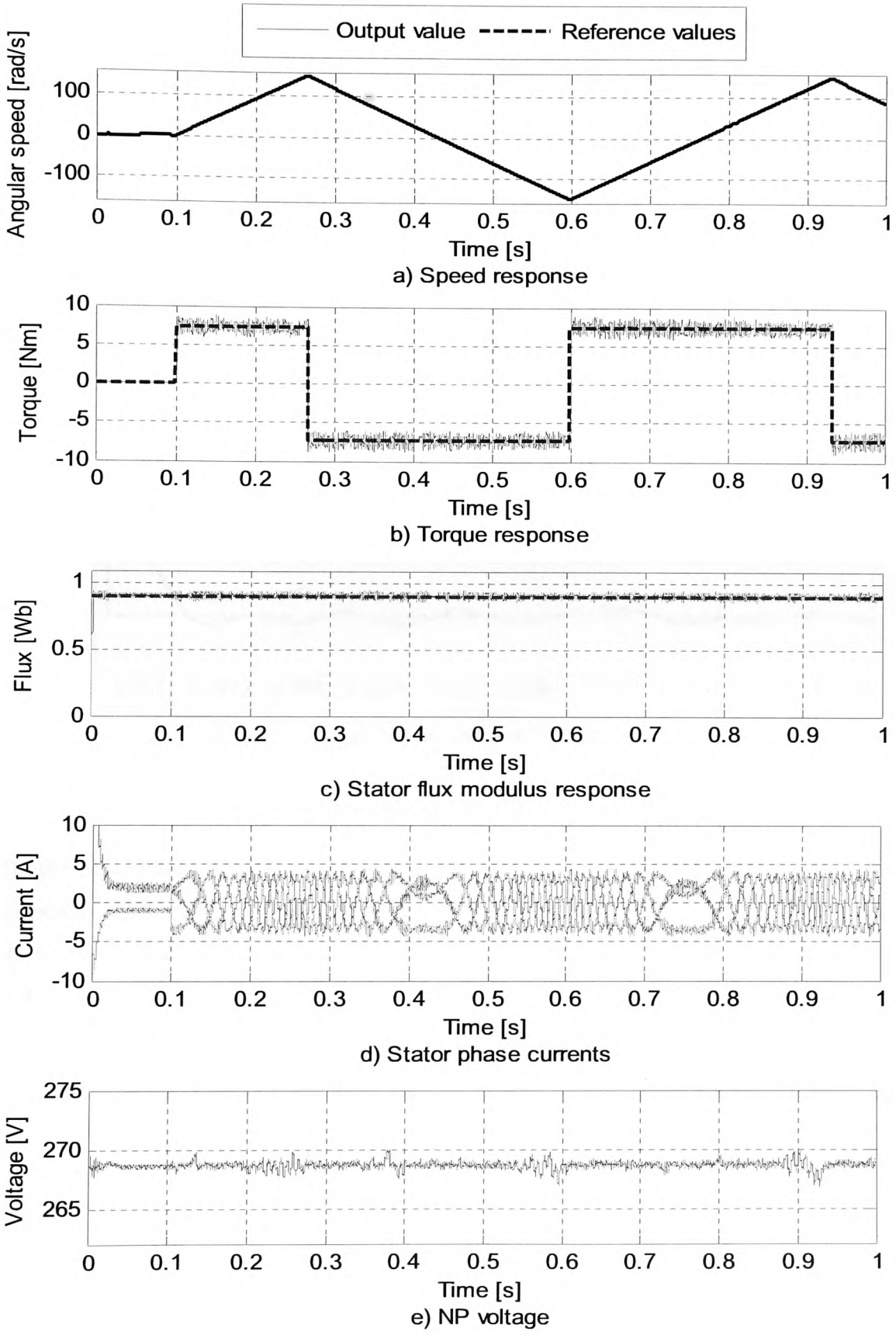

Fig. 5-38 Torque Test results for the PDTC3L system

If the torque response time is analyzed in Fig. 5-39 during the first torque inversion of the Torque Tests, it can be observed how both systems have almost the same response time. It can be concluded that the PDTC3L systems keeps the characteristic fast torque response associated with DTC.

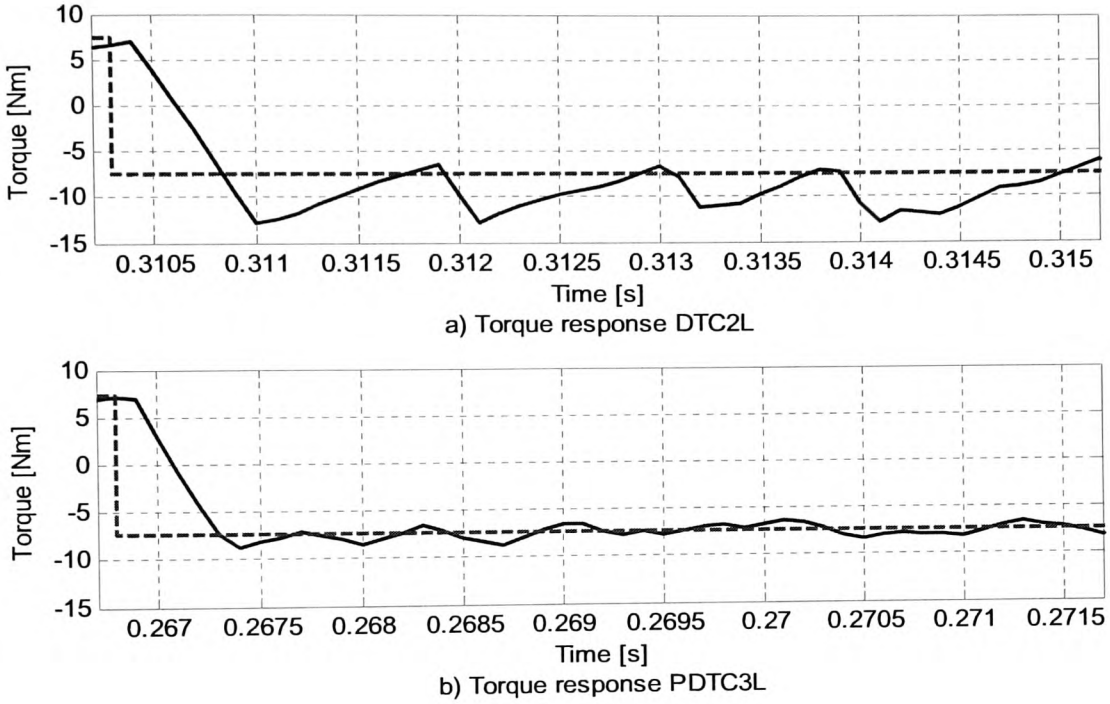

Fig. 5-39 Comparative torque response to a step change

On the other hand, if the torque start-up is analyzed, it can be observed how the torque response of the PDTC3L system is much quicker because the stator flux is already set to its nominal value. The comparative torque response during start-up is shown in Fig. 5-40.

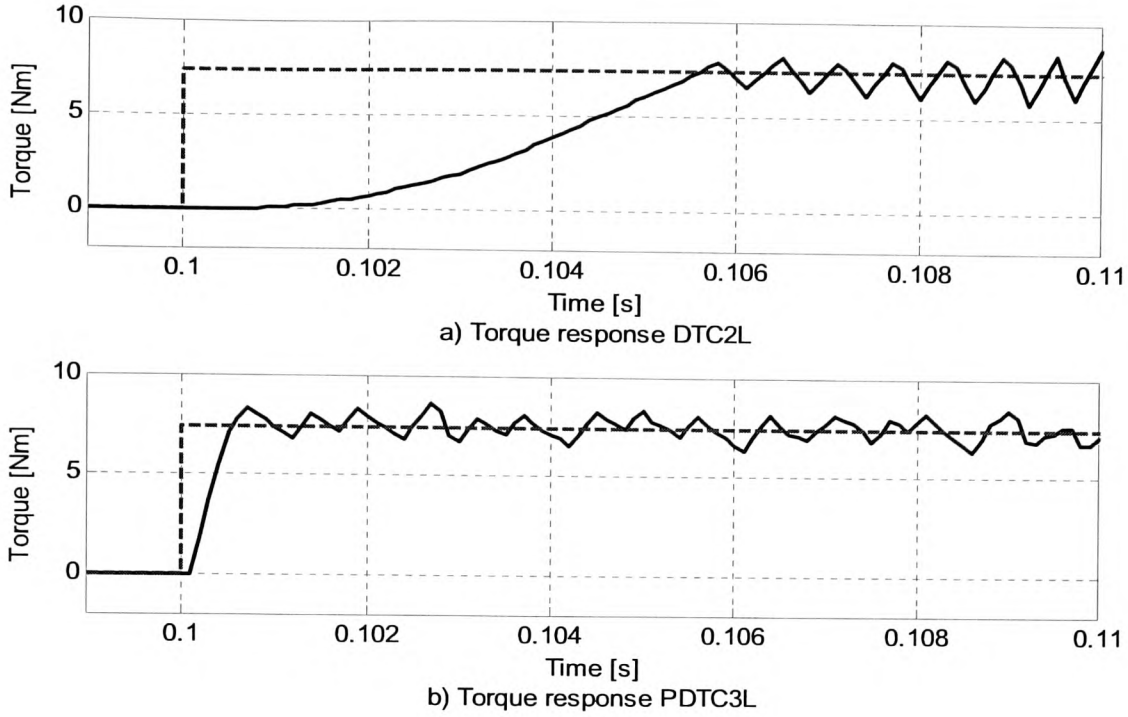

Fig. 5-40 Comparative torque response during start-up

Table 5-XI presents the performance indexes obtained in the dynamic tests for the DTC2L and the PDTC3L systems.

Table 5-XI Performance indexes of the simulated dynamic tests

Test	Index	DTC2L	PDTC3L	Reduction %
Speed Test	RMS $e_{\omega m}$ [rad/s]	7.799	7.448	**4.50**
	RMS $e_{\Gamma e}$ [Nm]	2.421	0.452	**81.33**
	RMS $e_{\psi s}$ [Wb]	0.036	0.018	**50.00**
	RMS (V_{C1}-V_{C2}) [V]		0.533	
	Mean (V_{C1}-V_{C2}) [V]		0.011	
	Mean i_{NP} [A]		0.0001	
Torque Test	RMS $e_{\Gamma e}$ [Nm]	2.316	0.653	**71.80**
	RMS $e_{\psi s}$ [Wb]	0.049	0.034	**30.61**
	RMS (V_{C1}-V_{C2}) [V]		0.580	
	Mean (V_{C1}-V_{C2}) [V]		0.046	
	Mean i_{NP} [A]		-0.0021	

The last column shows the percentage of reduction obtained with the PDTC3L system. It can be observed how the speed control performance is only slightly better while the torque control performance is clearly superior. Moreover the NP voltage control proves to be efficient.

5.10 Interim conclusions

This chapter has presented the new control system developed and reported in this thesis. Taking into account the desired features for a high performance motor drive system it seems that a solution combining the DTC method with the three-level VSI can bring some benefits. The literature review containing the proposed control methods presented by other researchers indicates that this solution can offer some advantages over the Classical DTC method with the two-level VSI. Nevertheless, it seems that with an approach based on hysteresis controllers and look-up tables it is difficult to fully exploit the potentialities of the three-level VSI.

The design of the new control system starts by analysing the DTC principle by means of the stator voltage equation expressed in the stator flux vector reference frame. This analysis shows how the decoupled control of stator flux modulus and torque is achieved by controlling the radial (x) and tangential (y) components respectively of the stator voltage vector. It is also deduced the strong influence of the BEMF term on the torque production.

The new control system developed generates a reference voltage vector based on the control laws derived from the stator voltage equation expressed in the stator flux vector reference frame. The stator flux modulus is controlled by means of the radial (x) component of the stator voltage vector employing a deadbeat controller, which gives the required voltage to cancel the stator flux modulus error at the end of each sampling period. Torque is controlled by means of the tangential (y) component of the stator voltage vector employing a combination of a proportional feed-back control loop with a feed-forward control. The feed-forward action consists of two terms: the required voltage to produce the torque reference and the required voltage to compensate the BEMF term in steady-state conditions. The reference voltage vector is then synthesized by choosing the nearest voltage vector that can be delivered by the three-level VSI. This solution is simpler than the use of modulation techniques.

The equations of the controller only contain the stator resistance and there is only one parameter to be tuned, which is the torque proportional gain. A very simple and efficient optimization method has been developed to tune this gain.

A PI controller is employed in the speed control loop. The tuning method employed is based on the SO criterion.

The redundancy of switching combinations for the zero vector is employed to reduced the switching frequency, while the redundancy of the small vectors is employed to control the voltage balance in the DC-link capacitors.

From the analysis of the steady-state and transient results it can be concluded that the advantages of the proposed control system when compared to the Classical DTC method with the two-level VSI are the following:

- A better torque and stator flux control is achieved with a reduction of the ripple and steady-state mean error. Fast torque response is kept and the stator flux modulus can be controlled when the torque reference is zero providing a faster start-up.
- Some improvement in the speed control is achieved as a consequence of the improvement in the torque control. The speed response presents smaller oscillations.
- The stator flux and current distortion caused by the sector boundaries effect is eliminated and a circular stator flux path is obtained for all operating conditions.
- The harmonic distortion of the stator voltage and current waveforms is reduced.
- The voltage derivatives and the CM voltage and currents are reduced.
- The mean switching frequency in the semiconductor devices is also reduced. The switching devices commute at only half of the DC-link voltage. Stress and power losses in the semiconductor devices are therefore reduced.
- The tuning of the new controller is based on a simple and efficient optimization method, where only the torque proportional gain has to be adjusted. The proposed method can be easily implemented as an auto-tuning method.
- The control structure is flexible and easy to adapt to other converter topologies. The use of modulation techniques to synthesize the reference voltage vector is also possible.

Chapter 6: Experimental Validation

Summary – *The first part of this chapter presents the experimental setup used to test and evaluate the control system developed in this research work. It gives a description of all the hardware components of the laboratory setup and the implementation of the control algorithms. The second part of the chapter presents the experimental results obtained to validate the proposed control system described in Chapter 5.*

6.1 General description of the laboratory setup

Nowadays most of the laboratory setups for motor control are based on DSPs. This type of processor provides fast calculation and wide Input/Output (I/O) capabilities such as analog I/O, serial communication and PWM outputs.

The experimental setup used in the research work described in this thesis was developed for the purpose of implementing different types of control strategies for electrical motors [92]. It was developed in the Department of Electronic Engineering of the "Universitat Politècnica de Catalunya" in Spain. The applications that can be developed are position, speed and torque control of IMs and Permanent Magnet Synchronous Motors (PMSM). Examples of these techniques would be scalar control, FOC and DTC. The system includes the control of the load torque by means of a PMSM attached to the other motors and fed by an industrial drive system. Load torque can be accurately controlled being a very important and useful feature for the development and test of position, speed and torque control strategies.

The control system is based on a dSPACE board, which is a very flexible fast-prototyping system that provides the hardware and software tools to host applications created in Matlab/Simulink or high-level programming languages such as C. The advantage of the dSPACE system is that it can be programmed using Simulink blocks. Therefore the simulation models developed in an early stage of the research can be easily transferred to the control system of the real plant. The system in Simulink blocks is directly compiled and uploaded in the digital processors of the dSPACE board and no knowledge of these processors or the programming using conventional tools such as assembler and C programming is needed.

Additionally, a software package called ControlDesk is supplied with the dSPACE system, which allows the user to interact in real time with the control system through a virtual control panel with a variety of instruments. Data from the process can be captured from the system and exported to Matlab for processing and analysis purposes. The general block diagram of the experimental setup used is shown in Fig. 6-1.

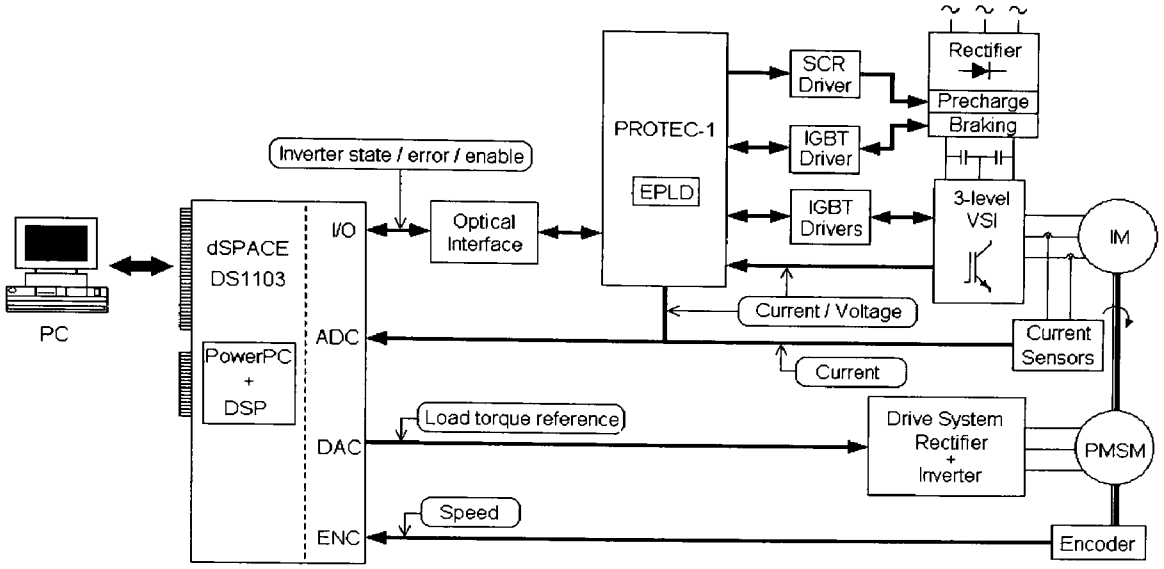

Fig. 6-1 General block diagram of the experimental setup

The complete system can be divided in three main parts described in the following sections:

- Control. It contains all the elements that perform control tasks and the required interface components to interact with the power converter and the sensors connected to the electrical motors. It includes the PC, the dSPACE board, the optical interface, the PROTEC-1 board (used for signal conditioning and protections), the IGBT drivers and the sensors. All the component employ low voltages. Electrical insulation through optical devices is used for protection to interface the control with other parts of the setup.
- Power conversion. This part contains all the high-power electronic devices employed to feed the electrical motors. It includes the VSIs and rectifiers connected to the grid and some passive components such as the capacitors of the DC-link.
- Electrical motors. This part includes one IM and two PMSMs.

The electrical diagrams of the experimental setup are included in Appendix B.

6.2 Control

The control part includes the following components:

- Computer (PC).
- DS1103 dSPACE board and external panel CP1103.
- Optical interface.

- Signal conditioning and protection board (PROTEC-1).
- IGBT drivers.
- Sensors.

6.2.1 Computer

The computer is where the dSPACE board is hosted. The processor is a Pentium III at 1 GHz with 512 MB of RAM memory. Matlab/Simulink is installed with the additional dSPACE software. The main special feature of this computer is the ISA slot included in the mother board. This feature is quite uncommon in computers nowadays due to the obsolescence of the ISA bus. This slot is where the dSPACE board is allocated.

6.2.2 dSPACE board

The control board DS1103 from dSPACE is based on a RISC/DSP architecture, which provides powerful floating-point processing, as well as wide Input/Output capabilities. Its main features are:

- Supply voltages and current consumption 5 V, 6 A; -12 V, 250 mA; 12 V, 750 mA
- Over-temperature sensor.
- 16-bit ISA bus.
- I/O connection through 3 connectors (100-pin high-density).
- BIOS Plug & Play

The RISC processor is a floating-point Motorola PowerPC 604e (PPC), which is the main processing unit of the system. The DSP processor is a fixed-point Texas Instrument TMS320F240. Among other I/O capabilities this DSP can generate three-phase PWM signals, which makes it very suitable for control of power converters and motor drives. In this sytem the PPC unit is the master device while the DSP is the slave device.

The DS1103 board is inserted in the ISA slot of the computer and the connectors available in the back panel of the computer are connected to the CP1103 external panel.

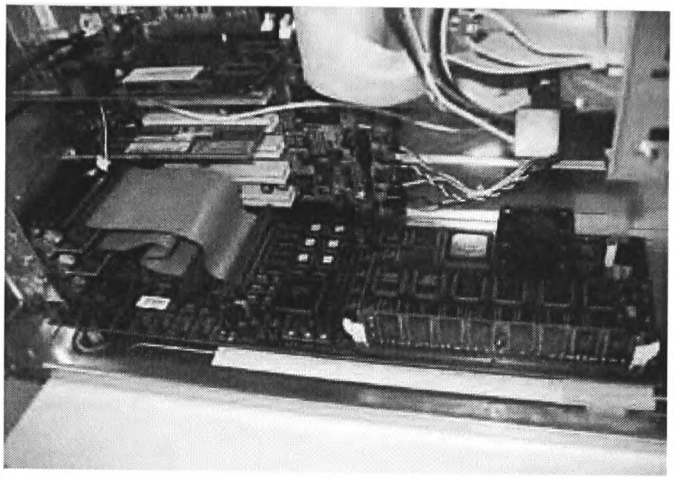

Fig. 6-2 DS1103 board (dSPACE)

The main characteristics of the Master PPC unit are:

- PowerPC 604e at 400 MHz.
- Superscalar processor.
- 3 integer units, 1 floating-point unit.
- 32 KBytes cache memory for instructions.
- 32 KBytes cache memory for data.

Timers

- 2 general-purpose timers.

Memory

- 2 MB of SRAM local memory for the program.
- 128 MB of DRAM global memory for data storage and exchange with the computer.

Interrupt Controller

- The sources of interrupt available are: Host computer interrupts, CAN, slave DSP, serial interface, incremental encoders and 4 user-defined interrupts for external devices.
- Slave DSP PWM interrupts.

Analog inputs (ADC)

- 4 parallel ADC multiplexed in 4 channels each (16-bit resolution, ±10 V input voltage range, ± 5 mV offset error, ± 0.25% gain error, > 80 dB Signal-to-Noise Ratio (SNR), sampling time of 4 μs).
- 4 parallel ADC (10-bit resolution, ±10 V input voltage range, ± 5 mV offset error, ± 0.5% gain error, > 65 dB SNR, sampling time of 800 ns).

Analog Outputs (DAC)

- 2 quad DAC with 4 channels each (14-bit resolution, ±10 V output voltage range, ± 1 mV offset error, 3 ppm/K offset drift, ± 0.5% gain error, 25 ppm/K gain drift, Transparent and latched mode, settling time 5 μs).

Incremental Encoders interface

- 6 digital encoder interfaces with noise filtering.
- 1 TC3005H Hanning interface with both square-wave incremental positions transducers and sinusoidal incremental position transducers.

Digital I/O

- 32-bit digital I/O organized in 4 groups of 8 bits. Each group can be configured as input or output.
- ±10 mA maximum output current.
- TTL voltage range for input and output.

Serial interface

- RS232 y RS422.
- Transmission speed up to 1 MBaud.

CAN interface

- Siemens SAB8CI 16-bit CPU.
- Clock frequency 10–20 MHz.
- Fully compatible with the ISO/DIS 11898 standard.
- Up to 1 MBaud.

The main characteristics of the Slave DSP are:

- Texas Instruments TMS320F240 at 20 MHz, optimized for motor/motion control applications.
- 64-KWords program memory.
- 28-KWords data memory.
- 4-KWord dual-port RAM memory.
- Support for symmetrical/asymmetrical PWM and SVM.
- Three-phase PWM output and 4 single PWM outputs.
- 4 capture inputs to measure frequency (F2D) and PWM analysis (PWM2D).
- 2 ADC multiplexed in 8 channels each (10-bit resolution, 0-5 V input voltage range, sampling time of 6.6 μs).

- 18 bits digital I/O, each channel is configured individually, ±13 mA maximum output current, TTL voltage range for input and output.

The external panel CP1103 shown in figure Fig. 6-3 is connected to the DS1103 and provides easy connection between the control and the plant.

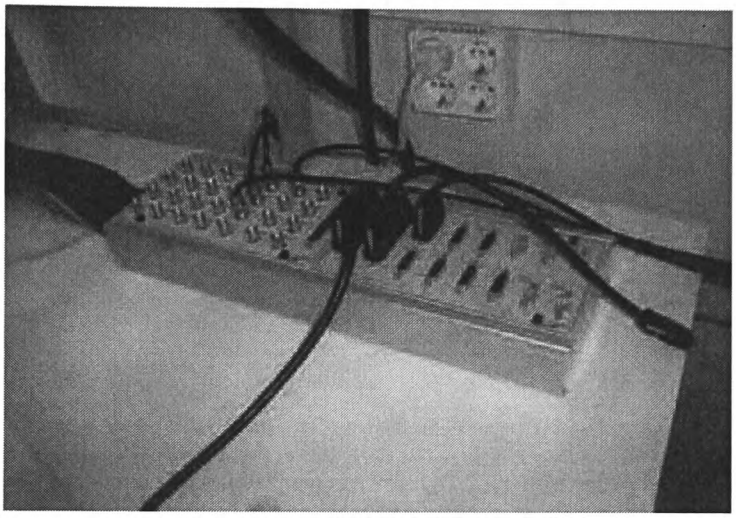

Fig. 6-3 CP1103 external panel

The following connectors are available in the panel:

- 20 BNC connectors for the ADCs (CP01 a CP20).
- 8 BNC connectors for the DACs (CP21 a CP28).
- 1 Sub-D connector with 37 pins for the ADC of the slave DSP (CP29).
- 1 Sub-D connector with 50 pins for the digital I/O (CP30).
- 1 Sub-D connector with 37 pins for the digital I/O of the slave DSP (CP31).
- 7 Sub-D connectors with 15 pins for the incremental encoder interfaces (CP32 a CP37 y CP39).
- 1 Sub-D connector with 9 pins for the CAN interface (CP38).
- 1 Sub-D connector with 9 pins for the UART RS232 of the master PPC (CP40).
- 1 Sub-D connector with 9 pins for the UART RS232 of the slave DSP (CP41).
- 1 Sub-D connector with 9 pins for the UART RS422 of the master PPC (CP42).
- 1 Sub-D connector with 9 pins for the UART RS422 of the slave DSP (CP43).

Fig. 6-4 shows the distribution of the connectors in the panel.

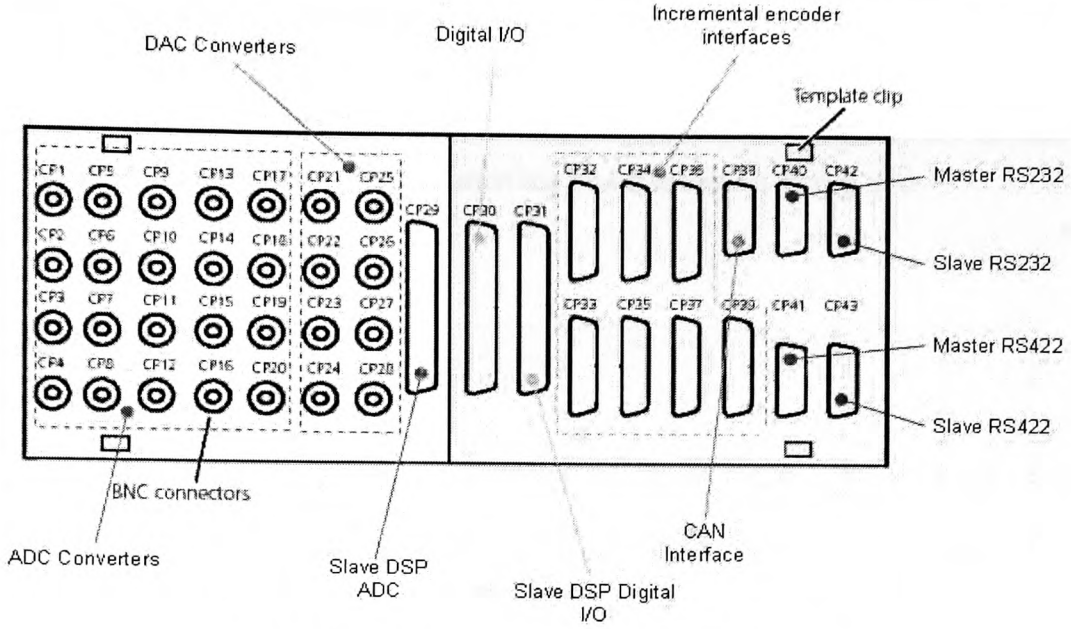

Fig. 6-4 Distribution of connectors in the CP1103 panel

6.2.3 Optical interface

The optical interface is used to communicate the dSPACE DS1103 board and the PROTEC-1 board that controls the three-level NPC VSI. It provides electrical insulation between both boards and eliminates the effect of electromagnetic perturbations on the control signals.

This interface is based on several photoemitters SFH750V and a non-inverting octal buffer 74HCT541B1 that supplies the current for proper operation and avoids overloads for the dSPACE digital outputs. It also includes LEDs for the user to easily check the state of the signals. The optical interface is connected to the CP1103 panel through a special cable plugged to a 9-pin Sub-D connector.

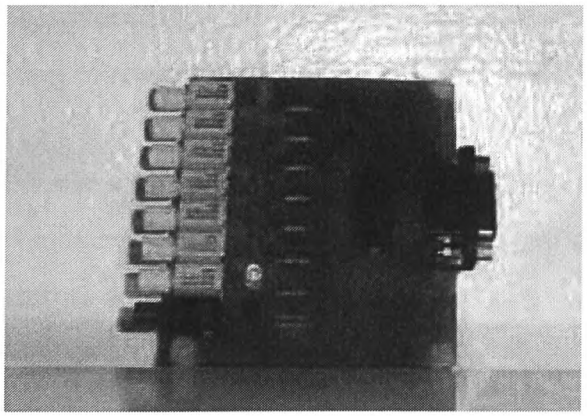

Fig. 6-5 Optical interface

7 signals are sent to the PROTEC-1 board through optical fibres containing the VSI state (6 lines, green LED's) and the enable signal (white LED). The error signal (red LED) is returned to the control system to notify about possible failures in the system. The schematic diagram of the optical interface board is shown in Fig. 6-6.

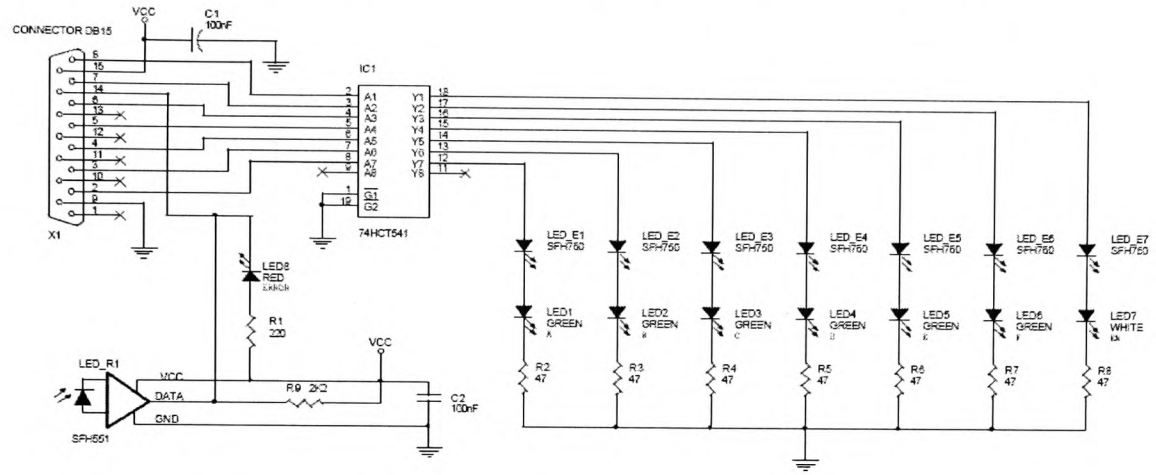

Fig. 6-6 Schematic diagram of the optical interface

6.2.4 PROTEC-1 board

The PROTEC-1 board (see Fig. 6-7) is an interface board devised to connect the dSPACE system to the three-level NPC VSI system. It was developed in the Department of Electronic Engineering of the "Universitat Politècnica de Catalunya" in Spain [93, 94]. The main functions of this board are the processing of the control signals sent by the dSPACE system, the conditioning of the currents and voltages measured in the VSI, and finally the protection of the system and generation of alarms. The main component of the PROTEC-1 board is a Programmable Logic Device (PLD), which performs all the processing tasks. The model used is the Lattice ISP 1032E. A more detailed list of functions performed by this board is given below:

- Processing and decoding of the control signals sent by the dSPACE control system to the VSI.
- Generation of dead times to avoid short-circuits in the VSI legs.
- Avoid forbidden combinations of switches and forbidden transitions between states.
- Detection of various errors such as overvoltages and overcurrents in the DC-link and VSI. Generation and visualization of alarms. Reset of the IGBT devices in case of alarm to inhibit the system.

- Monitoring and control of the DC-link voltage by means of the precharge and braking systems.
- Conditioning of the current and voltage signals measured to be sent to the dSPACE system.
- Electric insulation through optocoupler devices between the dSPACE system and the rest of components.

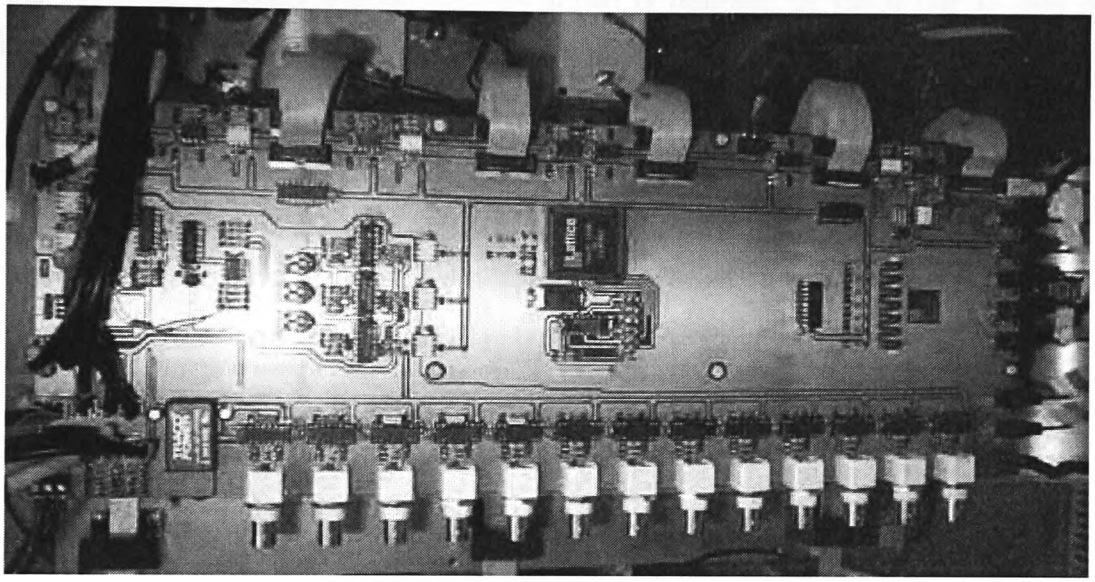

Fig. 6-7 PROTEC-1 board

The inputs and outputs of the PROTEC-1 board are shown in Fig. 6-8.

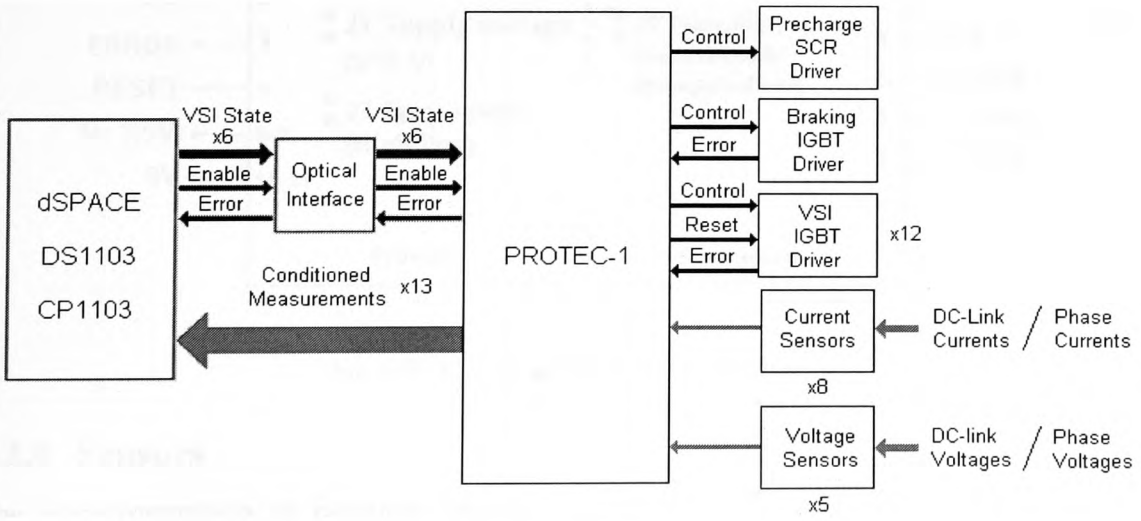

Fig. 6-8 Inputs and outputs PROTEC-1 board

6.2.5 IGBT drivers

In order control the state of the IGBT devices a driver circuit must be employed to adapt the control signals to the voltage and current required to commute the IGBT. Moreover, electrical insulation and some protection features against short-circuits are desired. For this purpose the driver SKHI10/17 from SEMIKRON has been used. 12 driver circuits are necessary, one for each IGBT of the three-level NPC VSI. Control signals are sent by the PROTEC-1 board and an error bit signal is returned by the driver in case of a failure. The main features of the IGBT drivers are:

- Compatible with IGBT devices up to V_{CE}=1700 V.
- CMOS/TTL control signals.
- 15 V / 5 V configurable supply voltage (jumper J1).
- Protection against short-circuits by monitoring V_{CE} level.
- Protection against power supply failure.
- Insulation through transformer.
- Error signal configurable to high or low level (jumper J3).
- Internal switching mode power supply.
- G_{ON} and G_{OFF} times independently configurable with RC networks, they can be connected or independent (jumper J2).

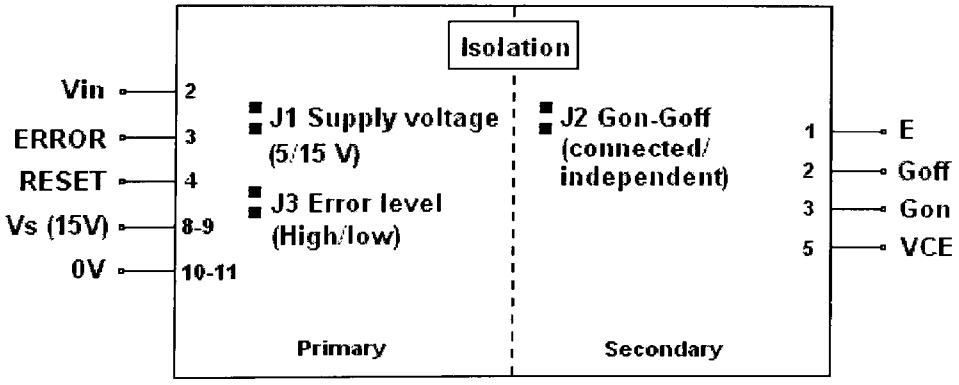

Fig. 6-9 I/O diagram of SKHI 10/17 driver

6.2.6 Sensors

The implementation of position, speed and torque controls for the IM requires the measurement of several variables to close the control loops. The measured variables to implement the control systems described in Chapter 5 are: the motor position, two of the

motor line currents, and the voltage in the capacitors of the DC-link. The sensors employed in the laboratory setup are described in the following sections.

6.2.6.1 Current sensors

Two of the IM line currents have to be measured (the third one can be calculated from the other two considering that the sum of them is equal to zero). The current sensors are built in a board with two Hall-effect sensors LEM LA 55-P with the following characteristics:

- Nominal RMS current in the primary: $I_{PN} = 50$ A.
- Range of measurement: $I_P = \pm 70$ A
- Nominal RMS current in the secondary: $I_{SN} = 50$ mA
- Conversion Ratio: $K_N = 1 : 1000$
- Supply voltage: ±12 / ±15 V
- Measurement resistance ($T_A = 70$ °C, $V_C = \pm 15$ V): $R_m = 50$–$160\ \Omega$
- Response time: <1μs (90% of I_{PN}).

The Hall-effect sensors are connected as shown in figure Fig. 6-10:

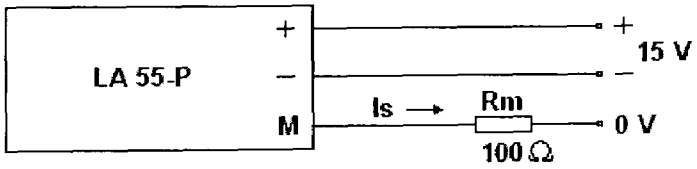

Fig. 6-10 Hall-effect sensor connection

A metallic film type measurement resistor is employed with a value of 100 Ω. The factor of conversion is therefore 0.1 V/A. The board is mounted on the side of the motor and supplied with ±15 V. The Current sensors board is shown in figure Fig. 6-11.

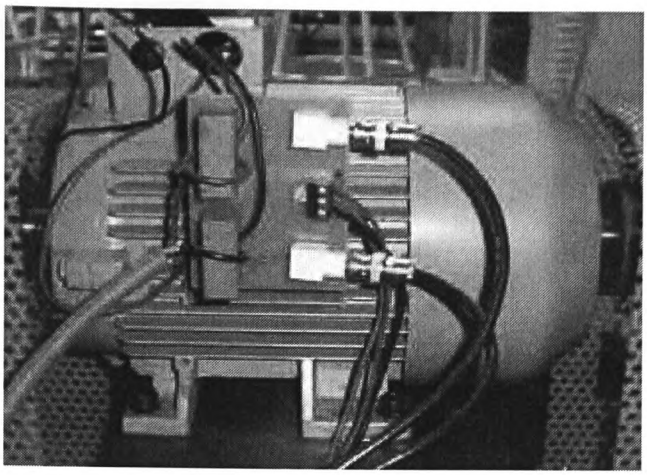

Fig. 6-11 Current sensors board

6.2.6.2 Voltage sensors

The voltage in the DC-link is measured in order to control it to the appropriate level, detect overvoltages and use the measured value in the control algorithm. For the particular case of the three-level NPC VSI, the DC-link contains two capacitors in series that divide it in two halves with the NP in the middle. Two voltage sensors are used to measure the DC-link voltage between the positive rail and the NP, and between the negative rail and the NP. By adding both voltages the total voltage of the DC-link is obtained. The type of sensor used is the ABB VS 500B, which has the following features:

- Nominal RMS voltage in the primary: 500 V.
- Maximum measurement range: ±750 V.
- Current in the secondary at nominal voltage conditions: 50 mA.
- Supply voltage: ± 15 V.

A 100 Ω measurement resistor is used in the secondary of the sensor to obtain 5 V at the output when the voltage in the primary is 500 V.

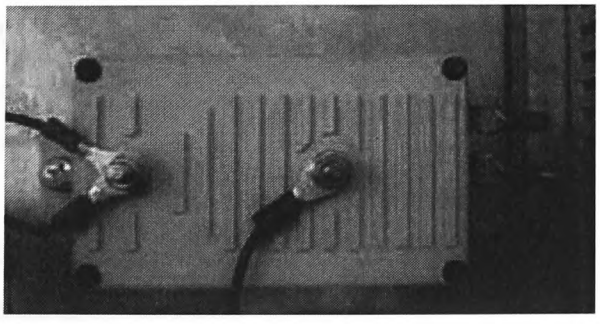

Fig. 6-12 Voltage sensor

6.2.6.3 Speed sensor

The PMSM used to control the load torque includes an incremental encoder integrated with the following characteristics:

- Supply voltage: 5 V.
- Current consumption: 300 mA.
- Number of pulses: 2048.
- Speed limit: 12000 rpm.

The signals at the output of the encoder are first transformed in the SBM board incorporated in the VSI SIMOVERT MC (see section 6.5.1). From that board the signals are then sent to the dSPACE board through one of the encoder connectors available in the CP1103 panel.

6.2.6.4 Additional sensors

The sensors described in the previous sections are those used to implement the control strategies developed in this research work. However, some additional voltage and current sensors are available in the three-level NPC VSI to provide more measurement points as illustrated in Fig. 6-13. Regarding the outputs of the VSI, the equivalent terminology "*RST*" has been used in the laboratory instead of "*ABC*", which is employed in other sections of this thesis.The output voltages of the VSI are measured with three voltage sensors of the same type as those described in section 6.2.6.2. According to Fig. 6-13 there are 5 current sensors in the DC-link side of the VSI and 3 current sensors for the VSI outputs. The sensor type employed for Ibus1, Ibus2, Iph1, Iph2 and Iph3 is the LEM LA 205-S. Its main characteristics are:

- Nominal RMS current in the primary: I_{PN} = 200 A.
- Range of measurement: I_P = ±300 A.
- Nominal RMS current in the secondary: I_{SN} = 100 mA.
- Conversion Ratio: K_N = 1:2000.
- Supply voltage: ±12 / ±15 V.
- Response time: <1μs (90% of I_{PN}).

The sensor type used in Ibus3, Ibus4 and Ibus5 is the LEM HAL 50-S. Its main characteristics are:

- Nominal RMS current in the primary: I_{PN} = 50 A.
- Range of measurement: I_P = ±150 A.
- V_{OUT} = ±4 V.

- Supply voltage: ±15 V.
- Response time: < 3 μs (90% of I_{PN}).

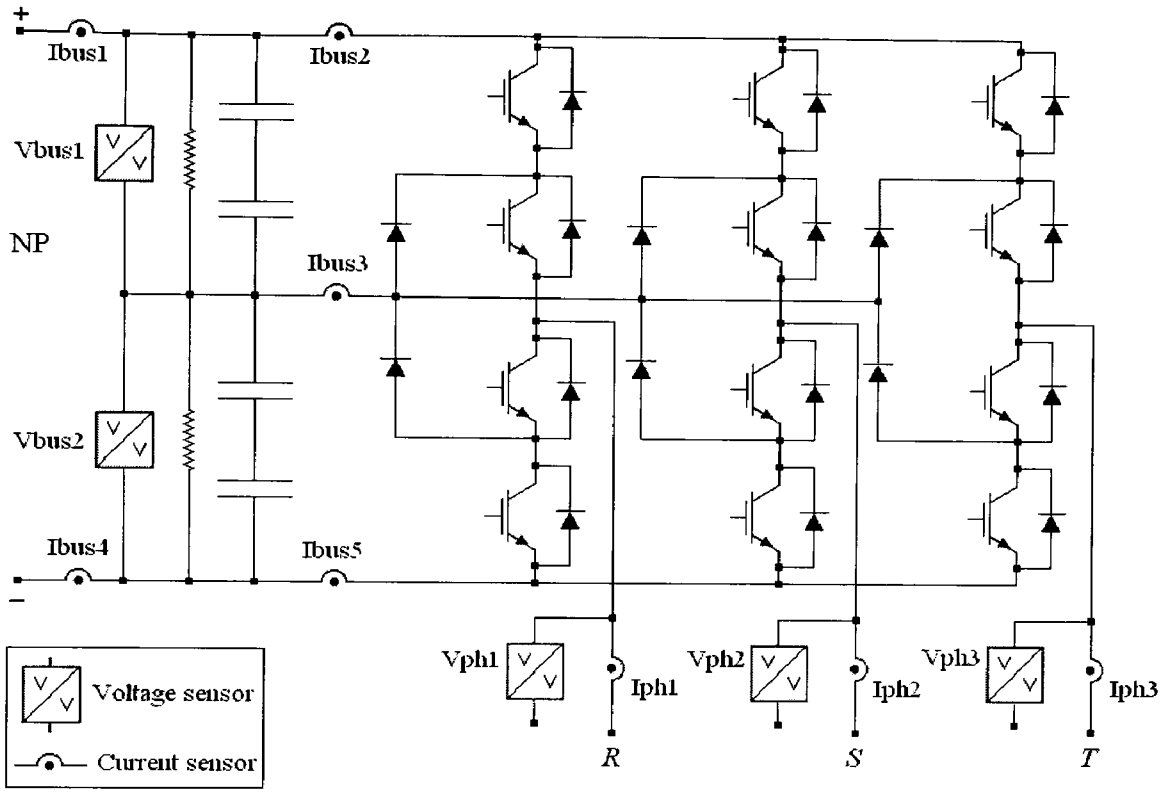

Fig. 6-13 Distribution of voltage and current sensors

6.3 Power conversion

This part of the setup is where the power electronics technology is employed. In most Variable Voltage and Variable Frequency drives (VVVF) used to control electrical machines a conversion from the AC network supply to DC and back to AC is utilised. A rectifier is used to perform the AC-to-DC conversion and the energy is stored in the DC-link by means of passive components, in this case capacitors. The DC-link voltage is then converted into AC with the desired voltage amplitude and frequency by means of the VSI. In this case a three-level NPC VSI is employed.

6.3.1 Rectifier

The rectifier employed is a three-phase non-controlled rectifier, the SEMIKRON B6U 380 510 50. This rectifier uses SEMIKRON SKKD 81/12 diodes. The main characteristics of the rectifier are:

- 380 V-50 Hz three-phase input.

• Maximum current 150 A.

A Precharge circuit is included after the rectifier to control the charge of the capacitors and avoid high currents when they are discharged. It consists of a thyristor in parallel with a resistor. The current flows through the resistor until the capacitors of the DC-link reach a certain voltage level. When this configurable level is reached the thyristor is fired and current flows through it. The thyristor module used is the SEMIKRON SKKT 92 with the following characteristics:

• V_{AKmax}=1200 V.

• I_{Dmax}=150 A.

A Braking circuit is also used to dissipate power when the motor returns energy to the DC-link. In this way the DC-link voltage cannot exceed a certain level. A resistor (33 Ω, 150 W) and an IGBT in series are connected in parallel with the DC-link capacitors. The IGBT is fired when the DC-link voltage exceeds a configurable value and then energy is dissipated in the resistor restoring the desired level of voltage in the DC-link. The IGBT module used is the SEMIKRON SKM 145 GB with a driver SEMIKRON SKHI 22 A. The main characteristics of the IGBT used are:

• V_{CEmax}=1200 V.

• I_{Cmax}=145 A.

The DC-link bus employs 4 capacitors connected in series with the following features:

• C=2200 μF, V_{Cmax}=450 V.

The resulting capacitance and maximum voltage of the DC-link is:

• $C_{DC\text{-}link}$=550 μF, $V_{DC\text{-}link\_max}$=1800 V.

Fig. 6-14 presents the schematic circuit with the elements described.

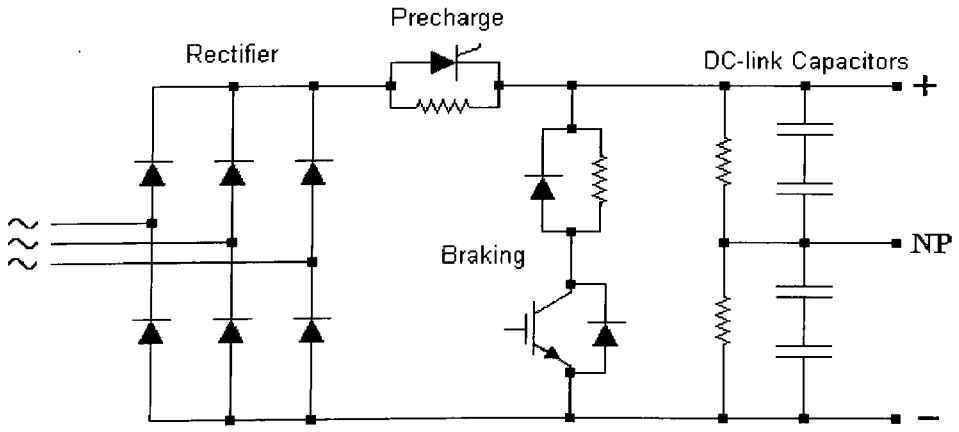

Fig. 6-14 Rectifier, precharge and braking schematic circuit

A photograph of the rectifier, Precharge and Braking circuits is shown in Fig. 6-15.

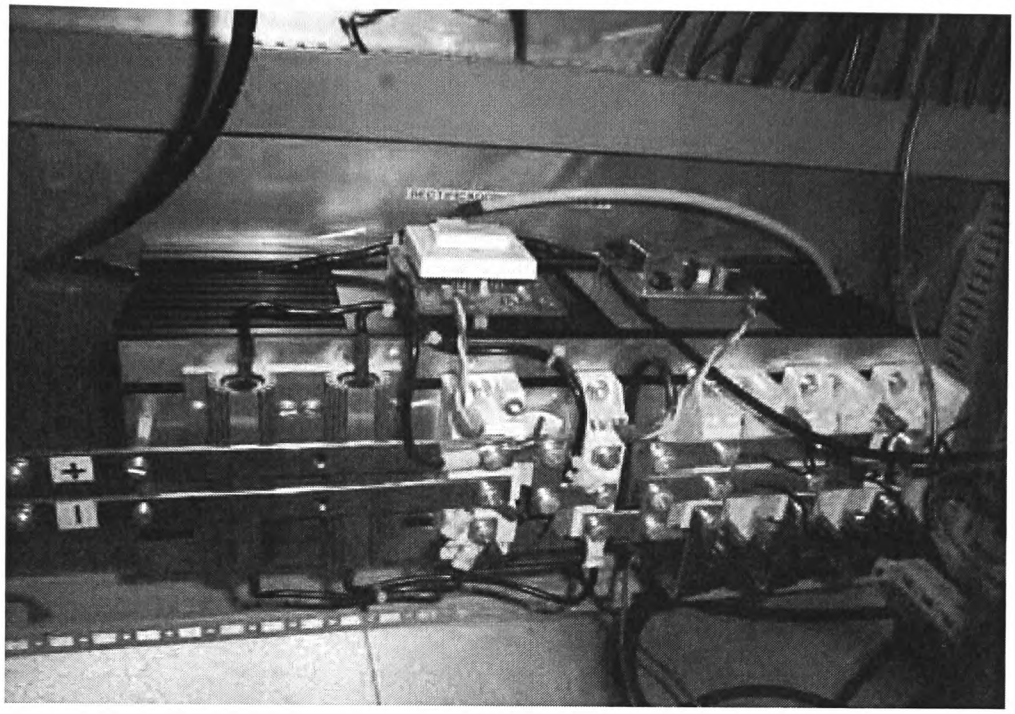

Fig. 6-15 Rectifier, precharge and braking circuits

The capacitors of the DC-link are shown in Fig. 6-16.

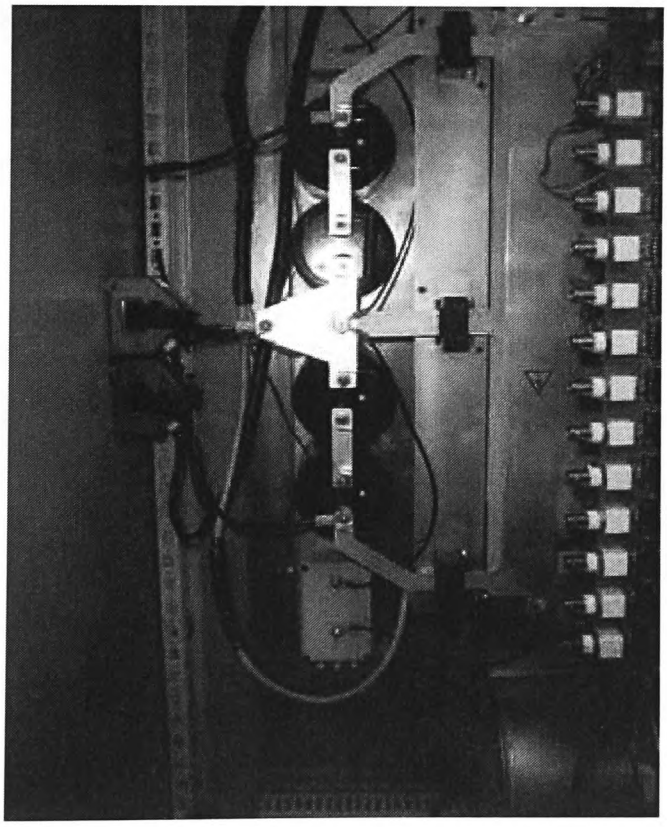

Fig. 6-16 DC-link capacitors

6.3.2 Three-level NPC VSI

In this experimental setup a prototype of a three-level NPC VSI has been used. It can be either connected to the rectifier or to an external DC power supply instead. The schematic circuit is shown in Fig. 6-13. The configuration of IGBT and diode modules (see Fig. 6-17) used to build every leg of the VSI is as follows:

- Module SEMIKRON SKM100 GAR 123D for the upper IGBT and clamping diode.
- Module SEMIKRON SKM100 GB 123D for the two IGBT devices in the middle of the leg.
- Module SEMIKRON SKM100 GAL 123D for the lower IGBT and clamping diode.

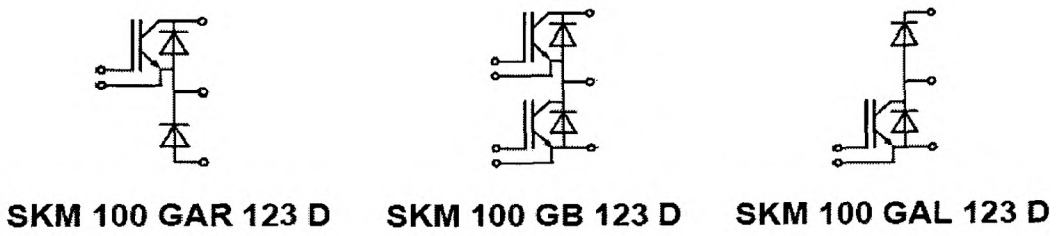

Fig. 6-17 IGBT and clamping diode modules

The main characteristics of these IGBT devices are:

- V_{CEmax}=1200 V.
- I_{Cmax}=100 A.

Fig. 6-18 shows the prototype of the three-level NPC VSI. The IGBT drivers are mounted on top of the IGBT modules. The capacitors, voltage and current sensors can be seen in first place.

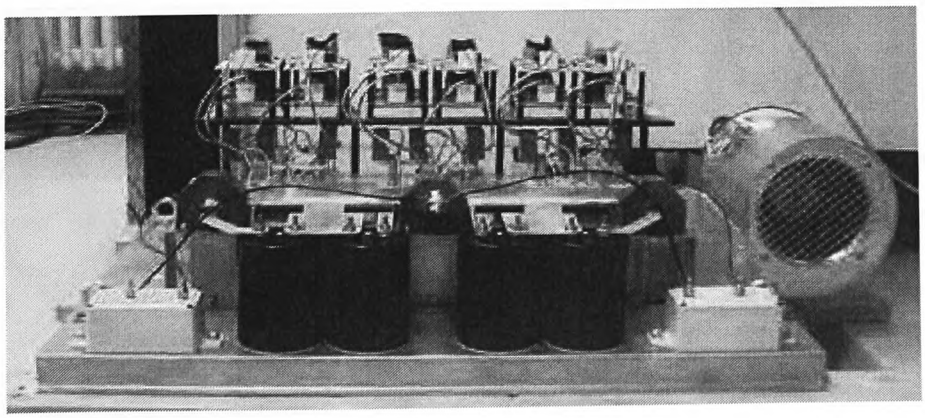

Fig. 6-18 Prototype of the three-level NPC VSI

6.4 Induction Motor

The IM used in the experimental setup is the Siemens 1LA7090-4AA10-Z. This is a three-phase squirrel-cage asynchronous motor. The main characteristics of this IM are described in Table 6-I.

Table 6-I IM characteristics

Rated speed	1415 rpm/148.17 rad/s
Rated power	1.1 kW
Rated torque	7.4 Nm
Rated voltage	230/400 V
Rated current	4.43/2.55 A
Rated frequency	50 Hz
Efficiency at P_{rated}	77%
Power Factor at P_{rated}	0.81
Starting/rated torque ratio	2.3
Breakdown/rated torque ratio	2.4
Starting/rated current ratio	4.6
No-load current	2.13 A
Moment of inertia	0.0024 kgm^2
Weight	13 kg
Stator windings resistance	9.21 Ω
Rotor windings resistance	6.644 Ω
Stator leakage inductance	32.07 mH
Rotor leakage inductance	8.47 mH
Three-phase magnetising inductance	444.15 mH

The IM is mounted in a rig with two other PMSM motors and their shafts connected. The moment of inertia of the whole system is therefore increased to J_{total}=0.00805 $kg{\cdot}m^2$. In Fig. 6-19 the motor rig employed is shown.

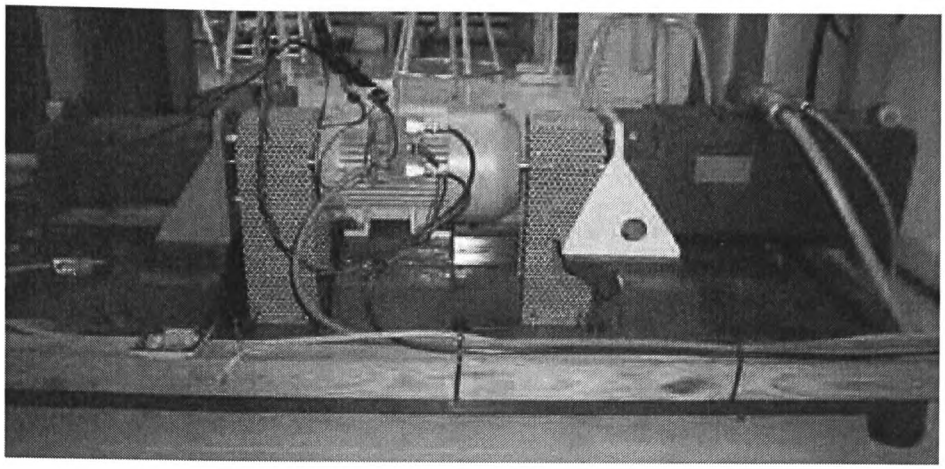

Fig. 6-19 Motor rig

6.5 Load control system

The load control system is based on a PMSM fed by a commercial drive system. The shafts of the IM and the PMSM are connected. The aim of this system is to provide an accurate control of the load torque. The load torque reference is generated by the dSPACE board and sent to the load control system.

6.5.1 Drive system

The load control system (see Fig. 6-20) is built with a Siemens SIMOVERT MC VSI that controls the PMSM. This system provides the possibility to implement a great variety of torque characteristics. The VSI is fed by a regenerative rectifier Siemens SIMOVERT RRU. The load control system is completed with the following components:

- An Electromagnetic Compatibility (EMC) filter.
- A reactance to reduce the current harmonics produced by the rectifier.
- An autotransformer to increase the input voltage of the rectifier by 20% an avoid voltage drops in regenerative mode.
- A 24 V power supply for the control circuits.

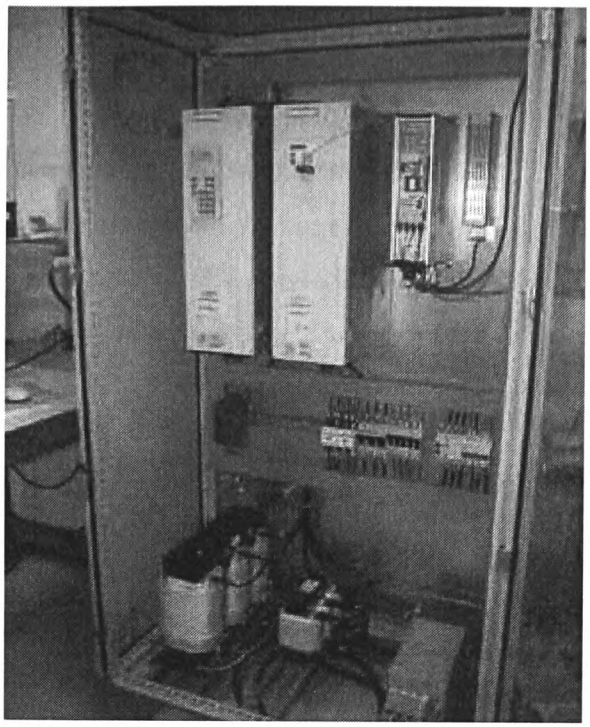

Fig. 6-20 Load control system

The regenerative rectifier converts the AC voltage coming from the network through the autotransformer into DC voltage to supply the VSI. It consists of two thyristor bridges connected in antiparallel that allow the power to flow in both directions. Its main features are:

- Input AC voltage: 380-480 V.
- Output DC voltage: 510-650 V.
- Maximum output current: 86 A.

The VSI is designed to control IMs and PMSMs with PWM techniques. The control is performed by a processor and a DSP and it includes some I/O capabilities such as digital and analog I/O, serial interface and encoder board (optional). The load torque reference is sent by means of one analog output of the dSPACE board which is connected to one analog input of the VSI control. The main characteristics of this equipment are:

- Power range: 2.2 kW-37 kW.
- Input voltage: 510-650 V.
- Input current: 40.5 A.
- Output voltage: 0-0.64 times the input voltage.
- Output current: 34 A.

- Output frequency: 0-400 Hz.
- Switching frequency: 5-10 kHz.

6.5.2 Permanent Magnet Synchronous Motor

The load control system is employed to supply one of the PMSMs and produce the desired load torque. This motor is a Siemens 1FT6084-8SH71-1AA0. It incorporates an incremental encoder (described in section 6.2.6.3), ventilation and thermal protection. The following table contains the main characteristics of this motor.

Table 6-II PMSM characteristics

Rated speed	4500 rpm/471.23 rad/s
Rated torque (100 K)	20 Nm
Rated current (100 K)	24.5 A
Starting torque (100 K)	26 Nm
Starting current (100 K)	28 A
Moment of inertia	0.0048 kgm^2
Maximum speed	7100 rpm
Maximum torque	65 Nm
Maximum current	86 A
Torque limit (600 V)	45 Nm
Current limit (600 V)	52 A
Torque constant	0.93 Nm/A
Voltage constant (between phases)	58 V/1000 rpm
Winding resistance	0.17 Ω
Three-phase inductance	2 mH
Electrical time constant	12 ms
Mechanical time constant	2.9 ms
Thermal time constant	42 min
Thermal resistance	0.09 W/K
Weight	25 kg

6.6 Programming of the control system

The implementation of the control strategies in the laboratory setup described involves some programming and the development of applications for various parts of the system. The programming can be split into the following parts:

1. **IM control.** The control algorithm is programmed using Simulink. The Simulink model is compiled and the code generated is uploaded in the dSPACE board.
2. **PROTEC-1 board.** The PLD is programmed using ABEL language and the software package ispDesignExpert. The main tasks of the PLD device are the decoding of the VSI state, to avoid forbidden combinations and transitions, the control of errors and the generation of alarms.
3. **ControlDesk.** An experiment file is created with a layout file associated. The layout file defines a Graphic User Interface (GUI) similar to a control panel. The main functionalities of the ControlDesk application generated are the control, monitoring and data capture from the system in real time.

Some extra code has been written in Matlab in the form of m-files to process and display the results obtained.

6.6.1 Induction Motor control

The control algorithms have been developed using Simulink. The Simulink models are then transferred to the dSPACE system. Two components need to be installed in the PC: the Real-Time Interface (RTI) library for Simulink and the software package ControlDesk (see section 6.6.3). The RTI adds a new group of blocks to the Simulink library that incorporate the I/O capabilities of the dSPACE system. Once the model is created it can be compiled using Real-Time Workshop (RTW) and the code is generated to be executed in real time in the dSPACE system. The library dSPACE RTI1103 for Simulink is divided in 4 sublibraries:

- DS1103 MASTER PPC. It contains all the blocks associated with the PowerPC 604e processor.
- DS1103 SLAVE DSP. It contains all the blocks associated with the DSP TMS320F240.
- Extras. Contains some special purpose blocks.
- TaskLib. It offers blocks to incorporate interruptions in the Simulink model.

The I/O blocks used from these libraries are shown in Table 6-III.

Table 6-III I/O Blocks used in the control system

INPUTS	
Signal	Library block
Motor speed (Incremental encoder)	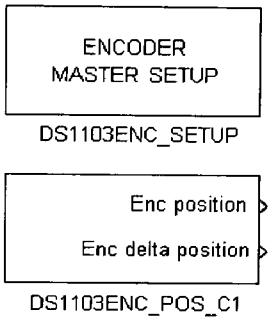
Motor line currents (i_{sa}, i_{sb}) and DC-link voltages (V_{DC}, V_{C1}, V_{C2}) (ADC)	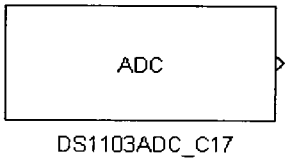
OUTPUTS	
Signal	Library block
A, B, C, D, E, F, Enable (Digital Outputs, bits 0-6)	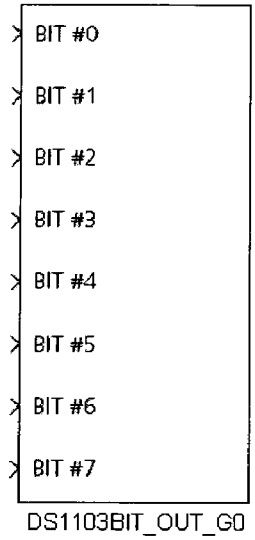
Load torque reference (DAC)	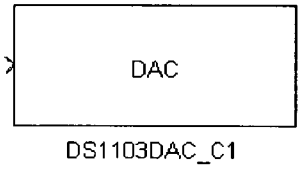

The structure of the control algorithm is presented in Fig. 6-21.

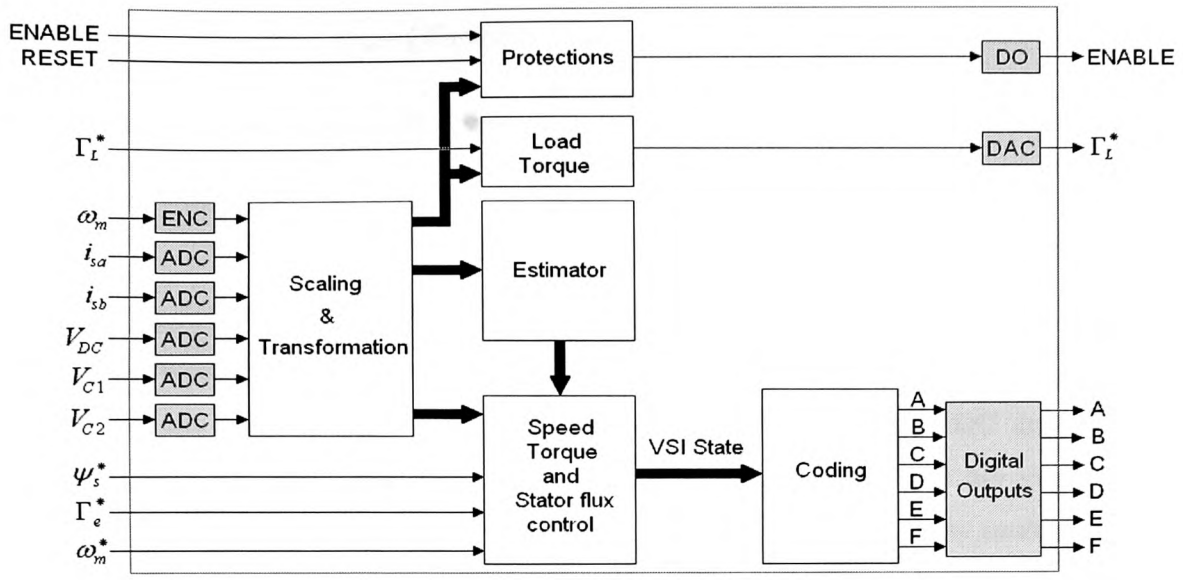

Fig. 6-21 General structure of the control algorithm

The control algorithm can be devided 6 different blocks:

- Scaling and transformation of the input signals.
- Estimator.
- Speed, torque and stator flux control.
- Coding of the VSI state.
- Protections.
- Load Torque generation.

Some of these blocks and the calculations involved are already presented in other sections of the thesis. The speed, torque and stator flux control is described for the Classical DTC method and the new control system presented in this thesis in Chapter 4 and Chapter 5 respectively. The stator flux and torque estimator is described in Chapter 4, and the method explained in section 4.4.2 is employed in the experimental implementation.

6.6.1.1 Scaling and transformation of input signals

The incremental encoder provides a train of pulses which gives the position of the motor. The variation of this position, which is given in number of pulses between samples (*Encoder_delta_position*), is transformed into radians. The speed in rad/s is obtained multiplying the variation of position in radians by the sampling frequency (10 kHz):

$$\omega_m = (Encoder\_delta\_position)\frac{2\pi f_s}{2048} \tag{6.1}$$

Finally the speed in rad/s can be expressed in rpm as follows:

$$n = \omega_m \frac{30}{\pi} \tag{6.2}$$

A low-pass filter is then applied to remove the noise from the signal. A 2nd order low-pass Butterworth filter with a pass-band edge frequency of 100 rad/s is employed.

Regarding the line currents i_{sa} and i_{sb} the measured value in the ADC converters is multiplied by a scaling factor (SCALE_ADC_CUR = 50 A/V) and the value of the currents is obtained in Amperes. The DC-link voltages are obtained by multiplying the value measured in the ADC by a scaling factor of 100.

6.6.1.2 Coding of the VSI state

The VSI state that has to be applied to the motor, which is calculated in the control system, defines the state (on-off) of the 12 VSI switches. Considering one leg of the VSI, which contains 4 switches, not all the combinations (2^4=16) are possible. Table 6-IV and Fig. 6-22 show the combinations allowed with the associated coding. As it can be seen only 4 combinations are possible and therefore the state of the leg can be expressed just using a two bits code. Moreover it should be noticed that only looking at the state of S_2 and S_3 the state of the leg is already defined. In order to reduce the number of lines sent from the dSPACE system to the PROTEC-1 board the state of each leg is coded using only two bits. The state of each leg is described by the following pairs of bits:

- Leg *R* (*A*): A & B.
- Leg *S* (*B*): C & D.
- Leg *T* (*C*): E & F.

Table 6-IV Possible combinations of states in a three-level NPC VSI and coding (0=off; 1=on)

Switches				Name	V_{ONP}	Coding	
S_1	S_2	S_3	S_4			A/C/E	B/D/F
off	off	off	off	E_REPOS	-	0	0
off	off	on	on	E_BAIX	$-V_{DC}/2$	0	1
off	on	on	off	E_MIG	0V	1	1
on	on	off	off	E_ALT	$+V_{DC}/2$	1	0

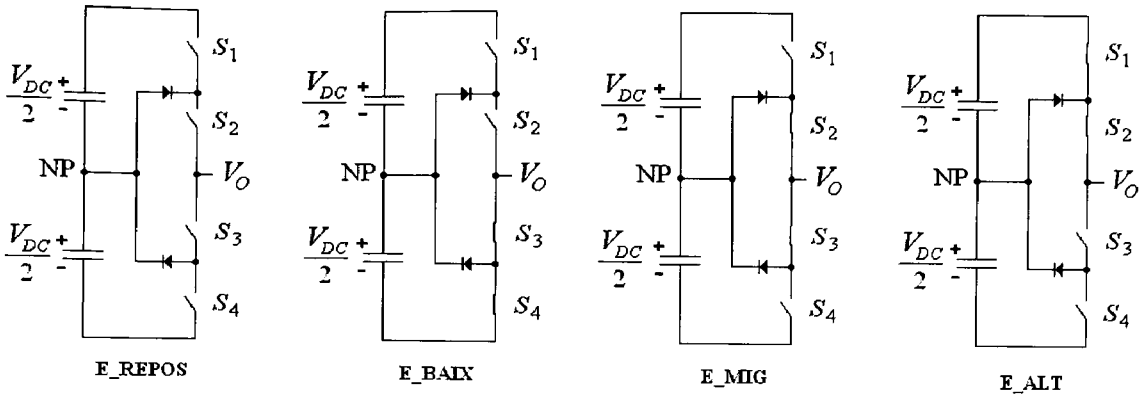

Fig. 6-22 Valid states in a leg of a three-level NPC VSI

Signals A, B, C, D, E and F are sent using digital outputs of the dSPACE board. These signals are inverted in the optical interface and this is taken into account in the PLD program.

6.6.1.3 Additional parts

Some extra parts have been programmed in Simulink to perform additional tasks. The load torque reference is generated and various modes are available to emulate different types of load: constant torque with the sign of the speed, linear, quadratic and cubic load torques. The maximum value that can be assigned is limited and finally it is multiplied by a scaling factor (SCALE_DAC_TQ=1/20 V/Nm) to transform from Nm to V. The final value is sent trougth the DAC to the load control system described in section 6.5.

The enable signal is created for a safe operation of the whole system. When this signal is off all the control is disabled. This signal is sent to the PROTEC-1 board using one of the digital outputs. Some protections are also implemented to disable the system in case of overcurrent or overspeed. The source of error can be displayed and identified with a code number.

6.6.2 PROTEC-1

The core element of the PROTEC-1 board is the PLD. Combinational and sequential circuits can be implemented in the PLD. The defined inputs and outputs of the PLD are shown in Table 6-V.

Table 6-V PLD inputs and outputs

INPUTS	
A	First bit coding leg *R*.
B	Second bit coding leg *R*.
C	First bit coding leg *S*.
D	Second bit coding leg *S*.
E	First bit coding leg *T*.
F	Second bit coding leg *T*.
EN	Enable
Err_R	IGBT driver error in leg *R*.
Err_S	IGBT driver error in leg *S*.
Err_T	IGBT driver error in leg *T*.
Err_V	Overvoltage error.
Err_If	Overcurrent error in a phase.
Err_Ib	Overcurrent error in the DC-link.
Err_Cho	Driver error in the Braking system.
R_DRIVER	Reset of the IGBT drivers when reset button is pressed.
OUTPUTS	
O1_R	Firing signal S_1 leg *R*.
O2_R	Firing signal S_2 leg *R*.
O3_R	Firing signal S_3 leg *R*.
O4_R	Firing signal S_4 leg *R*.
O1_S	Firing signal S_1 leg *S*.
O2_S	Firing signal S_2 leg *S*.
O3_S	Firing signal S_3 leg *S*.
O4_S	Firing signal S_4 leg *S*.
O1_T	Firing signal S_1 leg *T*.
O2_T	Firing signal S_2 leg *T*.
O3_T	Firing signal S_3 leg *T*.
O4_T	Firing signal S_4 leg *T*.
O_V	Overvoltage alarm.
O_If	Phase overcurrent alarm.
O_Ib	DC-link overcurrent alarm.
O_R	Driver error in leg *R* alarm.
O_S	Driver error in leg *S* alarm.
O_T	Driver error in leg *T* alarm.
O_Cho	Driver error in the Braking system alarm.
Err	Error signal sent to the dSPACE system.
RST_DRI	Reset signal sent to the IGBT drivers.

The finite state machine diagram that describes the sequential part of the program is shown in Fig. 6-23. The state name and the output values for the firing signals (S_1,S_2,S_3,S_4) are shown in each circle representing a state. The transitions caused by the combinations of inputs are shown next to the arrows. Only inputs A and B corresponding to leg *R* are used in this diagram for simplification. In the actual program the coding of the state defined by a pair of bits such as A and B is inverted.

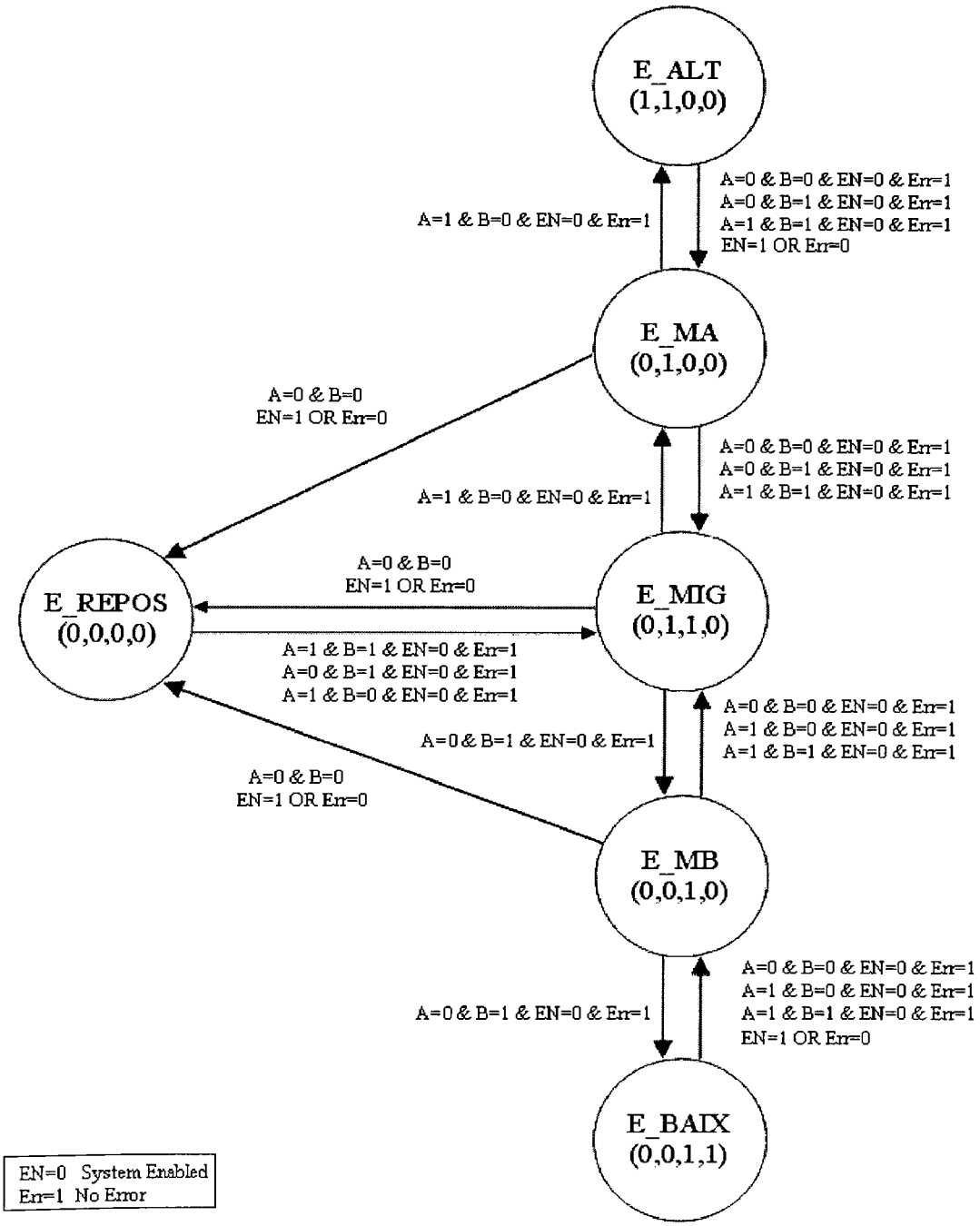

Fig. 6-23 Finite state machine diagram of the PLD program

As can be seen transitions between states are controlled and the program is forced to pass always through the state E_MIG (0,1,1,0) for safety. Two extra states are defined E_MA (0,1,0,0) and E_MB (0,0,1,0) to ensure that combinations (1,1,1,0) and (0,1,1,1) never happen, as these combinations would produce a short-circuit in the leg. A dead time of 2 μs is programmed for these transitions.

The combinational part of the program is basically associated with errors, alarms and the reset of the IGBT drivers. This part of the program is as follows:

```
"ERROR CONTROL, RESET AND ALARMS ACTIVATION

Err=(!Err_R&!Err_S&!Err_T&Err_V&Err_If&Err_Ib&!Err_Cho);
RST_DRI=!R_DRIVER;

O_Ib=Err_Ib;
O_V=Err_V;
O_If=Err_If;
O_T=!Err_T;
O_S=!Err_S;
O_R=!Err_R;
O_Cho=!Err_Cho;
```

The complete script of the program is included in Appendix C.

6.6.3 ControlDesk

The software package ControlDesk is provided with the dSPACE system. This program is devised to control, monitor and log data from experiments in real time. It is possible to set up a control panel in the PC with a GUI to perform all the tasks mentioned.

Different libraries with instruments are available to create layouts and experiments to evaluate the control strategies developed. The system parameters can be modified in real time to interact with the plant through virtual instruments. The main window of the application developed is shown in Fig. 6-24.

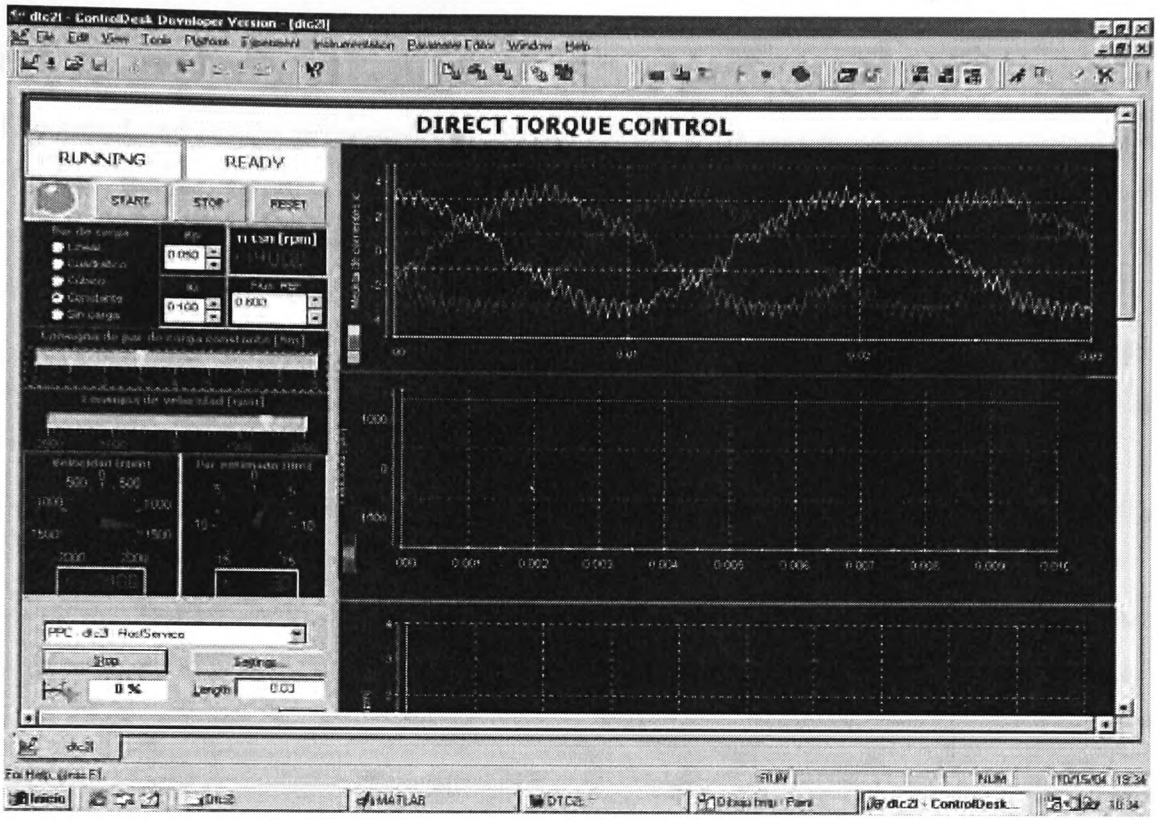

Fig. 6-24 ControlDesk experiment window

The main features of the application developed in ControlDesk to perform the experimental tests are:

- Enable/disable the control.
- Monitoring of errors and reset of them.
- Control of the speed, torque and stator flux modulus reference values.
- Control of the load torque.
- Tuning of several parameters of the control system (PI parameters, DTC hysteresis bands, torque gain of the proposed control).
- Log all the most interesting variables of the process.
- Visualization of variables such as speed, torque, stator flux, stator currents and the VSI state.

6.7 Experimental results

The simulated results presented in Chapter 5 have to be corroborated experimentally to validate the proposed control system. The experimental setup described has been employed for this purpose. However this setup was not fully operative when the experimental results were obtained and the following limitations were present:

- Several series-connected DC power supplies were employed to feed the DC-link. The voltage level employed was 200 V. The operating region in the speed-torque plane was therefore reduced.
- The braking system was not operative and only steady-state test were performed to avoid overvoltages in the DC-link.

Moreover an earlier version of the proposed control system described in Chapter 5 was employed during the experiments. The scheme employed in the experimental tests is shown in Fig. 6-25.

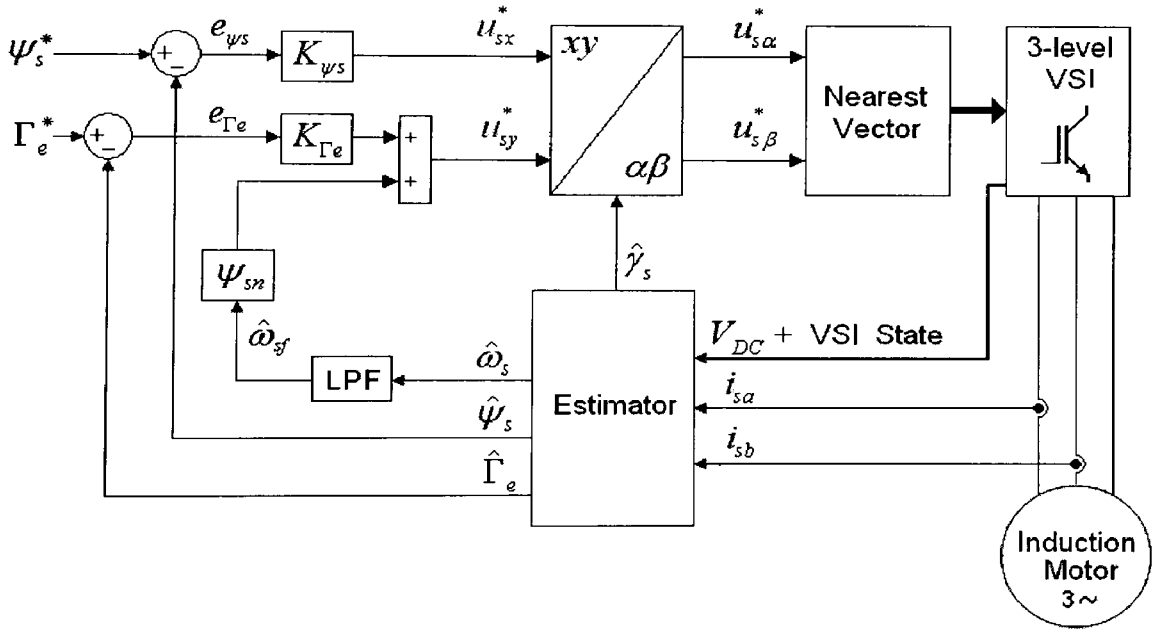

Fig. 6-25 Proposed control scheme employed in the experimental tests

This earlier version of the proposed control system is more simplified when compared to the scheme presented in Chapter 5. The stator flux modulus error and torque error are controlled in closed loop by means of proportional controllers to obtain the x and y components of the reference voltage vector in the stator flux vector reference frame.

Regarding the calculation of the y component of the reference voltage vector only the BEMF term is considered and added to the output of the torque proportional controller. As explained in Chapter 5, this term corresponds to the biggest part of u_{sy} in most of the IM operating region and is compensated in this way. Finally, the voltage drop in the stator resitance is not considered in the calculation of the x component of the reference voltage vector.

Once again, in order to assess the improvements achieved by the proposed control system described a comparative analysis with the Classical DTC method with a two-level VSI is presented. The following names are used to identify both systems:

- DTC2L: Classical DTC system with a two-level VSI.
- PDTC3L: Proposed control system with a three-level VSI employed for the experimental tests as shown in Fig. 6-25.

The control parameters employed for both systems in all the tests are shown in Table 6-VI. The parameters of the speed control loop are common for both systems. The torque and flux hysteresis bands in DTC2L are defined according to Fig. 4-4.

Table 6-VI Control parameters of the experimental tests

DTC2L	
Parameter	**Value**
Flux hysteresis bands ($H_{\psi s}$,-$H_{\psi s}$)	(0.001,-0.001) Wb
Torque hysteresis bands ($H_{\Gamma e}$,-$H_{\Gamma e}$)	(0.1,-0.1) Nm
Sampling period (T_s)	0.0001 s
PDTC3L	
Parameter	**Value**
Torque control proportional gain ($K_{\Gamma e}$)	60
Stator flux control proportional gain ($K_{\psi s}$)	900
Sampling period (T_s)	0.0001 s
Speed control loop	
Parameter	**Value**
PI proportional gain (K_p)	0.05
PI integral time (T_i)	0.1
PI output saturation (Γ_{lim})	±15 Nm
Speed filter type	Butterworth, 2nd order
Speed filter cut-off frequency	100 rad/s

The steady-state performance has been tested in four different operating points defined by the speed reference and load torque values. The operating points tested are shown in Table 6-VII.

Table 6-VII Operating points tested experimentally in steady-state conditions

Speed [rpm] / ω_m^* [rad/s]	**Γ_L [Nm]**
50 / 5.23	Γ_F
50 / 5.23	Γ_n
200 / 20.94	Γ_n
600 / 62.83	Γ_F

The same variables plotted in the simulated steady-state tests are shown for each experimental test:

- Stator flux modulus response.
- Stator flux vector path.
- Torque response.
- Speed response.
- i_{sa} current and frequency spectrum.

The same performance indexes calculated in the simulated steady-state tests are obtained for the experimental tests:

- Mean and RMS stator flux modulus error ($e_{\psi s}$).
- Mean and RMS torque error ($e_{\Gamma e}$).
- RMS speed error ($e_{\omega m}$).
- Stator current THD.
- Mean switching frequency of the semiconductor devices (f_{sw}). (Considering the ON-OFF sequence in a switch as one period).
- Percentage of utilisation for each type of voltage vector. (Large vector also refers to active vectors in the system which employs the two-level VSI).

The steady-state results obtained for the different operating points defined in Table 6-VII are shown in the following figures (Fig. 6-26 to Fig. 6-33).

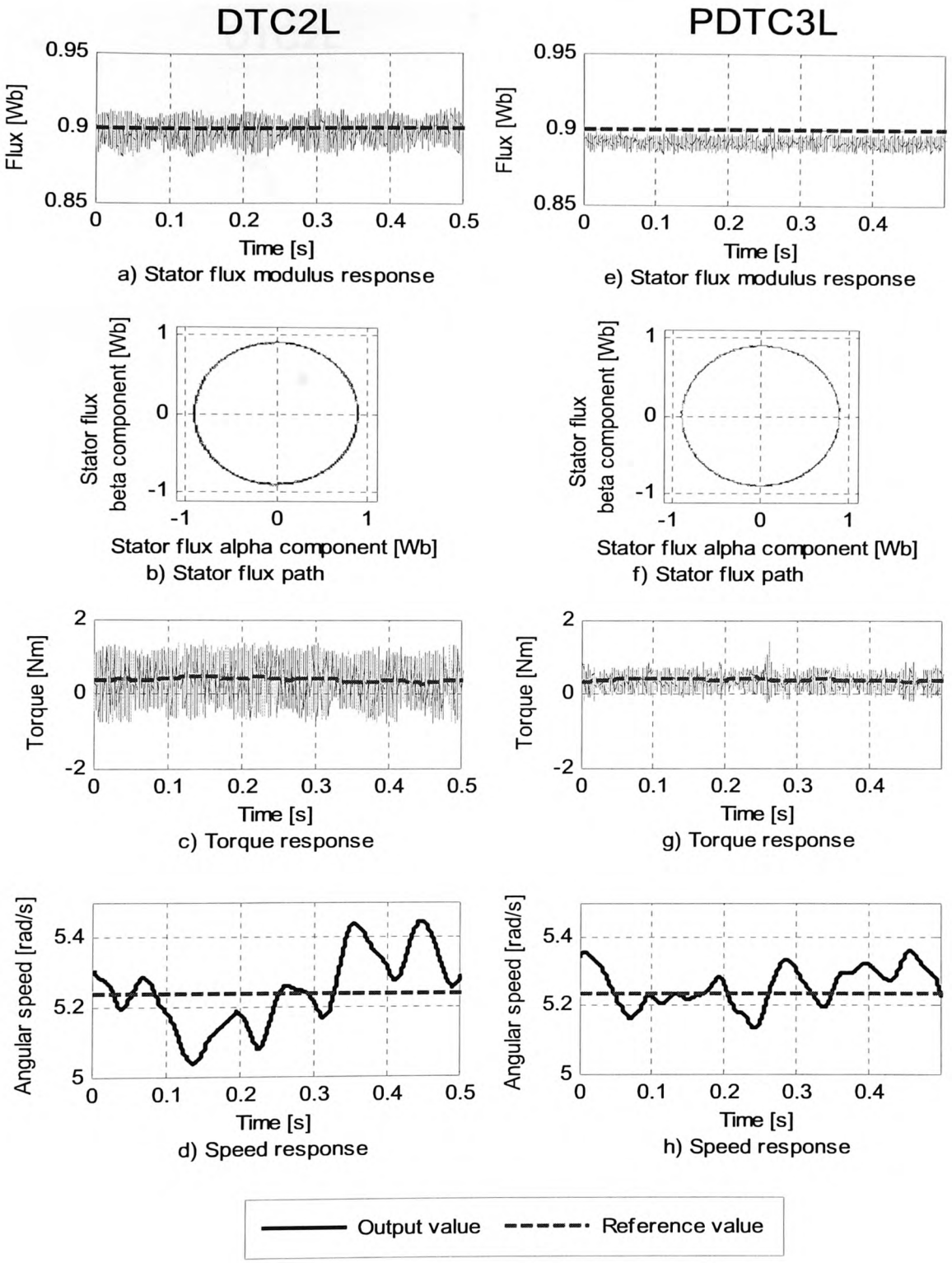

Fig. 6-26 Experimental results at 50 rpm and friction torque part I

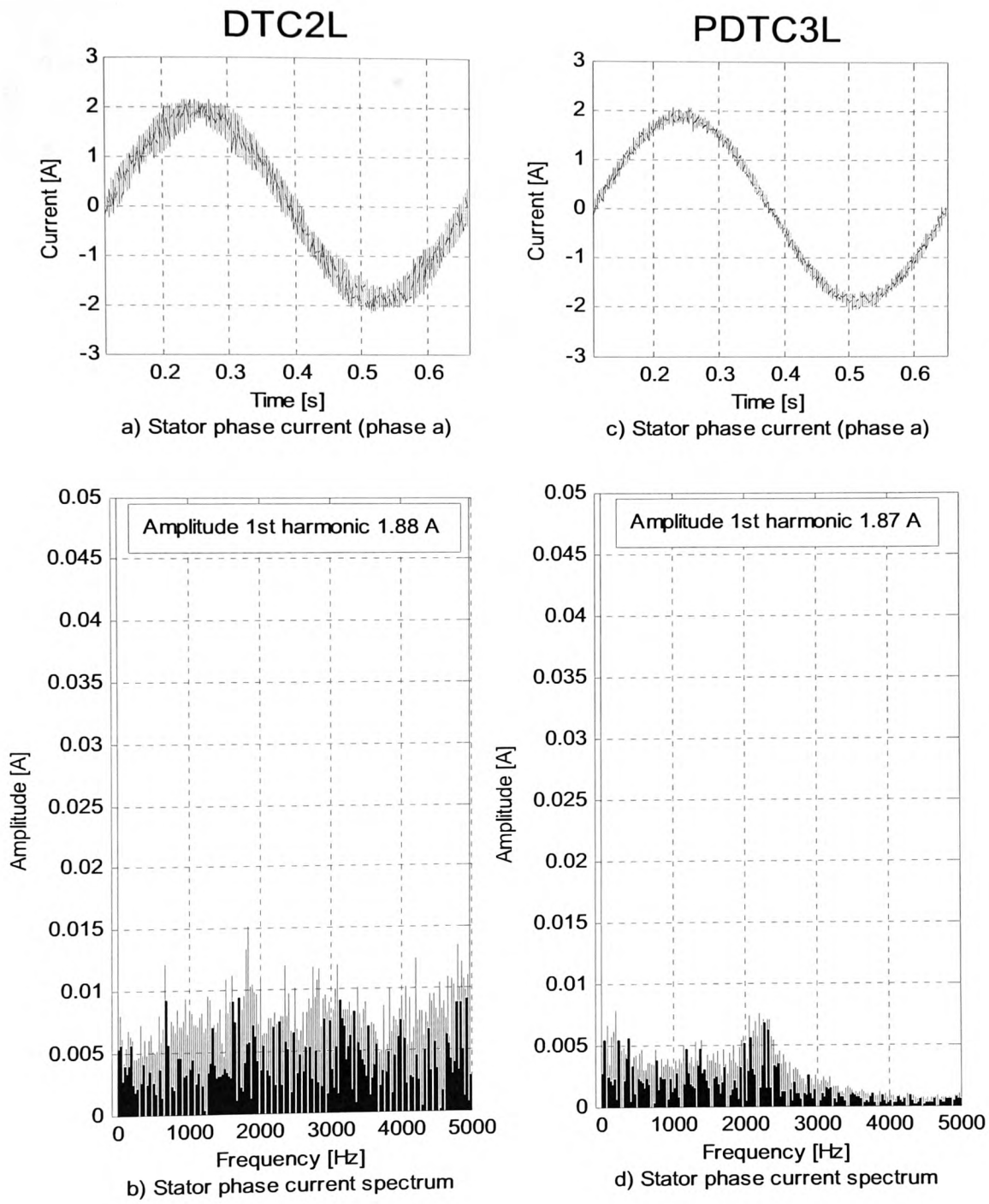

Fig. 6-27 Experimental results at 50 rpm and friction torque part II

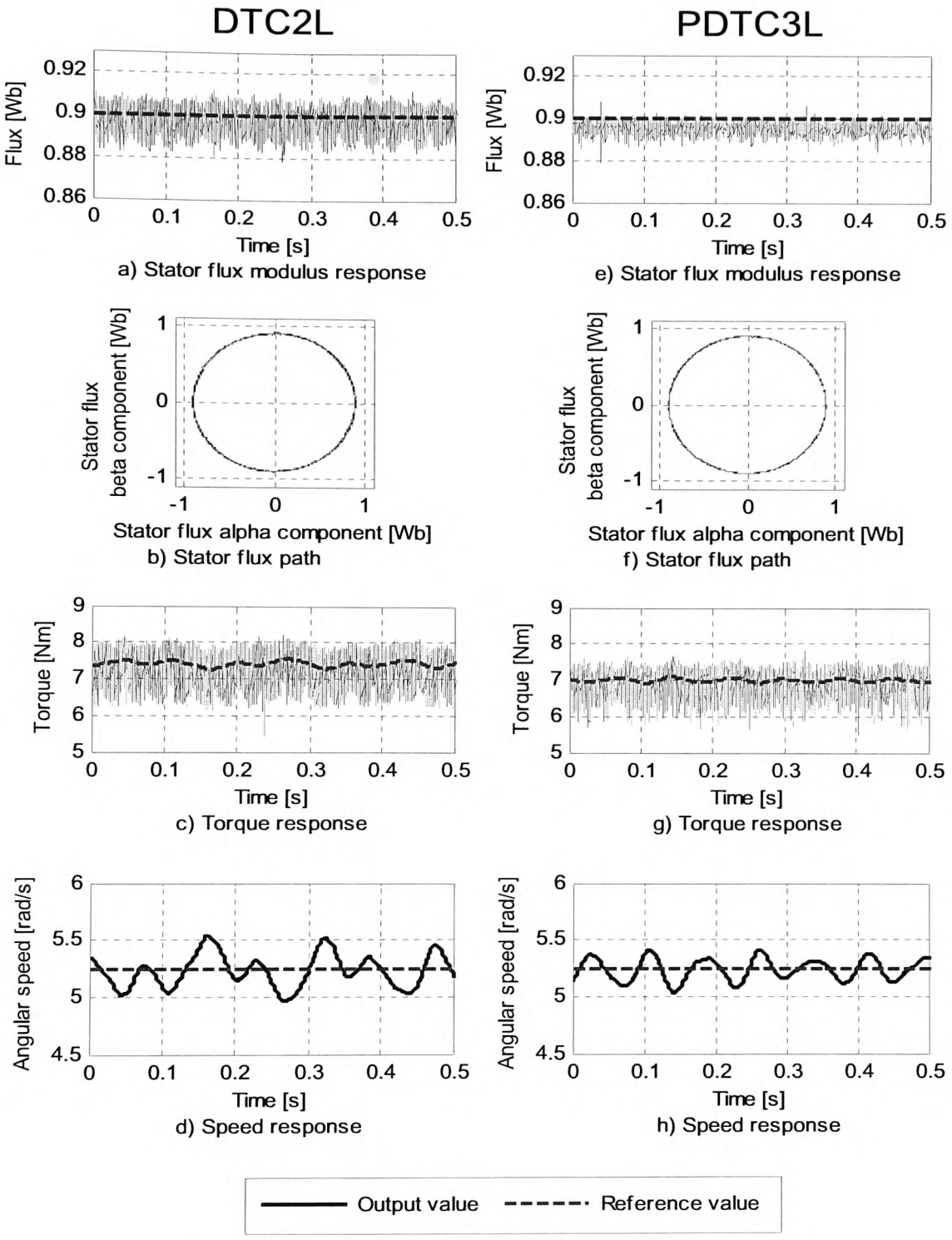

Fig. 6-28 Experimental results at 50 rpm and nominal torque part I

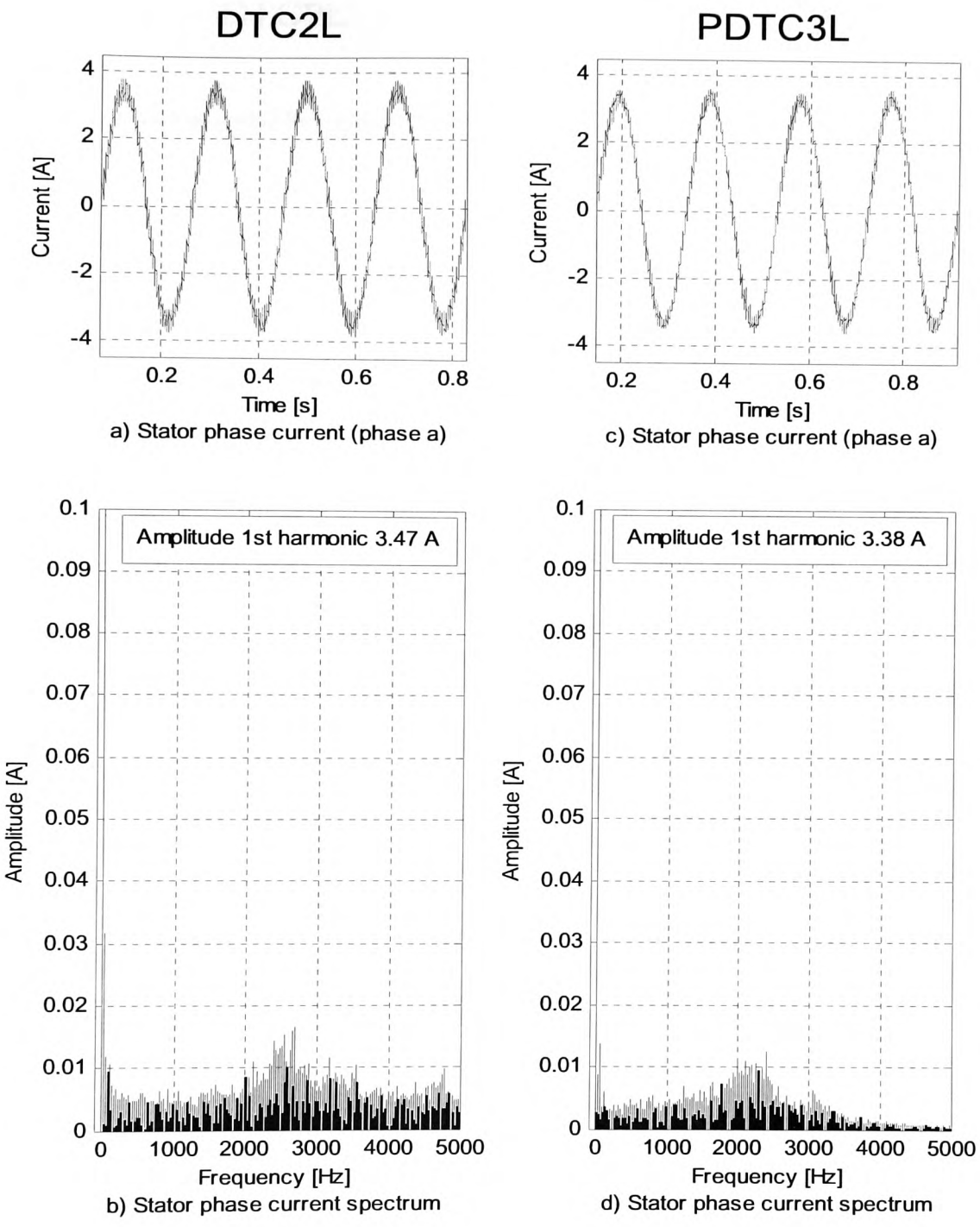

Fig. 6-29 Experimental results at 50 rpm and nominal torque part II

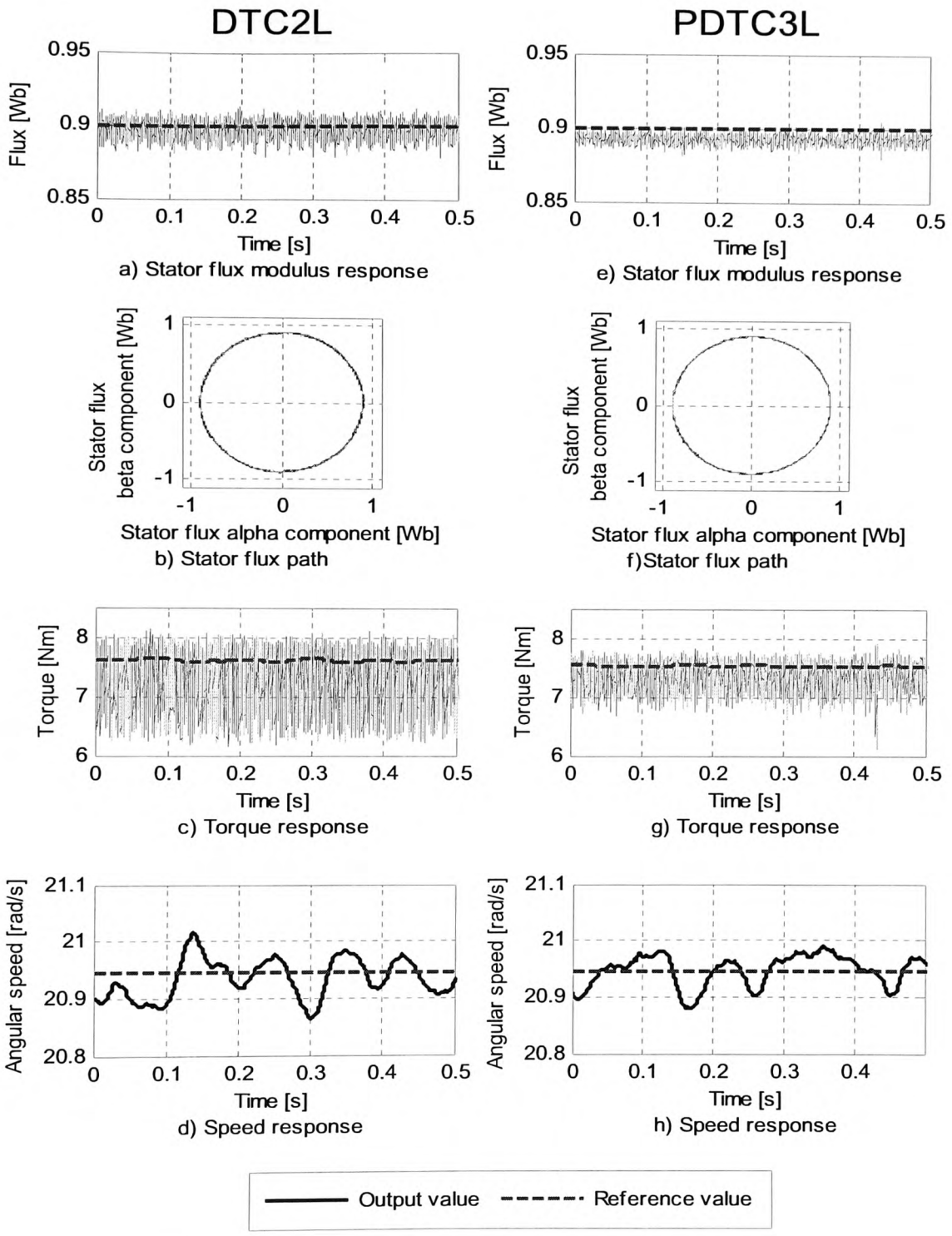

Fig. 6-30 Experimental results at 200 rpm and nominal torque part I

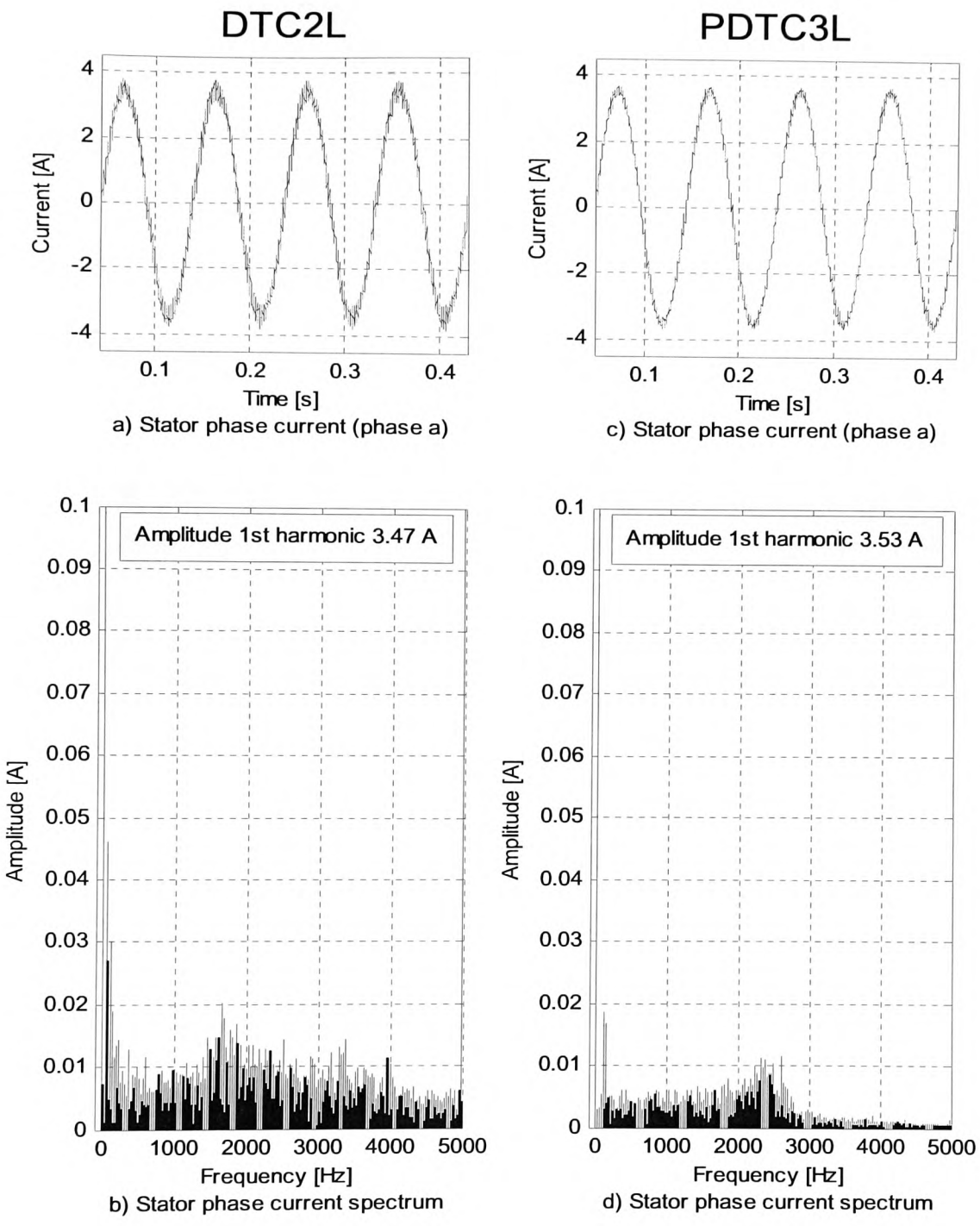

Fig. 6-31 Experimental results at 200 rpm and nominal torque part II

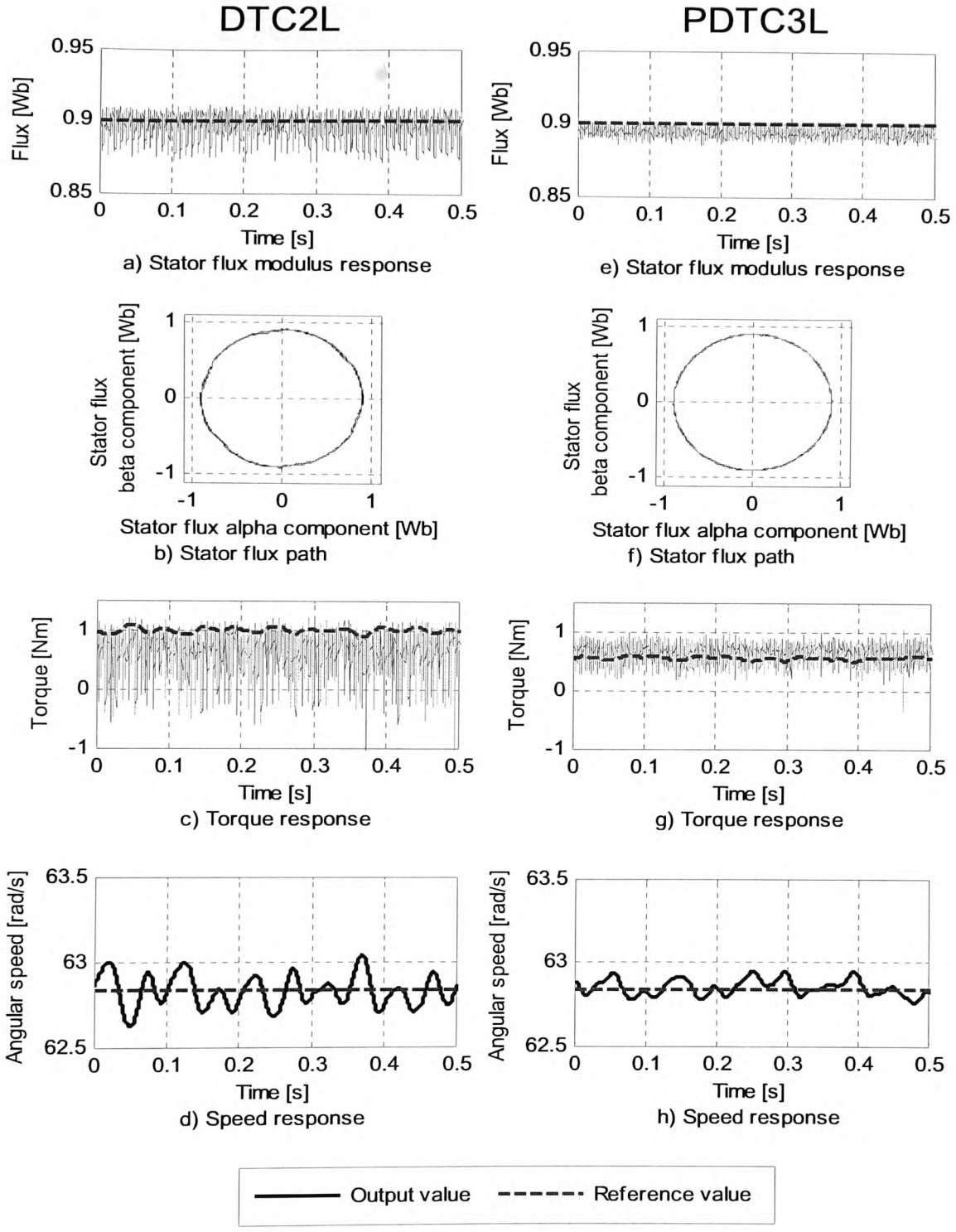

Fig. 6-32 Experimental results at 600 rpm and friction torque part I

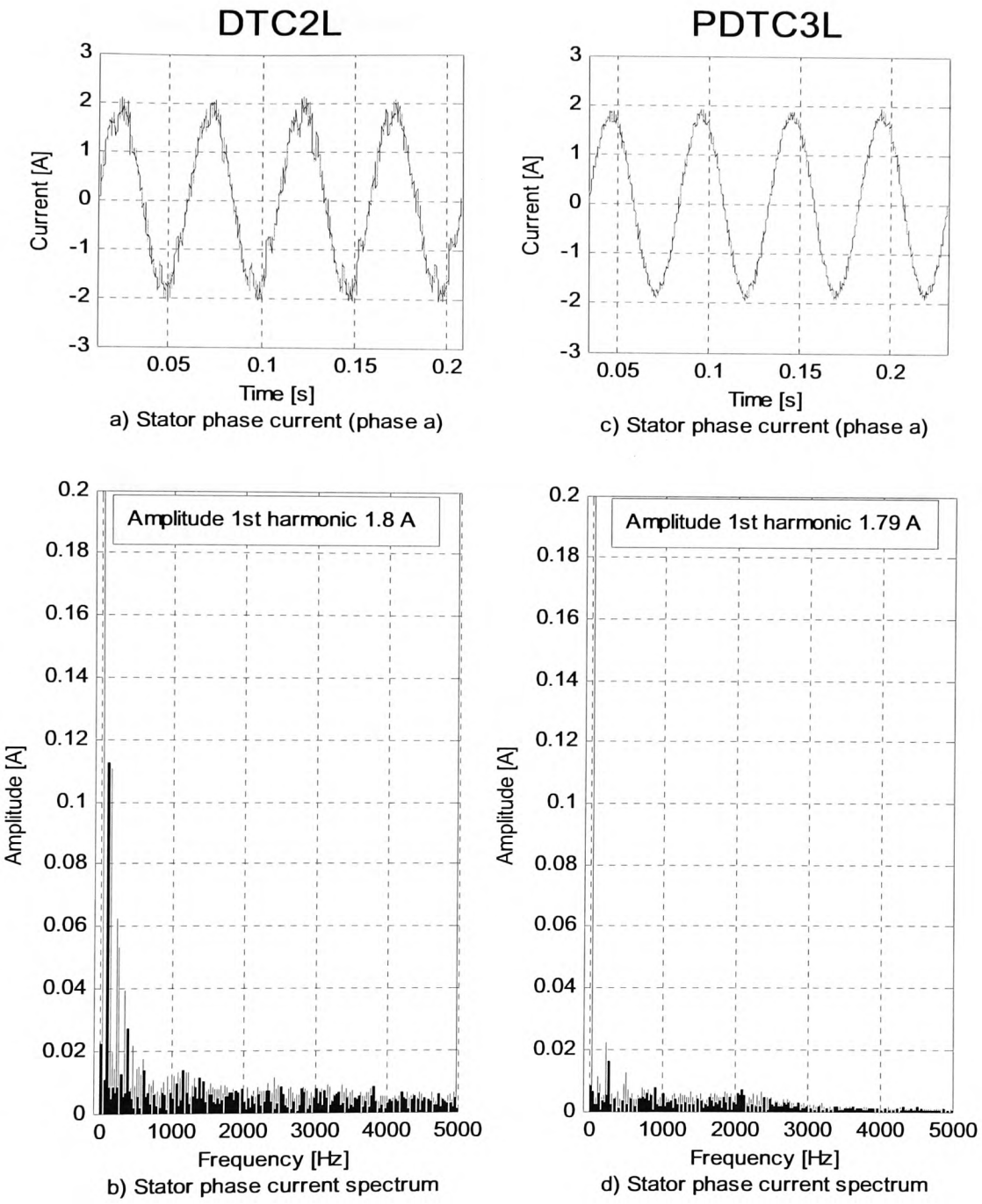

Fig. 6-33 Experimental results at 600 rpm and friction torque part II

The comparative results in steady-state conditions show a reduction of the ripple in the stator flux modulus and torque responses when using the PDTC3L system. A reduction of the speed oscillation is also achieved. The harmonic distortion in the stator phase current is lower in the results obtained with the PDTC3L system, as illustrated in the current waveforms and their frequency spectrum.

The only weakpoint observed in the results for the PDTC3L system is the mean error that appears in the stator flux modulus response. It should be noted however that this error is in all cases less than 1% and the ripple is considerably reduced when compared to the results of the DTC2L system. The presence of this mean error in the stator flux modulus response is mainly associated to the approach adopted based on a proportional controller. The mean error observed can be reduced by increasing the proportional gain. Moreover the voltage drop in the stator resistance can be added to the output of the proportional controller. An efficient solution to this problem is presented in the proposed control system described in Chapter 5, where a deadbeat control approach is employed instead and there is not a proportional gain to be adjusted, which simplifies the tuning of the controller.

Another weakpoint observed in the results of the PDTC3L system is the mean error that appears when the load torque value is high (50 rpm and 200 rpm with nominal torque). This mean error is still reduced in comparison with the results obtained by the DTC2L system but it is not completely eliminated. The presence of this error is caused by the torque production term of the u_{sy} voltage defined in equation (5.9) in Chapter 5, which is not added to the output of the proportional controller and the BEMF term. The problem is also solved by adding this term as explained in the new control system described in Chapter 5.

At 600 rpm with friction torque the DTC2L system presents some distortion in the stator flux path, like it was observed in some of the simulation tests, due to the effect of the sector boundaries. This confirms the existence of this effect, which is more noticeable when the stator flux vector rotates at high angular speeds. The spectrum of the currents also reflects this distortion with the presence of low frequency harmonics (harmonics 5^{th}, 7^{th}, 11^{th}, 13^{th},...) as can be seen in the current spectrum shown in Fig. 6-33.

Table 6-VIII presents the performance indexes obtained in the experimental steady-state tests for the DTC2L and the PDTC3L systems.

Table 6-VIII Performance indexes of the experimental tests

Index	System	Operating points (Speed [rpm] - Γ_L [Nm])				Mean Reduction %
		50 - Γ_F	50 - Γ_n	200 - Γ_n	600- Γ_F	
Mean $e_{\psi s}$ [Wb]	DTC2L	0.0027	0.0030	0.0033	0.0058	**-108.71**
	PDTC3L	0.0089	0.0053	0.0076	0.0057	
RMS $e_{\psi s}$ [Wb]	DTC2L	0.007	0.0066	0.0067	0.0108	**-0.95**
	PDTC3L	0.0094	0.0059	0.0081	0.0064	
Mean $e_{\Gamma e}$ [Nm]	DTC2L	0.0431	0.2490	0.4102	0.3818	**53.22**
	PDTC3L	0.0335	0.0962	0.1852	-0.0977	
RMS $e_{\Gamma e}$ [Nm]	DTC2L	0.4393	0.5100	0.6175	0.4857	**52.62**
	PDTC3L	0.1781	0.3521	0.2882	0.1614	
RMS $e_{\omega m}$ [rad/s]	DTC2L	0.1152	0.1389	0.0384	0.0870	**40.34**
	PDTC3L	0.0532	0.0999	0.0280	0.0414	
THD i_{sa} [%]	DTC2L	12.6	6.7	6.8	13.9	**52.17**
	PDTC3L	5.3	4.56	3.2	4.74	
Mean f_{sw} [Hz]	DTC2L	3174	2742	2039	934	**55.91**
	PDTC3L	673	1545	988	470	
Mean ω_s [rad/s]	DTC2L	11.49	33.51	65.01	127.97	
	PDTC3L	11.57	32.76	65.77	127.71	
% zero vectors	DTC2L	16.69	7.99	7.70	4.52	
	PDTC3L	49.52	11.85	10.13	0.06	
% large vectors	DTC2L	83.32	92.02	92.31	95.49	
	PDTC3L	0.04	22.31	17.26	40.12	
% medium vectors	DTC2L					
	PDTC3L	1.28	28.79	20.73	50.09	
% small vectors	DTC2L					
	PDTC3L	49.17	37.06	32.85	9.74	

The last column of the table shows the mean reduction of the performance indexes obtained for all the operating points. It can be observed how the PDTC3L system considerably reduces all the indexes and proves its superiority in comparison with the

DTC2L system. The only exception is the stator flux modulus response that contains a bigger mean error as explained before. Overall, the results obtained show that the PDTC3L system offers a more precise control of torque and speed with less distorted currents and a lower switching frequency in the semiconductor devices.

The resulting mean switching frequency for both systems and each operating point is shown in Fig. 6-34. It can be observed how the switching frequency is considerably reduced particularly for low angular speeds of the stator flux vector (ω_s) confirming the results obtained in simulation.

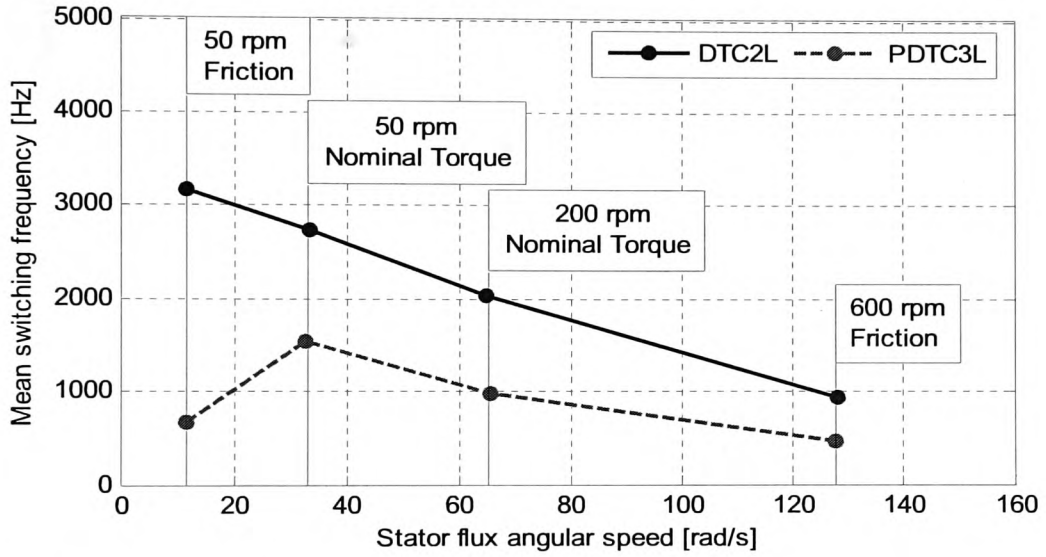

Fig. 6-34 Mean switching frequency depending on the operating point (experimental results)

The last 4 rows of Table 6-VIII present the percentage of utilisation of the different types of voltage vector in order to analyse how they contribute to the improvement of the control system. The results obtained (see Fig. 6-35) match with the simulation results presented in Chapter 5 and the same conclusions can be extracted. These results confirm experimentally the goodness of the solution based on the combination of DTC and the three-level VSI.

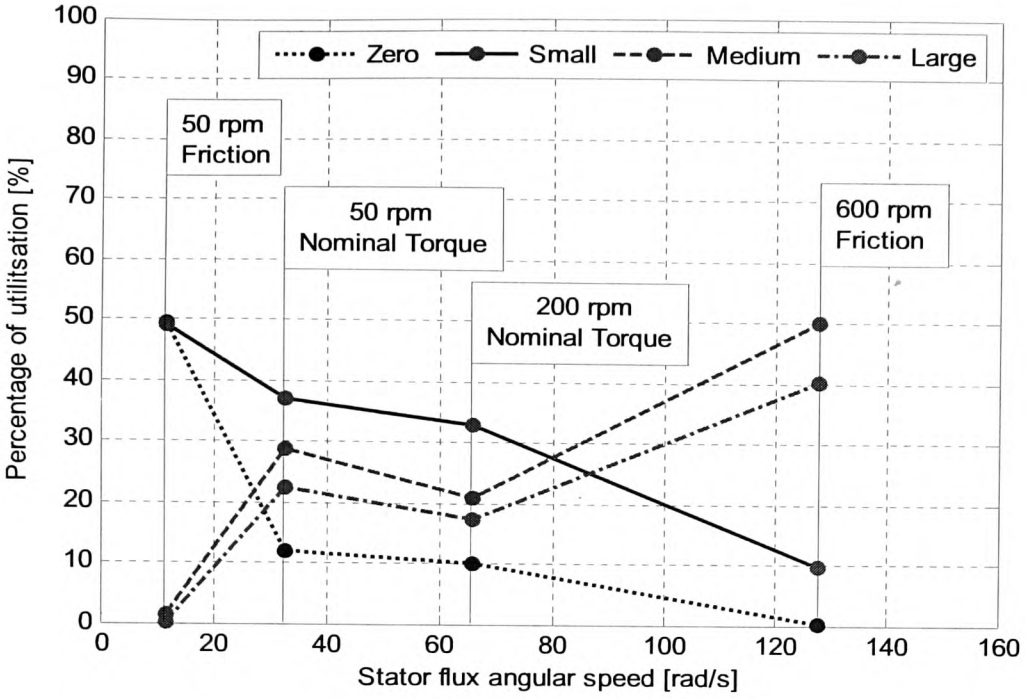

Fig. 6-35 Percentage of utilisation for the different types of vector depending on the operating point (experimental results)

Fig. 6-36 and Fig. 6-37 show the stator phase volatges and currents measured with the oscilloscope for some of the operating points tested experimentally.

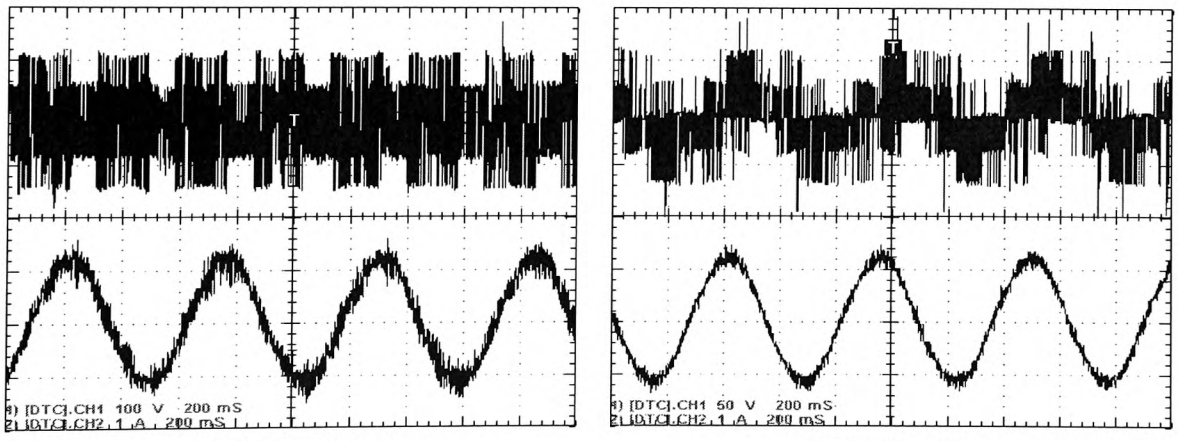

Fig. 6-36 Stator phase voltages and currents measured at 50 rpm and friction torque

It should be noted in Fig. 6-36 that the voltage scales are 100 V/division and 50 V/division for the DTC2L and PDTC3L systems respectively. The PDTC3L system can deliver reduced voltages at low speed operation thanks to three-level VSI and the

possibility of selecting small vectors. Thanks to this feature the results obtained at low speed operation are clearly superior.

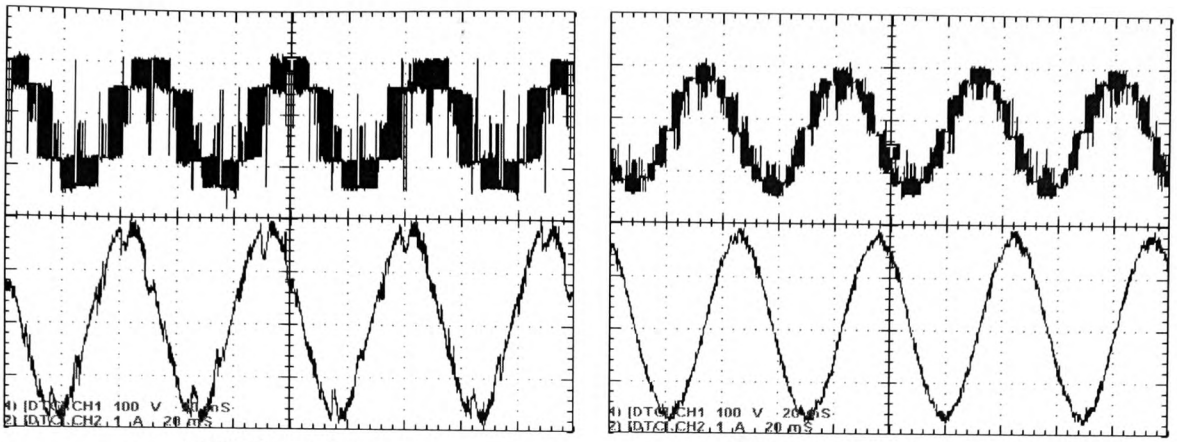

a) DTC2L system b) PDTC3L system

Fig. 6-37 Stator phase voltages and currents measured at 600 rpm and friction torque

6.8 Interim conclusions

The first part of this chapter describes the laboratory setup employed to experimentally validate the proposed control system. The equipment described provides a highly flexible system for research on the control of various types of electrical motors. An accurate system to control the load torque is one of the main features of the setup described. The system employs a fast-prototyping board (dSpace) that can be directly programmed from Simulink. The main advantage of this type of system when compared to a conventional DSP-based system programmed in C or assembler is the simplicity and time saved during the implementation of control algorithms. Moreover experiments can be easily implemented by means of an application (ControlDesk) to interact in real-time with the system and visualize and log the state of it using a wide variety of instruments.

In the second part of the chapter experimental results are presented to validate the proposed control system based on the DTC principle combined with the three-level VSI. Despite the limitations of the experimental tests carried out, the results obtained match with the simulation results presented in Chapter 5 confirming the advantages of the proposed control system in comparison with the Classical DTC method.

Chapter 7: Conclusions and Suggestions for Further Research

Summary – *This final chapter summarizes the research work presented in this thesis and the main conclusions extracted from it. The initial objectives are reviewed again followed by the description of the work completed and the results obtained. Finally the contributions of the thesis are stated and some future lines of work are suggested.*

7.1 Conclusions

The work presented in this thesis has been devoted to the study of advanced control systems for electrical motors. The study is focused on the control of the IM. The existing vector control strategies provide the best performance and have been incorporated to commercial motor drives for more than two decades. This family of control strategies can accurately control the instantaneous motor fluxes which are the key variables of the electrical motor in order to achieve precise control of position, speed and torque. Among the existing vector control strategies, one of the most recent developments was the strategy known as DTC, which has been employed in commercial drives for more than a decade. DTC still attracts the attention of many researchers where the aim is to improve the performance of the strategy. Following this direction, the main objective of the research work presented in this thesis has been the development of an improved control system for the IM based on the DTC principle. The DTC principle entails the direct control of the stator flux by means of the stator voltage applied to the IM. The control of the electromagnetic torque is achieved by controlling the modulus and rotation of the stator flux vector.

The technology employed in variable speed motor drives is mainly based on the VSI, being the two-level version the standard solution. This type of power converter can only apply a discrete number of voltage levels to the motor terminals. Consequently, only a discrete number of voltage vectors can be delivered by the VSI and selected by the DTC algorithm to control the stator flux modulus and torque of the motor. Several solutions can be employed to overcome this technological limitation. Some of these solutions are the following:

1. Reducing the control sampling period, which is the solution adopted in commercial drives based on DTC.
2. Employing PWM, which is the approach adopted in many of the proposed modifications of DTC. The use of PWM allows the application of a voltage vector with the desired direction and amplitude in average during the PWM period.
3. Employing multilevel converters to exploit the increased number of voltage vectors that they can deliver and enhance the vector selection possibilities of the DTC algorithm.

It is the last possibility based on the use of a multilevel VSI which has been explored in this thesis and the outcome has resulted in the development of a new control system for the IM. The multilevel topology employed is the three-level NPC VSI.

The research work completed commenced with the study of the IM to gain the necessary understanding of its mathematical model and derive a simulation model. The space vector notation with a common reference frame is employed which considerably simplifies the mathematical description of the IM. Different reference frames can be used to express the IM model. The reference frame fixed to the stator flux vector is particularly convenient to understand the DTC principle and develop a control strategy based upon it.

The existing technology for multilevel converters and the advantages associated with them in comparison with the standard two-level VSI have also been studied. The three-level NPC VSI has been chosen to be incorporated into the new control system and it has been analysed in more detail. The problem of the NP balance inherent to this topology has been studied and taken into consideration in the design of the new control system. Finally the two-level VSI and the three-level VSI have been compared and it has been concluded that the use of the three-level VSI provides a reduction of the voltage and current distortion, the voltage derivatives and the CM voltage and currents. Moreover, the switching frequency of the semiconductor devices is reduced and the voltage level that they have to withstand is halved for the equal DC-link voltage. Consequently the stress and power losses in the semiconductor devices are lower. Regarding the DTC algorithm, the number of non-redundant voltage vectors that can be selected is increased from 7 in a two-level VSI to 19 in a three-level VSI.

At the same time, the DTC strategy has been studied in detail. The main drawbacks of this control strategy have been identified and can be summarized as follows:

1. Poor performance at low speed operation.
2. Slow start-up.
3. Stator flux and torque estimators are required.
4. The switching frequency is variable and produces a spread frequency spectrum in the stator voltages and currents.
5. High torque and stator flux ripples are generated.
6. The torque steady-state mean error is not null due to the discrete-time implementation and delays of the control system. This error increases with the speed.

7. The stator flux and currents are distorted due to the sector boundaries of the stator flux position. This effect is more accentuated when the angular speed of the stator flux vector is high.
8. Higher harmonic distortion is present in the stator voltage and current waveforms when compared to FOC (employing a similar switching frequency).
9. Large voltage transitions can appear in the stator voltages.
10. Acoustical noise is produced, particularly at low speed.

From the literature review of the proposed solutions to these problems it is apparent that the amount of research devoted to the combination of DTC with multilevel converters is considerable small.

Taking into consideration the study of the IM, the three-level VSI and the DTC strategy a new control system has been developed. In first place a literature review was completed to analyse in detail the existing systems which combine the three-level VSI or some other multilevel topology with the DTC principle. From this study it was concluded that the benefits of employing a three-level VSI can only be achieved at the expense of increasing the complexity of the control system. Another conclusion drawn is that the adoption of an approach based on hysteresis regulators and a look-up table seems to be inadequate. With this control structure it becomes very complex to establish the appropriate dimensions of the look-up table and the variables to be considered in order to exploit the potential of the three-level VSI. Moreover, it is difficult to tune hysteresis regulators with multiple levels. The possible alternative that has been adopted is the calculation of a reference voltage vector to be directly synthesized by choosing the nearest voltage vector available in the three-level VSI. In order to calculate the reference voltage vector the stator voltage equation has been studied for a better understanding of the DTC principle. A coordinate system fixed to the stator flux vector has been employed to express the stator voltage equation. It has been observed how the stator flux modulus and torque can be controlled by means of the radial and tangential components of the stator voltage respectively. It has been demonstrated how the BEMF term, which depends on the stator flux angular speed and the stator flux modulus, is present in the tangential component of the stator voltage equation and it strongly affects the torque production. The BEMF term explains the influence of the operating point on the torque response obtained with the Classical DTC method. Consequently it has been decided to incorporate the BEMF term in the reference voltage vector calculation to improve the torque response.

The reference voltage vector is calculated as follows:

- The stator flux modulus is controlled by means of the radial component of the stator voltage vector employing a deadbeat controller, which gives the required voltage to cancel the stator flux modulus error at the end of each sampling period.
- Torque is controlled by means of the tangential component of the stator voltage vector employing a combination of a proportional closed-loop control with a feed-forward control. The feed-forward action consists of two terms: the required voltage to produce the torque reference and the required voltage to compensate the BEMF term in steady-state conditions.

The reference voltage vector is then transformed to stator-fixed coordinates. The nearest voltage vector that can be delivered by the three-level VSI is then selected to be applied during the next sampling period.

The resulting control system has only one parameter to be tuned, which is the proportional gain of the torque control loop. An optimization method has been developed to tune this gain based on the reduction of the torque RMS error. Due to the simplicity of the optimization algorithm it can be easily integrated into the control system to be executed online providing an auto-tuning method.

A PI controller has been employed in the speed control loop. The output of the PI controller is used as the reference value for the torque control loop. The tuning of the PI parameters has been done by means of the SO criterion. In order to apply this method, the delay considered for the torque control loop is the equivalent armature time constant of the IM. The use of a smoothing filter for the speed reference is proposed in order to attenuate the characteristic overshoot of the SO criterion while the disturbance rejection capability is kept.

The proposed control system has also considered some other issues related to the three-level VSI. The redundancy of some of the switching combinations has been used to:

- Reduce the switching frequency of the semiconductor devices by choosing the most appropriate configuration of the zero vector, which implies the smallest number of commutations.
- Balance the NP voltage of the DC-link by choosing the most appropriate configuration for small vectors.

Medium vectors also produce the variation of the NP voltage but only one switching combination is associated with each one of them. The lack of redundancy might cause

the increase of the NP voltage unbalance depending on the current direction of the phase connected to the NP. If the voltage drift exceeds a certain level, their use can be restricted when the current direction tends to increase this drift. It has been observed that this situation is more likely to happen during torque transients and at high speed and torque operating points. In these situations current values can be higher and medium vectors are selected more frequently while small vectors are employed less, which makes the control of the NP voltage more difficult.

In order to analyse the resulting control system, it has been tested in simulation for steady-state and transient conditions. Comparative results with the Classical DTC system with a two-level VSI have been obtained. The proposed control system has also been tested experimentally. Despite some limitations of the experimental setup, the results obtained corroborate the validity of the proposed approach.

The characteristics of the new control system observed from the analysis of the results and the comparison with the Classical DTC method with a two-level VSI are presented in the following points:

- The stator flux modulus and torque are more precisely controlled. In steady-state operation the ripples and mean error are considerably reduced. The torque mean error is virtually eliminated without using integration, which is an essential requirement for applications where the speed is not controlled and only torque control is required. Regarding the torque response, it should be noted that the improvement achieved is particularly remarkable at low speed operation where the voltage level required is much lower. In these conditions the three-level VSI can deliver small and medium vectors which are closer to the voltage level required and consequently the torque ripple is considerably reduced.
- The characteristic fast torque response of DTC is kept. This is achieved because no integration of the torque error is employed in the control. Moreover the stator flux modulus can be controlled when the torque reference is zero providing a faster start-up.
- The stator flux distortion which takes place in the Classical DTC method, particularly when the stator flux angular speed is high, is eliminated. This distortion can also be observed in the stator currents. This effect is caused by the division of the stator flux position in sectors, which is avoided in the proposed control system.

- The speed control is also improved thanks to the improved torque control. This can be observed in the reduction of the speed oscillation in steady-state conditions.
- The stator voltages and currents present less harmonic distortion.
- The mean switching frequency of the semiconductor devices is also reduced, and they only withstand half of the DC-link voltage. Stress and power losses are therefore reduced. The switching frequency is still variable but the variation for different operating points is reduced. The biggest reduction of the mean switching frequency is achieved in the low range of the stator flux angular speed.
- The voltage derivatives due to the utilisation of a VSI are reduced thanks to the three-level topology. Voltage peaks at the motor terminals due to the inductance and capacitance of the cables are therefore reduced. The CM voltage and currents are reduced as well. The resulting control system is therefore less damaging for the motor windings insulation and bearings. Longer cables can be utilised and the cost and size of the output filters and other additional components, when required, is reduced.
- The issue of the NP balance inherent to the three-level NPC VSI is solved in the proposed system by selecting the appropriate switching configuration for small vectors. The minimisation of commutations is also achieved with the selection of the appropriate switching configuration for the zero vector.
- The stator resistance is the only motor parameter involved in the calculation of the reference voltage vector. This parameter is already involved in the stator flux and torque estimation. The mechanical speed or position is not required and the flux and torque control is therefore sensorless as in the Classical DTC method.
- The torque proportional gain is the only parameter that has to be tuned in the controller. A simple, quick and reliable tuning method is provided. The method is very suitable to perform an online auto-tuning.
- The calculation of the reference voltage vector is independent of the type of VSI employed. The only parts of the algorithm that depend on the type of VSI employed are: the selection of the nearest VSI vector available, the selection of the appropriate switching configuration among the redundant possibilities to satisfy certain requirements such as the minimisation of commutations or the NP balance in the NPC topology. The proposed controller is therefore suitable for different VSI topologies and can be easily adapted. This is not the case of the approach based on hysteresis

regulators and look-up table which has to be specifically designed for a certain VSI topology.

- The main disadvantage of the proposed control system is the increase in complexity. This is unavoidable due to the utilisation of the three-level VSI, which is inherently more complex in structure and hardware requirements. Regarding the control algorithm an example of this increase in complexity is the use of a coordinate transformation to convert the reference voltage vector in stator flux vector coordinates to stator-fixed coordinates. This transformation is not necessary in the Classical DTC method.

The novelty of the work presented in this thesis consists in the following contributions:

1. The proposed control system based on the DTC principle employing a three-level VSI instead of the standard two-level VSI, which is described in Chapter 5.
2. The tuning method employed for the torque proportional gain of the proposed controller. The method consists in a local search optimization technique based on the Hooke-Jeeves algorithm. The tuning method is presented in section 5.5.
3. The tuning method employed for the speed PI controller employing the SO criterion, which is described in section 5.8. This method has been adapted to the proposed controller and can be applied to the Classical DTC strategy as well.

7.2 Suggestions for further research

From the work presented in this thesis some future lines of work can be suggested as a possible continuation.

The performance and validity of the proposed controller, which is the main contribution of the thesis, can be investigated for different types of electrical motor such as the Synchronous Motor (SM). In SMs the rotor flux is generated independently by constructing the rotor with an electrically excited winding or alternatively a Permanent Magnet (PM). In the second case the resulting motor is the PMSM. In this type of motors the rotating speed of the rotor is equal to the frequency of the supply voltage divided by the number of pole pairs. The IM is nowadays dominating the drive market and has substituted the DC motor in high performance applications where variable speed and torque control is needed. Nevertheless, the PMSM is gaining market since the introduction of new materials like neodymium-iron-boron (NdFeB) for the PM in 1983, which provide better magnetic properties. The main advantages of the PMSM are:

- No brushes and slip rings are required, reducing the maintenance.

- Inertia is lower and better dynamic performance is achieved.
- Efficiency is higher. There are no rotor losses.
- The power/weight ratio is higher.

These merits are counterbalanced by the higher cost and the variation of the PM properties during time and with temperature. PMSMs are currently employed in applications where high acceleration and precise control is required such as robotics and machine tools. PMSMs can be classified, according to how the PMs are mounted in the rotor, in Interior PMSMs (IPMSMs) and Surface Mounted PMSMs (SMPMSMs). In the second case the rotor saliency is reduced.

Similarly to the IM, the control of the PMSM is not a trivial matter when compared to the control of the DC motor. The FOC method has been successfully applied to PMSM drives in the past [91]. More recently DTC has also been adopted for the control of the PMSM and it was first reported by Zhong and Rahman in 1997 [95]. In the control scheme presented in [95], unlike the Classical DTC method for IMs, the hysteresis regulator for torque has two levels and the resulting look-up table is simplified and does not employ zero vectors. This detail of the control scheme has been corrected by other authors afterwards [96, 97], which have adopted the DTC scheme for IM as defined in [6]. The main reason is that the utilisation of zero vectors reduces the torque ripple, particularly at low speed. A comparison between FOC and DTC methods for PMSMs is presented in [98] to conclude that, similarly to the results obtained with the IM, FOC provides a better steady-state behaviour while DTC can achieve a faster torque response. However the successful application of the DTC method presents more difficulties when using the PMSM instead of the IM. The special features associated to the PMSM that need to be taken into account are the following:

- The inductances and electrical time constant of the PMSM are considerably smaller in comparison with the IM. Current rise is therefore much quicker leading to higher current, flux and torque ripples. Moreover the ratio of nominal stator flux to DC-link voltage is generally much lower in PMSMs than in IMs. A small sampling period is therefore necessary to achieve an acceptable level of ripple.
- The rotor flux has a constant component which is the PM flux. It is not necessary to create a rotor flux like in the IM in order to produce torque. Moreover the knowledge of the initial position of the rotor is necessary to know the initial value of the stator flux.

- The flux generated by the stator currents in the direction of the PM flux can affect the PM properties. In case of decreasing it, the demagnetization of the PM may occur, which is not desirable. For speeds above the nominal value if flux weakening is employed this effect is produced.

After the introduction of DTC for the PMSM the research carried out and reported in the literature has followed several lines of work:

1. **Sensorless implementation.** Some authors have concentrated on the sensorless implementation of the control. In [99] the stator flux and the torque angle are employed to estimate the speed of the IPMSM, while in [100] the use of high frequency injection to estimate the initial position is proposed. The Extended Kalman Filter (EKF) has been used in [101] to estimate the rotor position, speed, stator flux and torque.
2. **Stator resistance estimation.** The variation and correction of the stator resistance value employed in the stator flux estimator is a problem addressed in [102].
3. **Optimal flux reference.** The selection of the optimal flux reference is studied in order to minimise losses and currents in [103] and [104]. Operation above the nominal speed in the field weakening region is studied in [105] and [106].
4. **Modified control schemes.** Several modifications of the DTC control scheme have been presented to overcome the DTC drawbacks. These methods can summarised as follows:
   a. **Variable structure control.** A variable structure control is presented in [107]. SVM is employed to generate the voltage vector to be applied to the motor.
   b. **Predictive controller.** In [108] an optimum vector is calculated for quick transient responses and fast start-up. The optimum vector is then synthesized by means of SVM. Several authors present similar schemes where the optimum voltage vector is calculated and generated by means of SVM [109-111].
   c. **Virtual voltage vectors.** In [112] the authors increment the number of voltage vectors available in the VSI by adding some virtual vectors. These virtual vectors are synthesized by means of fixed modulation patterns between the existing active and null vectors. In the new control scheme the number of levels of the hysteresis regulators and the size of the look-up table are both increased.
   d. **Fuzzy logic controller.** The DTC controller is replaced by a Fuzzy logic controller in [113] and SVM has also been incorporated into the control.

The approach based on using multilevel converter topologies and DTC for PMSM drives has not been reported in literature, as far as known, except in [114]. In this paper the authors claim to be the first to investigate the use of DTC and the three-level NPC VSI topology for the control of the PMSM. The control scheme presented contains four-level hysteresis regulators for the stator flux and torque variables, and a new look-up table where only large and small vectors are employed. The balance of the NP voltage is kept by selecting the appropriate small vector configuration. The results presented show a reduction of the stator flux and torque ripples. The distortion in the voltage and current waveforms is also reduced. The results presented in [114] suggest that further work could be done in this direction by testing the control system presented in this thesis with the PMSM. As explained before, the smaller electrical time constant of the PMSM in comparison with the IM leads to very high torque ripple. It is apparent that the increased number of voltage vectors available in the three-level VSI enhances the vector selection possibilities and the torque ripple can be reduced.

A different line of work that can be investigated is the use of the proposed controller with different converter topologies such as: the two-level VSI, multilevel converters with more than three levels and matrix converters. Furthermore, some modifications in the control scheme can be added to improve the performance of the control system. One possibility is to incorporate modulation techniques, such as SVM, to synthesize the reference voltage vector calculated by the controller instead of selecting the nearest voltage vector available. Specific SVM algorithms for multilevel converters must be employed in this case [23, 26].

Finally, one last suggestion for further work can be the implementation of the proposed controller in a specific application such as an electric vehicle [52, 84]. The features of the new control system described in this thesis seem to offer a suitable solution for this type of application. This potential is mainly due to the fast and precise torque control achieved, together with the reduced distortion in the voltage and current waveforms and the low switching frequency of the semiconductor devices.

To conclude, it can be said that the DTC method steps into the 21st century as one of the best alternatives for high performance speed and torque control of IMs. Moreover, the DTC principle can be successfully extended to other types of electrical motors. The new control system presented in this thesis has combined the advantages of the DTC method and the three-level VSI. It is believed that the resulting solution leads to a good trade-

off between different requirements of a variable speed drive and further developments can follow this direction.

References

[1] I. Boldea and S. A. Nasar, "The induction motor machine handbook." CRC Press. 2002.

[2] T. Harder, et al., "Position Paper on Energy Efficiency - The Role of Power Electronics." EPE/ECPE European Workshop "Energy Efficiency in FP7? The Role of Power Electronics", <http://www.ecpe.org/download/power_electronic/Position_Paper_Energy_Efficiency.pdf>, May 2007.

[3] H. Shah, "Strong Growth Forecast for Both High and Low Power AC Drives Market." ARC Advisory Group, Press Center, <http://www.arcweb.com/txtlstvw.aspx?LstID=5eaeacfe-2050-426a-bb7d-48efe7c41b38>, 14 June 2007.

[4] K. Hasse, "Drehzahlgelverfahren für schnelle umkehrantriebe mit stromrichtergespeisten asynchron-kurzschlusslaufer-motoren." Reglungstechnik, vol 20, pp. 60-66, 1972.

[5] F. Blaschke, "The principle of field-orientation as applied to the transvector closed-loop control system for rotating-field machines." Siemens Rev., vol 34, pp. 217-220, 1972.

[6] I. Takahashi and T. Noguchi, "A new quick-response and high-efficiency control strategy of an induction motor." *IEEE Trans. on Ind. Appl.*, vol IA-22, no 5, pp. 820-827, September/October 1986.

[7] M. Depenbrock, "Direct Self-Control (DSC) of Inverter-Fed Induction Machine." *IEEE Trans. on Power Elec.*, vol 3, no 4, pp. 420-429, 1988.

[8] *"Direct Torque Control - the world's most advanced AC drive technology".* Technical guide no. 1. ABB, 1999.

[9] M. Aaltonen, P. Tiitinen, J. Lalu, and S. Heikkila, "Direct torque control of AC motor drives." The Plant Engineer, pp. 21-25, September/October 1995.

[10] P. Tiitinen and M. Surandra. "The Next Generation Motor Control Method, DTC Direct Torque Control." in Proc. International Conference on Power Electronics, Drives and Energy Systems for Industrial Growth 1996, 8-11 Jan 1996, pp. 37-43.

[11] J. Nash, "Direct Torque Control, Induction Motor Vector Control without an Encoder." *IEEE Trans. on Ind. Appl.*, vol 33, no 2, pp. 333-341, March/April 1997.

[12] G. Buja and M. P. Kazmierkowski, "Direct Torque Control of PWM Inverter-Fed AC Motors—A Survey." *IEEE Trans. on Ind. Elec.*, vol 51, no 4, pp. 744-757, August 2004.

[13] P. Vas, "Sensor-less and Direct Torque Control." Oxford University Press. 1998.

[14] I. Boldea and S. A. Nasar, "Electric Drives." CRC Press. 1999.

[15] J. Rodriguez, J. Lai, and F. Z. Peng, "Multilevel Inverters: A Survey of Topologies, Controls, and Applications." *IEEE Trans. on Ind. Elec.*, vol 49, no 4, pp. 724-738, August 2002.

[16] R. Teodorescu, et al. "Multilevel Converters - A Survey." in Proc. EPE Conference EPE99, September 1999, Lausanne, Switzerland, pp. 2-11.

[17] P. Vas, "Electrical machines and drives: a space-vector theory approach." Oxford University Press. 1992.

[18] I. Ludtke, "The Direct Torque Control of Induction Motors." PhD Thesis. University of Glamorgan, Pontypridd, UK. 1998.

[19] N. Mohan, T. M. Undeland, and W. P. Robbins, "Power Electronics: Converters, Applications and Design." John Wiley & Sons Inc. 1994.

[20] P. W. Wheeler, J. Rodriguez, J. C. Clare, L. Empringham, and A. Weinstein, "Matrix converters: a technology review." *IEEE Trans. on Ind. Elec.*, vol 49, no 2, pp. 276-288, April 2002.

[21] R. Sul, B. Dobrucky, and R. Ovcarcic, "New Possibilities of Power Electronic Structures Using SiC Technology." *Advances in Electrical and Electronic Engineering, Faculty of Electrical Engineering, University of Zilina, Slovakia*, vol 5/2006, no 1-2, pp. 64-67,

[22] C. A. Martins, T. A. Meynard, X. Roboam, and A. S. Carvalho, "A predictive sampling scale model for Direct Torque Control of the induction machine fed by multilevel voltage-source inverter." *The European Physical Journal Applied Physics*, vol 5, no 1, pp. 51-61, 1999.

[23] J. Pou, "Modulation and Control of Three-Phase PWM Multilevel Converters." PhD Thesis. Universitat Politècnica de Catalunya, Terrassa, Spain. 2002. <http://www.tesisenxarxa.net/TDX-0921104-155059/>.

[24] B. A. Welchko, M. Corrêa, and T. A. Lipo, "A Three-Level MOSFET Inverter for Low-Power Drives." *IEEE Trans. on Ind. Elec.*, vol 51, no 3, pp. 669-674, June 2004.

[25] Yaskawa Electric Inc., "Yaskawa G7 AC Drive the World's First 480V 3-level Inverter." Application Note AN.G7.01, <http://www.yaskawa.com>, 22 June 2005 (Rev. 05-06).

[26] N. Celanovic, "Space Vector Modulation and Control of Multilevel Converters." PhD Thesis. Faculty of the Virginia Polytechnic and State University, Blacksburg, Virginia, USA. 2000. <http://scholar.lib.vt.edu/theses/available/etd-10022000-00180032/unrestricted/dissertation.pdf>.

[27] B. Suh, G. Sinha, M. D. Manjrekar, and T. A. Lipo. "Multilevel Power Conversion - an Overview of Topologies and Modulation Strategies." in Proc. 6th International Conference on Optimization of Electrical and Electronic Equipments OPTIM98, 14-15 May 1998, Brasov, Romania, pp. AD11-AD24.

[28] A. Nabae, I. Takahashi, and H. Akagi, "A new neutral-point-clamped PWM inverter." *IEEE Trans. on Ind. Appl.*, vol IA-17, no 5, pp. 518-523, September/October 1981.

[29] T. A. Meynard and H. Foch. "Multi-Level Conversion: High Voltage Choppers and Voltage-Source Inverters." in Proc. IEEE Power Electronics Specialists Conference PESC92, June-July 1992, Toledo, Spain, pp. 397-403.

[30] M. D. Manjrekar, P. K. Steimer, and T. A. Lipo, "Hybrid Multilevel Power Conversion System: A Competitive Solution for High-Power Applications." *IEEE Trans. on Ind. Appl.*, vol 36, no 3, pp. 834-841, May/June 2000.

[31] Yaskawa Electric Inc., "Motor Bearing Current Phenomenon and 3-Level Inverter Technology." Application Note AN.G7.02, <http://www.yaskawa.com>, 22 June 2005 (Rev. 05-06).

[32] Yaskawa Electric Inc., "Drives for Industrial Automation." Catalog CA.G7.01. G7, <http://www.yaskawa.com>, 15 March 2007.

[33] K. Yamanaka, A. M. Hava, H. Kirino, Y. Tanaka, N. Koga, and T. Kume, "A Novel Neutral Point Potential Stabilization Technique Using the Information of Output Current Polarities and Voltage Vector." *IEEE Trans. on Ind. Appl.*, vol 38, no 6, pp. 1572-1580, November/December 2002.

[34] P. Lataire, "White paper on the new ABB medium voltage drive system, using IGCT power semiconductors and Direct Torque Control." *EPE Journal*, vol 7, no 3-4, pp. 40-45, December 1998.

[35] "*ACS 1000 Medium Voltage AC Drives for speed and torque control of 315 to 5000 kW / 400 to 6700 hp squirrel cage induction motors*". Technical Catalogue. ABB Industrie AG, 2000.

[36] S. Malik and D. Kluge, "*ACS 1000 - world's first standard AC drive for medium-voltage applications*". ABB Review 2/1998. pp. 1-11.

[37] Z. Tan, Y. Li, and M. Li. "A direct torque control of induction motor based on three-level NPC inverter." in Proc. IEEE Power Electronics Specialists Conference PESC01, June 2001, Vancouver, Canada, pp. 1435-1439.

[38] S. Busquest-Monge, J. Bordonau, D. Boroyevich, and S. Somavilla, "The Nearest Three Virtual Space Vector PWM—A Modulation for the Comprehensive Neutral-Point Balancing in the Three-Level NPC Inverter." *IEEE Power Electronics Letters*, vol 2, no 1, March 2004.

[39] G. Brando, A. Del Pizzo, S. Nocerino, and R. Rizzo. "Direct Torque Control with Variable Duty-Cycle in Induction Motor Drives using 3-Level Inverters." in Proc. IEEE 29th International Conference on Industrial Electronics IECON03, November 2003, Roanoke, Virginia, USA, pp. 306-311.

[40] V. Perelmuter. "Three-Level Inverters with Direct Torque Control." in Proc. IEEE Industry Applications Conference, October 2000, Rome, Italy, pp. 1368-1374.

[41] A. Sapin, P. K. Steimer, and J. Simond. "Modelling, Simulation and Test of a Three-level Voltage Source Inverter with Output LC Filter and Direct Torque Control." in Proc. IEEE IAS Annual Meeting 2003, October 2003, Salt Lake City, USA, pp. 492-498.

[42] M. Cirrincione, M. Pucci, G. Vitale, and G. Cirrincione, "A New Direct Torque Control Strategy for the Minimization of Common-Mode Emissions." *IEEE Trans. on Ind. Appl.*, vol 42, no 2, pp. 504-517, March/April 2006.

[43] A. BenAbdelghani, C. A. Martins, X. Roboam, and T. A. Meynard, "Use of Extra Degrees of Freedom in Multilevel Drives." *IEEE Trans. on Ind. Elec.*, vol 49, no 5, pp. 965-977, October 2002.

[44] M. Depenbrock, "Direct self-control of the flux and rotary moment of a rotary-field machine." U.S. Patent 4678248, 7th July 1987, <http://www.pat2pdf.org/patents/pat5734249.pdf>.

[45] P. Pohjalainen and C. Stulz, "Method and Apparatus for Direct Torque Control of a Three-phase Machine." U.S. Patent 5734249, 31st March 1998, <http://www.pat2pdf.org/patents/pat5734249.pdf>.

[46] P. Z. Grabowski, "Direct Flux and Torque Neuro-Fuzzy Control of Inverter Fed Induction Motor Drives." PhD Thesis. Politechnika Warszawska, Warsaw University of Technology, Warsaw, Poland. 1999.

[47] S. A. Mir, M. E. Elbuluk, and D. S. Zinger, "PI and Fuzzy Estimators for Tuning the Stator Resistance in Direct Torque Control of Induction Machines." *IEEE Trans. on Power Elec.*, vol 13, no 2, pp. 279 - 287, Mar 1998.

[48] A. Arias, "Improvements in Direct Torque Control of Induction Motors." PhD Thesis. Universitat Politècnica de Catalunya, Terrassa, Spain. 2001. <http://www.tesisenxarxa.net/TDX-0724101-144636/>.

[49] K.-B. Lee, J.-H. Song, I. Choy, and J.-Y. Yoo, "Improvement of Low-Speed Operation Performance of DTC for Three-Level Inverter-Fed Induction Motors." *IEEE Trans. on Ind. Elec.*, vol 48, no 5, pp. 1006-1014, October 2001.

[50] P. Vas, "Artificial-intelligence-based electrical machines and drives. Application of fuzzy, neural, fuzzy-neural, and genetic-algorithm-based techniques." Oxford University Press. 1999.

[51] D. Casadei, G. Serra, and A. Tani, "FOC and DTC: Two Viable Schemes for Induction Motors Torque Control." *IEEE Trans. on Power Elec.*, vol 17, no 5, pp. 779-787, September 2002.

[52] J. C. Trounce, S. D. Round, and R. M. Duke. "Comparison by Simulation of Three-Level Induction Motor Torque Control Schemes for Electric Vehicle Applications." in Proc. International Power Engineering Conference, May 2001, Singapore, pp. 294-299.

[53] C. Lascu, I. Boldea, and F. Blaabjerg, "Variable-Structure Direct Torque Control - A Class of Fast and Robust Controllers for Induction Machine Drives." *IEEE Trans. on Ind. Elec.*, vol 51, no 4, pp. 785-792, August 2004.

[54] G. Buja, D. Casadei, and G. Serra. "DTC-Based Strategies for Induction Motor Drives." in Proc. IEEE 23rd International Conference on Industrial Electronics IECON97, November 1997, New Orleans, USA, pp. 1506-1516.

[55] I. Ludtke and M. G. Jayne. "Direct Torque Control of Induction Motors." in Proc. IEE Colloquium on Vector Control and Direct Torque Control of Induction Motors, October 1995, London, UK, pp. 1-6.

[56] D. Casadei, G. Serra, and A. Tani. "Improvement of Direct Torque Control Performance by using a Discrete SVM Technique." in Proc. IEEE Power

Electronics Specialists Conference PESC98, May 1998, Fukukoa, Japan, pp. 997-1003.

[57] D. Casadei, G. Serra, and A. Tani, "Implementation of a Direct Torque Control Algorithm for Induction Motors Based on Discrete Space Vector Modulation." *IEEE Trans. on Power Elec.*, vol 15, no 4, pp. 769-777, July 2000.

[58] M. P. Kazmierkowski and A. Kasprowicz, "Improved Direct Torque and Flux Vector Control of PWM Inverter-Fed Induction Motor Drives." *IEEE Trans. on Ind. Elec.*, vol 42, no 4, pp. 344-350, August 1995.

[59] G. Habetler, F. Profumo, M. Pastorelli, and L. Tolbert, "Direct Torque Control of Induction Machines Using Space Vector Modulation." *IEEE Trans. on Ind. Appl.*, vol 28, no 5, pp. 1045-1053, September/October 1992.

[60] M. Zelechowski, M. P. Kazmierkowski, and F. Blaabjerg. "Controller Design for Direct Torque Controlled Space Vector Modulated (DTC-SVM) Induction Motor Drives." in Proc. IEEE International Symposium on Industrial Electronics ISIE05, 20-23 June 2005, Dubrovnik, Croatia, pp. 951-956.

[61] Y.-S. Lai and J.-H. Chen, "A New Approach to Direct Torque Control of Induction Motor Drives for Constant Inverter Switching Frequency and Torque Ripple Reduction." *IEEE Trans. on Energy Conversion*, vol 16, no 3, pp. 220-227, September 2001.

[62] J. Kang and S. Sul, "New Direct Torque Control of Induction Motor for Minimum Torque Ripple and Constant Switching Frequency." *IEEE Trans. on Ind. Appl.*, vol 35, no 5, pp. 1076-1082, September/October 1999.

[63] I. G. Bird and H. Zelaya, "Fuzzy logic torque ripple reduction for DTC based AC drives." *IEE Electronics Letters*, vol 33, no 17, August 1997.

[64] A. Arias, L. Romeral, E. Aldabas, and M. G. Jayne, "Improving Direct Torque Control by means of fuzzy logic." *IEE Electronics Letters*, vol 37, no 1, January 2001.

[65] I. Takahashi and Y. Ohmori, "High-performance direct torque control of an induction motor." *IEEE Trans. on Ind. Appl.*, vol 25, no 2, pp. 257-264, March/April 1989.

[66] D. Casadei, G. Serra, and A. Tani, "The Use of Matrix Converters in Direct Torque Control of Induction Machines." *IEEE Trans. on Ind. Elec.*, vol 48, no 6, pp. 1057-1064, December 2001.

[67] C. Ortega, A. Arias, X. del Toro Garcia, J. L. Romeral, and E. Aldabas. "Direct Torque Control for Induction Motors Using small voltage vectors of Matrix Converters." in Proc. 31st International Conference on Industrial Electronics IECON05, November 2005, Raleigh, USA, pp. 1353-1358.

[68] M. Azab, "Estudio y realización del control directo del par (DTC) para accionamientos de motores de inducción con inversores de diferentes topologías." PhD Thesis. Universitat Politecnica de Catalunya, Barcelona, Spain. 2002.

[69] B. K. Bose, "Fuzzy Logic and Neural Network Applications in Power Electronics." *IEEE Industrial Electronics Society Newsletter*, vol 50, no 2-3, pp. 6-13, June 2003.

[70] S. A. Mir, D. S. Zinger, and M. E. Elbuluk, "Fuzzy Controller for Inverter Fed Induction Machines." *IEEE Trans. on Ind. Appl.*, vol 30, no 1, pp. 78-84, January/February 1994.

[71] P. Ponce and J. C. Ramirez. "Fuzzy logic controller based on space vector modulation for induction motor control." in Proc. IEEE International Symposium on Industrial Electronics ISIE04, June 2004, Ajaccio, France, pp. 1285- 1290.

[72] X. Wu and L. Huang. "Direct Torque Control of Three-level Inverter Using Neural Networks as a Switching Vector Selection." in Proc. IEEE IEEE Industry Applications Conference IAS01, 30th Sept - 4th Oct 2001, Chicago, USA, pp. 939-944.

[73] G. Sowilan, "Application of Neural Networks on vector control systems of induction motors." PhD Thesis. Universitat Politecnica de Catalunya, Barcelona, Spain. 2000.

[74] P. Z. Grabowski, M. P. Kazmierkowski, B. K. Bose, and F. Blaabjerg, "A Simple Direct-Torque Neuro-Fuzzy Control of PWM-Inverter-Fed Induction Motor Drive." *IEEE Trans. on Ind. Elec.*, vol 47, no 4, pp. 863-870, August 2000.

[75] X. Wang and M. E. Elbuluk. "Neural Network control of Induction machines using genetic algorithm training." in Proc. IEEE Industry Applications Conference IAS96, 6-10 Oct 1996, San Diego, USA, pp. 1733-1740.

[76] H.-P. Pham and H. Le-Huy. "Direct torque control with switching frequency limitation for three-level inverter-fed induction motors." in Proc. 29th International Conference on Industrial Electronics IECON03, 2-6 Nov. 2003, Roanoke, Virginia, USA, pp. 2783 - 2788.

[77] M. Cirrincione, M. Pucci, and G. Vitale. "A novel direct torque control of an induction motor drive with a three-level inverter." in Proc. IEEE Power Tech Conference 2003, 23-26 June 2003, Bologna, Italy, pp. 7.

[78] J. K. Steinke and P. K. Steimer. "Medium Voltage Drive Converter for Industrial Applications in the Power Range from 0.5 MW to 5 MW based on a three-level Converter equipped with IGCTs." in Proc. IEE Seminar on PWM Medium Voltage Drives 2000, May 2000, Birmingham, UK, pp. 6/1-6/4.

[79] X. Hu and L. Zhang. "A Predictive Direct Torque Control Scheme for a Three-Level VSI-Fed Induction Motor Drive." in Proc. IEE 9th International Conference on Electrical Machines and Drives, September 1999, Canterbury, UK, pp. 334-338.

[80] M. A. Martín, G. Escobar, E. Galván, J. M. Carrasco, and R. Portillo, "A Switching Control Strategy Based on Output Regulation Subspaces for the Control of Induction Motors Using a Three-Level Inverter." *IEEE Power Electronics Letters*, vol 1, no 2, pp. 29-32, June 2003.

[81] K.-B. Lee, J.-H. Song, I. Choy, and J.-Y. Yoo, "Torque Ripple Reduction in DTC of Induction Motor Driven by Three-Level Inverter With Low Switching Frequency." *IEEE Trans. on Power Elec.*, vol 17, no 2, pp. 255-264, March 2002.

[82] G. Brando and R. Rizzo. "An Optimized Algorithm for Torque Oscillation Reduction in DTC-Induction Motor Drives using 3-Level NPC Inverter." in Proc. IEEE International Symposium on Industrial Electronics ISIE04, June 2004, Ajaccio, France, pp. 1215-1220.

[83] G. Brando, A. D. Pizzo, and R. Rizzo. "Three Level Rectifier versus Three Level Inverter with DTC controlled Induction Motor." in Proc. The Fifth International Conference on Power Electronics and Drive Systems PEDS03, 17-20 Nov. 2003, Singapore, pp. 1286 - 1290.

[84] J. C. Trounce, S. D. Round, and R. M. Duke. "Evaluation of Direct Torque Control Using Space Vector Modulation for Electric Vehicle Applications." in Proc. Australasian Universities Power Engineering Conference, September 2001, Perth, Australia, pp. 292-297.

[85] R. Hooke and T. A. Jeeves, "Direct search solution of numerical and statistical problems." *Journal of the ACM*, vol 8, pp. 212-229, March 1961.

[86] Kessler, "Das symmetrische Optimum, Teil I." *Regelungstechnik*, vol 6:11, pp. 395-400, 1958.

[87] Kessler, "Das symmetrische Optimum, Teil II." *Regelungstechnik*, vol 6:12, pp. 432-436, 1958.

[88] H. Gross, J. Hamann, and G. Wiegärtner, "Electrical Feed Drives in Automation." Siemens. Publicis MCD Corporate Publishing. 2001.

[89] W. Leonhard, "Control of Electrical Drives." Springer. 1996.

[90] A. Terlizzi, X. del Toro Garcia, B. Zigmund, R. Pavlanin, and L. Salvatore, "Experimental Evaluation of PI Tuning Techniques for Field Oriented Control of Permanent Magnet Synchronous Motors." *Advances in Electrical and Electronic Engineering, Faculty of Electrical Engineering, University of Zilina, Slovakia*, vol 5/2006, no 1-2, pp. 114-119, May 2006.

[91] R. Krishnan, "Electric Motor Drives. Modelling, analysis and control." Prentice Hall. 2001.

[92] D. Saltiveri, "Manual de puesta en marcha y funcionamiento del sistema dSPACE v2.0." Department of Electronic Engineering, Universitat Politècnica de Catalunya, Terrassa, Spain. 2004.

[93] G. López, *"Disseny d'una placa de control i adaptacio de senyals per a un inversor trinivell NPC"*. Final year project. Departament d'Enginyeria Electrònica, Universitat Politècnica de Catalunya, Terrassa, Spain, 2004.

[94] H. Lama, *"Puesta a punto de placa de control y adaptación de señales para un inversor de tres niveles"*. Final Year Project. Departament d'Enginyeria Electrònica, Universitat Politècnica de Catalunya, Terrassa, Spain, 2004.

[95] L. Zhong, M. F. Rahman, W. Y. Hu, and K. W. Lim, "Analysis of Direct Torque Control in Permanent Magnet Synchronous Motor Drives." *IEEE Trans. on Power Elec.*, vol 12, no 3, pp. 528-536, May 1997.

[96] J. Luukko, "Direct torque control of permanent magnet synchronous machines – analysis and implementation." PhD Thesis. Lappeenranta University of Technology, 2000.

[97] Y. Hu, C. Tian, Y. Gu, Z. You, L.X. Tang, and M.F. Rahman. "In-depth Research on Direct Torque Control of Permanent Magnet Synchronous Motor." in Proc. 28th International Conference on Industrial Electronics IECON02, 5-8 Nov. 2002, Sevilla, Spain, pp. 1060-1065.

[98] X. del Toro Garcia, B. Zigmund, A. Terlizzi, R. Pavlanin, and L. Salvatore, "Comparison between FOC and DTC Strategies for Permanent Magnet Synchronous Motors." *Advances in Electrical and Electronic Engineering, Faculty*

of Electrical Engineering, University of Zilina, Slovakia, vol 5, no 1-2, pp. 76-81, May 2006.

[99] M. F. Rahman, L. Zhong, M. E. Haque, and M. A. Rahman, "A Direct Torque-Controlled Interior Permanent-Magnet Synchronous Motor Drive Without a Speed Sensor." *IEEE Trans. on Energy Conversion*, vol 18, no 1, pp. 17-22, March 2003.

[100] M. E. Haque, L. Zhong, and M. F. Rahman, "A Sensorless Initial Rotor Position Estimation Scheme for a Direct Torque Controlled Interior Permanent Magnet Synchronous Motor Drive." *IEEE Trans. on Power Elec.*, vol 18, no 6, pp. 1376-1383, November 2003.

[101] Z. Xu and M. F. Rahman. "An Extended Kalman Filter Observer for the Direct Torque Controlled Interior Permanent Magnet Synchronous Motor Drive." in Proc. Fifth International Conference on Power Electronics and Drive Systems PEDS03, 17-20 Nov. 2003, Singapore, pp. 686-691.

[102] T. Tang, M. F. Rahman, and M. E. Haque. "Low Speed Performance Improvement of a Direct Torque Controlled Interior Permanent Magnet Synchronous Machine Drive." in Proc. Nineteenth Annual IEEE Applied Power Electronics Conference and Exposition APEC04, 22-26 Feb. 2004, Anaheim, USA, pp. 558- 564.

[103] J. Luukko and J. Pyrhonen. "Selection of the Flux Linkage Reference in a Direct Torque Controlled Permanent Magnet Synchronous Motor Drive." in Proc. 5th International Workshop on Advanced Motion Control, AMC98, 29 Jun-1Jul 1998, Coimbra, Portugal, pp. 198-203.

[104] C. Tian, H. Li, and Y. Hu. "A Novel Scheme of Direct Torque Control in the Permanent Magnet Synchronous Motor Drive." in Proc. IEEE Workshop on Power Electronics in Transportation 2002, 24-25 October 2002, Auburn Hills, Michigan, USA, pp. 47-52.

[105] M. F. Rahman, L. Zhong, and K. W. Lim, "A Direct Torque-Controlled Interior Permanent Magnet Synchronous Motor Drive Incorporating Field Weakening." *IEEE Trans. on Ind. Appl.*, vol 34, no 6, pp. 1246-1253, November/December 1998.

[106] M. Zordan, P. Vas, M. Rashed, S. Bolognani, and M. Zigliotto. "Field-Weakening in Vector Controlled and DTC PMSM Drives, A Comparative Analysis." in Proc. IEE 8th International Conference on Power Electronics and Variable Speed Drives 2000, 18-19 September 2000, London, UK, pp. 493-499.

[107] Z. Xu and M. F. Rahman. "Direct Torque and Flux Regulation of an IPM Synchronous Motor Drive Using Variable Structure Control Approach." in Proc. 30th International Conference on Industrial Electronics IECON04, 2-6 November 2004, Busan, Korea, pp. 2733-2738.

[108] H. Ghasemi and S. Vaez-Zadeh. "A Very Fast Direct Torque Control for Permanent Magnet Synchronous Motors Start up." in Proc. Canadian Conference on Electrical and Computer Engineering, 2004, 2-5 May 2004, Niagara Falls, Canada, pp. 1673-1677.

[109] L. Tang, L. Zhong, M. F. Rahman, and Y. Hu, "A Novel Direct Torque Controlled Interior Permanent Magnet Synchronous Machine Drive with Low Ripple in Flux and Torque and Fixed Switching Frequency." *IEEE Trans. on Power Elec.*, vol 19, no 2, pp. 346-354, March 2004.

[110] D. Swierczynski and M. P. Kazmierkowski. "Direct Torque control of Permanent Magnet Synchronous Motor (PMSM) using Space Vector Modulation (DTC-SVM) - Simulation and Experimental Results." in Proc. IEEE 2002 28th Annual Conference of the Industrial Electronics Society IECON02, 5-8 Nov. 2002, pp. 751-755.

[111] D. Sun, J. G. Zhu, and Y. K. He. "A Space Vector Modulation Direct Torque Control for Permanent Magnet Synchronous Motor Drive Systems." in Proc. Fifth International Conference on Power Electronics and Drive Systems PEDS 2003, 17-20 Nov. 2003, Singapore, pp. 692-697.

[112] L. Li, H. Sun, X. Wang, and Y. Tian. "A High-Performance Direct Torque Control Based on DSP in Permanent Magnet Synchronous Motor Drive." in Proc. 4th World Congress on Intelligent Control and Automation 2002, Shangai, China, pp. 1622-1625.

[113] M. Jin, J. Qiu, C. Shi, and R. Lin. "A Fuzzy DTC Method with a SVM Defuzzification to Permanent Magnet Synchronous Machine." in Proc. 30th Annual Conference of IEEE Industrial Electronics Society IECON 2004, 2-6 Nov. 2004, Busan, Korea, pp. 3196-3199.

[114] K. E. B. Quindere, E. Ruppert, and M. E. de Oliveira. "A Three-Level Inverter Direct Torque Control of a Permanent Magnet Synchronous Motor." in Proc. IEEE International Symposium on Industrial Electronics, ISIE06, 9-12 July 2006, Montreal, Canada, pp. 2361-2366.

Appendix A: Optimization algorithm

```
% Optimization algorithm for Matlab to tune Kte (based on the Hooke-Jeeves algorithm).
clear all;
Siemens; Tsimstop=9; % Load system parameters and Simulation time
Fluxsp=1; wm0=0; % Initialize stator flux reference and motor initial speed
% Initialize the algorithm
h=16; % Initial exploratory radius
Kc=0; Kte=Kc; % Initial solution
nev=0; %Initialize the number of evaluations
% Ending conditions
hmin=1; budget=100;
sim('pdtc3l_imxOptim'); % Fitness evaluation of the initial solution
fc=norm(Teref-Te)/sqrt(length(Teref)); % Torque RMS error calculation
nev=nev+1; % Increment the number of evaluations
hist=[Kc,fc,h,nev]; % Save the evolution of the algorithm
% Start by checking the ending conditions
while h>=hmin && nev<budget
   % Exploratory move
   Ku=Kc+h; Kte=Ku;
   sim('pdtc3l_imxOptim'); % Fitness evaluation
   nev=nev+1;
   fu=norm(Teref-Te)/sqrt(length(Teref)); % Torque RMS error calculation
   Kl=Kc-h; Kte=Kl;
   sim('pdtc3l_imxOptim'); % Fitness evaluation
   nev=nev+1;
   fl=norm(Teref-Te)/sqrt(length(Teref)); % Torque RMS error calculation
   fmin=min([fc,fu,fl]); % Best solution
   % Pattern move
   if fc==fmin
      h=h/2;
   elseif fu==fmin
      Kf=Kc+2*h; Kte=Kf;
      sim('pdtc3l_imxOptim'); % Fitness evaluation
      nev=nev+1;
      ff=norm(Teref-Te)/sqrt(length(Teref)); % Torque RMS error calculation
      if ff<fu
         Kc=Kf;
         fc=ff;
      else
         Kc=Ku;
         fc=fu;
      end
   else
      Kf=Kc-2*h; Kte=Kf;
      sim('pdtc3l_imxOptim'); % Fitness evaluation
      nev=nev+1;
      ff=norm(Teref-Te)/sqrt(length(Teref)); % Torque RMS error calculation
      if ff<fl
         Kc=Kf;
         fc=ff;
      else
         Kc=Kl;
         fc=fl;
      end
   end
   hist=[hist;[Kc,fc,h,nev]]; % Save the evolution of the algorithm
end
```

Appendix B: Electrical diagrams of the laboratory setup

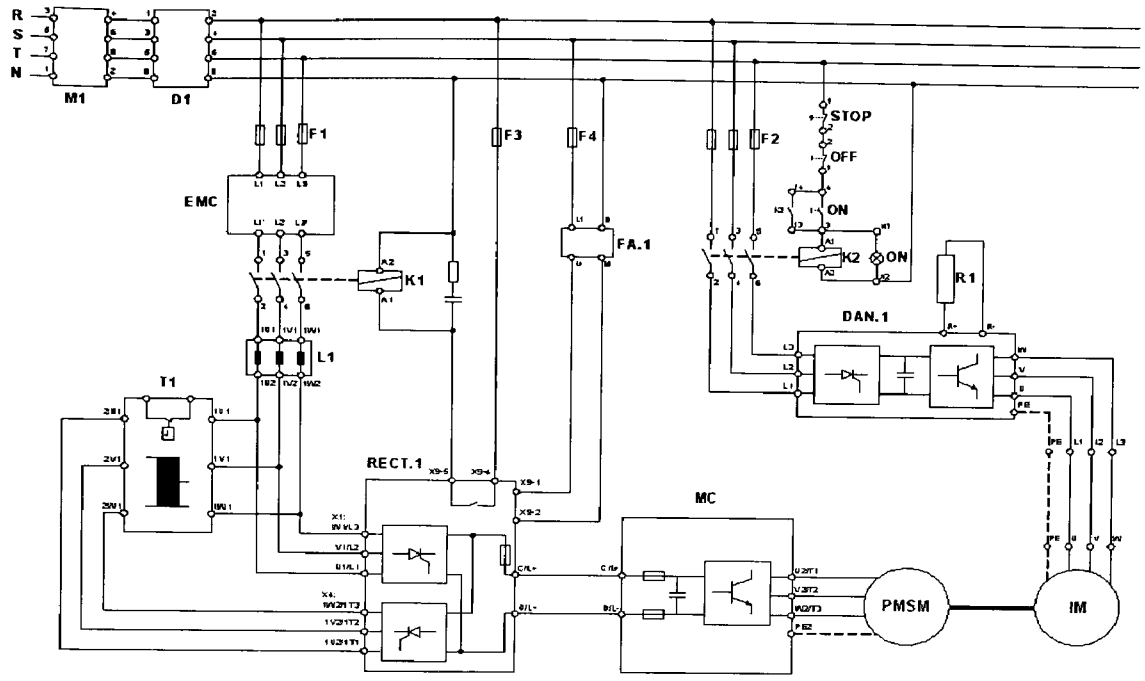

Fig. B. 1 Electrical diagram of the motor control cabinet

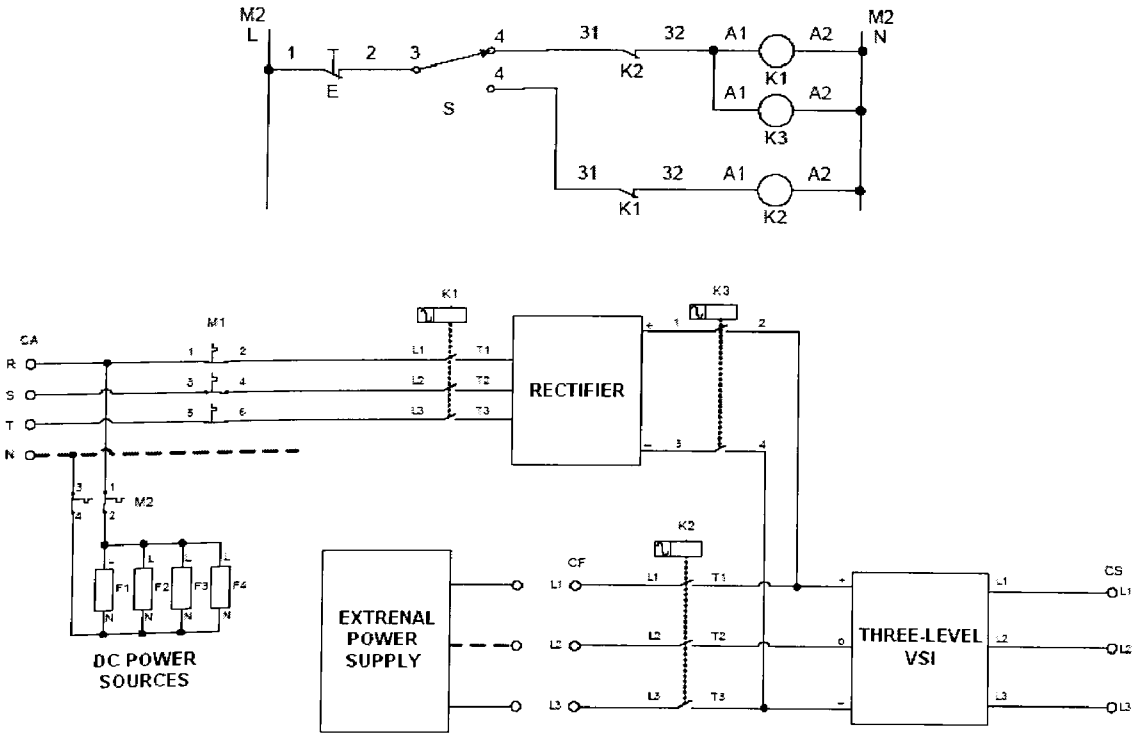

Fig. B. 2 Electrical diagram of the three-level VSI cabinet

Appendix C: PLD program

```
MODULE Protec_1

TITLE 'Program for the Protec_1 board'

DECLARATIONS

"INPUTS

CLK    PIN 20;
RESET   PIN 24;
R_DRIVER  PIN   83;

A    PIN 34;
B    PIN 35;
C    PIN 36;
D    PIN 37;
E    PIN 38;
F    PIN 39;
EN    PIN 40;

Err_R   PIN 74;
Err_S   PIN 60;
Err_T   PIN 53;
Err_V   PIN 78;
Err_If    PIN 77;
Err_Ib    PIN 76;
Err_Cho   PIN 75;

"OUTPUTS

O1_R    PIN 72  ISTYPE 'reg,buffer';
O2_R    PIN 73  ISTYPE 'reg,buffer';
O3_R    PIN 70  ISTYPE 'reg,buffer';
O4_R    PIN 71  ISTYPE 'reg,buffer';

Q1_R    NODE  ISTYPE 'reg,buffer';
Q2_R    NODE  ISTYPE 'reg,buffer';
Q3_R    NODE  ISTYPE 'reg,buffer';

O1_S    PIN 68  ISTYPE 'reg,buffer';
O2_S    PIN 69  ISTYPE 'reg,buffer';
O3_S    PIN 58  ISTYPE 'reg,buffer';
O4_S    PIN 59  ISTYPE 'reg,buffer';

Q1_S    NODE  ISTYPE 'reg,buffer';
Q2_S    NODE  ISTYPE 'reg,buffer';
Q3_S    NODE  ISTYPE 'reg,buffer';

O1_T    PIN 56  ISTYPE 'reg,buffer';
O2_T    PIN 57  ISTYPE 'reg,buffer';
O3_T    PIN 54  ISTYPE 'reg,buffer';
O4_T    PIN 55  ISTYPE 'reg,buffer';

Q1_T    NODE  ISTYPE 'reg,buffer';
Q2_T    NODE  ISTYPE 'reg,buffer';
Q3_T    NODE  ISTYPE 'reg,buffer';

O_Ib    PIN 45  ISTYPE 'com';
O_V   PIN 46  ISTYPE 'com';
O_If    PIN 47  ISTYPE 'com';
O_T   PIN 48  ISTYPE 'com';
O_S   PIN 49  ISTYPE 'com';
O_R   PIN 50  ISTYPE 'com';
O_Cho   PIN 51  ISTYPE 'com';

RST_DRI   PIN 52  ISTYPE 'com';

Err   PIN 41  ISTYPE 'com';

CONT_R7..CONT_R0 NODE  ISTYPE 'reg';
CONT_S7..CONT_S0 NODE  ISTYPE 'reg';
CONT_T7..CONT_T0 NODE  ISTYPE 'reg';
CONT_RA7..CONT_RA0 NODEISTYPE 'reg';
CONT_SA7..CONT_SA0 NODEISTYPE 'reg';
```

```
CONT_TA7..CONT_TA0 NODEISTYPE 'reg';

"ASSIGNATION OF STATES

E_SORT_R  = [Q1_R,Q2_R,Q3_R];
E_REPOS_R   = [  0,   0,   0 ];
E_ALT_R   = [  0,   0,   1 ];
E_MIG_R   = [  0,   1,   0 ];
E_BAIX_R  = [  0,   1,   1 ];
E_MA_R    = [  1,   0,   0 ];
E_MB_R    = [  1,   0,   1 ];
E_NO_US_1_R  = [  1,   1,   0 ];
E_NO_US_2_R  = [  1,   1,   1 ];

O_SORT_R  = [O1_R,O2_R,O3_R,O4_R];
O_REPOS_R   = [  0,   0,   0,   0 ];
O_ALT_R   = [  1,   1,   0,   0 ];
O_MIG_R   = [  0,   1,   1,   0 ];
O_BAIX_R  = [  0,   0,   1,   1 ];
O_MA_R    = [  0,   1,   0,   0 ];
O_MB_R    = [  0,   0,   1,   0 ];

E_SORT_S  = [Q1_S,Q2_S,Q3_S];
E_REPOS_S   = [  0,   0,   0 ];
E_ALT_S   = [  0,   0,   1 ];
E_MIG_S   = [  0,   1,   0 ];
E_BAIX_S  = [  0,   1,   1 ];
E_MA_S    = [  1,   0,   0 ];
E_MB_S    = [  1,   0,   1 ];
E_NO_US_1_S  = [  1,   1,   0 ];
E_NO_US_2_S  = [  1,   1,   1 ];

O_SORT_S  = [O1_S,O2_S,O3_S,O4_S];
O_REPOS_S   = [  0,   0,   0,   0 ];
O_ALT_S   = [  1,   1,   0,   0 ];
O_MIG_S   = [  0,   1,   1,   0 ];
O_BAIX_S  = [  0,   0,   1,   1 ];
O_MA_S    = [  0,   1,   0,   0 ];
O_MB_S    = [  0,   0,   1,   0 ];

E_SORT_T  = [Q1_T,Q2_T,Q3_T];
E_REPOS_T   = [  0,   0,   0 ];
E_ALT_T   = [  0,   0,   1 ];
E_MIG_T   = [  0,   1,   0 ];
E_BAIX_T  = [  0,   1,   1 ];
E_MA_T    = [  1,   0,   0 ];
E_MB_T    = [  1,   0,   1 ];
E_NO_US_1_T  = [  1,   1,   0 ];
E_NO_US_2_T  = [  1,   1,   1 ];

O_SORT_T  = [O1_T,O2_T,O3_T,O4_T];
O_REPOS_T   = [  0,   0,   0,   0 ];
O_ALT_T   = [  1,   1,   0,   0 ];
O_MIG_T   = [  0,   1,   1,   0 ];
O_BAIX_T  = [  0,   0,   1,   1 ];
O_MA_T    = [  0,   1,   0,   0 ];
O_MB_T    = [  0,   0,   1,   0 ];

CONT_R  = [CONT_R7..CONT_R0];
CONT_S  = [CONT_S7..CONT_S0];
CONT_T  = [CONT_T7..CONT_T0];
CONT_RA = [CONT_RA7..CONT_RA0];
CONT_SA = [CONT_SA7..CONT_SA0];
CONT_TA = [CONT_TA7..CONT_TA0];

"DELAY IN THE TRANSITIONS THROUGH THE MEDIUM STATE

RETRAS  = 64;

"RETRAS 255 --> 1111 1111b --> 8us
"RETRAS 224 --> 1110 0000b --> 7us
"RETRAS 192 --> 1100 0000b --> 6us
"RETRAS 160 --> 1010 0000b --> 5us
"RETRAS 128 --> 1000 0000b --> 4us
"RETRAS 096 --> 0110 0000b --> 3us
"RETRAS 064 --> 0100 0000b --> 2us
"RETRAS 032 --> 0010 0000b --> 1us
```

```
EQUATIONS

E_SORT_R.CLK=CLK;
E_SORT_R.AR=!RESET;

O_SORT_R.CLK=CLK;
O_SORT_R.AR=!RESET;

E_SORT_S.CLK=CLK;
E_SORT_S.AR=!RESET;

O_SORT_S.CLK=CLK;
O_SORT_S.AR=!RESET;

E_SORT_T.CLK=CLK;
E_SORT_T.AR=!RESET;

O_SORT_T.CLK=CLK;
O_SORT_T.AR=!RESET;

CONT_R.CLK=CLK;
CONT_R.AR=!RESET;

CONT_S.CLK=CLK;
CONT_S.AR=!RESET;

CONT_T.CLK=CLK;
CONT_T.AR=!RESET;

CONT_RA.CLK=CLK;
CONT_RA.AR=!RESET;

CONT_SA.CLK=CLK;
CONT_SA.AR=!RESET;

CONT_TA.CLK=CLK;
CONT_TA.AR=!RESET;

"ERROR CONTROL, RESET AND ALARMS ACTIVATION

Err = (!Err_R&!Err_S&!Err_T&Err_V&Err_If&Err_Ib&!Err_Cho);
RST_DRI= !R_DRIVER;

O_Ib = Err_Ib;
O_V = Err_V;
O_If = Err_If;
O_T = !Err_T;
O_S = !Err_S;
O_R = !Err_R;
O_Cho = !Err_Cho;

"R LEG

STATE_DIAGRAM E_SORT_R;

STATE E_REPOS_R:

  O_SORT_R=O_REPOS_R;
  CONT_R:=0;
  CONT_RA:=0;

  IF (EN#!Err#(A&B))  THEN E_REPOS_R

  ELSE E_MIG_R;

STATE E_MIG_R:

  O_SORT_R=O_MIG_R;
  CONT_RA:=0;

IF (CONT_R<RETRAS)  THEN E_MIG_R  WITH CONT_R:=(CONT_R+1);ENDWITH

ELSE IF (!A&B&!EN&Err) THEN E_MA_R

  ELSE IF (A&!B&!EN&Err) THEN E_MB_R
```

```
  ELSE IF (EN#!Err#(A&B))THEN E_REPOS_R

  ELSE E_MIG_R;

STATE E_ALT_R:

  O_SORT_R=O_ALT_R;
  CONT_R:=0;
  CONT_RA:=0;

  IF (!A&B&!EN&Err) THEN E_ALT_R

  ELSE E_MA_R;

STATE E_BAIX_R:

  O_SORT_R=O_BAIX_R;
  CONT_R:=0;
  CONT_RA:=0;

  IF (A&!B&!EN&Err)   THEN E_BAIX_R

  ELSE E_MB_R;

STATE E_MA_R:

  O_SORT_R=O_MA_R;
  CONT_R:=0;

IF (CONT_RA<RETRAS) THEN E_MA_R  WITH CONT_RA:=(CONT_RA+1);ENDWITH

ELSE IF (!A&B&!EN&Err) THEN E_ALT_R

  ELSE IF (A&!B&!EN&Err)    THEN E_MIG_R

  ELSE IF (EN#!Err#(A&B))THEN E_REPOS_R

  ELSE E_MIG_R;

STATE E_MB_R:

  O_SORT_R=O_MB_R;
  CONT_R:=0;

IF (CONT_RA<RETRAS) THEN E_MB_R  WITH CONT_RA:=(CONT_RA+1);ENDWITH

ELSE IF (!A&B&!EN&Err) THEN E_MIG_R

  ELSE IF (A&!B&!EN&Err)    THEN E_BAIX_R

  ELSE IF (EN#!Err#(A&B))THEN E_REPOS_R

  ELSE E_MIG_R;

STATE E_NO_US_1_R:

  CONT_R:=0;
  CONT_RA:=0;

  GOTO E_MIG_R;

STATE E_NO_US_2_R:

  CONT_R:=0;
  CONT_RA:=0;

  GOTO E_MIG_R;

"S LEG

STATE_DIAGRAM E_SORT_S;

STATE E_REPOS_S:

  O_SORT_S=O_REPOS_S;
  CONT_S:=0;
  CONT_SA:=0;
```

```
  IF (EN#!Err#(C&D))  THEN E_REPOS_S

  ELSE E_MIG_S;

STATE E_MIG_S:

  O_SORT_S=O_MIG_S;
  CONT_SA:=0;

IF (CONT_S<RETRAS)  THEN E_MIG_S  WITH CONT_S:=(CONT_S+1);ENDWITH

ELSE IF (!C&D&!EN&Err) THEN E_MA_S

  ELSE IF (C&!D&!EN&Err)   THEN E_MB_S

  ELSE IF (EN#!Err#(C&D))THEN E_REPOS_S

  ELSE E_MIG_S;

STATE E_ALT_S:

  O_SORT_S=O_ALT_S;
  CONT_S:=0;
  CONT_SA:=0;

  IF (!C&D&!EN&Err) THEN E_ALT_S

  ELSE E_MA_S;

STATE E_BAIX_S:

  O_SORT_S=O_BAIX_S;
  CONT_S:=0;
  CONT_SA:=0;

  IF (C&!D&!EN&Err)   THEN E_BAIX_S

  ELSE E_MB_S;

STATE E_MA_S:

  O_SORT_S=O_MA_S;
  CONT_S:=0;

IF (CONT_SA<RETRAS) THEN E_MA_S  WITH CONT_SA:=(CONT_SA+1);ENDWITH

ELSE IF (!C&D&!EN&Err) THEN E_ALT_S

  ELSE IF (C&!D&!EN&Err)   THEN E_MIG_S

  ELSE IF (EN#!Err#(C&D))THEN E_REPOS_S

  ELSE E_MIG_S;

STATE E_MB_S:

  O_SORT_S=O_MB_S;
  CONT_S:=0;

IF (CONT_SA<RETRAS) THEN E_MB_S  WITH CONT_SA:=(CONT_SA+1);ENDWITH

ELSE IF (!C&D&!EN&Err) THEN E_MIG_S

  ELSE IF (C&!D&!EN&Err)   THEN E_BAIX_S

  ELSE IF (EN#!Err#(C&D))THEN E_REPOS_S

  ELSE E_MIG_S;

STATE E_NO_US_1_S:

  CONT_S:=0;
  CONT_SA:=0;

  GOTO E_MIG_S;
```

```
STATE E_NO_US_2_S:

  CONT_S:=0;
  CONT_SA:=0;

  GOTO E_MIG_S;

"T LEG

STATE_DIAGRAM E_SORT_T;

STATE E_REPOS_T:

  O_SORT_T=O_REPOS_T;
  CONT_T:=0;
  CONT_TA:=0;

  IF (EN#!Err#(E&F)) THEN E_REPOS_T

  ELSE E_MIG_T;

STATE E_MIG_T:

  O_SORT_T=O_MIG_T;
  CONT_TA:=0;

IF (CONT_T<RETRAS) THEN E_MIG_T  WITH CONT_T:=(CONT_T+1);ENDWITH

ELSE IF (!E&F&!EN&Err) THEN E_MA_T

  ELSE IF (E&!F&!EN&Err)   THEN E_MB_T

  ELSE IF (EN#!Err#(E&F))THEN E_REPOS_T

  ELSE E_MIG_T;

STATE E_ALT_T:

  O_SORT_T=O_ALT_T;
  CONT_T:=0;
  CONT_TA:=0;

  IF (!E&F&!EN&Err) THEN E_ALT_T

  ELSE E_MA_T;

STATE E_BAIX_T:

  O_SORT_T=O_BAIX_T;
  CONT_T:=0;
  CONT_TA:=0;

  IF (E&!F&!EN&Err)   THEN E_BAIX_T

  ELSE E_MB_T;

STATE E_MA_T:

  O_SORT_T=O_MA_T;
  CONT_T:=0;

IF (CONT_TA<RETRAS) THEN E_MA_T  WITH CONT_TA:=(CONT_TA+1);ENDWITH

ELSE IF (!E&F&!EN&Err) THEN E_ALT_T

  ELSE IF (E&!F&!EN&Err)   THEN E_MIG_T

  ELSE IF (EN#!Err#(E&F))THEN E_REPOS_T

  ELSE E_MIG_T;

STATE E_MB_T:

  O_SORT_T=O_MB_T;
  CONT_T:=0;

IF (CONT_TA<RETRAS) THEN E_MB_T  WITH CONT_TA:=(CONT_TA+1);ENDWITH
```

```
ELSE IF (!E&F&!EN&Err) THEN E_MIG_T

  ELSE IF (E&!F&!EN&Err)   THEN E_BAIX_T

  ELSE IF (EN#!Err#(E&F))THEN E_REPOS_T

  ELSE E_MIG_T;

STATE E_NO_US_1_T:

  CONT_T:=0;
  CONT_TA:=0;

  GOTO E_MIG_T;

STATE E_NO_US_2_T:

  CONT_T:=0;
  CONT_TA:=0;

  GOTO E_MIG_T;

END
```

Appendix D: Author's publications

The following list contains all the papers published by the author of this thesis during the duration of the PhD studies. The list is divided into publications directly related to the thesis and other publications covering different topics. The most relevant publication in the list directly related to the research presented in this thesis is attached after the list of publications.

Publications directly related to the thesis:

1. X. del Toro Garcia, A. Arias, M. G. Jayne and P. A. Witting. "Direct Torque Control of Induction Motors Utilising Three-level Voltage Source Inverters". *IEEE Transaction on Industrial Electronics*, vol 55, no 2, pp. 956-958, February 2008.
2. X. del Toro Garcia, A. Arias, M. G. Jayne, P. A. Witting, V. M. Sala and J. L. Romeral. "New DTC Control Scheme for Induction Motors fed with a Three-level Inverter". *Automatika, journal for control, measurement, electronics, computing and communications*, no 46 , vol 1-2, pp. 73-81, 2005. **(Publication attached).**
3. X. del Toro Garcia, M. G. Jayne, P. A. Witting, J. Pou, A. Arias and J. L. Romeral. "New DTC Control Scheme for Induction Motors". Proceedings of the 11th European Conference on Power Electronics and Applications EPE05, Dresden, Germany, September 2005.
4. X. del Toro Garcia, M. G. Jayne, P. A. Witting, V. M. Sala, A. Arias, J. L. Romeral "New DTC Control Scheme for the Induction Motor fed with a Three-level Inverter". Proceedings of the IEEE Symposium on Industrial Electronics ISIE05, Dubrovnik, Croatia, 20-23 June 2005, pp.893-898.
5. X. del Toro Garcia, S. Calls, M. G. Jayne, P. A. Witting, A. Arias, J. L. Romeral. "Direct Torque Control of an Induction Motor using a Three-level Inverter and Fuzzy Logic". Proceedings of the IEEE Symposium on Industrial Electronics ISIE04, Ajaccio, France, 4-7 May 2004, pp. 923-927.
6. S. Calls, X. del Toro Garcia, M. G. Jayne, P. A. Witting, A. Arias, J. L. Romeral. "Direct Torque Control of Induction Motors with a Three-Level Inverter". Proceedings of the 4th International Research and Educational Colloquium on Electronics IRECE03, University of Glamorgan, July 2003. pp. 35-43.

Other publications:

7. F. Neri, X. del Toro García, G.L. Cascella, N. Salvatore "Surrogate Assisted Local Search in PMSM Drive Design". Accepted for publication in COMPEL: The International Journal for Computation and Mathematics in Electrical and Electronic Engineering, December 2007.
8. V. M. Sala, J. Cusidó, X. del Toro Garcia "Nuevo Amplificador Clase-D de Alta Potencia y Calidad de Sonido a Baja Frecuencia de Conmutación". Proceedings of the XIII Seminario Anual de Automática, Electrónica Industrial e Instrumentación, SAAEI06, Spain, 12-15 September 2006, pp. 895-898.
9. Terlizzi, X. del Toro Garcia, B. Zigmund, R. Pavlanin, Luigi Salvatore "Experimental Evaluation of PI Tuning Techniques for Field Oriented Control of Permanent Magnet Synchronous Motors". *Advances in Electrical and Electronic Engineering* (selected papers from ELEKTRO 2006, 6th International Conference in Electrical and Electronic Engineering, Zilina, Slovak Republic, 23-24th May 2006), no 1-2, vol 5/2006, pp. 114-119.
10. X. del Toro Garcia, B. Zigmund, A. Terlizzi, R. Pavlanin, L. Salvatore "Comparison between FOC and DTC Strategies for Permanent Magnet Synchronous Motors". *Advances in Electrical and Electronic Engineering* (selected papers from ELEKTRO 2006, 6th International Conference in Electrical and Electronic Engineering, Zilina, Slovak Republic, 23-24th May 2006), no 1-2, vol 5/2006, pp. 76-81.
11. V. M. Sala, X. del Toro Garcia, J. Pou, A. Arias "New High Power D-Class Amplifier with High Quality of Sound at Low switching Frequency". Proceedings of the 6th International Conference Elektro 2006, Zilina, Slovak Republic, 23-24th May 2006, pp. 56-59.
12. X. del Toro Garcia, F. Neri, G. L. Cascella, N. Salvatore "A Surrogate Assisted Hooke-Jeeves Algorithm to Optimize the Control System of a PMSM Drive". Proceedings of the IEEE Symposium on Industrial Electronics ISIE06, Montreal, Canada, 9-12th July 2006, pp. 347-352.
13. C. Ortega, A. Arias, X. del Toro Garcia, J. L. Romeral, E. Aldabas. "Direct Torque Control for Induction Motors Using small voltage vectors of Matrix Converters". Proceedings of the IEEE 31st International Conference on Industrial Electronics IECON05, Raleigh, USA, November 2005, pp. 1353-1358.

New DTC Control Scheme for Induction Motors fed with a Three-level Inverter

Xavier del Toro Garcia*, Antoni Arias**,Marcel G. Jayne*, Phil A. Witting*, Vicenç M. Sala**, Jose Luis Romeral**

*School of Electronics, University of Glamorgan, Pontypridd, Wales, United Kingdom.
**Electronic Engineering Department, Universitat Politècnica de Catalunya, Terrassa, Catalunya, Spain.

Abstract **– This paper presents a novel controller based on Direct Torque Control (DTC) strategy. This controller is designed to be applied in the control of Induction Motors (IM) fed with a three-level Voltage Source Inverter (VSI). This type of inverter has several advantages over the standard two-level VSI, such as a greater number of levels in the output voltage waveforms, lower dV/dt, less harmonic distortion in voltage and current waveforms and lower switching frequencies. In the new controller, torque and stator flux errors are used together with the stator flux angular frequency to generate a reference voltage vector. Experimental results of the novel system are presented and compared with those obtained for Classical DTC system employing a two-level VSI. The new controller is shown to reduce the ripple in the torque and flux responses. Lower current distortion and switching frequency of the semiconductor devices are also obtained in the new system presented.**

Keywords **– Adjustable speed drives, Direct Torque and Flux Control, Induction Motors, Multilevel Converters.**

I. INTRODUCTION

Direct Torque Control (DTC) is a method that has emerged to become one possible alternative to the well-known Vector Control of Induction Motors [1-3]. This method provides a good performance with a simpler structure and control diagram. In DTC it is possible to control directly the stator flux and the torque by selecting the appropriate VSI state. The main advantages offered by DTC are:

- Decoupled control of torque and stator flux.
- Excellent torque dynamics with minimal response time.
- Inherent motion-sensorless control method since the motor speed is not required to achieve the torque control.
- Absence of coordinate transformation (required in Field Oriented Control (FOC)).
- Absence of voltage modulator, as well as other controllers such as PID and current controllers (used in FOC).
- Robustness for rotor parameters variation. Only the stator resistance is needed for the torque and stator flux estimator.

These merits are counterbalanced by some drawbacks:

- Possible problems during starting and low speed operation and during changes in torque command.
- Requirement of torque and flux estimators, implying the consequent parameters identification (the same as for other vector controls).
- Variable switching frequency caused by the hysteresis controllers employed.
- Inherent torque and stator flux ripples.
- Flux and current distortion caused by sector changes of the flux position.
- Higher harmonic distortion of the stator voltage and current waveforms compared to other methods such as FOC.
- Acoustical noise produced due to the variable switching frequency. This noise can be particularly high at low speed operation.

A variety of techniques have been proposed to overcome some of the drawbacks present in DTC [4]. Some solutions proposed are: DTC with Space Vector Modulation (SVM) [5]; the use of a duty-ratio controller to introduce a modulation between active vectors chosen from the look-up table and the zero vectors [6-8]; use of artificial intelligence techniques, such as Neuro-Fuzzy controllers with SVM [9]. These methods achieve some improvements such as torque ripple reduction and fixed switching frequency operation. However, the complexity of the control is considerably increased.

A different approach to improve DTC features is to employ different converter topologies from the standard two-level VSI. Some authors have presented different implementations of DTC for the three-level Neutral Point Clamped (NPC) VSI [10-15]. This work will present a new control scheme based on DTC designed to be applied to an Induction Motor fed with a three-level VSI. The major advantage of the three-level VSI topology when applied to DTC is the increase in the number of voltage vectors available. This means the number of possibilities in the vector selection process is greatly increased and may lead to a more accurate control system, which may result in a reduction in the torque and flux ripples. This is of course achieved, at the expense of an increase in the complexity of the vector selection process.

II. THE THREE-LEVEL NPC INVERTER

The standard VSI traditionally used in electrical drive systems is the two-level VSI, which unfortunately has a

number of inherent limitations. For example the maximum voltage that can be supported by the semiconductor switching devices in the inverter limits the maximum value of DC bus voltage. Similarly the output voltages and currents from the inverter can contain high harmonic distortion. The output voltage waveforms can also contain large values of dV/dt, which contribute to the degradation of the machine windings insulation and also produce considerable electromagnetic interference during operation. New multilevel VSI topologies however can considerably reduce many of these limitations [16].

The three-level NPC VSI, presented in Fig. 1, is one of the most commonly applied multilevel topologies [17]. This type of VSI has several advantages over the standard two-level VSI, such as a greater number of levels in the output voltage waveforms, lower dV/dt, less harmonic distortion and lower switching frequencies. The main drawback of this type of converter is the voltage imbalance produced in the capacitors of the DC-link when one of the phases is connected to the middle point or Neutral Point (NP).

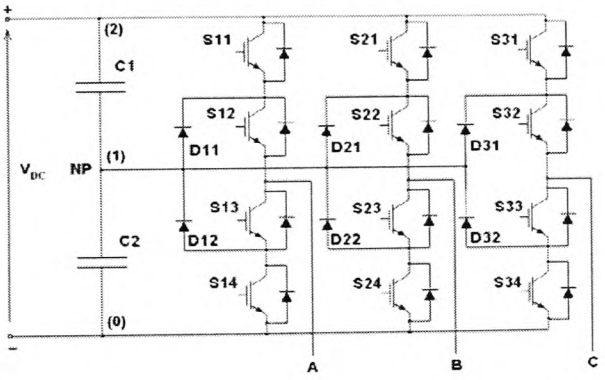

Fig. 1 Three-level NPC VSI

In Fig. 2, the different vectors or VSI states available in a three-level VSI are presented. As it can be seen, there are 4 different kinds of vectors depending on the module:

- Zero vectors: Vz (with 3 possible configurations).
- Large vectors: V1l, V2l, V3l, V4l, V5l, V6l.
- Medium vectors: V1m, V2m, V3m, V4m, V5m, V6m.
- Small vectors: V1s, V2s, V3s, V4s, V5s, V6s. (with 2 possible configurations for each).

The state of the switches for each leg (C_A, C_B and C_C) is shown in brackets (2: phase connected to the positive of the DC-link; 1: phase connected to the middle point of the DC-link (NP); 0: phase connected to the negative of the DC-link). The output voltage vector is defined by the following expression:

$$\vec{v} = \frac{V_{DC}}{9}\left(3C_A + bC_B + b^* C_C\right); \quad C_A, C_B, C_C \in \{0,1,2\} \quad (1)$$

Where $a = e^{j\frac{2\pi}{3}}$ and $b = 2a - a^2 - 1$.

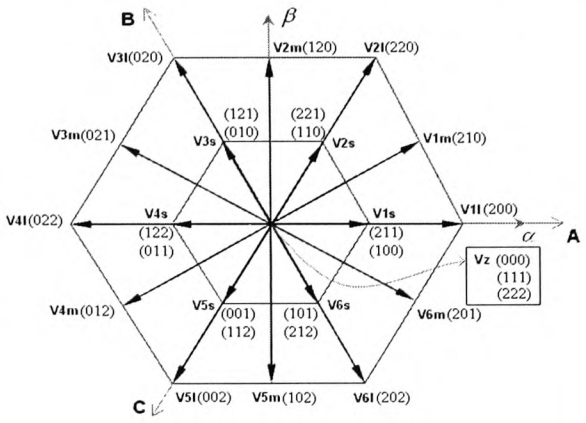

Fig. 2 Voltage space vectors for a three-level NPC VSI

III. DTC Principle Review

In order to understand DTC principle some of the equations of the Induction Motor need to be reviewed. The electromagnetic torque can be expressed as a function of the stator flux and the rotor flux space vectors as follows:

$$\Gamma_e = -\frac{3}{2} P \frac{L_m}{L_s L_r - L_m^2} \vec{\psi}_s \times \vec{\psi}_r' \quad (2)$$

If the modulus of the previous expression is evaluated it is obtained:

$$\Gamma_e = \frac{3}{2} P \frac{L_m}{L_s L_r - L_m^2} \left|\vec{\psi}_r'\right| \left|\vec{\psi}_s\right| \sin\left(\gamma_s - \gamma_r\right) \quad (3)$$

Considering the modulus of the rotor and stator fluxes constant, torque can be controlled by changing the relative angle between both flux vectors. Stator flux can be adjusted by the stator voltage according to the stator voltage equation in stator fixed coordinates:

$$\vec{u}_s = R_s \vec{i}_s + \frac{d\vec{\psi}_s}{dt} \quad (4)$$

If the voltage drop in the stator resistance is neglected the variation of the stator flux is directly proportional to the stator voltage applied:

$$\vec{u}_s \approx \frac{d\vec{\psi}_s}{dt} \qquad \vec{u}_s \approx \frac{\Delta\vec{\psi}_s}{\Delta t} \quad (5)$$

Because the rotor time constant is larger than the stator one, the rotor flux changes slowly compared to the stator flux. Thus torque can be controlled by quickly varying the stator flux position by means of the stator voltage applied to the motor. The desired decoupled control of the stator flux modulus and torque is achieved by acting on the radial (x) and tangential (y) components respectively of the stator flux vector. According to (5) these two components will depend on the components of the stator voltage vector applied in the same directions. The tangential component of the

stator voltage will affect the relative angle between the rotor and the stator flux vectors and in turns will control the torque variation according to (3). The radial component will affect the amplitude of the stator flux vector.

Fig. 3 shows the stator flux in the α-β plane, and the effect of the different states of a two-level VSI regarding torque and stator flux modulus variation. The α-β plane is divided into six different sectors. As an example, for sector 1 (K=1), V2 can increase both stator flux and torque.

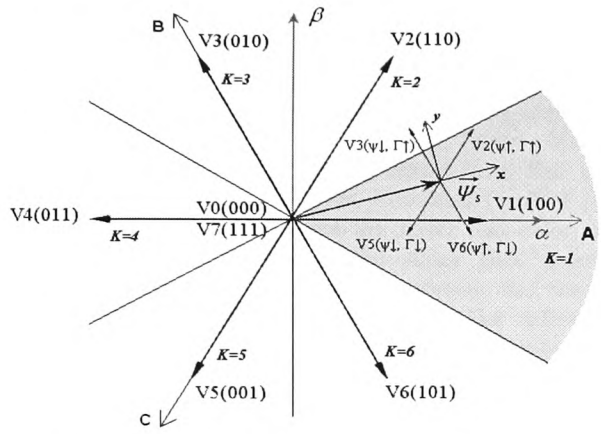

Fig. 3 Influence of the voltage vector selected on the variation of stator flux modulus and torque

According to the considerations illustrated in Fig. 3 the generic or Classical DTC scheme for a VSI-fed Induction Motor was developed [1] as shown in Fig. 4.

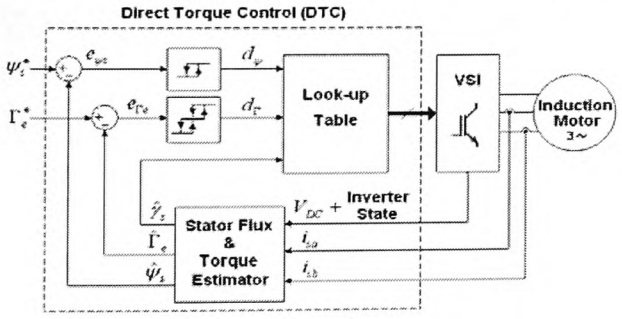

Fig. 4 Classical DTC scheme

As it can be seen, there are two different loops corresponding to the magnitudes of the stator flux modulus and torque. The reference values for the stator flux modulus and the torque are compared with the estimated values, the resulting error values are fed into a two-level and a three-level hysteresis block respectively. The outputs of the stator flux error and torque error hysteresis blocks, together with the position of the stator flux are used as inputs to the look-up table (Table I). The position of the stator flux is divided into six different sectors. The output of the look-up table is the VSI state that will be applied during a sampling period. The stator flux modulus and torque errors tend to be restricted within its respective hysteresis bands.

Table I Classical DTC look-up table

$K(\gamma_s)$		1	2	3	4	5	6
$d_\psi = 1$	$d_\Gamma = 1$	V2	V3	V4	V5	V6	V1
	$d_\Gamma = 0$	V7	V0	V7	V0	V7	V0
	$d_\Gamma = -1$	V6	V1	V2	V3	V4	V5
$d_\psi = -1$	$d_\Gamma = 1$	V3	V4	V5	V6	V1	V2
	$d_\Gamma = 0$	V0	V7	V0	V7	V0	V7
	$d_\Gamma = -1$	V5	V6	V1	V2	V3	V4

The principle of DTC operation can also be explained by analysing the Induction Motor stator voltage equation in the stator flux reference frame.

$$\bar{u}_s = R_s \bar{i}_s + \frac{d\bar{\psi}_s}{dt} + j\omega_s \bar{\psi}_s \tag{6}$$

If this expression is separated into de direct (x) and the quadrature component (y) of the stator voltage, the following expressions are can be obtained:

$$u_{sx} = R_s i_{sx} + \frac{d\psi_{sx}}{dt} \tag{7}$$

$$u_{sy} = R_s i_{sy} + \omega_s \psi_{sx} \tag{8}$$

In the same reference frame fixed to the stator flux vector the electromagnetic torque can be expressed as:

$$\Gamma_e = \frac{3}{2} P \bar{\psi}_s \times \bar{i}_s \tag{9}$$

$$\Gamma_e = \frac{3}{2} P\left(\psi_{sx} i_{sy} - \psi_{sy} i_{sx}\right) = \frac{3}{2} P \psi_{sx} i_{sy} \tag{10}$$

Combining expression (8) with (10) the following torque expression is obtained:

$$\Gamma_e = \frac{3}{2} P \frac{\psi_{sx}\left(u_{sy} - \omega_s \psi_{sx}\right)}{R_s} \tag{11}$$

From expression (7) it can be concluded that stator flux amplitude can be controlled by means of the direct (or radial) component of the stator voltage. It is also evident from equation (11) that the electromagnetic torque can be controlled by means of the quadrature (or tangential) component of the stator voltage, under adequate decoupling of the stator flux. From equation (11) some other considerations can be made:

- Torque depends on the stator flux amplitude as well.
- It also depends on the stator flux angular speed, which depends on the operating point of the machine. It can be seen that as the speed of the machine and the slip increase the effect of the voltage vectors applied on the produced torque is lower. It is also obvious that zero vectors will produce a high torque decrease at high speeds.

DTC requires the estimation of stator flux and torque, which can be performed by means of two different phase currents, the state of the VSI and the voltage level in the DC-link. This estimation is based in the stator voltage equation [3]:

$$\vec{\psi}_s = \int \left(\vec{u}_s - R_s \vec{i}_s \right) dt \qquad (12)$$

Torque expression is then obtained using (9).

IV. New DTC Scheme

In the new controller, shown in Fig. 5, a reference voltage vector (V_{ref}) in α-β coordinates is generated according to the DTC basic principle explained in the previous section, rather than using the inverter state look-up table as used in classical DTC. This approach adopted is close to the DTC with Space Vector Modulation (SVM) scheme with closed-loop flux and torque control, and Stator Flux Oriented Control [4]. The inputs to the controller are the stator flux error, the torque error and additionally the stator flux angular speed, which is incorporated to improve the torque response at different operating points. The reference voltage generated as a control action can be synthesised using different techniques with different degrees of complexity such as choosing the nearest vector available or using modulation techniques. This controller can be applied to any topology because the type of VSI will only affect the way the reference voltage vector has to be synthesised.

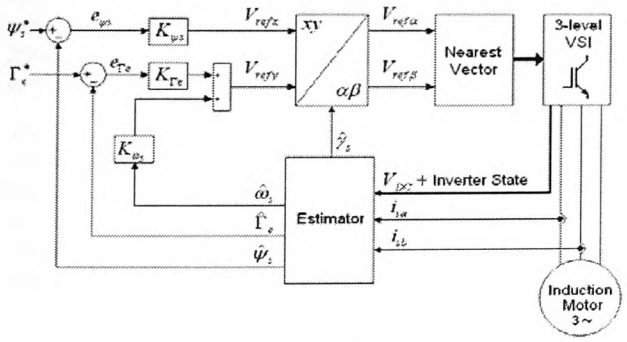

Fig. 5 New DTC scheme

Following the conclusions extracted from (7) and (11), when calculating the reference voltage (in x-y coordinates fixed to the stator flux vector) the radial or x component will depend on the stator flux error, while the tangential or y component will depend on the torque error. A feed-forward action depending on the stator flux angular speed is added in the calculation of the stator voltage y component. This action will compensate the effect of the operating point on the torque production. Initially a preliminary reference vector in x-y coordinates is calculated; where some gain factors have been introduced to tune the controller.

$$V_{refx} = K_{\psi s} e_{\psi s} \qquad (13)$$

$$V_{refy} = K_{\Gamma e} e_{\Gamma e} + K_{\omega s} \hat{\omega}_s \qquad (14)$$

Then a transformation x-y to α-β is performed to obtain the reference vector in fixed coordinates. In this point, the new controller synthesises the reference voltage vector by choosing the nearest vector available that can be delivered by the VSI. The nearest vector is found by means of calculating the minimum distance of the voltage vectors that can be delivered by the VSI to the reference voltage vector.

A different possibility instead of choosing the nearest vector and applying it for the whole sampling period is to use modulation techniques such as Space Vector Modulation (SVM) or some active-null vector modulation like in a duty-ratio controller. These possibilities will also provide a higher but constant switching frequency.

V. Experimental Setup

The novel controller has been tested in an experimental setup. This setup contains the following components as shown in Fig. 6:

- A dSpace DS1103 board that performs the control tasks. This board contains a PowerPC and a DSP.
- A 30A three-level NPC VSI with Insulated Gate Bipolar Transistors (IGBT) to supply an Induction Motor.
- A 1.1kW Induction Motor to be controlled. Table II shows the parameters of this motor.
- A permanent magnet synchronous motor (PMSM) attached to the Induction Motor shaft and supplied with an industrial rectifier and inverter. Torque load can be controlled with this equipment by sending the load torque reference signal from the control board.
- The control algorithm has been created using Matlab/Simulink.

Table II Induction Motor parameters

Rated power	1.1kW (Y: 380V/4.43A)
Poles	4
Nominal speed	1415rpm=148.17rad/s
Nominal torque	7.4Nm
Nominal Flux	0.96Wb
Rs	9.21Ω
Rr	6.644Ω
Lm	0.44415H
Ls	0.03207H
Lr	0.00847H

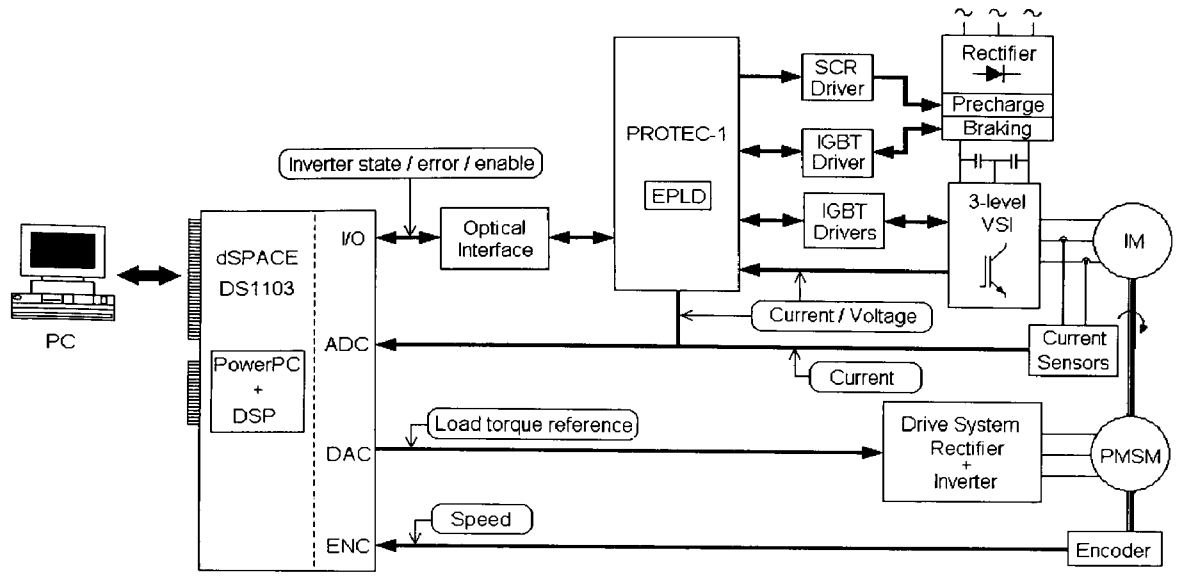

Fig. 6 Experimental setup

VI. Experimental Results

Some experimental results have been obtained for the Classical DTC control system with a two-level VSI (DTC2L) and the new control technique with a three-level VSI (NDTC3L) to establish a comparison between both systems. Fig. 7 and Fig. 8 show the torque response, stator flux response and stator currents at 50rpm and no load conditions for both systems respectively. Fig. 9 and Fig. 10 show the torque response, stator flux response and stator currents at 200rpm and nominal torque conditions (7.4Nm) for both systems respectively.

The sample time used in the control system is 100μs. In order to assess the performance of both systems, the torque standard deviation and stator flux standard deviation are calculated to evaluate the ripple of both variables. The expression for the standard deviation of a generic variable employed is as follows (being n the number of samples):

$$\sigma = \left(\frac{1}{n-1} \sum_{i=1}^{n} (x_i - \bar{x})^2 \right)^{1/2} \qquad \bar{x} = \frac{1}{n} \sum_{i=1}^{n} x_i \quad (15)$$

Additionally the Total Harmonic Distortion (THD) of the stator current is calculated and the mean switching frequency of the inverter IGBT devices has been obtained for both systems. These results are shown in Table IV, where two additional operating points are incorporated: 50rpm and nominal load, and 600rpm with no load.

From the experimental results presented in Fig. 7 to Fig. 10 it is apparent that the torque and flux ripple for the new system utilising a three-level VSI is considerably reduced. Stator current waveforms also show less distortion for the new system. Measurements made on the results obtained (see Table IV) also show that the THD of the stator currents and the switching frequency of the inverter switches in the proposed system can be both reduced by more than 50%. Switching frequency is reduced due to the utilisation of a three-level VSI topology. In this type of inverter some transitions between the three possible states of a leg do not involve the commutation of all the semiconductors of the leg. With the new proposed system, NDTC3L, a higher efficiency can be achieved due to the reduction of switching frequencies and THD. This feature together with the improved torque control makes this system an interesting alternative in applications such as electrical vehicles [18].

In Table III it is shown the percentage of utilisation for every different type of vector that can be delivered by the three-level VSI at different operating points. It is interesting to see how the small and medium vectors, which do not exist in the two-level topology, play an important role in reducing the torque ripples. This is particularly important for small vectors at low speed and low load operation. It can be seen that in this condition (50rpm and no load) medium and large vectors are hardly ever employed.

Finally, in Fig. 11 it can be seen the stator voltage waveforms captured with the oscilloscope in the star-connected motor phases. The number of voltage levels delivered by the two-level VSI is 5, while in the case of the three level VSI this number is increased to 9 voltage levels, achieving a more sinusoidal and motor-friendly waveform. It is evident that voltage dV/dt is reduced with the three-level VSI.

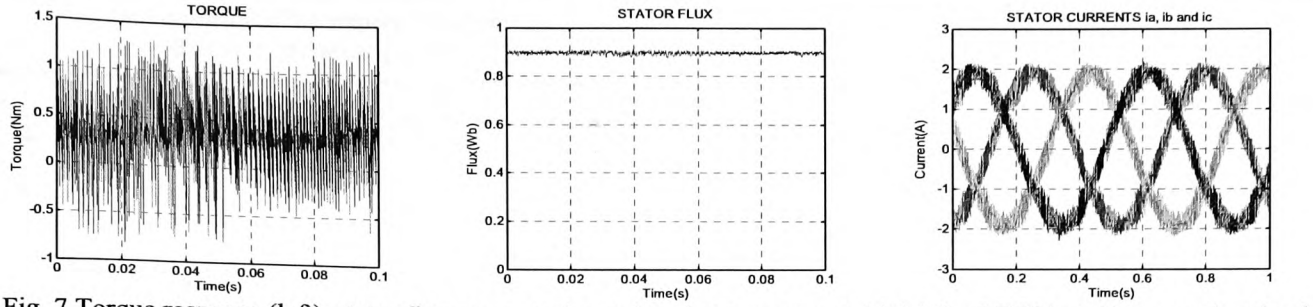

Fig. 7 Torque response (left), stator flux response (centre) and stator currents (right) for DTC2L at 50 rpm and no load

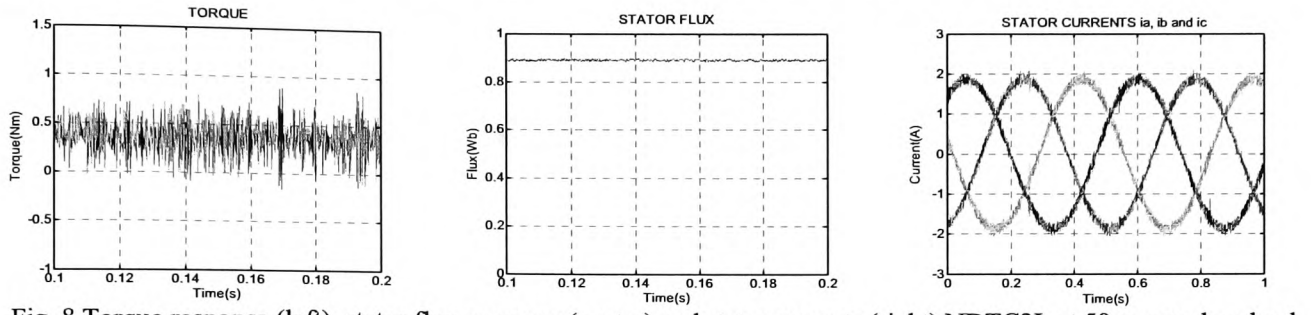

Fig. 8 Torque response (left), stator flux response (centre) and stator currents (right) NDTC3L at 50 rpm and no load

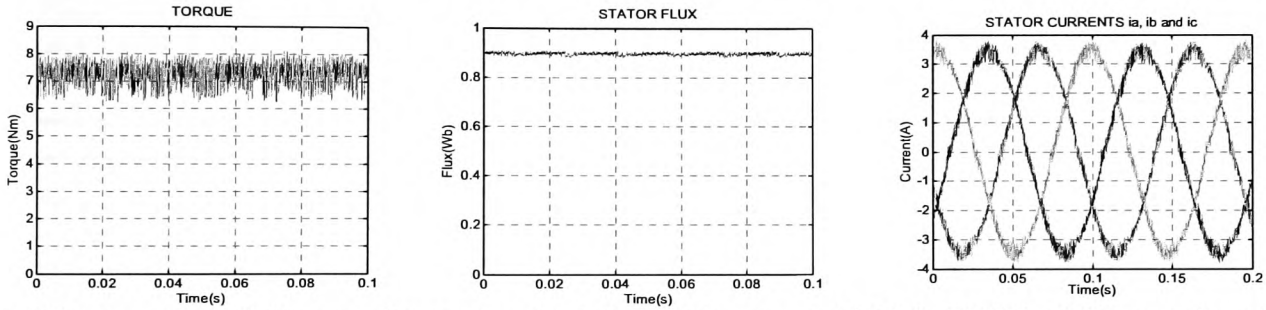

Fig. 9 Torque response (left), stator flux response (centre) and stator currents (right) for DTC2L at 200 rpm and nominal load

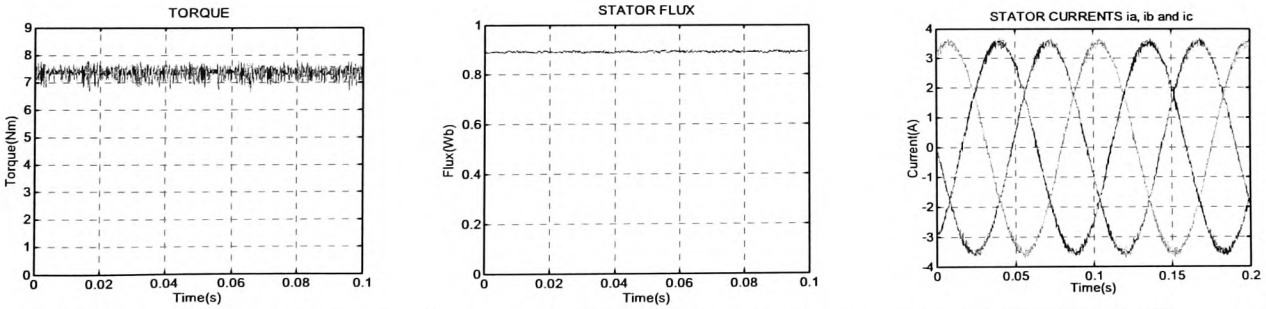

Fig. 10 Torque response (left), stator flux response (centre) and stator currents (right) for NDTC3L at 200 rpm and nominal load

Table III Use of the different types of vector in the NDTC3L system

Operating point	% zero vectors	% small vectors	% medium vectors	% large vectors
50 rpm and no load	49.52	49.17	1.28	0.04
200 rpm and nominal load	12.51	40.57	26.6	21.32
50 rpm and nominal load	11.85	37.07	28.79	22.31
600 rpm and no load	0.06	9.74	50.08	40.12

Table IV Summary of the experimental results at different operating points

50 rpm and no load		
SYSTEM	DTC2L	NDTC3L
Torque Standard Deviation	0.44Nm	0.17Nm
Flux Standard Deviation	0.0065Wb	0.003Wb
Stator current THD	11.89%	5.07%
Mean Switching Frequency	6350Hz	1380Hz
200 rpm and nominal load		
SYSTEM	DTC2L	NDTC3L
Torque Standard Deviation	0.46Nm	0.22Nm
Flux Standard Deviation	0.0059Wb	0.0029Wb
Stator current THD	2.62%	1.17%
Mean Switching Frequency	4078Hz	1977Hz
50 rpm and nominal load		
SYSTEM	DTC2L	NDTC3L
Torque Standard Deviation	0.45Nm	0.34Nm
Flux Standard Deviation	0.0059Wb	0.0027Wb
Stator current THD	3.20%	2.04%
Mean Switching Frequency	5484Hz	3090Hz
600 rpm and no load		
SYSTEM	DTC2L	NDTC3L
Torque Standard Deviation	0.30Nm	0.13Nm
Flux Standard Deviation	0.0091Wb	0.0028Wb
Stator current THD	6.58%	1.43%
Mean Switching Frequency	1869Hz	940Hz

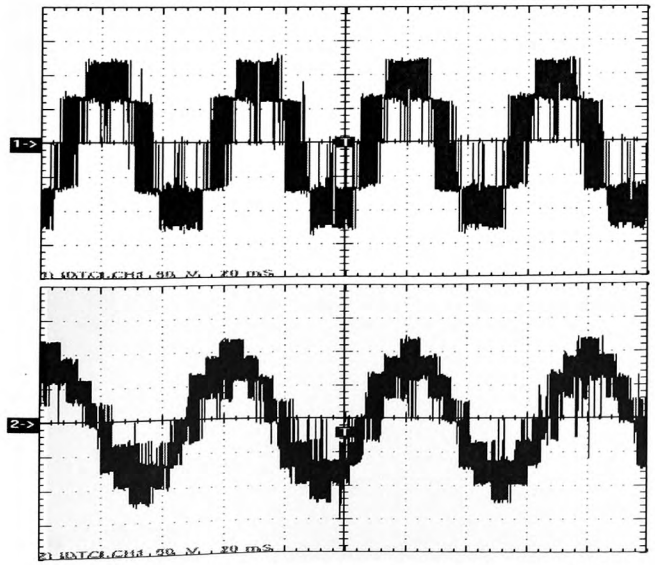

Fig. 11 Stator phase voltage for DTC2L (up) and NDTC3L (down)

VII. Conclusions

A novel controller based on the DTC principle is presented and it is shown that it can be easily implemented in a three-level VSI drive system. The inputs of the controller are the stator flux error, the torque error and additionally the stator flux angular speed. A reference voltage vector is then generated instead of choosing the inverter state through a look-up table as in the Classical DTC system. The reference voltage generated at the output of the controller is then synthesised applying the nearest vector available. This controller can be easily applied to different VSI topologies. The novel controller equations do not involve the use of motor parameters. Motor parameters are only used in the inherent torque and stator flux estimation necessary in any DTC system. The experimental results obtained for the new DTC scheme with a three-level VSI illustrate a considerable reduction in torque ripple, flux ripple, harmonic distortion in stator currents and switching frequency when compared to the existing Classical DTC system utilising two-level VSI.

List of Symbols

Γ_e : Electromagnetic torque.

Γ_e^* : Torque reference.

$\hat{\Gamma}_e$: Estimated torque.

$e_{\Gamma e}$: Torque error.

d_Γ : Torque error label.

$\vec{\psi}_s$: Stator flux vector.

ψ_{sx} : x component of the stator flux vector.

ψ_{sy} : y component of the stator flux vector.

ψ_s^* : Stator flux module reference.

$\hat{\psi}_s$: Estimated stator flux.

$\hat{\gamma}_s$: Estimated stator flux angle.

ω_s : Stator flux angular speed.

$\hat{\omega}_s$: Estimated stator flux angular speed.

$e_{\psi s}$: Stator flux error.

K : Stator flux sector position.

d_ψ : Stator flux error label.

P : Pole pairs.

L_m : Magnetising inductance.

L_s : Stator inductance.

L_r : Rotor inductance.

R_s : Stator resistance.

R_r : Rotor resistance.

$\vec{\psi}_r'$: Rotor flux vector referred to the stator.

$\vec{u}_s$: Stator voltage vector.

u_{sx} : x component of the stator voltage vector.

u_{sy} : y component of the stator voltage vector.

$\vec{i}_s$: Stator current vector.

i_{sx} : x component of the stator current vector.

i_{sy} : y component of the stator current vector.

i_{sa} : Stator current phase a.

i_{sb} : Stator current phase b.

V_{DC} : DC-link voltage.

V_{refx} : x component of the voltage reference.

V_{refy} : y component of the voltage reference.

$V_{ref\alpha}$: α component of the voltage reference.

$V_{ref\beta}$: β component of the voltage reference.

$K_{\Gamma e}$: Torque gain.

$K_{\psi s}$: Stator flux gain.

$K_{\omega s}$: Stator flux angular speed gain.

REFERENCES

[1] Takahashi, I.; Noguchi, T. "A new quick-response and high-efficiency control strategy of an induction motor." *IEEE Transactions on Industrial Applications*, vol. IA-22, no.5, pages 820-827, 1986.

[2] Depenbrock, M. "Direct self control of inverter-fed induction machines." *IEEE Transactions in Power Electronics*, vol. PE-3, no. 4, pp. 420-429, Oct. 1988.

[3] ABB. "Direct Torque Control – the world's most advanced AC drive technology" Technical guide no. 1, 1999.

[4] Buja, G.; Kazmierkowski, M. P. "Direct Torque Control of PWM Inverter-Fed AC Motors - A Survey", *IEEE Transactions on Industrial Electronics*, vol. 51, no. 4, pp. 744-757, August 2004.

[5] Habetler, T.G.; Profumo, F.; Pastorelli, M.; Tolbert, L. "Direct Torque Control of Induction Machines Using Space Vector Modulation"; *IEEE Transactions on Industry Applications*, vol. 28, no. 5, pages 1045-1053, September/October 1992.

[6] Romeral, J.L.; Arias, A.; Aldabas, E.; Jayne, M. G. "Novel Direct Torque Control (DTC) Scheme with Fuzzy Adaptive Torque Ripple Reduction." *IEEE Transactions on Industrial Electronics*, vol. 50, no. 3, pp. 487-492, June 2003.

[7] Bird, I. G.; Zelaya, H. "Fuzzy logic torque ripple reduction for DTC based AC drives." *IEE Electronics Letters*, vol. 33, no. 17 August 1997.

[8] Kang, J.; Sul, S. "New Direct Torque Control of Induction Motor for Minimum Torque Ripple and Constant Switching Frequency" *IEEE Transactions on Industry Applications*, vol. 35, no. 5, pages 1076-1082, September/October 1999.

[9] Grabowsky, P. Z. "Direct Flux and Torque Neuro-Fuzzy Control of Inverter Fed Induction Motor Drives." Thesis. Faculty of Electrical Engineering. Politecnicka Warszawaska, Warsaw University of Technology. 1999.

[10] Perelmuter, V. "Three-Level Inverters with Direct Torque Control." *Industry Applications Conference*, pp. 1368-1374, Rome, October 2000.

[11] Tan, Z.; Li, Y.; Li, Min. "A Direct Torque Control of Induction Motor Based on Three-level NPC Inverter." *Power Electronics Specialists Conference*, vol. 3, pp. 1435-1439, June 2001.

[12] Lee, K.B.; Song, J.H.; Choy, I.; Yoon, J.Y. "Improvement of Low-Speed Operation Performance of DTC for Three-Level Inverter-Fed Induction Motors." *IEEE Transactions in Power Electronics*, vol. 48, no. 5, pp. 1006-1014, October 2001.

[13] Lee, K.B.; Song, J.H.; Choy, I.; Yoon, J.Y. "Torque Ripple Reduction in DTC of Induction Motor Driven by Three-level Inverter with Low Switching Frequency." *IEEE Transactions in Power Electronics*, vol. 17, no. 2, pp. 255-264, March 2002.

[14] Prats, Ma A.M.; Escobar, G.; Galvan, E.; Carrasco, J.M.; Portillo, R. "A switching control strategy based on output regulation subspaces for the control of induction motors using a three-level inverter." *IEEE Power Electronics Letters*, vol. 1, no. 2, pp. 29-32, June 2003.

[15] G. Brando and R. Rizzo. "An Optimized Algorithm for Torque Oscillation Reduction in DTC-Induction Motor Drives using 3-Level NPC Inverter." in Proc. IEEE International Symposium on Industrial Electronics ISIE04, June 2004, Ajaccio, France, pp. 1215-1220.

[16] J. Rodriguez, J. Lai, and F.Z. Peng, "Multilevel Inverters: A Survey of Topologies, Controls, and Applications." *IEEE Trans. on Ind. Elec.*, vol 49, no 4, pp. 724-738, August 2002.

[17] Nabae, A.; Takahashi, I.; Akagi, H. "A new neutral-point-clamped PWM inverter." *IEEE Transactions on Industrial Applications*, vol. IA-17, no. 5, pages 518-523, Sept./Oct. 1981.

[18] J.C. Trounce, S.D. Round, and R.M. Duke. "Comparison by Simulation of Three-Level Induction Motor Torque Control Schemes for Electric Vehicle Applications." in Proc. International Power Engineering Conference, May 2001, Singapore, pp. 294-299.